MECHANISMS AND EFFECT OF DEEP CRYOGENIC TREATMENT ON STEEL PROPERTIES

Patricia Jovičević Klug

Doctoral Dissertation
Jožef Stefan International Postgraduate School
Ljubljana, Slovenia

Supervisor: Prof. Bojan Podgornik, Department of Metallic Materials and Technology, Institute of Metals and Technology and Jožef Stefan International Postgraduate School, Ljubljana, Slovenia

Evaluation Board:
Prof. Vojteh Leskovšek, Chair, Institute of Metals and Technology and Jožef Stefan International Postgraduate School, Ljubljana, Slovenia
Prof. Miha Čekada, Department of Thin Films and Surfaces, Jožef Stefan Institute and Jožef Stefan International Postgraduate School, Ljubljana, Slovenia
Prof. Dario Iljkić, Department of Materials Science and Engineering, Faculty of Engineering, University of Rijeka, Rijeka, Croatia

MEDNARODNA PODIPLOMSKA ŠOLA JOŽEFA STEFANA
JOŽEF STEFAN INTERNATIONAL POSTGRADUATE SCHOOL

Patricia Jovičević Klug

MECHANISMS AND EFFECT OF DEEP CRYOGENIC TREATMENT ON STEEL PROPERTIES

Doctoral Dissertation

MEHANIZMI IN VPLIV GLOBOKEGA PODHLAJEVANJA NA LASTNOSTI JEKEL

Doktorska disertacija

Supervisor: Prof. Bojan Podgornik

Ljubljana, Slovenia, May 2022

I dedicate this work to my beloved family and all women in science.

"To female scientists...
…their names and faces are mostly unknown to me,
yet somehow, I carry their legacy.
These women have shaped me. They have influenced me. They have inspired me beyond measure. Deep within me are the flames of these female hearts whom I have never met. Their strength seems to find me when my own fire is dwindling, and I am emboldened
by their everlasting spirits.
Their past has been an investment into my future. Their strength has become my tenacity. Their victories have become my opportunities. The existence of their generation has allowed for the emergence of mine.
We may have been born into different eras, we may have journeyed on roads that were unfair or unequal, the divides between us may seem illimitable and titanic. But we are forever united by the irrefutable truth of our common bond: We are women.
Because of them, I have a pathway. Because of me, I walk it."
-Adapted from a quote by Skylar Liberty Rose (writer).

Acknowledgments

This thesis was carried out under the financial support of the *Slovenian Research Agency (ARRS*).

When doing PhD research and to achieve the best results, you need the whole village to stand behind you to support, motivate and sometimes criticize you. Therefore, this is now the time to proudly present and express gratitude to my village, which is now already more like a miniature city.

First and foremost, I must thank my supervisor *Prof. Bojan Podgornik*, Institute of Metals and Technology (IMT), Department of Metallic Materials and Technology. He has been an outstanding mentor to me, he is the true definition of a leader and the ultimate role model. I have been extremely lucky to have had a supervisor who cared about my project and was eager to answer all of my (numerous) queries and listen to all my ideas. He has been supportive and encouraging (He said: *"Patricia, show them what they are missing. Let them mock you, laugh at you, hurt you and ignore you, BUT never let them stop you in achieving your carrier and scientific goals."* –May 2020). For this advice and encouragement, I will be forever grateful. Furthermore, he has pushed me to take on challenges and gain experiences that will and have made me a better scientist. I would like to thank him for all the help, professional opinion and productive discussions throughout my PhD work.

I would also like to express my gratitude to my guest supervisor *Dr. Michael Rohwerder*, Max-Planck Institute for Iron Research (MPIE), Department of Interface Chemistry and Surface Engineering. I am extremely grateful that he welcomed me to his group as a guest PhD researcher and for all his guidance and support. Sincere gratitude is extended to his generous participation in guiding, constructive feedback, kind support, and advice during my research stay at his group. Furthermore, I would also like to extend my gratitude to my fellow colleagues from MPIE, to *Haroon Christopher Sam, Manoj Prabhakar, Alexandra Vogel and Dirk Vogel*, for all the help with analyses and our synchrotron talks.

Special thanks go to *Prof. Jeffrey McCord*, University of Kiel, Department of Nanoscale Magnetic Materials-Magnetic Domains, who warmly welcomed me to his group and helped me with interpretation and suggestions for development of my results. At the same time, I would like to express my gratitude to my dear colleagues from the University of Kiel, *Lars Thormählen* and *Dennis Seidler*, for all the help with my experiments.

I would like to express my gratitude to my fellow colleague *Dr. Levi Tegg*, University of Sydney, Australian Centre for Microscopy and Microanalysis. I would like to thank him for his enthusiasm, cooperation and his willingness to extend my and also his research to new dimensions. His brilliant and skillful assistance enriched my study beyond my expectation. At the same time, I would like to thank *Prof. Julie Cairney*, University of Sydney, Australian Centre for Microscopy and Microanalysis, for her support and openness to our ideas; without her our collaboration and in-depth unraveling studies would not be possible.

I would also like to thank *Dr. Matteo Amatti* and *Dr. Luca Gregoratti*, synchrotron Elettra, ESCA beamline. You have my immense thanks for all the support you have given me during my stays at the synchrotron. Your guidance and productive discussions have helped me and motivated me to extend my interest of research and methods of testing also to surface science. Working with you was truly a pleasure.

Specific in-depth analyses would not have been possible without the support and assistance of *Dr. Nathalie Valle*, Luxembourg Institute of Science and technology (LIST), Nanomaterials and Nanotechnologies, *Dr. Laszlo Almasy*, Budapest Neutron Centre (BNC), SANS beamline and *Dr. Efthymios Polatidis*, Paul Scherrer Institute (PSI), POLDI beamline, thank you for your help and collaboration.

This work would also not have been possible without *Prof. Goran Dražić*, National Institute of Chemistry (KI), Department of Electronic Ceramics and *Dr. Bojan Ambrožič*, Center of Excellence on Nanoscience and Nanotechnology (Nanocenter). I would like to thank you both for your direct and indirect support and assistance, discussions, inspirations and valuable suggestions during the course of this study.

Special thanks go to uplifting women in science *Nataša Lipovšek, Tjaša Kranjec and Tina Sever*. Thank you all for putting up with all my experimental ideas, discussions and mini projects, working with you was truly a pleasure.

I would like to thank *my beloved parents Tatjana and Boris* for their love and support that helped me to take on challenges and for raising me to have a curios personality, which helped in achieving and expanding my own life goals. They often thought what is going on in that mind of hers and they sometimes did not know where this magical mystery ride of a scientific carrier will take me, but no matter what, they always supported me. They also taught me that women's rights are equal to men's rights and that I should not succumb to the stereotypes that science and leadership are not for women. And for that I will be forever grateful to them.

I would also like to express my gratitude to *my treasured husband Matic*, fellow scientist and partner in crime, my personal hero of antiheros, who has always supported me with my ideas and getting my creative endeavors out there. *Matic, in a night sky full of stars I saw galaxies in your eyes, because you light up my path and ignite eternal flame. We are embers from the same fire and we are dust from the same star.* You love my curves and edges and all my perfect imperfections, as you are my heart's rhythm and blues. During my PhD you gave me strength when I needed it and provided me with unconditional love, which helped to achieve my life and carrier goal(s).

Thank you all with all my heart.
Patricia

Abstract

Deep cryogenic treatment (DCT) is a type of cryogenic treatment, during which a material is subjected to temperatures below −160 °C. When a metallic material is modified with DCT, changes occur down to the nanoscopic level. DCT induces microstructural changes such as grain size refinement, formation of new grains, movement of dislocations, change of solubility of alloying atoms, alteration of crystal structure and new phase formation. Changes in the material can have positive or negative effects or can conjointly render negligible changes on the final properties of steels, which was evaluated and proven within this work. The steel's performance and later performance of manufactured components and tools from this specific material strongly depend on the selection of proper material, proper design, accuracy with which the tool is made from untreated material and application of proper heat treatment, including DCT. Furthermore, DCT treatment has shown to reduce density of defects in crystal structure, increase wear resistance of steel, increase hardness, improve toughness, tensile strength as well as corrosion resistance. However, the performance of DCT strongly depends on steel type as well as manufacturing type (wrought or powder metallurgy steel), chemical composition of steel (the ratio of alloying elements, such as chromium, tungsten etc.). Additionally, heat treatment parameters (austenitizing and tempering temperature) and presence of microstructure-related phenomena within the steel (such as transformation-induced plasticity (TRIP)) also influence DCT effectiveness. This study provides a systematic approach and research of DCT and its effectiveness on steels. The study also aims at unravelling the underlying mechanisms in selected ferrous alloys (high-speed steels, tool steels, stainless steel and bearing steel) to provide in-depth fundamental understanding of DCT on ferrous alloys.

Keywords: deep cryogenic treatment (DCT), ferrous alloys, microscopy, microstructure, surface analysis, mechanical properties, wear resistance, fatigue

Povzetek

Globoko podhlajevanje (v angleščini izraz “deep cryogenic treatment”, iz tega sledi kratica DCT) je tip podhlajevanja, pri katerem je material izpostavljen temperaturam, nižjim od −160 °C. Ko je kovina modificirana z DCT, se pojavijo spremembe materiala vse do nanonivoja. DCT povzroči spremembe v mikrostrukturi kot so zmanjšanje velikosti zrn, tvorjenje novih zrn, premik dislokacij, sprememba topnosti legirnih atomov, sprememba kristalne strukture in tvorjenje novih faz. Nastale spremembe imajo lahko pozitiven ali negativen vpliv ali pa skupaj tvorijo zanemarljive spremembe posameznih končnih lastnosti jekel, kar je tudi evalvirano in dokazano znotraj te disertacije. Lastnosti jekla in kasneje zmogljivosti izdelanih komponent iz le-tega so močno odvisne od izbire podtipa materiala, oblike, natančnosti izdelave in izbire primerne toplotne obdelave, vključno z DCT. Dokazano je bilo, da DCT zmanjša gostoto napak v kristalni mreži, izboljša odpornost na obrabo, poveča trdoto, trdnost in natezno trdnost ter prav tako odpornost jekla na korozijo. Kakor koli, vpliv ter uspešnost DCT-ja na izbrano jeklo sta tesno povezana tudi z vrsto jekla, načinom proizvodnje jekla (kovano jeklo ali jeklo, izdelano preko praškovne metalurgije), kemijsko sestavo jekla (razmerje med legirnimi elementi kot so krom, volfram itd.). Prav tako parametri toplotne obdelave (temperatura avstenitizacije in popuščanja) ter prisotnostjo posebnih mikrostrukturnih fenomenov znotraj jekla (npr. transformacijsko inducirana plastičnost (TRIP)) imajo vpliv na učinkovitost DCT-ja. Izbrana študija predstavlja tudi sistematični pristop in raziskave o DCT vplivu na jekla. Cilj raziskave je tudi razvozlati mehanizme v izbranih jeklih (hitrorezna jekla, orodna jekla, nerjavno jeklo ter ležajno jeklo) z namenom podajanja temeljnega razumevanja DCT vpliva na železne zlitine (jekla).

Ključne besede: globoko podhlajevanje, železne zlitine, mikroskopija, mikrostruktura, površinska analiza, mehanske lastnosti, odpornost na obrabo, utrujanje

Contents

List of Figures

List of Tables

Abbreviations

BP	. . .	Boiling point
BSE	. . .	Back-scatter electrons
CCT	. . .	Conventional cold treatment
CHT	. . .	Conventional heat treatment
CNPTB	. . .	Circumferentially notched and fatigue pre-cracked tensile bar
COF	. . .	Coefficient of friction
DCT	. . .	Deep cryogenic treatment
EBSD	. . .	Electron backscatter diffraction
ECD	. . .	Equivalent carbide diameter
EDS	. . .	Energy-dispersive X-ray spectroscopy
HSS	. . .	High-speed steel(s)
ICP-OES	. . .	Inductively coupled plasma - optical emission spectrometry
LM	. . .	Light microscope
MCT	. . .	Multistage cryogenic treatment
PAG	. . .	Prior austenite grain
PM	. . .	Powder metallurgy
SCT	. . .	Shallow cryogenic treatment
SEI	. . .	Secondary electron imaging
SEM	. . .	Scanning electron microscopy
STEM	. . .	Scanning transmission electron microscopy
TEM	. . .	Transmission electron microscopy
XPS	. . .	X-ray photoelectron spectroscopy
XRD	. . .	X-ray diffraction
XRF	. . .	X-ray fluorescence

Chapter 1

Introduction

1.1 Deep Cryogenic Treatment

1.1.1 Short history of research of cryogenic treatment

Cryogenic treatment is a type of heat treatment, the name is formed by combining two Greek words: "*kryo*", which means very cold, and "*genics*", which means to produce. From this, one can describe cryogenic treatment as a type of method or technology, where the main goal of the process is to expose matter to temperatures below 0 °C (< 273 K) [1]. In literature, several terms for the same method of cryogenic treatment can be found, such as cryo, cryogenics, cryoprocessing, cryogenic processing, cryogenating, cryogenic stress relief, cryogenically treated, cryotempering, cryogenic hardening, cryo-treated, cryogenic thermal cycling treatment [1]–[7]. In the last century, cryogenic treatment has obtained an important role in the heat treatment of ferrous and non-ferrous alloys in changing their properties (Figure 1). Heat treatment procedures of different materials are constantly altering and improving throughout centuries from blacksmith's art to high-tech science technology nowadays. Similarly, cryogenic treatment also follows this trend, especially due to its effect on modifying the material from bulk to surface. With the limitations being slowly reached for improving metallic materials through chemical composition modification, an increasing interest has evoked in the last decade for the understanding of cryogenics techniques and their possible application in material science [8], [9].

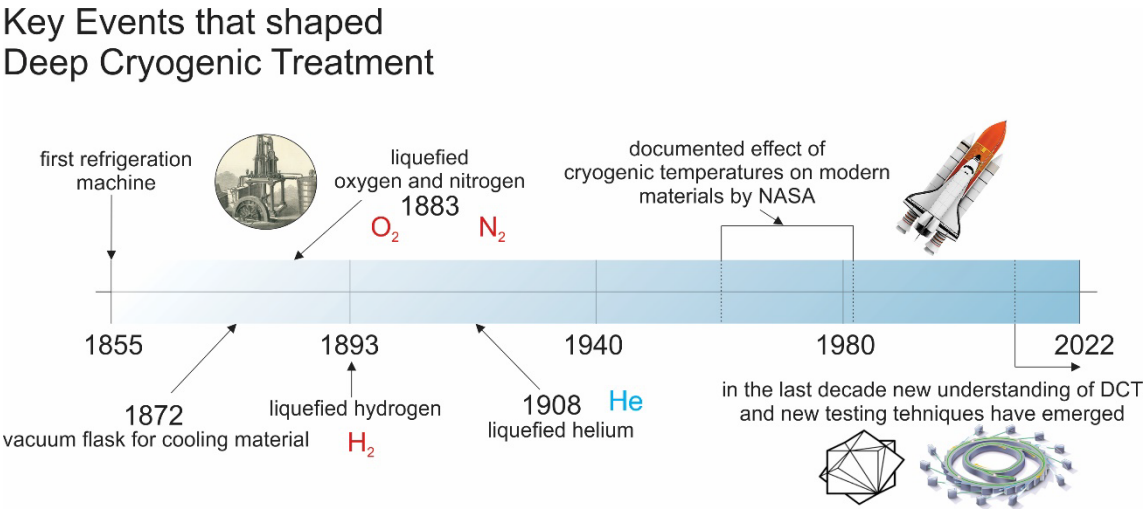

Figure 1: Key events that shaped deep cryogenic treatment (DCT) throughout history.

However, the topic of cryogenic treatment is not new (Figure 1). Some attempts of reverse heat treatment – cooling, were already conducted at the beginning of the 20th century, mostly to improve properties of cutting tools [10]. Then in 1872, James Dewar invented the vacuum flask for cooling and storing refrigerated liquids under vacuum. In 1883, Karol Olszewski liquefied

oxygen and 10 years later, in 1893, he and James Dewar liquefied hydrogen. Later in 1908 also liquefied helium was produced by Kamerlingh Onnes, and with liquid helium new research options of cryogenic treatments had opened [11]–[16]. Aerospace industry and research was one of the first to actually notice and technically document the effects of cryogenic temperatures on modern and more advanced materials, including specialized steels and non-ferrous alloys. National Aeronautics and Space Administration (NASA) engineers documented that many of the metal parts of the space aircraft, which had returned from space, where condition is vacuum at cryogenic temperatures, were stronger than before leaving Earth (before the flight). Since then, the pioneers and researchers have been searching, improving and analyzing new ideas and methods/techniques in the field of cryogenics and cryogenic treatment of materials for improving their macroscopic properties [17].

1.1.2 Types of cryogenic treatments

The cryogenic treatment of metals is divided into three systematically different temperature systems. First and foremost is the conventional cold treatment (CCT), for which the temperature is reduced down to −80 °C (≥ 193 K) [9]. CCT was common in the past, because it was believed that temperatures down to −80 °C (≥ 193 K) were adequate to transform most of the retained austenite into martensite in steels, establishing improved fatigue strength and dimensional stability and increased wear performance [18], [19]. The promotion of this idea was done by several experiments, where the material was directly soaked into containers with dry ice (solid CO_2). Unfortunately, the negative results of these experiments emerged, where CCT supposedly led to thermal shock and later to failure of tools, instigating that companies abstained from developing and using such treatment (1940s–1950s). However, only years later, experiments at lower temperatures and more careful handling during the procedure proved and showed a general improvement of material properties with CCT and later shallow and/or deep cryogenic treatment [20]–[22] (Figure 2).

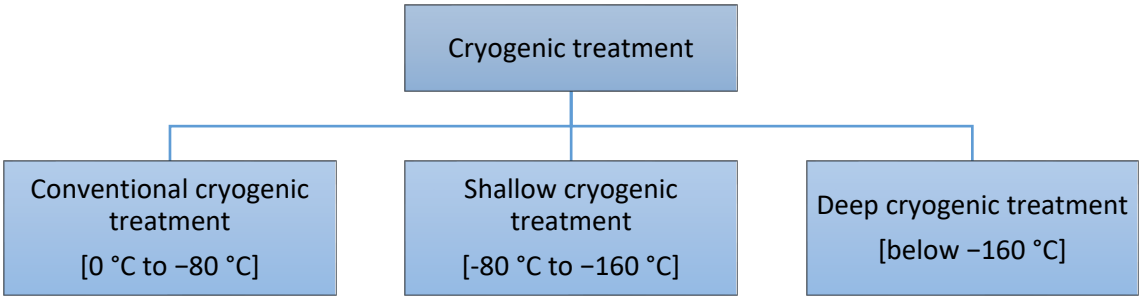

Figure 2: Schematic presentation of division of cryogenic treatment.

The second type, shallow cryogenic treatment (SCT), occurs from −80 °C to −160 °C (193 K to 113 K), however, CCT is often considered to be a part of SCT (0 °C - −160 °C) [23]–[27]. SCT causes transformation of retained austenite into martensite (increase in hardness) and allows size reduction of carbides and thus increased number of them [28], [29]. After SCT, the last type is deep cryogenic treatment. In Celsius scale, the deep cryogenic treatment (DCT) is in some literatures below −160 °C (113 K) and other literatures −153 °C (120 K), depending on corresponding author and their views. DCT can be also found in literature named as sub-zero treatment (SZT) [24] or ultra-low temperature process (ULTP) [30]. In case of metallic materials, DCT is placed normally after quenching under −160 °C for a certain period of time (often for 24 hours [11]–[13], [15], [16]).

Deep cryogenic treatment is described separately in more detail in the next subchapter 1.1.3.

1.1.3 Deep cryogenic treatment

1.1.3.1 Deep cryogenic treatment effect on material

Under DCT several mechanisms occur in metallic materials: the conversion of retained austenite into martensite, carbon redistribution and grain size reductions [2], [31], [32], precipitation of fine carbides [2], [31]–[35] and reduction of free energy of crystal structure [36], [37]. Furthermore, DCT has beneficial effects on the alteration of residual stress [38]–[41], redistribution of atoms [42] and binding energy [43]. Moreover, DCT additionally creates a denser molecular structure in semiconductors, increases tool life, reduces time of machine parts for replacement, increases Schottky barrier height and thus, significantly reduces material reverse leakage current [44]–[47]. It also improves grinding forces [47], cuts operating costs [48], improves specific gravity requirements [47], decreases H solubility [49], as well as alters Curie temperature of Fe-B-based material [49]. DCT can also decrease brittleness, reduces friction and improves thermal conductivity and wear resistance [48].

In terms of mechanical properties, DCT was found to have an effect on hardness [26], [50]–[52], fracture toughness [2], [31], [52], [53], impact toughness [52], [54]–[57], compressive strength [52], [58] and values of strain-hardening exponent [52]. DCT has also been proven to have an effect on wear resistance [25], [31], [59]–[66], corrosion resistance [67]–[72], oxidation dynamics [43], [73], fatigue properties [52], [64], [74]–[77] and magnetic properties [41]. However, the consensus of when and how DCT influences different materials has still not been set. For this reason, different materials and their multiple properties are being tested with DCT in order to understand the mechanism behind it and to provide meaningful correlations to the different DCT effects with respect to selected materials (Figure 3).

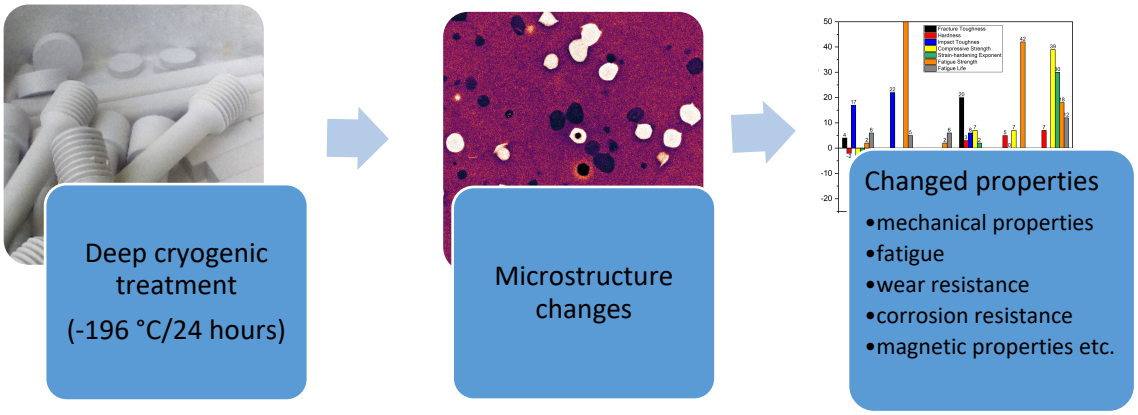

Figure 3: Schematic representation of deep cryogenic treatment (DCT) and its influence on materials.

DCT has been mostly used for metallic materials, however, its application can extend also to non-metallic materials. Non-metallic materials, such as polymers, are in recent years drawing attention with new applications in medicine, aerospace, space and electronics. DCT on polymers has also clearly shown an improvement of hardness, mechanical strength, relaxation behavior of material as well as wear resistance [15], [78]–[81].

1.1.3.2 Deep cryogenic treatment parameters of ferrous alloys

When ferrous alloys are exposed to DCT, several parameters have to be taken into account. The importance factor of individual parameters was statistically determined with the Taguchi method in the study of Darwin et al. (2008) [82], where the aim was to optimize and identify the importance of the critical processing parameters. The far most important factor is selected soaking temperature (72 %) of selected media, followed by holding time of the material under selected deep cryogenic temperature (24 %). The cooling rate and warming rate (10 %) and sequence of cryogenic treatment (2 %) have a lower impact on DCT effectiveness. The selection

of the soaking period depends on the type of material (ferrous (steel) or non-ferrous alloys) and applied cryogenic treatment. Cryogenic temperature depends on the type of research and individually selected temperature [83]. DCT is usually placed immediately after the quenching stage of ferrous alloys, followed by a single tempering cycle [8], [84], [85]. However, there are also studies, where DCT is done after tempering [78], [86] (Figure 4).

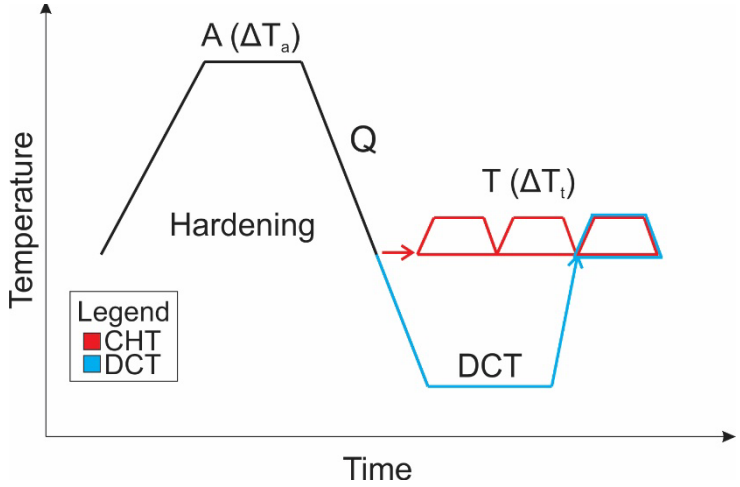

Figure 4: Schematic presentation of the most commonly used deep cryogenic heat treatment route (DCT) compared to conventional heat treatment route (CHT).

In recent years, more and more research is also conducted with a specific type of DCT described as multistage deep cryogenic treatment (MCT) (Figure 5). In this case the treatment consists of rapid cooling down to DCT temperature (below −160 °C) and heating up to SCT temperature (−80 °C) or even to room temperatures (20 °C or more) [86]–[89] in a cyclic manner with several repetition cycles (usually at least 3).

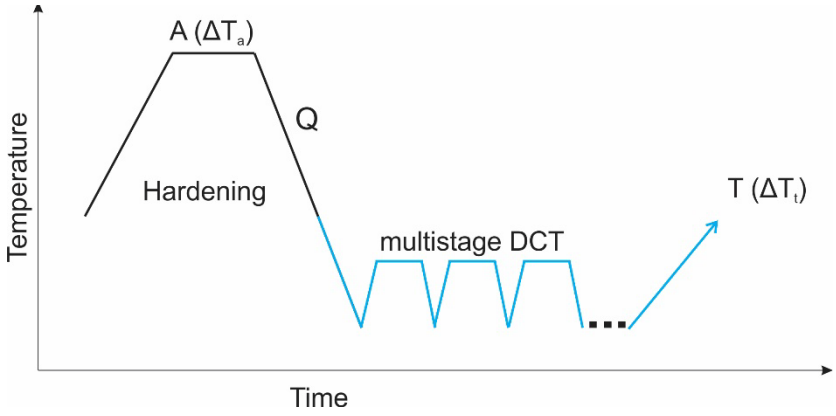

Figure 5: Example of multistage deep cryogenic treatment (MCT).

Beside DCT processing parameters, the performance of DCT is also influenced by the chemical composition of steel [32], [90], [91], steel type (wrought production or powder metallurgy steel (PM)) [52], [91], heat treatment parameters, such as austenitizing and tempering temperature [52], [59], [68], [91], [92], and also microstructural phenomenon, such as transformation-induced plasticity (TRIP) [93] etc.

1.1.3.3 Deep cryogenic treatment methods and gases

Four main methods of applications of DCT on ferrous alloys can be found in literature. The first is gradual immersion, where the sample is directly immersed (soaked) in liquid nitrogen for a predetermined time and then gradually warmed back to room temperature. The second is the heat exchanger, where liquid nitrogen flows through chamber, at which the cooled gas is dispersed by a fan inside the sample chamber. The third option is direct nebulization, where

liquid nitrogen is nebulized directly into a chamber and homogenous distribution is obtained by a fan. The fourth option is a hybrid method, which is actually a combination of first nebulization followed by gradual immersion, in order to provide improved control of the cooling whilst maintaining a high cooling rate [8], [13], [94]. For the different techniques different cooling media, mostly gases, are used. The common gases used for DCT are presented in Table 1.

Table 1: The common gases used in deep cryogenic treatment (DCT) with their chemical formula and boiling point, based on [15], [95], [96].

Gas	Chemical formula	Boiling point (°C/K)
Methane	CH_4	−162/111
Oxygen	O_2	−183/90
Nitrogen	N_2	−196/77
Hydrogen	H_2	−253/20
Helium	He	−269/4

Some gases tend to be more preferable compared to others for usage in DCT due to the properties of the selected gas. For example, liquid hydrogen can cause metals to undergo hydrogen embrittlement, which promotes brittleness and induces fracturing of the material. Additionally, hydrogen is considerably harder to store and is very explosive, making it difficult to handle with ease. Another example is helium, which can solidify other gases, such as oxygen, in localized areas, where pressure-relief passages occur that lead to dimensional instability of the material [97]. However, in most cases nitrogen is preferred due to its high availability, low cost, inertness, easy handling and storage.

1.1.4 Application of deep cryogenic treatment

Increasing demands on the market for material's performance improvement, material life cycle enhancement, cost savings, reduction of material for production and increased fraction of used green energy/technology are causing shifts in science and industry to adapt to these demands [8], [10]. One of the possible solutions is also DCT, which is cost-effective and can be marketed as green technology. As such it does not have a negative impact on the environment, which is a win-win combination for industry and the environment [98].

Application of DCT can be found in various industries : in medicine for improvement of implants [99], [100]; automotive industry for body parts, drivetrains, suspension and other parts of car/motorbike [8]; aerospace industry for shuttles, tools and robotics [101]–[103]; tool industry for tools, casings and electronics [8], [10]; energy sector/industry for increased corrosion resistance of pipes for oil and gas [104], [105], mining equipment [106] and nuclear power sector for improvement of the material used for storage [107]. DCT is becoming nowadays more and more applied also in the musical industry, where brass and plucked string instruments are treated by DCT to improve the acoustic effect [19], [108]. With all the above DCT has also attracted attention from nanosciences and nanotechnologies as a part of the heat transfer application in nanomaterials, nanofluids and resolving the agglomeration issue of particles [18]. Furthermore, DCT is also becoming an interesting possibility for applications in 3D printing [109], microscopy [110] and laser technology [111].

1.2 State of Art

As presented in the previous section DCT can influence on various perspectives of materials properties. However, the literature overview shows that DCT is still under research and all the benefits and drawbacks are still unknown and not fully understood [21]. In continuation of this section the varying effects of DCT on different steels are presented.

Table 2: Main steel groups and grades used for deep cryogenic treatment (DCT) from literature overview.

Group of steel	Grade of steel	Literature
Cold work steel	X210Cr12	[24], [26], [112]–[116]
	X153CrMoV12	[48], [88], [117], [118]
	X220CrVMo13-4	[119]
	X210CrW12	[120]
	45WCrV7	[121]
	60WCrV8	[122]
	X165CrMoV12	[118], [123]
	X50CrMoW9-1-1	[123]
	lower C and high W and C content	[2], [31], [124]
	X110CrMoV82	[40], [117]
Hot work steel	X37CrMoV5-1	[125], [126]
	X40CrMoV5-1	[40], [126]–[129]
	X30WCrV9-3	[130]
	QRO90 supreme	[78]
Structural steel	C40	[17], [39], [131]
	C50	[132]
	C40E	[17], [39], [131]–[133]
	C40R	[17], [39], [131]
	C45E	[134], [135]
	15NiCr13	[132]
	20NiCrMo2-2	[113], [136]
	17NiCrMo6-4	[137]
	18CrNiMo7-6	[138]
	16MnCrS5	[136]
	42CrMo4V	[17], [39], [40], [131], [139]–[141]
	S275JR	[142]
High-speed steel	HS10-4-3-10	[143]
	HS2-5-1-3	[144], [145]
	HS6-5-2-5	[78], [91]
	HS2-9-1-8	[146]
	HS18-1-2-5	[146]
	HS18-0-1	[146]
	HS6-5-2C	[47], [91], [112], [147]–[151]
Stainless steel	X30Cr13	[138], [139], [152]
	X30CrMoN15-1	[51]
	X105CrMo17	[153]
	X10CrNi18-8	[154]–[156]
	X4CrNiMo16-5-1	[157]
	X45CrSi9-3	[68], [158]
	X20CrMoV12-1	[159]
	X55CrMo14	[160]
	GX4CrNi13-4	[155], [161]
	X22CrMoV12-1	[159]
	X2CrNIMoN17-13-3	[162]
	GX23CrMoV12-1	[159]

The main groups of steels, which are being studied are cold work tool steels, hot work tool steels, high speed steels, stainless steels and structural steels. As such, the majority of research is focused on tool steels, due to the fact that tool steels are the most frequently used steel type and their application depends strongly on the properties that DCT is most known to positively alter (Table 2). For this reason, steels such as construction, high strength, bearing, duplex, maraging and other steels not designated as tool steels, are commonly not handled and tested with DCT.

During ascertainment of DCT literature, the following grades of steel were also encountered: bearing steel 100Cr6 [163]–[166] and low carbon martensitic bearing steel [163]. Additionally, also specific types of the steel, such as gear steel 600TG178 [167], plain carbon steel (1%) [168], super-bainitic steel [169], eutectoid steel [170], Cr-V ledeburitic tool steel [24], [50], high carbon alloyed tool steel [171], carburized steel [172], X165CrMoV12 [118], austempered ductile iron ADI 1000 grade [173], grey cast iron steel [174], 20NiCrMo2-2 [175], 16MnCr5 [175], W-C-Fe-Ni cemented carbides steel [176] and cold rolled low C steel CR3 [7], [66], [177], [178], have been treated with DCT.

As mentioned before, the DCT parameters are also important for DCT effectiveness. The literature conveys that soaking temperature of DCT can vary from −153 °C to −269 °C (Table 3). The reason behind this variability is the medium used for DCT and author's decision. Generally, many authors convey that temperatures below −196 °C impact the material properties and microstructure in a stronger fashion than with temperatures above −196 °C. Senthilkumar (2016) [29] described these differences to be related mostly to the improved complete austenite transformation to martensite, as well as to the enchanted carbon redistribution through segregation and clustering, when temperatures below −196 °C are applied.

Table 3: Soaking temperatures used in deep cryogenic treatment (DCT).

Temperature (°C)	Temperature (K)	Literature
−153	120	[24]
−154	119	[126]
−160	113	[149]
−163	110	[182]
−173	100	[183]
−175	98	[112], [156], [173]
−176	97	[133]
−180	93	[78], [84], [145], [183]–[186]
−184	89	[102], [124], [132]
−185	88	[30], [83], [92], [102], [109], [140], [150], [153], [154], [170], [187]–[189]
−186	87	[155]
−188	86	[68], [158]
−190	84	[173], [175], [190]–[192]
−193	81	[1]
−195	79	[157]
−196	77	most authors used it, liquid nitrogen temperature
−198	76	[51]
−243	30	[183]
−252	21	[193]
−269	4	[157], [162]

The most commonly used cooling and warming rate of metallic materials is 0.3–0.5 °C/min [94], [121], [192], [193], but some studies also provided considerably different rates such as 1 °C/min [172], 1.8 °C/min [196], 4.5 °C/min [5] or even 6–10 °C/min [197].

The last factor, which is important for DCT, is the soaking period (time), which can be from minute to days, depending on each author and selected metallic material (Table 4). In most cases this parameter is set to 24 h [40], [68], [136], [137], [195], but some divergences can also be found such as 0.5, 2, 16 h and more than 40 h [17], [113], [169]. However, the variety of soaking time applied on the steels shows that the temporal dynamics of DCT is still not well understood,

as some studies report a similar resulting effect with shorter soaking time [17], [169], [196] and others with longer soaking period (most of them). Furthermore, the temporal dependency is also not clear due to the high divergence in holding time related to the differently used steel grades and types.

Table 4: Soaking time of deep cryogenic treatment (DCT).

Time	Literature
3 min	[198]
5 min	[40]
10 min	[193]
15 min	[199], [200]
30 min	[162]
1 hour	[90], [115], [141], [156], [172], [177], [199]
2 hours	[99], [130], [146], [169]
4 hours	[50], [108], [187], [200]
6 hours	[92], [121], [132]
8 hours	[172], [203]–[205]
9 hours	[154]
10 hours	[120], [168], [173]
11 hours	[205]
12 hours	[144], [162], [170], [181], [185], [206], [207]
14 hours	[117]
15 hours	[99], [123], [203]
16 hours	[29], [182]
17 hours	[202]
18 hours	[21], [147]
20 hours	[47], [181], [182]
21 hours	[126]
22 hours	[39], [170]
24 hours (1 day)	most of authors used it
25 hours	[66], [123], [152], [206]–[209]
32 hours	[118], [125], [137], [178],
33 hours	[189]
35 hours	[117]
36 hours	[25], [48], [105], [106], [118], [127], [130], [168], [170], [188], [205], [210], [211]
40 hours	[66], [152], [194], [209]
48 hours (2 days)	[48], [83], [99], [105], [106], [109], [126], [127], [171], [205], [212]
72 hours (3 days)	[208], [216]
96 hours (4 days)	[217]
100 hours	[40]
120 hours	[217]
1 week	[150]

1.2.1 Deep cryogenic treatment influence on the microstructure of steels

When explaining the reasons for properties change of the steels, when treated by DCT, different theories have been proposed. Leskovšek and Ule (2002) [218], Bensely et al. (2006) [5], Podgornik et al. (2012) [66], Jaswin and Mohan Lal (2015) [68] and Kumar et al. (2016) [197] proposed that the main reason of improvement is attributed to grain refinement and precipitation of very fine carbides. Jaswin and Mohan Lal (2015) [68] and Kumar et al. (2016) [197] postulated DCT increases the driving force for the carbide nucleation (through lattice energy reduction and finer martensite formation from transforming retained austenite), which results in increased precipitation and finer carbides. Additionally, the refinement has also been assumed to originate from the precipitation of η-carbides instead of ε-carbides that normally form during conventional heat treatment, as suggested by Meng et al. (1994) [219]. However, Gavriljuk et al. (2013) [119] suggested that the theory related to these transiting carbides is vague due to their short lifetime and metastability in the initial stage of tempering, making them hard to track and analyze. In contrast, Gavriljuk et al. (2013) [119] explained that the additional carbides nucleation occurs from direct plastic deformation of the martensite during exposure to DCT, which yields carbon displacement and agglomeration with gliding dislocations.

The next possible mechanism is described by Collins (1996) [28], who stated that DCT influences the production of internal stresses that result from the austenite to martensite transformation. This effect, as proposed by Moore and Collins (1999) [199], results in martensite conditioning, which promotes formation of fine carbides through additional formation of nucleation sites. They assumed that the additional nucleation sites are activated by recombination and formation of crystal defects and/or carbon clusters that inhibit a lower energy potential for carbide nucleation. Furthermore, Collins (1996) [28] stated that internal stresses may spawn twins and dislocations in crystal lattice defects. Huang et al. (2003) [150] suggested that supersaturation of martensite during DCT increases its lattice distortion and thermodynamic instability, due to the extremely low temperature, which then promotes the atomic migration of carbon and alloying elements towards nearby crystal defects. Akhbarizadeh et al. (2009) [65] also explained that another possibility for induced carbide precipitation results from martensite and austenite lattice contraction. As a result of martensitic contraction and conditioning, residual stresses in the material change into a more compressive character [39]. This has been shown to have a positive effect on steels, as DCT reduces tensile residual stresses or even forms compressive stresses that benefit material performance and lifetime [220].

Hu et al. (2014) [169], Koneshlou et al. (2011) [221] and Prudhvi et al. (2016) [17] concluded that the main mechanism behind DCT is also the transformation of austenite to martensite, where smaller martensite laths are uniformly formed in the matrix. Niessen et al. (2018) [196] and Villa and Somers (2020) [222] provided an useful input on the thermal formation of the martensite from austenite, from which a strong influence of holding time on properties of steel has been suggested, especially in terms of impact toughness. They postulate based on previous research that impact toughness scales with austenite fraction, which is expected due to the higher ductility properties of austenite compared to martensite.

Zhirafar et al. (2007) [195] and Dhokey et al. (2014) [144] suggested that the mechanism behind the properties' change is densified martensite, precipitation of secondary martensite and precipitation of finer carbides. Formation of secondary martensite may occur because of martensitic transformation during DCT. The other explanation could also be that secondary martensite is formed after DCT during tempering, throughout which the relief of phase hardening stimulated precipitation of secondary martensite is proposed to form [223].

1.3 Motivation and Research Objectives

The most widely used cryogenic treatment is CCT, because the media can be simply ice and dry ice, which yield low costs and are easy to handle. As the temperatures are getting lower, the more complex systems, machineries and other media have to be used. Despite the tremendous potential and ability of DCT processes to improve the properties of materials, these processes are still not well known and understood, much less applied in practice. In addition, the metallurgical basis behind these processes is partially researched without adequate experimental evidence and therefore poorly described in the literature. As the cryogenic treatment (conventional, shallow and deep) has expanded into different branches and is used for different applications, it was expected to have some uniform guidelines/instructions for heat treatment for specific steel grades and types. Conversely, till now there are no uniform guidelines/instructions and also no clear assortment of suggested conditions, under which DCT positively affects individual steel grades. In this study, a detailed systematic approach with experiments for ferrous alloys (steels) in correlation to deep cryogenic treatment has been procured. For this reason, the dissertation strives to reveal the fundamental microscopic/nanoscopic processes occurring in ferrous alloys during DCT. The main reason for the uncertainty and lack of understanding of DCT lies in the fact that the development of DCT technology was mainly empirical, mostly based on trial and error, without a clear understanding of the scientific basis and mechanisms of microstructural transformations caused by DCT. As such, DCT is used primarily as an attempt to solve existing problems by considering positive experiences without proper scientific basis or in-depth incremental exploration of individual effects. This has in many cases led to misapplication of DCT procedures and thus to inconsistencies, unreliable results or even negative effects that resulted in the negative connotation and dismissal of DCT in industry. To amend this issue, the dissertation explores the applicability of DCT on a variety of steels to provide evidence of DCT applicability and positive effectiveness on the steels' properties.

The aims of the dissertation are:

I. To move from a trial-and-error approach to a scientifically supported and systematic framework of DCT applicability and development, thus gaining in-depth fundamental knowledge of the different mechanisms of DCT in steels and the impact on the targeted properties.

II. Investigation of the influence of DCT on microstructural mechanisms, phase transformations and related microscopic and nanoscopic changes in steels.

III. Investigation of the influence of DCT on mechanical, physical, wear and corrosion properties according to the type and composition of steel.

IV. The aim of the research is also to provide a reliable approach and guidelines for the use of DCT for large-scale potential applications in industry.

The chosen topic of DCT has several major contributions to science. By knowing the influence of DCT parameters on the change of microstructure, depending on the composition and type of material, it is possible to accurately predict the change of properties and thus successfully place the DCT process instead of the heat treatment processes in the final product manufacturing process. As such, DCT has the potential to reduce heat treatment costs as well as processing time with costly high-temperature treatments of steels. With knowledge of microstructural changes at all levels (from macro to nano-level), the use of DCT will no longer be left to trial and error, but to a carefully planned process in order to significantly improve the properties of steels.

To address the previously mentioned aims, the following hypotheses were set:

I. **Hypothesis 1:** *In addition to the parameters of the deep cryogenic treatment process, the efficiency of deep cryogenic treatment and thus the final properties of the material are also influenced by the parameters of the basic heat treatment of steel (higher/lower austenitizing and tempering temperature).*

II. **Hypothesis 2:** *The effect of deep cryogenic treatment is not the same for all types of steels, but depends on the type and chemical composition of steel or main alloying elements, where deep cryogenic treatment affects the mechanical and anti-wear properties, corrosion resistance and fatigue resistance.*

III. **Hypothesis 3:** *Deep cryogenic treatment causes microstructural changes at the macro, micro and nano-level and affects the dynamics of precipitation and growth of phases. At the same time, deep cryogenic treatment enables the achievement of a fine-grained microstructure with a homogeneous distribution of finer carbides with an increased degree of nucleation or precipitation and a reduced tendency for clustering. Furthermore, in the metal matrix, deep cryogenic treatment leads to the elimination of retained austenite and the formation of very fine lattice martensite by non-diffuse martensitic transformation before and during deep cryogenic treatment*.

1.3.1 Materials and methods used in this research

For the research and validation of research hypotheses of this work several steels with different chemical composition were selected, which are presented in the Table 5.

Table 5: Selected steels with chemical composition in weight percentage (wt. %).

AISI M2	C	Mn	S	Cr	Mo	V	W	other	Fe
high-speed steel	0.90	0.28	0.002	4.00	4.70	1.70	6.00		base
AISI M3:2	C	Mn	S	Cr	Mo	V	W	Co	Fe
high-speed steel	1.29	0.31	0.006	3.90	4.80	3.00	5.90	0.69	base
AISI M35	C	Mn	S	Cr	Mo	V	W	Co	Fe
high-speed steel	0.90	0.34	0.004	4.10	5.20	2.01	6.20	4.50	base
AISI H11	C	Mn	S	Cr	Mo	V	Si	Ni	Fe
hot work tool steel	0.38	0.43	0.001	4.90	2.90	0.57	0.30	0.14	base
AISI 431	C	Mn	S	Cr	Mo	Cu	Si	Ni	Fe
stainless steel	0.17	0.83	0.017	15.20	0.11	0.19	0.29	1.50	base
AISI 52100	C	Mn	S	Cr	Si	-	-	-	Fe
bearing steel	0.93	0.41	0.004	1.41	0.30	-	-	-	base
AISI D3	C	Mn	S	Cr	Mo	V	Si	Ni	Fe
cold work tool steel	2.07	0.35	0.002	12.40	0.35	0.16	0.23	0.11	base

For each steel four different heat treatment parameters were used in order to identify the effect of austentizing and tempering temperature on the performance of DCT. All steels were vacuum heat-treated with quenching N_2 gas quenched at 5 bars, except for AISI H11, which was quenched at 1.05 bar. The treatment parameters for each steel are provided in Table 6.

The analyses of selected steels were conducted systematically from various perspectives ranging from chemical, microstructural to mechanical and tribological testing. The list of numerous applied techniques is provided in Table 7. With all the listed techniques, the DCT induced microstructural changes were correlated with the changes in surface, bulk, mechanical and tribological properties.

Table 6: Treatment parameters of selected steels.

Group	Subgroup	Austenitizing		DCT		Tempering (°C)
		Temperature (°C)	Time (min)	Temperature (°C)	Immersion time (h)	
AISI M2	A1	1230	2	-	-	550/550/550/1 h
	A2	1230	2	−196	24	550/1 h
	A3	1180	2	-	-	620/620/620/1 h
	A4	1180	2	−196	24	620/ 1 h
AISI M3:2	B1	1180	2	-	-	540/540/540/2 h
	B2	1180	2	−196	24	540/2 h
	B3	1050	2	-	-	600/600/600/2 h
	B4	1050	2	−196	24	600/2 h
AISI M35	C1	1230	2	-	-	550/550/550/2 h
	C2	1230	2	−196	24	550/2 h
	C3	1160	2	-	-	620/620/620/2 h
	C4	1160	2	−196	24	620/2 h
AISI H11	D1	1080	20	-	-	525/525/525/2 h
	D2	1080	20	−196	24	525/2 h
	D3	1030	20	-	-	600/600/600/2 h
	D4	1030	20	−196	24	600/2 h
AISI 431	E1	1050	30	-	-	480/2 h
	E2	1050	30	−196	24	480/2 h
	E3	980	30	-	-	600/2 h
	E4	980	30	−196	24	600/2 h
AISI 52100	X1	870	30	-	-	150/1 h
	X2	870	30	−196	24	150/1 h
	X3	830	30	-	-	350/1 h
	X4	830	30	−196	24	350/1 h
AISI D3	Y1	980	20	-	-	350/2 h
	Y2	980	20	−196	24	350/2 h
	Y3	950	20	-	-	300/2 h
	Y4	950	20	−196	24	300/2 h

Within this work all the selected steels were investigated in the relation to microstructural changes induced with DCT (Chapter 2–Chapter 5). Special consideration was carried out on the high-speed steels (AISI M2, AISI M3:2 and AISI M35), which were also tested by surface sensitive technique X-ray photoelectron spectroscopy (XPS) (Chapter 4). Furthermore, the selected high-speed steels were also tested for their mechanical and tribological properties as well as fatigue, which were correlated to the microstructural changes instigated by DCT (Chapter 3).

Table 7: List of used techniques for investigation of selected steels.

Technique	Machine	Place
Heat treatment	Horizontal Vacuum Furnace Ipsen VTTC324-R	Institute of Metals and Technology
	Chemical analysis	
X-ray fluorescence (XRF)	Thermo Scientific Niton XL3t GOLDD+	Institute of Metals and Technology
Inductively coupled plasma - optical emission spectrometry (ICP-OES)	Agilent 5800 VDV	Institute of Metals and Technology
Surface chemistry analysis		
X-ray photoelectron spectroscopy (XPS)	Physical Electronics PHI TFA XPS	Jožef Stefan Institute
Phase analysis		
X-ray diffraction (XRD)	PANalytical 3040/60	Institute of Metals and Technology
Microstructural, phase and fractographic analysis		
Light microscope (LM/OM)	Zeiss Axio Imager.Z2m	Institute of Metals and Technology
Scanning electron microscopes (SEM)	Jeol JSM-6500F and ZEISS Crossbeam 550 FIB-SEM Gemini II	Institute of Metals and Technology
Transmission electron microscope (TEM)	JEOL JEM-2100 HR TEM	Institute of Metals and Technology
Energy-dispersive X-ray spectroscopy (EDS)	Detector Oxford EDS INCA Energy 450	Institute of Metals and Technology
Electron backscatter diffraction (EBSD)	Hikari Super plus camera with Apex	Institute of Metals and Technology
Scanning transmission electron microscopy (STEM)	Gatan Orius SC 1000 CCD camera	Institute of Metals and Technology
Mechanical testing and fatigue		
Hardness in HRC	Wilson Instruments B2000 machine, standard SIST EN ISO 6508–1:2016	Institute of Metals and Technology
Fracture toughness	Instron 1255	Institute of Metals and Technology
Impact toughness	Charpy impact test, standard SIST EN ISO 148-1:2017	Institute of Metals and Technology
Compressive strength	Instron 1255, ASTM E9-19	Institute of Metals and Technology
Strain-hardening exponent	Instron 1255, ASTM E9-19	Institute of Metals and Technology
Fatigue	Rumul resonant fatigue testing machine Cracktronic	Institute of Metals and Technology
Tribological testing		
Reciprocating sliding testing	inhouse-assemebled sliding machine	Institute of Metals and Technology
Dynamic impact wear	Instron 8802	Institute of Metals and Technology
Galling	inhouse-assemebled sliding machine	Institute of Metals and Technology

1.4 Significance of This Research

The results of the doctoral thesis have a direct impact on the understanding of DCT of steels, which will enable the effective implementation of DCT in industry and research and faster and more efficient development of new applications. This will certainly help to guide future applied research to industrial needs and increase their scientific and technological level. From a scientific point of view, the results will contribute to the fundamental understanding of the material and metallurgical processes and transformations that occur in steels during DCT. Of course, one of the main challenges here is the extremely wide range of types of steels that can be treated with DCT. Understanding the basics with a scientifically supported explanation will enable the identification of steel types suitable for DCT processing. Newly coordinated research covered by the doctoral dissertation is crucial for the expansion of fundamental knowledge, understanding and development of DCT technologies. The starting point is to increase the level of knowledge, especially in the field of microstructural changes (at the macro, micro and nano-level) that occur during DCT and identify and explain the associated changes in macroscopic properties, including mechanical properties, wear and corrosion resistance, fatigue resistance, etc. In this case, the research will not be limited to one steel, but will be systematically extended to individual groups of steels (high-speed, tool, structural and stainless steels), which will determine the DCT efficiency according to the type and chemical composition of selected steels. Based on the acquired fundamental knowledge and understanding of microstructural changes, further targeted applied research in the field of modeling, correlation research, optimization of DCT processes and their integration into conventional heat treatment processes will be enabled and stimulated.

Originality of results and progress is expected in the following areas:

I. in-depth knowledge of theoretical metallurgical processes of DCT technology for application on steels,

II. determination of the optimal factors for the best usage of DCT with highest impact and positive yield on selected steel properties,

III. modeling and simulation of physical-mechanical properties,

IV. standardization of the DCT procedure according to the type and composition of steel and application,

V. integration of DCT processes into the heat treatment process and providing the possible extension of DCT applicability to the entire field of metallic materials research.

From a technological point of view, it is important that DCT gains industrial relevance, which will increase its implementation in practice. The empirical strategies used so far do not help in any way. By raising the technological understanding of DCT processing and identifying suitable materials, the industry will also be ready to use this new technology. The results of the research will contribute to a better understanding and in-depth insight into the DCT technology, which will enable the maximum use of the effects of DCT in order to improve the properties of the material and thus their industrial implementation.

Chapter 2

Influence of Deep Cryogenic Treatment on Microstructure

This chapter tends to provide some basic introduction into DCT. Simultaneously, it discusses and explains the microstructural changes induced by DCT in selected high-speed steels (HSS), which are widely used in tool industry (cutting tools etc.). To observe the influence of chemical composition of steel and type of steel (wrought/PM) on DCT performance, the same group of tool steels – HSS (AISI M2, AISI M3:2 and AISI M35) was investigated with different variation of alloying elements. In this study, a detailed analysis of carbide precipitation and formation was made with X-ray diffraction (XRD), scanning electron microscopy (SEM), energy-dispersive X-ray spectroscopy (EDS), fractography, electron backscatter diffraction (EBSD) and transmission electron microscopy (TEM). The emphasis of the evaluation of DCT effect on the microstructure and furthermore on carbide precipitation is evaluated based on carbide distribution, morphology, density, volumetric fraction, size and chemical composition of carbides.

Brief discussion: The concentration of alloying elements in HSS shapes the final microstructure and its evolution during selected heat treatment. In addition to chemical composition, selected heat treatment (CHT (conventional heat treatment)/DCT) also has a major influence on the microstructure (carbide precipitation, transformation of phases etc.). DCT influences the steels' matrix by significantly refining the martensitic laths compared to CHT and also the amount of retained austenite is reduced to values under 1 vol. %, whereas for CHT, the fraction is above 1 vol. %. In correlation to carbide precipitation, DCT has the following effects: less frequent occurrence of carbide clusters, more homogeneous distribution of carbides, up to 30 % increased carbide precipitation, more spherical form of carbides and stronger carbide to matrix cohesion (fractography analysis showed that the detached carbides in DCT samples leave stronger deformed zones) compared to carbides within CHT samples. All of these effects can be explained by stress-state modification, more homogenous distribution of alloying elements and increased nucleation of carbides. Furthermore, different chemical composition (the content of cobalt) showed that DCT in cobalt-free and cobalt-low HSS induced denser formation of $M_{23}C_6$ carbides and cuboidal shaped carbides compared to cobalt-bearing HSS. Moreover, DCT also affected the precipitated carbide preferential type, where lower presence of MC and M_6C and higher presence (up to 3–5 %) of $M_{23}C_6$ is observed compared to CHT counterparts. In addition, in this article/chapter, the impact of preexisting M_2C is also evaluated in correlation to the volumetric fraction of $M_{23}C_6$ carbides. The research reveals that the chemical composition of the residual M_2C is modified based on $M_{23}C_6$ precipitation and modified carbide nucleation through DCT, leading to different decomposition behavior with DCT. This provides a unique view and explanation for different microstructure and properties development of HSS with DCT.

The ***author's contribution,*** as the first author, to the paper ***Effectiveness of deep cryogenic treatment on carbide precipitation***, published in the Journal of Materials Research and Technology, was: conceptualization, planning of experiments, visualization, modelling, evaluation and writing (original draft and editing).

Chapter 2 addresses thesis ***Hypotheses 2 and 3***.

J MATER RES TECHNOL. 2020;9(6):13014–13026

Available online at www.sciencedirect.com

jmr&t Journal of Materials Research and Technology

https://www.journals.elsevier.com/journal-of-materials-research-and-technology

Original Article

Effectiveness of deep cryogenic treatment on carbide precipitation

Patricia Jovičević-Klug[a,b,*], *Matic Jovičević-Klug*[a], *Bojan Podgornik*[a,b]

[a] *Department of Metallic Materials and Technology, Institute of Metals and Technology, Lepi pot 11, 1000 Ljubljana, Slovenia*
[b] *Jožef Stefan International Postgraduate School, Jamova cesta 39, 1000 Ljubljana, Slovenia*

ARTICLE INFO

Article history:
Received 25 August 2020
Accepted 12 September 2020
Available online 25 September 2020

Keywords:
Deep cryogenic treatment
High-speed steels
Microstructure
Carbides
Thermodynamic modelling

ABSTRACT

The study discusses the effectiveness of deep cryogenic treatment (DCT) on selected steels and its effectiveness on carbide precipitation. The investigation of DCT influence on the precipitation of different carbide types in three selected high-speed steels (M2, M3:2 and M35) has been carried out by a combination of x-ray diffraction (XRD), scanning electron microscopy (SEM), fractography, energy-dispersive X-ray spectroscopy (EBSD) and transmission electron microscopy (TEM). Three different steels with different chemical composition were selected in order to observe and correlate DCT induced carbide precipitation phenomena with varying concentration of alloying elements (Co, Cr, Mo, V and W). The study discloses the DCT effect on carbide distribution, morphology, size, and the mechanism of their formation. Using thermodynamic modeling the precipitation and origin of specific carbides is discussed and confirmed. This research proves that DCT has an impact on precipitation of carbides by increasing their volumetric fraction (overall up to 23%, up to 140% for $M_{23}C_6$), density (up to 30% for MC and M_6C carbides), reducing their mean size and inducing a more homogeneous distribution of them. Low-cobalt-bearing steels exposed to DCT display an increased volume fraction of $M_{23}C_6$ carbides that presumably originate from the precipitation of additional embryos formed during DCT. However, selected steel with high Co content showed no significant changes in the volumetric fraction of carbides after DCT. The impact of preexisting M_2C carbides and their decomposition on the final carbide formation is also discussed.

1. Introduction

Deep cryogenic treatment (DCT) is a heat treatment, which is normally performed after quenching and before tempering [1–4]. It is applied, when the steel properties, such as hardness, toughness and wear resistance, are desired to be enhanced by exposing the material to temperatures below −196 °C. Based on preexisting literature reviews on DCT [1–6], high-speed steels (HSS) are indicated as the second most common group of steels for which DCT is used to achieve improved properties. HSS are desired in steel industry for production of cutting tools, punches and dies, due to their unique combination of

* Corresponding author at: Institute of Metals and Technology, Lepi pot 11, 1000 Ljubljana Slovenia.
E-mail: patricia.jovicevicklug@imt.si (P. Jovičević-Klug).
https://doi.org/10.1016/j.jmrt.2020.09.063

properties with uniform and high hardness from center to surface, resulting from the high-alloy content (Co, Cr, Mo, V and W) [7]. Selected alloying elements Cr, Mo, V and W can also induce precipitation of carbides [8], which allows further manipulation of steel properties for various applications. In HSS, mainly MC, M_2C, M_3C, M_7C_3, M_6C and $M_{23}C_6$ types of carbides form [7,9]. Co is mainly dissolved in the matrix and has a low probability to form carbides due to the high positive free energy [9,10]. Nevertheless, a low Co amount in the steel can induce formation of fine and complex carbides enriched with Fe and with moderate amount of other alloying elements such as Cr, Co, V [11].

For DCT the main purpose is to reduce retained austenite and convert it into daughter phase martensite, which causes increase in hardness and removes residual stresses, which has been reported to improve wear resistance [1,12]. However, additional mechanisms have been reported to occur, when HSS are exposed to DCT: carbon redistribution and site reduction [2], reduction of free energy of crystal structure [13], increase of precipitation of fine submicroscopic carbides (secondary and tertiary) [14–21].

The efficiency of DCT on precipitation, (re)distribution and homogeneity of the microstructure, as well as on the resulting material properties, has been in the past evaluated via Taguchi method. The evaluation revealed that the DCT parametrization can be narrowed down to 4 main influencing factors; selected deep cryogenic temperature, holding time (soaking period), cooling and warming rate and sequence of DCT [1,22–24]. Longer DCT soaking period leads to a more homogeneous carbon distribution, which induces an overall increase in lattice distortion [25]. By exposing the steel to cryogenic temperatures, the martensite matrix progresses into a supersaturated state (with all alloying elements). Consequently, the lattice distortion of the martensite matrix leads to segregation of alloying elements and carbon to nearby defects. These locations then act as centers for forming clusters that later develop into carbide nuclei during tempering [26]. When the steel undergoes tempering, the martensite matrix rejects carbon and alloying elements in the form of finely divided carbide phases, causing (re)distribution of fine carbides and consequentially increased structural stability [27].

Several theories have been proposed to explain the increase of carbide precipitation with DCT. (1) First theory and the oldest one states, that improved carbide formation is a product of low temperatures and volumetric contraction of phases (retained austenite to martensite change). The contraction of different phases (different contraction coefficients) causes carbon atoms to move into neighboring dislocations, which after DCT and during tempering act as inhibitor sites for carbide precipitation [21,28]. (2) Second theory discusses the possibility that the high degree of contraction of both phases (austenite and martensite) causes dislocations in the structure to move and agglomerate due to local plastic deformation. The dislocations attract carbon atoms to these areas during tempering which leads to increased carbide precipitation. For this case, the carbon content plays an important role as higher carbon content causes more carbon atoms to mobilize to the dislocations leading to an increased amount of sufficiently large nuclei for subsequent carbide growth [29]. (3) Third theory proposes the precipitation of fine η-carbides. The precipitation mechanism of η-carbides is a result of contraction and expansion of the martensitic lattice in different directions, when it is in a so-called "low-temperature condition". As a result, the carbon atoms are slightly shifted which leads to segregation of η-carbides along the carbon-rich bands during stress relieving and/or tempering [30,31]. (4) The fourth theory is based more on the function of the carbides and their placement in the matrix. During tempering the carbides fill preexisting microvoids in the matrix leading to an increase in carbide density and coherence of the steel structure [32].

This study focuses on the effectiveness of DCT on the carbide precipitation in three HSS M2, M3:2 and M35 with regards to the distribution, type and possible mechanism of carbide formation in the selected steels. To explain possible phenomena behind carbide formation in selected HSS, microstructural changes are studied by scanning electron microscopy (SEM), energy-dispersive X-ray spectroscopy (EDS), SEM-feature, electron backscatter diffraction (EBSD), fractography and X-ray diffraction (XRD). To provide more theoretical insight in the development of carbides with DCT, additional thermodynamic modeling is employed in this research.

2. Experiments

Rolled and peeled bars of selected steels AISI M2 (EN 1.3343), M3:2 (EN 1.3395) and M35 (EN 1.3243) in soft annealed form are used for the experimental tests. The standard value range from the EN standards and actual chemical composition of selected steels are provided in Table 1.

Samples for fractography, XRD and SEM were cut out from bigger samples after the designated heat treatments (Table 2) into pieces with 10 mm diameter and 5 mm height. All the samples were austenitized and quenched in a single step in a horizontal vacuum furnace Ipsen VTTC324-R. The quenching is performed with N_2 gas at pressure of 5 bars. After this process, the samples of all three steels (A, B, C), were divided into two groups where one group is conventionally vacuum heat-treated (CHT) with a three-step tempering sequence. The parameters of the CHT were chosen according to the suppliers' recommendations for the heat treatment for each steel grade aimed at obtaining good combination of toughness at working hardness from 58 HRC to 60 HRC. The second group of samples is exposed to DCT, performed in a controlled environment with gradual immersion in liquid nitrogen for 24 h (cooling rate of about 10 °C/min), followed by single-step tempering in the vacuum furnace. The exact parameters of each heat treatment are provided in Table 2.

Microstructural characterization was done by SEM and XRD analysis. SEM analysis was performed on JSM-6500 F, Jeol, Tokyo, Japan, where secondary electron detector (SEI), back-scattered (BSE) detector and energy dispersive X-Ray spectroscopy (EDS) were employed for imaging and chemical composition determination. The feature analysis was conducted with program INCA, Oxford Instruments plc, Abingdon, UK. Samples were analyzed in a polished, fatigue fractured state and in an etched state (etching by Nital and Villellaś reagent for a few second, depending on each sample [33]).

Table 1 – Chemical composition of the selected steels in mass contents (%). Nominal values based on EN standards. Analyzed values measured with ICP-OES Agilent 720.

Steel	C	Mn	S	Cr	Mo	W	V	Co
AISI M2 (EN 1.3343) – A group								
standard	0.80 – 0.90	<=0.40	<=0.030	3.80 – 4.50	4.70 – 5.20	6.00 – 6.70	1.70 – 2.00	–
analyzed	0.90	0.28	0.002	4.00	4.70	6.00	1.70	–
AISI M3:2 (EN 1.3395) – B group								
standard	1.15 – 1.25	0.15 – 0.40	<=0.030	3.75 – 4.50	4.75 – 6.50	5.00 – 6.75	2.75 – 3.75	–
analyzed	1.29	0.31	0.006	3.90	4.80	5.90	3.00	0.69
AISI M35 (EN 1.3243) – C group								
standard	0.87 – 0.95	<=0.40	<=0.030	3.80 – 4.50	4.70 – 5.20	5.90 – 6.70	1.70 – 2.10	4.50 – 5.00
analyzed	0.90	0.34	0.004	4.10	5.20	6.20	2.00	4.50

Table 2 – Vacuum heat treatments: conventional heat treatment (CHT) and deep cryogenic treatment (DCT).

Group	Subgroup	Austenitizing		DCT		Tempering (°C/h)
		Temperature (°C)	Time (min)	Temperature (°C)	Immersion time (h)	
A	A-CHT	1180	2			3 × 620/1 h
	A-DCT	1180	2	–196	24	620/1 h
B	B-CHT	1050	6			3 × 600/2 h
	B-DCT	1050	6	–196	24	600/2 h
C	C-CHT	1160	2			3 × 620/2 h
	C-DCT	1160	2	–196	24	620/2 h

XRD analysis was carried out on PANalytical 3040/60, Almelo, Netherlands.

3. Results and discussion

3.1. *Microstructure*

The concentration of alloying elements in HSS defines the microstructure and its evolution during heat treatment (CHT and DCT) which in turn determines the mechanical and tribological properties. For this reason, a detailed microstructural analysis of samples was carried out. Each steel is divided into two groups; CHT and DCT samples. It is observed that in both cases of heat treatment (CHT and DCT) for all investigated steels the matrix is composed of lath type martensite (Fig. 1 e, k, Fig. 2 e, k and Fig. 3 e, k, l). A large amount of carbides is present in the microstructure of all steel samples, which is expected for HSS. The coarser carbides are situated along lath boundaries and on primary austenite grain boundaries, whereas fine carbides are also dispersed within the martensitic laths [34]. The grain boundaries are also enriched with carbides in form of colonies (Fig. 1 k and Fig. 3 k). The first significant change for all steels is that the microstructure of DCT samples (g, h, k of Fig. 1, Fig. 2 and Fig. 3) shows finer martensite structure compared to CHT samples (a, b, e of Fig. 1, Fig. 2 and Fig. 3). The smaller size of the martensite laths is promoted by plastic deformation, that results from austenite to martensite transformation at low temperatures [35,36]. The DCT samples also show a significantly smaller occurrence of carbide clustering compared to CHT samples, best seen by comparing Fig. 1 a to Fig. 1 g (clusters are marked with dashed circle). Steel B does not show such changes in clustering as this steel predominantly forms less clusters due to lower austenitization temperature and higher carbon content as well as due to the powder metallurgy production technique. The third observed difference is the more homogenous microstructure of the DCT samples compared to their CHT counterparts. This is also visible from the carbide distribution (relative frequency), which is presented more in next section.

From the analysis of fractured samples, a difference is visible in the fracturing of the material between CHT and DCT samples. The DCT samples show on average a larger amount of dimple and void formations compared to the CHT samples (the biggest impact visible for steel B in Fig. 2 c and i). Furthermore, the detached carbides leave a more deformed matrix zone for the DCT samples (compare Fig. 2 d and j). These changes can be induced by stress-state modification [37] and more homogeneous distribution of alloying elements [25] in the material induced by DCT. The homogenized structure additionally leads to a stronger cohesion of the carbide grain boundary to the matrix, as the depleted zone around the carbide is narrower and yields a smaller concentration gradient. As a result, the depleted zone around the carbide is etched stronger than the matrix and carbides (visible from the etched samples Fig. 1 f and l). Furthermore, the grain boundary between two coalescing carbides of the same type is also altered by the DCT due to the homogenized structure and distribution of alloying elements (grain boundary marked by dashed arrows in Fig. 1 f and l).

From the microstructural evaluation, the growth mechanism of secondary carbides can be also described. The clusters observed in CHT and DCT samples show the presence of two types of carbides, bright and dark carbides that correspond to heavier and lighter chemical composition respectively. It is visible that heterogeneous nucleation and growth is present for both carbides (Fig. 1 e and Fig. 3 e, l). The highly coherent grain boundaries (marked with solid arrow in Fig. 1 f) display the possibility of the lighter carbides nucleating subsequent to the heavier carbides. Such carbide formation has already

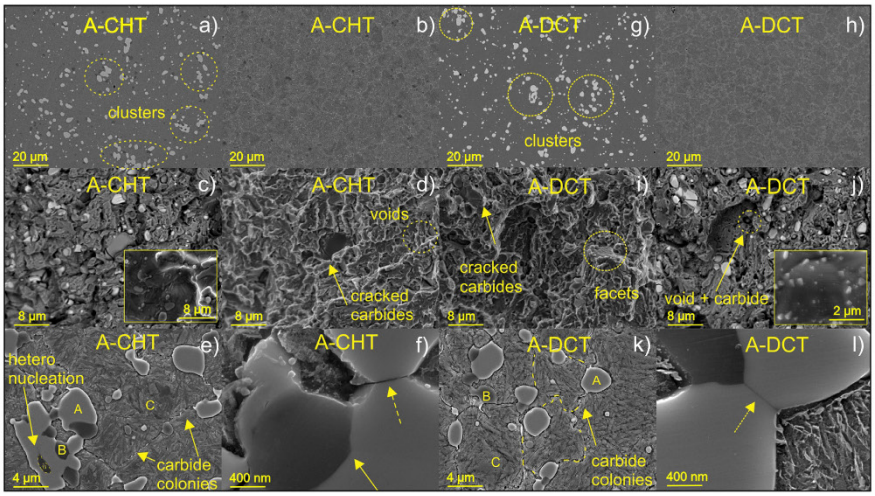

Fig. 1 – SEM micrographs of steel A (M2), treated by conventional heat treatment (CHT) and deep cryogenic treatment (DCT). Images a, c, g and i are acquired with back-scattered electron emission imaging mode. The rest of the images is acquired with secondary electrons emission imaging mode.

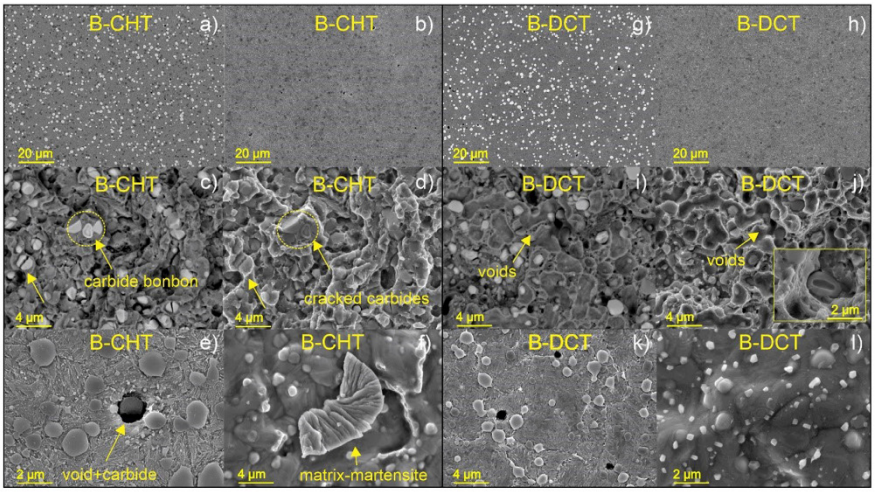

Fig. 2 – SEM Micrographs of steel B (M3:2), treated by conventional heat treatment (CHT) and deep cryogenic treatment (DCT). Images a, c, g and i are acquired with back-scattered electron emission imaging mode. The rest of the images is acquired with secondary electrons emission imaging mode.

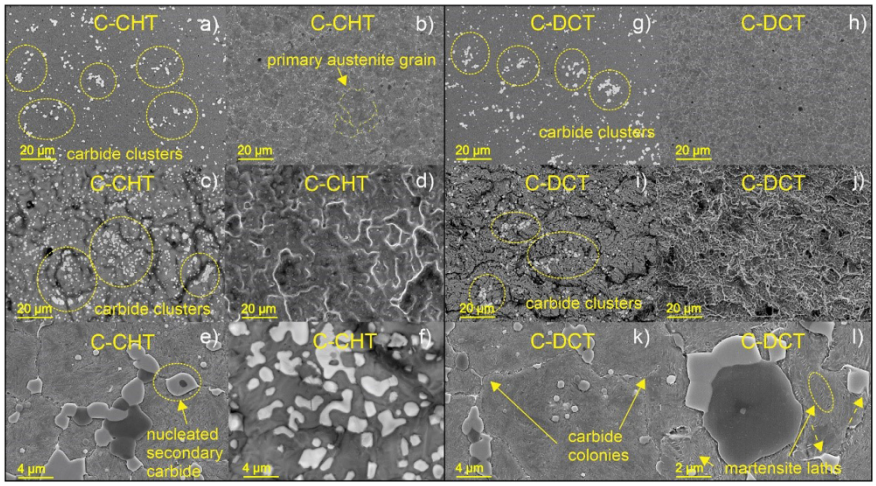

Fig. 3 – SEM Micrographs of steel C (M35), treated by conventional heat treatment (CHT) and deep cryogenic treatment (DCT). Images a, c, f, g and i are acquired with back-scattered electron emission imaging mode. The rest of the images is acquired with secondary electrons emission imaging mode.

been reported in the past for similar HSS [38]. The behavior also correlates with the formation of stable carbides from prior existing carbides with different carbon content [39]. The clusters correlate with their shape and carbide distribution to the decomposition of M_2C carbides into M_6C and MC carbides, which has been reported by previous research [40,41]. Further analysis of fractured samples allowed additional confirmation of secondary growth on preexisting carbides of similar chemical composition that were either not dissolved during austenitization or they correspond to intermediate metastable carbide formation. The incomplete decomposition and secondary growth results in a carbide formation that we have dubbed as "bonbon" carbide, which can be seen in the insert of Fig. 2 j.

Another crucial microstructural difference between CHT and DCT steels is the formation of tertiary carbides that evenly precipitate for all three steel grades. In the case of Co-free and low-Co HSS (steels A and B), DCT induces a denser formation of tertiary precipitates (see inserts in Fig. 1 d and j and Fig. 2 f and l). Furthermore, DCT samples have more faceted (cuboidal) elongated carbides than their CHT counterparts. On the other hand, higher Co-bearing HSS (steel C) shows no differences in the tertiary carbide formation between CHT and DCT samples. It is excluded, that the different density of tertiary carbides is a result of Ostwald ripening, as tertiary carbides of similar morphology and size are present in the steels for both treatments. The lack of faceted carbides in C steel is a very important aspect that will be further discussed in the modeling section 3.4.

3.2. *Carbide distribution and size*

Carbide distribution is best presented with relative frequency (the number of carbides per area) and area fraction (percentage of steel area represented by carbides) in correlation with the carbide size threshold. The carbide size is expressed as carbide equivalent diameter (ECD) [42] and was measured by SEM feature at area $400 \times 400\,\mu m$. The analysis for each steel type and heat treatment was conducted only on one sample area, since the homogeneity of the material was determined to be statistically relevant with the selected measurement area. The total number of carbides measured in A-CHT is 5823 and in A-DCT it is 7810 (Fig. 4). The carbides in A-CHT steel are in majority below $1\,\mu m$ size, but the most contributing carbides to the area fraction are between $1\,\mu m$ and $2\,\mu m$. The average nearest neighbor mean distance between carbides smaller than $1\,\mu m$ is measured to be $4.5\,\mu m$. While the mean distance for carbides larger than $1\,\mu m$ is $19.4\,\mu m$. A-DCT showed that the average size of carbides is under $1\,\mu m$ and mean area fraction of them is at around $2.2\,\mu m$. The mean distance between carbides smaller than $1\,\mu m$ is $8.4\,\mu m$ and for carbides larger than $1\,\mu m$ it is $32.4\,\mu m$.

In the case steel B only minor differences in carbides relative frequency and area fraction have been observed between CHT and DCT samples. The total number of carbides measured in B-CHT is 10979 and in B-DCT it is 11502 (Fig. 5). The carbides in B-CHT have mean relative frequency under $1\,\mu m$ size, but their mean area fraction is at around $1.5\,\mu m$ size. The nearest

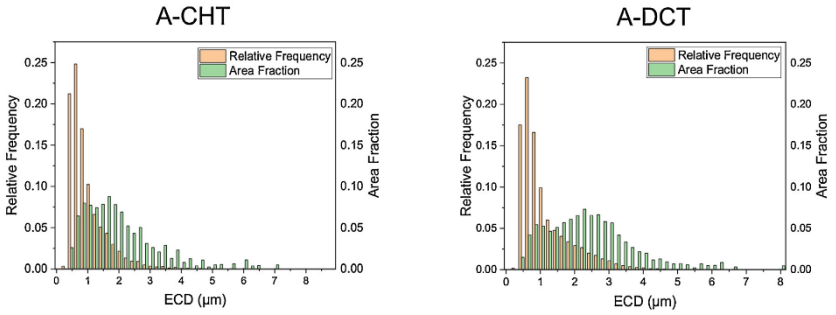

Fig. 4 – Carbide relative frequency and area fraction regarding ECD for conventionally (A-CHT) and deep cryogenic treated (A-DCT) steel A.

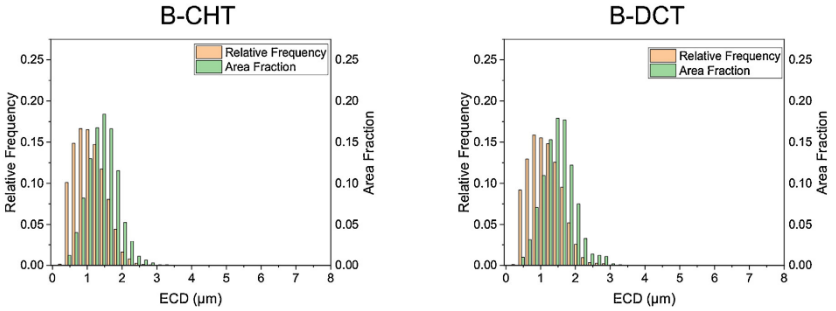

Fig. 5 – Carbide relative frequency and area fraction regarding ECD for conventionally (B-CHT) and deep cryogenic treated (B-DCT) steel B.

neighbor mean distance between carbides smaller than 1 μm for B-CHT is 6.9 μm and 8.9 μm for B-DCT. While the mean distance of carbides larger than 1 μm is 25.6 μm for B-CHT and 22.5 μm for B-DCT.

In C steel the total number of carbides in C-CHT is 6936 and 8323 in C-DCT (Fig. 6). The carbides in C-CHT and C-DCT samples have an average relative frequency under 1 μm (approximately 0.5 μm), whereas mean area fraction for both samples is at around 2 μm (1.75–1.80 μm). The nearest neighbor mean distance between carbides smaller than 1 μm for C-CHT is 5.1 μm and 5.4 μm for C-DCT. While the mean distance for carbides greater than 1 μm is 30.3 μm for C-CHT and 33.4 μm for C-DCT.

From the feature analysis four major observations can be given: DCT samples have an increased number of carbides of up to 30 % of the number of carbides determined for their CHT counterparts. The average nearest-neighbor carbide distance is generally larger for DCT samples (exception is steel B for which carbides larger than 1 μm have a shorter nearest-neighbor distance). No significant difference in the relative frequency is visible between DCT and CHT samples. On the other hand, when steel A is exposed to DCT, the region of most contributing carbides in terms of the area fraction is shifted towards larger carbide size and broadened. In the case of steel B a shift towards larger carbides is observed. For DCT steel C the region of most contributing carbides portrays only marginal differences compared to its CHT counterpart. Finally, the DCT samples of all steels have in general more spherically shaped larger carbides than CHT, which are more aspherical (data not shown).

3.3. *XRD and SEM-EDS*

The different types of steels were also investigated with XRD to determine the carbide types and influence of the heat treatment on their volumetric fraction within the selected steels. From the XRD data in Fig. 7, the typically expected carbides of MC-type and M_6C-type were determined for all steel samples, regardless of the heat treatment strategy used (CHT and DCT). The MC-type corresponds to a VC structure whereas the M_6C-type corresponds to a $Fe_3(Mo, W)_3C$ structure. Next to the M_6C peaks, smaller amplitude peaks are found, that are positioned 0.3° to 0.8° higher. These peaks are a possible contribution from the residual M_2C carbides that were not dissolved during austenitization (insufficient time to dissolve and/or decompose). The regions with these low-amplitude

13020 J MATER RES TECHNOL. 2020;9(6):13014–13026

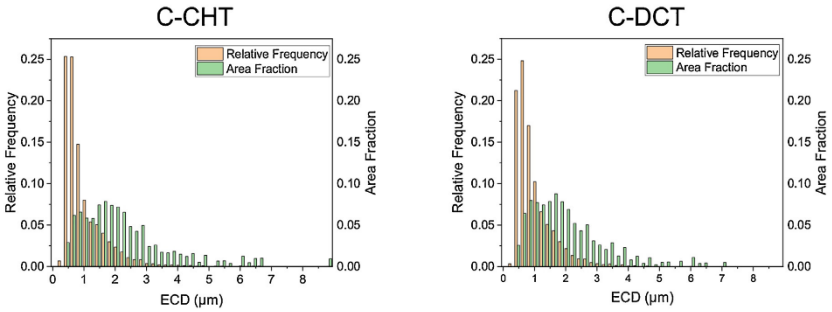

Fig. 6 – Carbide relative frequency and area fraction regarding ECD for conventionally (C-CHT) and deep cryogenic treated (C-DCT) steel C.

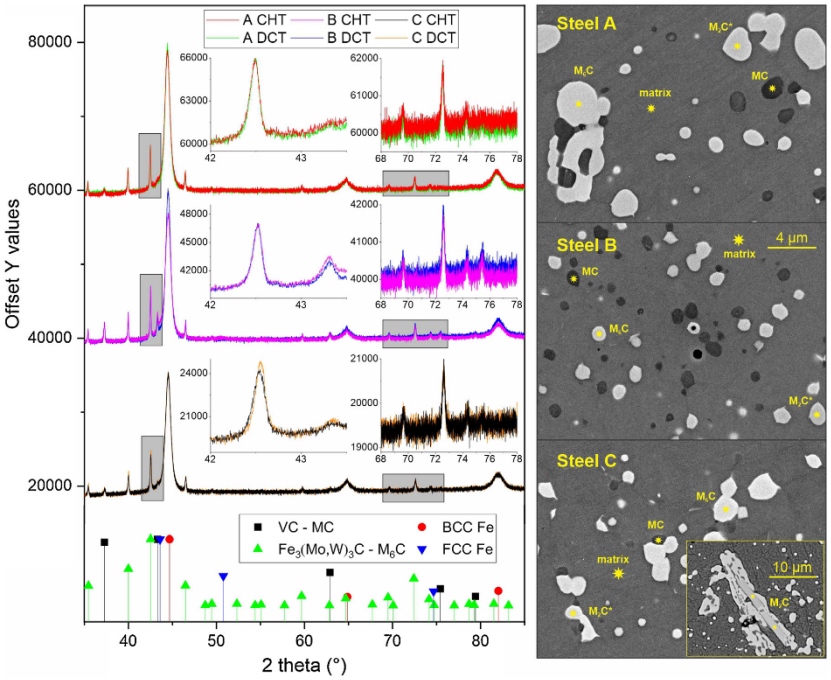

Fig. 7 – XRD spectrums for all analyzed steels treated with CHT and DCT. The inserts present the regions where additional low-amplitude peaks are present that are potentially related to residuals of M_2C carbides. On the right-hand side, SEM micrographs are given for each steel type indicating exemplar positions of EDS analysis for the different carbide types and matrix.

peaks are presented in the enlargements of the XRD data on the left-hand side of Fig. 7. The possible carbides contributing to these peaks are probably the inner parts of the "bonbon" carbide formations observed during microstructural analysis (see section 3.1). SEM-EDS analysis confirms the presence of both M_6C and M_2C carbides that are distinguishable by their carbon content. In steel B, also inclusions enriched with Fe, Si and O are present next to the carbides.

Table 3 – Average chemical composition of microstructural features determined for steel A, B and C in both heat-treated conditions. The variations next to the values are the average deviations and they do not represent the uncertainty of the measured values. The MC-type carbide is vanadium enriched VC carbide. The M_6C-type carbide is $Fe_3(Mo,W)_3C$ carbide. The M_2C^* is an iron-enriched variant of the M_2C carbide which is a $Mo_1(W,V)_1C$.

Steel A							
Composition (wt. %)	C	W	Mo	Cr	V	Co	Fe
matrix	0.45 ± 0.3	4.42 ± 0.5	3.91 ± 0.4	4.73 ± 0.2	1.13 ± 0.3	0	85.65 ± 1.3
MC	13.09 ± 0.8	18.28 ± 0.3	19.85 ± 0.5	4.07 ± 0.4	38.55 ± 0.7	0	6.16 ± 0.8
M_6C	2.81 ± 0.7	36.05 ± 0.6	24.78 ± 0.8	3.17 ± 0.1	2.97 ± 0.2	0	30.21 ± 0.4
M_2C^*	9.17 ± 0.5	35.16 ± 0.5	21.86 ± 1.0	3.04 ± 0.2	2.60 ± 0.1	0	28.16 ± 0.3
steel B							
matrix	0.54 ± 0.3	2.64 ± 0.4	2.94 ± 0.0	4.26 ± 0.3	1.12 ± 0.3	2.13 ± 0.9	86.67 ± 1.2
MC	11.76 ± 0.3	16.83 ± 0.9	14.99 ± 0.6	4.59 ± 0.2	36.93 ± 0.8	4.08 ± 0.7	10.81 ± 0.8
M_6C	2.71 ± 0.4	35.15 ± 0.6	24.57 ± 0.5	3.12 ± 0.1	2.41 ± 0.2	3.22 ± 0.1	28.80 ± 1.5
M_2C^*	8.25 ± 0.9	34.87 ± 0.6	23.76 ± 0.4	2.47 ± 0.0	2.57 ± 0.1	0	28.08 ± 0.8
steel C							
matrix	0.38 ± 0.3	4.45 ± 0.3	3.93 ± 0.7	4.65 ± 0.0	1.45 ± 0.2	5.48 ± 0.2	79.95 ± 1.0
MC	13.25 ± 2.9	17.11 ± 1.3	16.57 ± 0.5	4.66 ± 0.5	36.17 ± 0.4	5.09 ± 0.0	7.15 ± 2.3
M_6C	3.51 ± 0.4	33.44 ± 0.1	25.99 ± 0.9	3.09 ± 0.2	3.30 ± 0.3	2.45 ± 0.1	28.22 ± 0.0
M_2C^*	10.02 ± 0.3	31.29 ± 0.1	24.45 ± 0.3	2.93 ± 0.2	2.61 ± 0.2	1.96 ± 0.3	26.73 ± 0.3
M_2C	9.05 ± 0.4	31.24 ± 0.2	35.28 ± 0.2	7.44 ± 0.2	11.05 ± 0.3	0.43 ± 0.0	5.51 ± 0.1

matrix-tetragonal martensite; MC–face centered cubic (FCC); M6C–face centered cubic (FCC); M2C, M2C* – hexagonal closed packed (HCP).

The composition of the different carbide types is determined using EDS analysis (results given in Table 3 and exemplar microstructure images with positions of acquired EDS spectra are presented on the right-hand side of Fig. 7). To ensure proper characterization of carbon content in the system, the weight fraction of carbon is normalized by using the average measured carbon content of the VC carbides corrected to the expected carbon values in VC for the different steel grades (determined with thermodynamic calculations).

The chemical compositions of carbides are similar for CHT and DCT samples (Table 3). The MC carbides were confirmed to be VC carbides with enrichment of Mo and W (both in the range of 15–19 wt. %). For the M_6C carbides, the main alloying composition is $Fe_{2.65-2.75}Mo_{1.3-1.5}W_1$ for all steels. For steel B and C the M_6C carbides have an additional Co content of 0.3 atm. % and 0.2 atm. % respectively. Some of the carbides that morphologically coincide with the M_6C carbides (and are not part of the clusters) show a similar alloying composition, but with a larger carbon content. The carbon content coincides with coherently formed M_2C carbide as modeled by Grujicic, 1989 [43]. However, the rest of the alloying composition, especially the high iron content, does not match the typical M_2C carbide composition [40].

To confirm the presence of the characteristic M_2C carbides, rigorous microstructural observation with several samples and etching steps was conducted. A handful of plate-type M_2C carbides were found in steel C which have an alloying composition similar to reported values from previous researchers [40,43]. From the measurements, we conclude that there is indeed a presence of semi-decomposed M_2C carbides with carbon content typical for M_2C carbide and a chemical composition of other alloying elements similar to M_6C carbides. To distinguish these carbides from other carbides, they are addressed as M_2C^*.

From the SEM observations, the occurrence of the M_2C^* carbides seems to be less often in DCT samples compared to their CHT counterparts, however a clear statistical confirmation of this relation is not possible, due to the low amount of M_2C^* in the steel samples.

Table 4 – Mean volumetric fractions of carbides and matrix for differently treated steels quantified from XRD and SEM data. XRD evaluation was performed with a combination of the Toraya method [46] and Rietveld refinement [47].

Steel	MC	M_6C	$M_{23}C_6$	Matrix
A-CHT	2	6.9	2.2	88.9
A-DCT	1.5	6.7	5.3	86.3
B-CHT	6.6	7.6	4.3	81.5
B-DCT	5.9	7.2	7.7	79.2
C-CHT	3	7.3	5.1	84.6
C-DCT	3.1	7.6	4.9	84.4

The $M_{23}C_6$ carbides could not be determined with XRD and SEM-EDS, as the XRD peak signals of these crystallites overlap with the α-Iron, γ-iron and M_6C peaks and the carbides are too small for reliable EDS analysis. To identify and confirm their presence, TEM investigation was employed to quantify the structural and chemical composition of the supposed $M_{23}C_6$ carbides.

The TEM results disclose that these carbides belong to the space group Fm $\bar{3}$ m (FCC structure) and that their chemical composition is on average $Fe_{22}Cr_1C_6$ (steel A) and $Fe_{21}Co_1Cr_1C_6$ (steel B and C). The average D-spacing between the {220} planes is 0.371 ± 0.016 nm and lattice parameter of the carbide is 1.049 ± 0.045 nm which correspond well with literature values [44,45]. The carbides nucleate preferentially on the martensitic lath boundaries and demonstrate nanocluster growth in carbon enriched areas (see Fig. 8) for all steel samples (CHT and DCT).

From EDS, SEM and XRD data, the volumetric fraction of all carbides is quantitatively determined and presented in Table 4. The largest difference in carbide formation between

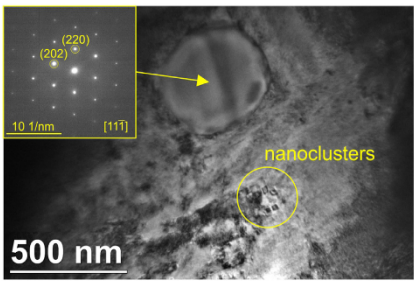

Fig. 8 – TEM image of $M_{23}C_6$ carbides with complementary selected area electron diffraction (SAED) pattern.

CHT and DCT samples is for steels A and B. For DCT samples, the MC and M_6C have a 0.3–0.7 vol. % and 0.2–0.4 vol. % lower presence respectively. The reduced presence of both carbides is considered to be a result of the shorter tempering time that is used for the DCT (1 tempering cycle) compared to CHT (3 tempering cycles). The higher amount of MC carbides for steel B compared to the other two steels is a result of the higher carbon and vanadium content as well as due to the small presence of cobalt that promotes VC carbide nucleation [10]. The volumetric fraction of M_2C and M_2C^* carbides is considered to be under 1 % for all steel samples (CHT and DCT), however due to their low volumetric presence and chemical similarity with M_6C carbides the exact values were not possible to determine.

Using SEM images at high magnification an estimate of the fraction of $M_{23}C_6$ carbides is determined. The DCT steels A and B showed a significantly higher fraction of $M_{23}C_6$ carbides compared to their CHT counterparts (about 3 % more). Steel B shows a larger amount of $M_{23}C_6$ carbides resulting from higher carbon content and presence of Co that promotes carbide precipitation [10,48]. On the other hand, C-DCT has similar $M_{23}C_6$ carbide quantity as C-CHT. For steel C-DCT there is a tendency of larger volume fraction of M_6C and MC carbides, however the difference to CHT counterpart is minor compared to the other two steels. The carbide volume fractions show, that the main difference and advantage of DCT to CHT is the promotion of tertiary carbide formation. Together with statistical and morphological analysis in section 3.2 it is also shown that despite similar volumetric content of MC and M_6C carbides, DCT steels contain larger number of carbides with smaller average size and more homogeneous distribution.

3.4. *Thermodynamic modeling*

In order to understand the ratio and formation of the carbide types for the selected steels and heat treatments, thermodynamic modeling was performed for all selected HSS with Thermo-Calc Software using TCFE8 database and JMatPro. The thermodynamic modeling (Fig. 10) suggests that the large plate-like M_2C carbides originate from the preexisting microstructure of the as-supplied steel, as these carbides should be considerably smaller in size (under 2 μm), if originating from precipitation effects (data not shown). However, the

Table 5 – Calculated volume fraction of carbides after austenitization by assumed ideal homogeneous condition of the as-received steel.

Steel	Volume fraction after austenitization	
	MC	M_6C
A	1.11	6.7
B	6.55	7.99
C	2.53	7.22

smaller carbides, that partially decompose into M_2C^*, are most probably a result of the heating to the austenitization temperature (growth of preexisting M_2C precipitates) and short holding time that halted the decomposition into M_6C and MC carbides [39]. It is proposed that during tempering, these carbides are infused with elements from the matrix (mainly iron). As a result, the carbide partially decomposes by which a shell of M_6C is formed around it, due to carbon rejection from the surface of the M_2C^* carbide (leading to the "bonbon" formation seen in section 3.1). The complete and partial decomposition are schematically presented in Fig. 9.

The previously discussed decomposition mechanics are important for the final properties of the steel as the M_2C carbides are the main intermediate carbides responsible for the precipitation and evolution of the fine $M_{23}C_6$ carbides (can be seen from the simulated data in Fig. 10 d–f). The simulations also indicate that the volumetric amount of M_6C and MC carbides mainly originate from the state achieved at the austenitization temperature (compare Table 4 and Table 5). As such, it is clear that the tempering process has minor contribution on the volume fraction of MC and M_6C carbides, which is mainly related to the carbide growth with tempering time and decomposition of M_2C carbides.

The $M_{23}C_6$ carbides are not present at the austenitization temperature as they dissolve at the transition from ferrite to austenite. From the simultaneous precipitation modeling (Fig. 10 d–f), it is clear that for the CHT samples the limitation in the volumetric amount is the amount of precipitated M_2C carbides and their dissolvement/transformation into $M_{23}C_6$ carbides. For all three CHT steels, the measured volume fraction of $M_{23}C_6$ carbides (Table 4) corresponds to the values achieved at tempering where the M_2C carbides are not present anymore. It should be stated, that the simulated tempering times are not realistic, as the simulation considers simultaneous precipitation from a homogeneous material, which is not the case in reality. Additionally, the model does not take into account growth mechanisms of preexisting carbides and Ostwald ripening of the larger preexisting carbides. Nevertheless, the model allows the interpretation of existence of additional nucleation sites for DCT steels.

The results of stable phases at different temperatures for steels A and B (Fig. 10 a–c) show that at cryogenic temperatures M_7C_3 carbides are present. These carbides could indeed be the reason for the increase of $M_{23}C_6$ precipitation in the case of DCT samples. If the crystal structure of M_7C_3 is of hexagonal structure [49–51], the two different morphologies of $M_{23}C_6$ carbides can be explained. It is proposed that the smaller cuboidal $M_{23}C_6$ carbides are formed from the M_7C_3 carbide embryos that emerge during DCT. During tempering,

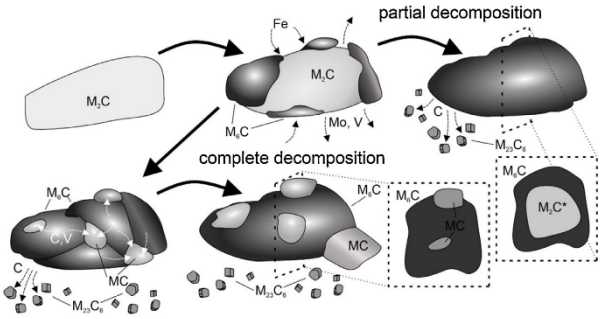

Fig. 9 – Schematic representation of carbide transformation during tempering.

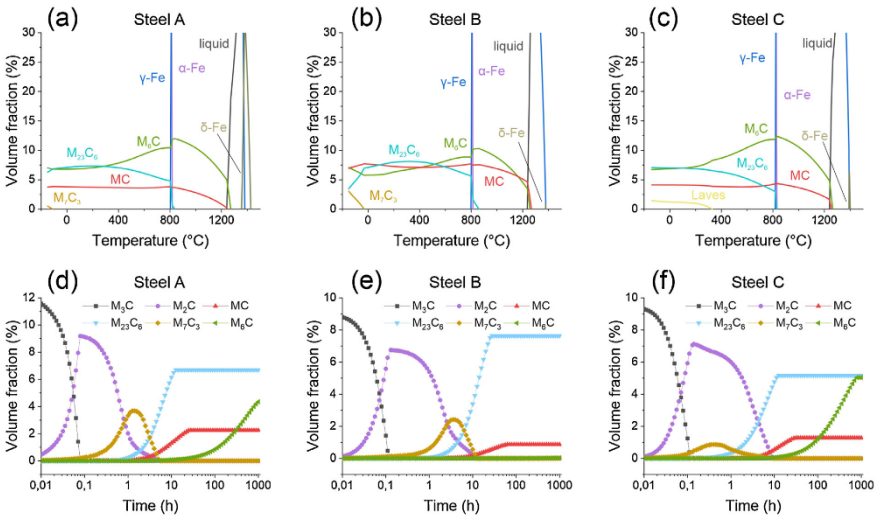

Fig. 10 – Thermodynamically modeled volumetric fractions of stable phases in equilibrium vs. temperature for (a) steel A, (b) steel B and (c) steel C. In (d), (e) and (f) the evolution of volumetric fractions of precipitates (metastable and stable) with tempering time is given for steel A, B and C respectively. The model incorporates preexisting carbide after austenitization (values provided in Table 5) and heat treatment temperatures provided in Table 2.

the embryos then grow into small hexagonal pillars at which they slowly enlarge (up to about 1 μm) and transform into the complex cubic $M_{23}C_6$ carbides conserving the pillar-cuboidal morphology. The larger and more spherical $M_{23}C_6$ carbides originate from the precipitation of M_3C/M_2C carbides. These carbides will endure Ostwald ripening during the tempering process, which causes their larger and spherical form. As a result, the DCT steels have a much larger amount of $M_{23}C_6$ carbides, as the additional embryos allow large quantity of nuclei to form. This in turn induces the full volume development of these carbides that are possible at the selected tempering temperature. Furthermore, these results suggest that in DCT steels the M_2C carbide decomposition inclines to be more complete as the preexisting formation of M_7C_3 carbides increases the $M_{23}C_6$ carbide fraction to maximum. For such a process to occur, the amount of available carbon in the matrix needs to be increased, which is possible by the dissolvement and complete decomposition of the preexisting M_2C carbides. As a result, the full transformation time of M_2C carbides for the DCT samples should be sufficiently shorter compared to the modeled data in Fig. 10 d–e. This coincides well with the obtainment of maximum $M_{23}C_6$ volume fraction for the samples with DCT and

tempering times that are significantly shorter than the ones expected from the modeled data. This also coincides well with the SEM observation of less frequent occurrence of M_2C^* carbides and lower amount of clusters in DCT samples (section 3.3 and 3.1 respectively).

However, the above does not hold for steel C for which the $M_{23}C_6$ carbides do not show distinct differences in morphology. This steel also shows no difference in the volume fraction of carbides between CHT and DCT. The main reason for this minute effect is the high Co concentration that increases alloying elements dissolution into the matrix and promotes faster carbide nucleation due to increased chemical potential of the alloying elements [52]. As a result, the nucleation barrier of all carbide types is considerably lower and allows formation and growth in the early stages of the heat treatment and sufficient formation of nuclei to attain full volume fraction of $M_{23}C_6$ carbides. Furthermore, the modeling suggests that instead of M_7C_3 carbides Laves phases form at temperatures lower than 400 °C. The replacement of the M_7C_3 carbides with Laves phase at cryogenic temperatures could be another reason for the indifference between DCT and CHT steel C.

4. Conclusion

In this paper, the effectiveness of deep cryogenic treatment (DCT) on the carbide precipitation in selected high-speed steels (HSS) was investigated. The carbide precipitation, change in microstructure, types and size of carbides were analyzed. It is concluded, that DCT increases the density of precipitation of all carbides (up to 30 %). The size of carbides is also on average smaller with the average carbide size reduced down to 20 %. The redistribution does not influence the volumetric fraction of M_6C and MC carbides for all selected steels (DCT) compared to conventionally heat-treated (CHT) counterparts. However, HSS with no or low cobalt content have a substantial increase in volume fraction of $M_{23}C_6$ (up to 140 % increase) carbides when exposed to DCT (corresponding to about 3 % higher volume fraction compared to CHT samples). The increase is correlated with the higher number of carbides with cuboidal morphology that are presumed (based on modeling results) to evolve from M_7C_3 carbides forming at cryogenic temperatures. The presence of larger $M_{23}C_6$ carbides originating from the conventional transformation from M_3C/M_2C carbides that are present in both CHT and DCT samples support the claim of two separate nucleation processes that occur for DCT steels. For the selected steel with higher Co content, no influence of DCT on the volume fraction of $M_{23}C_6$ carbides was determined, which is attributed to the lower nucleation energy barrier of carbides resulting from the high cobalt content. With this research, also the dynamics of the M_2C decomposition are addressed. It is shown that the M_2C decomposition with selected heat treatments is incomplete, leading to a partial decomposed M_2C carbide formation with larger iron content. Such decomposition is another influencing factor on the ending quantity of M_6C and MC carbides that are formed through the decomposition of M_2C carbides. It was determined by modeling and observations with SEM, that the complete decomposition of M_2C carbides occurs more frequently for DCT samples compared to their CHT counterparts.

Conflicts of interest

The authors declare no conflicts of interest.

Author contributions

P.J.-K.: Conceptualization, Visualization, Modelling, Writing. M.J.-K.: Visualization, Modelling, Writing, Editing. B.P.: Conceptualization, Supervision, Writing-editing and review. All authors have read and agreed to the published version of the manuscript.

Funding

This work was supported by Slovenian Research Agency (ARRS), Ljubljana, Slovenia [No. P2-0050 & No. J2-9211].

Acknowledgement

Acknowledgement goes to IMT metallographic lab and microscope operators.

REFERENCES

[1] Baldissera P, Delprete C. Deep cryogenic treatment: a bibliographic review. Open Mech Eng J 2008;2:1–11, http://dx.doi.org/10.2174/1874155X00802010001.
[2] Senthilkumar D. Cryogenic treatment:shallow and deep. In: Totten GE, Colas R, editors. Encyclopedia of iron, steel, and their alloys, New York, NY. NY, USA: Taylor and Francis; 2016. p. 995–1007, http://dx.doi.org/10.1081/E-EISA-120052805.
[3] Jovičević-Klug P, Podgornik B. Deep cryogenic treatment of metallic materials. Encyclopedia 2020:1–11.
[4] Jovičević-Klug P, Podgornik B. Review on the effect of deep cryogenic treatment of metallic materials in automotive applications. Metals 2020;10:434, http://dx.doi.org/10.3390/met10040434.
[5] Vengatesh M, Srivignesh R, Pradeep T, Karthik NR. Review on cryogenic trearment of steels. Int Res J Eng Sci Technol Innov 2016;3:417–22.
[6] Singla AK, Singh J, Sharma VS. Processing of materials at cryogenic temperature and its implications in manufacturing: a review. Mater Manuf Process 2018;33:1–38, http://dx.doi.org/10.1080/10426914.2018.1424908.
[7] Bayer AM, Becherer BA, Vasco T. High-speed tool steels. In: ASM handbook, volume 16: machining. Cleveland, OH, USA: ASM International; 1989. p. 51–9, http://dx.doi.org/10.31399/asm.hb.v16.9781627081887.
[8] Mukherjee T. Materials for metal cutting. Brain Inform Health (2015) 1970.
[9] Rong W, Andrén HO, Wisell H, Dunlop GL. The role of alloy composition in the precipitation behaviour of high speed steels. Acta Metall Mater 1992;40:1727–38, http://dx.doi.org/10.1016/0956-7151(92)90116-V.
[10] Gogte C.L., Peshwe D.R., Paretkar R.K. Influence of cobalt on the cryogenically treated W-Mo-V high speed steel. Advances in Cryogenic Engineering, vol. 1434, Spokane, WA, USA: n.d., p. 1175–1182. https://doi.org/10.1063/1.4707039.
[11] Davis JR. Wrought High-speed tool steels. In: ASM specialty handbook: tool materials. Cleveland, OH, USA: ASM International; 1995. p. 13.

[12] Barron RF. Cryogenic treatment of metals to improve wear resistance. Cryogenics 1982;22:409–13, http://dx.doi.org/10.1016/0011-2275(82)90085-6.

[13] Diekman F. Cold and cryogenic treatment of steel. In: Dossett J, Totten GE, editors. Steel heat treating fundamentals and processes-ASM handbook. Cleveland, OH, USA: ASM International; 2013. p. 382–6.

[14] Timmerhaus KD. Superconductivity. Advances in cryogenic engineering, Boulder, CO, USA: cryogenic engineering conference university of colorado and national bureau of standards boulder, CO; 1960. p. 145–8, http://dx.doi.org/10.1007/978-1-4613-2213-9.

[15] Jones JN, Rogers CB. The acoustic effect of cryogenically treating. J Acoust Soc Am 2013;114:2349.

[16] Ming CJ. Cryogenic treatment of music wire. National university of singapure; 2004.

[17] Paul S, Chattopadhyay AB. Environmentally conscious machining and grinding with cryogenic cooling. Mach Sci Technol 2007;10:87–131.

[18] Govindaraju N, Shakeel AL, Pradeep Kumar M. Experimental investigations on cryogenic cooling in the drilling of AISI 1045 steel. Mater Manuf Process 2014;29:1417–21.

[19] Pérez M, Rodríguez C, Belzunce FJ. The use of cryogenic thermal treatments to increase the fracture toughness of a hot work tool steel used to make forging dies. Procedia Mater Sci 2014;3:604–9, http://dx.doi.org/10.1016/j.mspro.2014.06.100.

[20] Das D, Dutta AK, Ray KK. Influence of varied cryotreatment on the wear behavior of AISI D2 steel. Wear 2009;266:297–309, http://dx.doi.org/10.1016/j.wear.2008.07.001.

[21] Akhbarizadeh A, Shafyei A, Golozar MA. Effects of cryogenic treatment on wear behavior of D6 tool steel. Mater Des 2009;30:3259–64, http://dx.doi.org/10.1016/j.matdes.2008.11.016.

[22] Kalia S. Cryogenic processing: a study of materials at low temperatures. J Low Temp Phys 2010;158:934–45, http://dx.doi.org/10.1007/s10909-009-0058-x.

[23] Joshi P, Singh J, Dhiman P, Shekhar H, Kumar V. Effect of cryogenic treatment on various materials: a review. Open International Journal of Technology Innovations and Research 2015;14:1–11.

[24] Darwin JD, Mohan Lal D, Nagarajan G. Optimization of cryogenic treatment to maximize the wear resistance of 18% Cr martensitic stainless steel by Taguchi method. J Mater Process Technol 2008;195:241–7, http://dx.doi.org/10.1016/j.jmatprotec.2007.05.005.

[25] Huang JY, Zhu YT, Liao XZ, Beyerlein IJ, Bourke MA, Mitchell TE. Microstructure of cryogenic treated M2 tool steel. Mater Sci Eng A 2003;339:241–4, http://dx.doi.org/10.1016/S0921-5093(02)00165-X.

[26] Su YY, Chiu LH, Chen FS, Lin SC, Pan YT. Residual stresses and dimensional changes related to the lattice parameter changes of heat- treated JIS SKD 11 tool steels. Mater Trans 2014;55:831–7.

[27] Bensely A, Prabhakaran A, Mohan Lal D, Nagarajan G. Enhancing the wear resistance of case carburized steel (En 353) by cryogenic treatment. Cryogenics 2006;45:747–54, http://dx.doi.org/10.1016/j.cryogenics.2005.10.004.

[28] Amini K, Nategh S, Shafyei A. Influence of different cryotreatments on tribological behavior of 80CrMo12 5 cold work tool steel. Mater Des 2010, http://dx.doi.org/10.1016/j.matdes.2010.05.028.

[29] Oppenkowski A, Weber S, Theisen W. Evaluation of factors influencing deep cryogenic treatment that affect the properties of tool steels. J Mater Process Technol 2010;210:1949–55, http://dx.doi.org/10.1016/j.jmatprotec.2010.07.007.

[30] Meng F, Tagashira K, Sohma H. Wear resistance and microstructure of cryogenic treated Fe-1.4Cr-1C bearing steel. Scr Metall Mater 1994;31:865–8.

[31] Meng F, Tagashira K, Azuma R, Sohma H. Role of eta-carbide precipitations in the wear resistance improvements of Fe-12Cr-Mo-V-1.4C tool steel by cryogenic treatment. Isij Int 1994;34:205–10, http://dx.doi.org/10.2355/isijinternational.34.205.

[32] Collins DN, Dormer J. Deep cryogenic treatment of a D2 cold-work tool steel. Heat Treatment Of Metals 1997;3:71–4.

[33] Osborne AK. An encyclopedia of the Iron & steel Industry. New York, NY: Philosophical Library Inc.; 1956.

[34] Kim S, Im Y-R, Lee S, Lee H-C, Oh YJ, Hong JH. Effects of alloying elements on mechanical and fracture properties of base metals and simulated heat-affected zones of SA 508 steels. Metallurgical and Materials Transactions A: Physical Metallurgy and Materials Science 2001;32A:903–11.

[35] Kumar TV, Thirumurugan R, Viswanath B. Influence of cryogenic treatment on the metallurgy of ferrous alloys: a review. Mater Manuf Process 2017;32:1789–805.

[36] Lee S, Kim S, Hwang B, Lee BS, Lee CG. Effect of carbide distribution on the fracture toughness in the transition temperature region of an SA 508 steel. Acta Mater 2002;50:4755–62, http://dx.doi.org/10.1016/S1359-6454(02)00313-0.

[37] Demir E, Toktas I. Effects of cryogenic treatment on residual stresses of AISI D2 tool steel. Kovove Materialy 2018;56:153–61, http://dx.doi.org/10.4149/km20183153.

[38] Inoue A, Masumoto T. Carbide reactions (M3C→M7C3→M23C6→M6C) during tempering of rapidly solidified high carbon Cr-W and Cr-Mo steels. Metall Trans A 1980;11:739–47, http://dx.doi.org/10.1007/BF02661203.

[39] long Liu B, qing LüZ, wei Feng W, zhi Ren T, W tang Fu. Precipitation and decomposition behaviors of carbides in AISI M2 high-speed steel with nitrogen and mischmetal. J Cent South Univ 2017;24:782–8, http://dx.doi.org/10.1007/s11771-017-3480-2.

[40] Zhou X, Liu D, Zhu W, Fang F, Tu Y, Jiang J. Morphology, microstructure and decomposition behavior of M2C carbides in high speed steel. J Iron Steel Res Int 2017;24:43–9, http://dx.doi.org/10.1016/S1006-706X(17)30007-9.

[41] Pan FS, Wang WQ, Tang AT, Wu LZ, Liu TT, Cheng RJ. Phase transformation refinement of coarse primary carbides in M2 high speed steel. Prog Nat Sci 2011;21:180–6, http://dx.doi.org/10.1016/S1002-0071(12)60053-7.

[42] Kostoj V, Mithieux JD, Fröhlich T. Influence of chromium carbide size on the austenization kinetics of a martensitic stainless steel measured by dilatometry. Solid State Phenom 2011;172–174:426–31.

[43] Grujicic M. Coherent precipitation of M2C carbides in AF1410 steel. Mater Sci Eng A 1989;117:215–20, http://dx.doi.org/10.1016/0921-5093(89)90103-2.

[44] Hou TP, Wu KM, Liu WM, Peet MJ, Hulme-Smith CN, Guo L, et al. Magnetism and high magnetic-field-induced stability of alloy carbides in Fe-based materials. Sci Rep 2018;8:1–10, http://dx.doi.org/10.1038/s41598-018-20910-3.

[45] Fang CM, Van Huis MA, Sluiter MHF. Formation, structure and magnetism of the γ-(Fe,M)23C6 (M = Cr, Ni) phases: a first-principles study. Acta Mater 2016;103:273–9, http://dx.doi.org/10.1016/j.actamat.2015.08.078.

[46] Toraya H. A new method for quantitative phase analysis using X-ray powder diffraction: direct derivation of weight fractions from observed integrated intensities and chemical compositions of individual phases. J Appl Crystallogr 2016;49:1508–16, http://dx.doi.org/10.1107/S1600576716010451.

[47] Rietveld HM. A profile refinement method for nuclear and magnetic structures. J Appl Crystallogr 1969;2:65–71, http://dx.doi.org/10.1107/s0021889869006558.
[48] Dhokey NB, Hake A, Kadu S, Bhoskar I, Dey GK. Influence of cryoprocessing on mechanism of carbide development in cobalt-bearing high-speed steel (M35). Metallurgical and Materials Transactions A: Physical Metallurgy and Materials Science 2014;45:1508–16, http://dx.doi.org/10.1007/s11661-013-2067-2.
[49] Ernst F, Li D, Kahn H, Michal GM, Heuer AH. The carbide M7C3 in low-temperature-carburized austenitic stainless steel. Acta Mater 2011;59:2268–76, http://dx.doi.org/10.1016/j.actamat.2010.11.058.
[50] Liu S, Zhou Y, Xing X, Wang J, Ren X, Yang Q. Growth characteristics of primary M7C3 carbide in hypereutectic Fe-Cr-C alloy. Sci Rep 2016;6:1–8, http://dx.doi.org/10.1038/srep32941.
[51] Yamamoto K, Inthidech S, Sasaguri N, Matsubara Y. Influence of Mo and W on high temperature hardness of m&sub&7&/sub&C&sub&3&/sub& carbide in high chromium white cast Iron. Mater Trans 2014;55:684–9, http://dx.doi.org/10.2320/matertrans.F-M2014801.
[52] Nishizawa T, Hasebe M, Ko M. Thermodynamic analysis of solubility and miscibility gap in ferromagnetic alpha iron alloys. Acta Metall 1979;27:817–28.

Chapter 3

Influence of Deep Cryogenic Treatment on Material's Properties

Chapter 3 is concentrated on the changes in material's properties induced by DCT. The tested materials were three steel grades (AISI M2, AISI M3:2 and AISI M35), all from the HSS group. The representative selection was based on previous research conducted on the selected grades in correlation to microstructure and surface properties. A variety of mechanical properties was tested, which were selected based on their commonness as tested properties in relation to the DCT effect. On the other hand, additional properties were also researched that are unconventionally tested properties of a selected steel group. It is postulated that these uncommonly tested properties can reveal/indicate additional features of DCT-induced properties change. Additionally, they can provide explanations to the possible mechanisms behind DCT, which can be further unraveled with further in-situ observation(s). For this reason, the material's life cycle via fatigue testing, compressive strength, strain-hardening exponent and impact toughness were carried out on both control (CHT) and tested (DCT) groups to observe proposed changes and indicators of modified properties with DCT.

The second aspect of materials properties in relation to the HSS group is their surface resistance to wear and friction properties, as these are key features that need to be controlled for cutting tools. For this reason, DCT influence on friction, wear resistance and galling was tested on the same steels. The wear resistance was tested in three different conditions, the first one favoring abrasion, the second one adhesion and the last one considers a mixed type maintaining both abrasion and adhesion. This way, a variety of different steel properties were tested in order to provide systematic approach of unraveling the DCT mechanism(s) and also to test and provide guidelines for DCT incorporation into classical heat treatment schemes in industry for applications, where wear and friction play an important role (tool industry, aerospace, medicine etc.).

A detailed description of DCT influence on the selected materials properties is provided in the next two subchapters:

3.1. Mechanical properties and fatigue
The first subchapter/article discusses the influence of DCT on the microstructure and changes in selected tested mechanical properties (hardness, fracture toughness, impact toughness, compressive strength and strain-hardening exponent) and fatigue (fatigue cycle and limit).

3.2. Friction, wear resistance and galling
In the second subchapter/article, the research goes even further, where impact of DCT is tested with friction, wear resistance and galling are researched in correlation to changed microstructure and mechanical properties.

Chapter 3 addresses ***Hypotheses*** **1, 2 and partly 3**.

3.1 Mechanical Properties and Fatigue

This subchapter presents and discusses the influence of heat treatment parameters and chemical composition of steel on the effectiveness of DCT. Within this research, three grades of HSS, AISI M2, AISI M3:2 and M35 were tested in relation to their fatigue resistance, hardness, fracture and impact toughness, compressive strength and strain-hardening exponent in order to observe changes induced by DCT in comparative relation to CHT counterparts. Results of this study indicate that the influence and effectiveness of DCT is strongly guided by the manufacturing type (wrought or powder metallurgy (PM) steel), chemical composition of the selected steel grade and selected heat treatment parameters (austenitizing and tempering temperature), resulting in either degradation or improvement of individual properties and different combination of effect on the variety of tested properties. With this study, a strong emphasis is given to the tailoring of the DCT effect on different HSS grades based on the selected heat treatment temperatures (austenitization and tempering).

Brief discussion: The study showed that DCT generally improves the fatigue properties (2–50 %) and mechanical properties, such as hardness (3–7 %), fracture (4–20 %) and impact toughness (6–22 %), compressive strength (7–39 %) and strain-hardening exponent (2–30 %), of HSS. The predominant reason for the properties change is related to the selected heat treatment temperature. However, on the DCT improvement of the properties other factors also play an important role. The increase of fatigue resistance is attributed to the increased size of MC carbides after DCT, which is also dependent on the Co content. The latter is postulated from the fact that Co allows the limited formation of $M_{23}C_6$ carbides, which induces formation of larger carbides with lower overall density. Additionally, the M_2C carbide presence, size and decomposition also strongly affect the fatigue properties by acting as weak points for crack nucleation and propagation. The increase in hardness is strongly correlated to the more effective change of the retained austenite into martensite and to the increased precipitation of carbides with DCT. Improvement in fracture toughness is strongly contributed to the homogeneity of the microstructure, especially related to the presence of carbide clusters, which are less common in the DCT samples compared to the CHT counterparts. Additional factors, which play an important role, are carbide density and the size of prior austenite grains (PAGs), which can be larger or smaller, depending on the combination of heat treatment parameters, that act as additional weak points for crack propagation. If PAGs are smaller, the toughness is improved, whereas the improvement of impact toughness is more correlated to the matrix, which exhibits refinement of martensitic laths and overall decrease in C content (7-36 %) after DCT. The improvement of compressive strength and strain-hardening exponent is considerably more complex compared to other investigated properties, since all previously mentioned factors conjointly contribute to their final state. Nevertheless, overall, the increased formation of $M_{23}C_6$ after DCT shows the strongest and most positive trend on compressive strength, which is also proposed to be related to the concurrent reduction of residual stresses with DCT. On the contrary, the increase in carbide precipitation reduced the strain-hardening exponent. Furthermore, the study shows that the lower austenitizing and higher tempering temperature resulted in a general improvement of selected properties in comparison to higher austenitization and lower tempering temperature. Additionally, the higher presence of Co content and precipitation of $M_{23}C_6$ carbides with morphologies displaying sharp edges additionally contributed to a predominantly negative or negligible effect on investigated properties.

The ***author's contribution,*** as the first author, to the paper ***Influence of heat treatment parameters on effectiveness of deep cryogenic treatment on properties of high-speed steels***, published in the Journal of Materials Science and Engineering A, was: conceptualization, investigation, planning of experiments, visualization, evaluation and writing (original draft and editing).

This subchapter addresses thesis ***Hypotheses 1, 2 and 3***.

Materials Science & Engineering A 829 (2022) 142157

Contents lists available at ScienceDirect

Materials Science & Engineering A

journal homepage: www.elsevier.com/locate/msea

Influence of heat treatment parameters on effectiveness of deep cryogenic treatment on properties of high-speed steels

Patricia Jovičević-Klug [a,b,*], Gašper Puš [a], Matic Jovičević-Klug [a], Borut Žužek [a], Bojan Podgornik [a,b]

[a] Department of Metallic Materials and Technology, Institute of Metals and Technology, Lepi pot 11, 1000, Ljubljana, Slovenia
[b] Jožef Stefan International Postgraduate School, Jamova cesta 39, 1000, Ljubljana, Slovenia

ARTICLE INFO

Keywords:
Characterization
Fatigue properties
Fracture mechanics
Hardness
Iron alloys
Phase transformation

ABSTRACT

This study investigates the influence of heat treatment parameters on effectiveness of deep cryogenic treatment (DCT) and on properties of three high-speed steels (HSS) (AISI M2, AISI M3:2 and AISI M35) with different chemical composition. Within this research the same preselected soaking temperature, time, cooling/warming rate and placement of DCT, being found in the literature as the most effective, were applied to the selected HSS grades. The fatigue resistance, hardness, impact and fracture toughness, compressive strength and strain-hardening exponent were selected as the evaluators of DCT effectiveness. The results indicate that the influence and effectiveness of DCT is strongly subjected by the type (wrought or PM steel), chemical composition of the particular steel grade and heat treatment parameters, resulting in either degradation or improvement of the steel properties. Furthermore, the study elucidates the effect of DCT on different HSS grades based on the selected heat treatment temperatures (austenitization and tempering). The research confirms that DCT generally improves the hardness, fatigue properties, fracture and impact toughness, compressive strength and strain-hardening exponent for HSS grades. However, it may also have negative impact on HSS properties. For all HSS investigated, the level of DCT effect depended also on the heat treatment conditions, i.e. austenitization and tempering temperature. The lower austenitization and higher tempering temperature in general resulted in improvement of steel properties, as compared to higher austenitization and lower tempering temperature with predominantly negative effect.

1. Introduction

Deep cryogenic treatment (DCT) of materials is employed in many different applications (medicine, aerospace, oil and gas industry, automotive industry, musical instruments, electronics, tool and tooling industry as well as additive manufacturing) [1–3]. For DCT certain variables have to be taken into account, such as (following the order of importance): selected soaking media and/or temperature, holding time of the material under selected deep cryogenic temperature, cooling rate/warming rate and sequence of cryogenic treatment [4–7]. The main proposed mechanism of DCT induced changes in steels is the transformation of retained austenite into martensite with carbide precipitation [2,3]. The microstructural changes have in general a positive effect on the mechanical properties such as hardness and toughness [8,9]. However, also negative effects of DCT have been observed for different steels, leading to degradation of certain properties such as impact toughness [10], hardness [11] etc. Such contradictory results and unclear mechanisms lead to a lack of consistency and reliability of the treatment process, which is required for the integration of DCT in various industries [12]. Reasons for such ambiguity of results reside in the unsystematic research of DCT and inadequacy of studies with limited and inconsistent parametric evaluation as well as questionable and unconventional experimental procedures. Furthermore, even for specific grades of materials there is no clear designation of DCT procedure, which creates limited applicability of DCT in industry. The most common material in tooling industry, showing good productivity at low costs are high-speed steels (HSS). HSS have distinctive mechanical properties such as superior hardness and abrasive wear resistance, high temperature stability and high strength [13]. However, HSS are also very brittle [13], which limits their use in more demanding applications involving high impact forces and fatigue. Material brittleness, toughness and ductility are characterized by its sudden failure energy (impact

* Corresponding author. Institute of Metals and Technology, Lepi pot 11, 1000, Ljubljana, Slovenia.
E-mail address: patricia.jovicevicklug@imt.si (P. Jovičević-Klug).

https://doi.org/10.1016/j.msea.2021.142157
Received 24 May 2021; Received in revised form 1 October 2021; Accepted 5 October 2021
Available online 6 October 2021

toughness), resistance to crack propagation (fracture toughness), strain-hardening (strain-hardening exponent) and fatigue life. In terms of tool steel properties enhancement, DCT has been found to effectively increase hardness and strength, without having negative effect on toughness [14]. Moreover, work of Podgornik et al., 2016 [14] indicates that DCT can simultaneously increase hardness and toughness. However, the effect is linked to be strongly dependent on steel type and chemical composition.

Among HSS, AISI M2 has been most commonly associated with DCT and properties enhancement [15–18]. Literature review of DCT AISI M2 shows increased hardness [8,18–20], resulting from the change of retained austenite (RA) into martensite and redistribution and refinement of carbides. Pellizzari et al., 2008 [8] also noticed that DCT is not effective in increasing the fracture toughness of AISI M2. Contrary, it showed increased embrittlement after DCT application. However, Sola et al., 2017 [21] stated that DCT has improved fracture toughness of AISI M2. Also Fantineli et al., 2020 [22] observed improvement in impact toughness of AISI M2 after DCT, which was attributed to the lower carbon amount in the martensite matrix and finer and more homogeneous carbide precipitation. Similar observation of improved impact toughness of AISI M2 steel after DCT was reported also by Pellizzari et al., 2012 [16], but it required alteration of heat treatment parameters and DCT route. In contrast to the research of AISI M2 HSS, DCT research on other types of HSS is much scarcer. The available studies on AISI M3:2 HSS [11,20] and the effect of DCT show increase in fracture toughness after DCT without any significant change in hardness. On the other hand, research on AISI M35 steel performed by Candane et al., 2013 [23] and Jelenkowski et al., 2010 [24] showed increase in hardness after application of DCT, but no significant change in toughness [23]. In contrast, Pellizzari 2008 [20] observed drop in hardness and fracture toughness after DCT. Negative effect of DCT on fracture toughness of Co-containing AISI M35 HSS has been mainly attributed to the Co-dynamics. Pellizzari 2008 [20] has concluded that the effectiveness of DCT on mechanical properties of HSS is influenced by Co presence, where Co-free HSS grades will in general display improved fracture toughness and vice versa. In addition, most studies of DCT in combination with HSS are concentrated on one set of heat treatment parameters and mainly on hardness and toughness, whereas research of other mechanical properties such as fatigue, compressive strength and strain-hardening exponent is limited. Furthermore, there is no clear understanding of how different heat treatment parameters influence the whole ensemble of mechanical properties, which is crucial knowledge in the development of complementary heat treatments for preferential improvement of material properties.

This study continues work from our previous microstructural studies of high-speed steels (HSS) by Jovičević-Klug et al., 2020 [25] and Jovičević-Klug et al., 2021 [26], which provides systematic research of DCT effect on the microstructure and surface changes of selected steels (HSS) AISI M2, AISI M3:2 and AISI M35. To resolve the previously mentioned issues of contradictory reports and lack of research, this study considers a broad range of mechanical properties in connection to varying heat treatment parameters to provide more insight into the DCT effectiveness on HSS and its dependency on selected heat treatment parameters. Furthermore, to expand the knowledge of DCT effectiveness on HSS, the selected HSS steels are further investigated for the DCT effect on fatigue and mechanical properties of HSS steels. The main aim of the research is to demonstrate and explain DCT induced changes of material properties in relation to HSS steel composition and heat treatment conditions. Additionally, the study intends to provide correlations between selected properties (fatigue resistance, strength, hardness, impact and fracture toughness and strain-hardening exponent) and microstructure/phase alterations for selected HSS.

2. Methods and methods

2.1. Material and heat treatment

The following high-speed steels were tested: AISI M2 (EN HS6-5-2) - A, AISI M3:2 (EN HS6-5-3) - B and AISI M35 (EN HS6-5-2-5) - C. The investigated steels, where A and C are wrought steels and B produced through powder metallurgy (PM) were delivered in the shape of rolled, soft-annealed and peeled rods. Chemical compositions of selected steels given in wt. % in Table 1 are within the value range of corresponding steel standards.

From the received material, CNPTB - Circumferentially Notched and fatigue Pre-cracked Tensile Bar [27] specimens (for fracture toughness and hardness) and CVN - Charpy V-notch (for impact toughness and fatigue) specimens were machined for the different testing methods. The sample for compressive strength and strain-hardening exponent were cut from CNPTB samples. All samples were first austenitized and quenched in a single step in a horizontal vacuum furnace IPSEN VTTC-324R with uniform high-pressure gas quenching using N_2 at the pressure of 5 bars (average quenching rate was for all steels approximately 7–8 °C s^{-1}). After hardening, one group of specimens was conventional heat-treated (CHT), comprising of triple tempering according to the steel producer recommendation. On the other hand, the second group was subjected to DCT, performed immediately after quenching by gradual immersion of the samples in liquid nitrogen for 24 h, followed by just a single tempering cycle, proven to be sufficient due to almost complete retained austenite transformation by DCT [20]. To take eventual effect of austenitizing temperature into account, specimens were hardened from two austenitizing temperatures, selected within the steel producer recommended range. One set of specimens was hardened from upper austenitizing temperature and tempered at lower temperature in order to promote high hardness over toughness. The other set was hardened from lower austenitizing temperature and tempered at high tempering temperature, thus promoting toughness over hardness. Details of heat treatment procedures and parameters are given in Table 2.

2.2. Microstructure and phase analysis

Microstructural characterization after CHT and heat treatment including DCT was conducted on microsectioned and metallographically prepared samples with scanning electron microscope (SEM) (JEOL JSM-6500F). The light microscope images were mainly obtained to acquire an overall picture of the microstructure (grains and their grain boundaries), while with SEM the microstructure (type, size and distribution of precipitates, inclusions and phases) of each subgroup for all three steel grades was precisely determined. To estimate the number of precipitates and their distribution, the SEM-feature technique was employed over the analyzing area of 400 × 400 μm^2. Analysis of carbon depletion was made by SEM-EDS (EDS is energy dispersive X-ray spectroscopy) in the most representative part of samples' matrix, where the influence of carbides was the smallest and it is provided in SM1. A detailed microstructural and surface investigation was performed in our previous studies by Jovičević-Klug et al., 2020 [25] and Jovičević-Klug et al., 2021 [26]. In addition, phase analysis of subgroups was performed with X-ray diffraction (XRD). The XRD analysis was carried out on PANalytical 3040/60, Almelo, Netherlands and the XRD data was measured from 15° to 90° of 2θ angle. The phase identification was performed using COD database references and followed by evaluated using a

Table 1
Actual chemical composition of the investigated steel in *wt. %*.

Steel grade AISI	C	Mn	S	Cr	Mo	V	W	Co
M2 (A)	0.90	0.28	0.002	4.00	4.70	1.70	6.00	–
M3:2 (B)	1.29	0.31	0.006	3.90	4.80	3.00	5.90	0.69
M35 (C)	0.90	0.34	0.004	4.10	5.20	2.01	6.20	4.50

Table 2
Heat treatment parameters.

Group	Subgroup	Austenitizing		DCT		Tempering (°C)
		Temperature (°C)	Time (min)	Temperature (°C)	Immersion time (h)	
A (AISI M2)	A1-CHT	1230	2	–	–	3 × 550/1 h
	A2-DCT	1230	2	−196	24	1 × 550/1 h
	A3-CHT	1180	2	–	–	3 × 620/1 h
	A4-DCT	1180	2	−196	24	1 × 620/1 h
B (AISI M 3:2)	B1-CHT	1180	2	–	–	3 × 540/2 h
	B2-DCT	1180	2	−196	24	1 × 540/2 h
	B3-CHT	1050	2	–	–	3 × 600/2 h
	B4-DCT	1050	2	−196	24	1 × 600/2 h
C (AISI M35)	C1-CHT	1230	2	–	–	3 × 550/2 h
	C2-DCT	1230	2	−196	24	1 × 550/2 h
	C3-CHT	1160	2	–	–	3 × 620/2 h
	C4-DCT	1160	2	−196	24	1 × 620/2 h

combination of Rietveld refinement [28] and Toraya method [29].

2.3. Mechanical and fatigue testing

Mechanical testing involved 6 characteristic properties: fatigue resistance, impact and fracture toughness, hardness, compressive strength and strain-hardening exponent. The properties were selected as these are considered as the most important properties for tool steel evaluation and performance determination in cutting tool applications.

2.3.1. Impact toughness

Impact toughness was measured with the Charpy impact test at room temperature (21 °C and 50% humidity) according to international standard SIST EN ISO 148-1:2017, using standard Charpy V-notch specimens (at least 3) and 300 J pendulum.

2.3.2. Fracture toughness

Fracture toughness of investigated steels was determined with CNPTB specimens, which were fatigue pre-cracked prior to heat treatment by being subjected to a single point cyclic loading for several minutes in order to produce pre-crack region of about 0.5 mm width. After heat treatment, the specimens (at least 6) were mounted into universal INSTRON 1255 500 KN tensile testing machine and axially loaded at the displacement speed of 0.0167 mm s^{-1} until failure at room temperature (21 °C and 50% humidity). Loading is performed according to ASTM E1820-01 standard. Fracture toughness calculation is then based on the measured load at fracture and the size of brittle fractured area. Details on specimens' preparation, pre-cracking, loading and fracture toughness calculation are given in Podgornik et al., 2014 [30].

2.3.3. Hardness

Hardness obtained after different heat treatment procedure and parameters was measured using Rockwell C method at room temperature (21 °C and 50% humidity). For each steel grade and heat treatment group, multiple measurements were performed on several specimens (at least 6) and average value calculated. For hardness measurement performed on cylindrical specimens, the curvature correction was applied according to SIST EN ISO 6508-1 (2016).

2.3.4. Compressive strength and strain-hardening exponent

Due to the high strength and brittle nature of HSS, tensile testing was replaced by compressive testing. Compressive strength was measured according to ASTM E9-19 standard on test specimens (at least 3) of cylindrical shape with 10 mm diameter and L/D ratio of 1.0 (length/diameter ratio). Specimens were cut from a section of the previously tested CNPTB specimen. Testing was performed using universal testing machine INSTRON 1255 at room temperature (21 °C and 50% humidity) and a constant compressive speed of 2 mm min^{-1} until maximum plastic deformation or sudden fracture of the specimen occurred. From the compressive tests, the strain-hardening exponent was determined from the true stress – true strain curve. The evaluation range was set from the beginning of plastic deformation to the maximum compressive stress.

2.3.5. Fatigue testing

Fatigue resistance of the investigated HSS after CHT and DCT was tested under dynamic loading in bending mode using Rumul resonant fatigue testing machine Cracktronic with an operating frequency of around 180 Hz. The fatigue (S/N) curves were obtained by performing room temperature (21 °C and 50% humidity) fatigue tests on standard Charpy V-notched (CVN) samples (10 × 10 × 55 mm) and using constant amplitude bending stress between 220 MPa and 460 MPa, stress ratio R of 0.1 and a sinusoidal waveform. Sample failure criterion was set as a drop of inherent oscillation by more than 3%, where the fatigue cracks occurred in a depth of up to 3 mm. The data was fitted according to Pearl-String method derivation and presented with linear function.

3. Results

3.1. Microstructure

The summary of microstructure is described in this section, however a more detailed microstructural, fractography and surface investigation with SEM and, transmission electron microscopy (TEM) is described in our previous studies by Jovičević-Klug et al., 2020 [25] and Jovičević-Klug et al., 2021 [26] and in SM 1. XRD results are provided in Table 3.

Fig. 1 presents SEM images of steel A (AISI M2) for all four heat treatments (A1-A4). Micrographs display precipitation of fine carbides within the lath-type martensite matrix. Additionally, they reveal dense precipitation of spherical carbides MC (M = V) (dark), M_6C (M = Fe, Mo, W) (bright), M_2C (M = Fe, Mo, W) (bright) and $M_{23}C_6$ (M = Fe, Cr) (light

Table 3
The phase composition of all subgroups for AISI M2, AISI M3:2 and AISI M35 steels.

Steel subgroup	Carbides			Matrix
	MC (V)	M_6C (W, Mo, Fe)	$M_{23}C_6$ (Fe, Cr)	
A1-CHT	2.1	6.9	2.2	88.8
A2-DCT	1.5	6.7	5.3	86.3
A3-CHT	1.8	6.7	2.5	89.1
A4-DCT	1.6	6.8	6.8	84.8
B1-CHT	6.6	7.6	4.3	81.5
B2-DCT	5.9	7.2	7.7	79.2
B3-CHT	7.5	8.4	3.1	81.1
B4-DCT	7.5	9.3	8.2	75.1
C1-CHT	3.0	7.3	5.1	84.6
C2-DCT	3.1	7.6	4.9	84.4
C3-CHT	2.8	7.1	3.4	86.7
C4-DCT	3.2	8.4	3.6	84.8

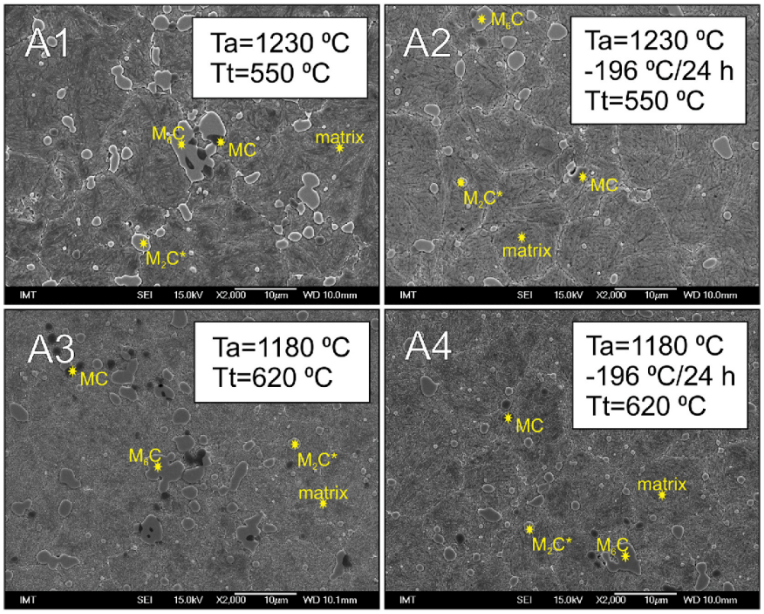

Fig. 1. Microstructure obtained by scanning electron microscope for all four groups of steel A (AISI M2): Groups A1/A3 are conventional heat-treated and A2/A4 are deep cryogenic treated.

bright), as proven by our previous studies [25,26], where MC, M_6C and M_2C are primary carbides and $M_{23}C_6$ are secondary carbides (see SM 1). The identification of the generation of carbides is referenced to the original state of microstructure of steel before being heat-treated. DCT samples have less agglomerated carbides and the carbides are more homogenously distributed. The average number of carbides of CHT treated samples is about 25% lower as compared to samples treated with DCT. At the same time, the subgroups with higher austenitization temperature and lower tempering temperature show approximately 40% lower number of carbides (A1-CHT/A2-DCT = ~23000 mm ^{2}/~29000 mm ^{2}) as compared to the other two subgroups with lower austenitization temperature and higher tempering temperature (A3-CHT/A4-DCT = ~36500 mm ^{2}/~49000 mm ^{2}). The relative frequency of equivalent carbide diameter (ECD) of carbides in CHT and DCT samples (A1-CHT/A2-DCT/A3-CHT/A4-DCT), regardless of the subgroup, is ~0.65 μm.

Fig. 2 shows SEM micrographs for all four subgroups (B1–B4) of steel B (AISI M3:2). Micrographs show precipitation of fine carbides within the lath martensite matrix. The carbides were the same types as found for steel A (MC (M = V) (dark), M_6C (M = Fe, Mo, W) (bright), M_2C (M = Fe, Mo, W) (bright) and $M_{23}C_6$ (M = Fe, Cr) (light bright), where MC, M_6C and M_2C are primary carbides and $M_{23}C_6$ are secondary carbides (see SM 1). On average, 4% less carbides is present in CHT samples than in DCT samples. The subgroups with higher austenitization temperature and lower tempering temperature have about 25% less precipitated carbides (B1-CHT/B2-DCT = ~50500 mm ^{2}/~53000 mm ^{2}) in comparison to the other two subgroups with lower austenitization temperature and higher tempering temperature (B3-CHT/B4-DCT = ~68500 mm ^{2}/~72000 mm ^{2}). The relative frequency of ECD in B1-CHT/B3-CHT/B4-DCT samples is ~0.85 μm, except for B2-DCT, for which it is ~1.05 μm. The high number of precipitated carbides could be theoretically even higher, due to the fact that in this study only carbides greater than 0.5 μm were included (SEM limitations for high confidence feature analysis).

The micrographs of steel C (AISI M35) are presented in Fig. 3 (C1–C4). These micrographs also reveal spherical carbide precipitation within the lath martensite matrix as seen for steel A and B. DCT samples have less agglomerated carbides, and the carbides are more homogenously distributed. The average number of carbides of CHT treated samples is 17% (C1-CHT/C2-DCT) and 37% (C3-CHT/C4-DCT) lower than in DCT samples. The number of precipitated carbides is increased significantly after DCT and from this, it can be concluded that the strongest DCT influence on the carbide precipitation is present for AISI M35 steel as compared to the other two steels AISI M2 and AISI M3:2. At the same time, the subgroups with higher austenitization temperature and lower tempering temperature also have substantially lower number of carbides (C1-CHT/C2-DCT = ~43500 mm ^{2}/~52000 mm ^{2}) as compared to the other two subgroups with lower austenitization temperature and higher tempering temperature (C3-CHT/C4-DCT = ~156000 mm ^{2}/~247000 mm ^{2}). The relative frequency of ECD in C1-CHT/C2-DCT samples is ~0.65 μm. The relative frequency of the other two subgroups C3-CHT/C4-DCT is ~0.55 μm.

Additional observation of prior austenitic grains (PAG) showed that PAG are larger in all three HSS groups of higher austenitization and lower tempering heat treatment, compare to groups of lower austenitization and higher tempering heat treatment.

3.2. Mechanical testing

3.2.1. Hardness

From Fig. 4, decrease in hardness is observed for AISI M2 steel when DCT is applied in combination with high austenitizing temperature.

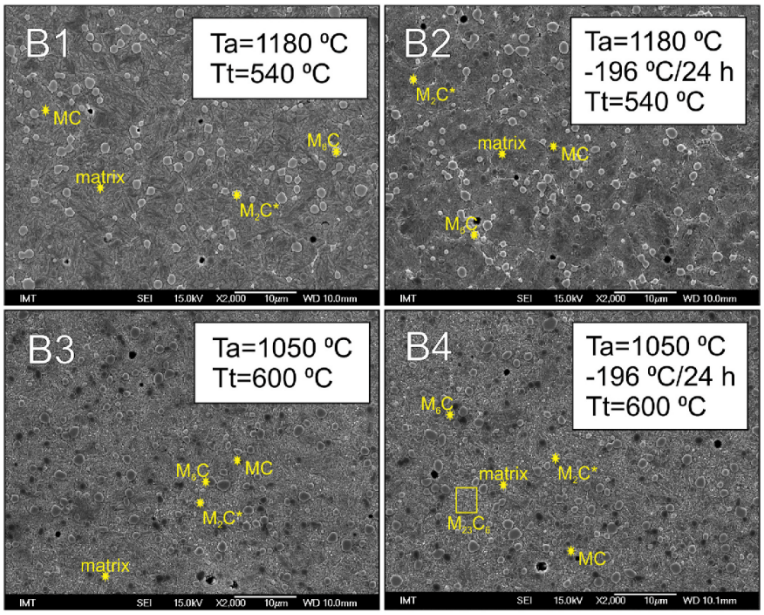

Fig. 2. Microstructure obtained by scanning electron microscope for all four groups of steel B (AISI M3:2). Groups B1/B3 are conventional heat-treated and B2/B4 are deep cryogenic treated.

However, the comparison of A1-CHT/A2-DCT subgroups indicates very minor or insignificant decrease (~2%) in hardness (from 65.99 ± 0.25 HRC for A1-CHT to 64.65 ± 0.65 HRC for A2-DCT). On the other hand, for low austenitizing temperature and lower working hardness range (A3-CHT/A4-DCT) DCT provides improvement in hardness of about 3% (from 57.93 ± 0.12 HRC for A3-CHT to 59.64 ± 0.15 HRC for A4-DCT). From this, it is suggested that DCT has no or very limited effect on the hardness of AISI M2 steel, becoming positive with reduced austenitization temperature. In the case of steel B (AISI M3:2), again for the first subgroups (B1-CHT/B2-DCT), austenitized from the upper temperature an insignificant decrease in hardness from 66.03 ± 0.04 HRC to 65.25 ± 0.11 HRC (~2%) can be seen, when the steel is exposed to DCT. Furthermore, for the second two subgroups (B3-CHT/B4-DCT) austenitized from the lower temperature the hardness again increased with DCT by ~5%, from 53.33 ± 0.11 HRC to 56.21 ± 0.12 HRC. Completely the same trends were found also for steel C – AISI M35, as shown in Fig. 4. For the first subgroup (C1-CHT/C2-DCT) implementation of DCT gives almost no change in hardness (drop from 66.16 ± 0.26 HRC for C1-CHT to 65.43 ± 0.38 HRC for C2-DCT; ~1%). For lower austenitization temperature (C3-CHT/C4-DCT) the DCT has a positive effect on the hardness, as the hardness increased for about 7% from 53.15 ± 0.55 HRC (C3-CHT) to 56.93 ± 0.26 HRC (C4-DCT). From this, it can be concluded that DCT has practically no effect on the hardness of HSS for high austenitizing temperatures and upper working hardness range (low tempering temperature), but positive when combined with lower austenitizing temperatures and low working hardness range (high tempering temperature).

3.2.2. *Impact and fracture toughness*

In Fig. 5, results of impact (Fig. 5 a) and fracture toughness (Fig. 5 b) for all HSS are provided. For steel A (AISI M2) (Fig. 5 a) higher impact toughness is observed for both DCT samples as compared to their CHT counterparts, by approximately 17% for high hardness group (A1-CHT = 35.42 ± 2.94 kJ m ^{2}, A2-DCT = 41.66 ± 2.94 kJ m ^{2}) and 6% for lower hardness group (A3-CHT = 37.50 kJ m ^{2}, A4-DCT = 39.58 ± 2.94 kJ m ^{2}). However, when scattering of results and standard deviation (SD) is taken into account, all four values lie within the same range, making the probable change in impact toughness induced by DCT very limited. Fracture toughness shows very similar trend in terms of DCT effect, being increased by 4% for the first group (A1-CHT/A2-DCT), from 10.51 ± 1.93 MPa$\sqrt{m}$ (A1-CHT) to 10.92 ± 1.64 MPa$\sqrt{m}$ (A2-DCT). However, when DCT is combined with lower austenitizing temperatures and lower hardness range a significant improvement in the fracture toughness of AISI M2 steel of 20% has been observed, increasing it from 11.92 ± 1.17 MPa$\sqrt{m}$ (A3-CHT) to 14.33 ± 1.17 MPa$\sqrt{m}$ (A4-DCT). The results suggest that DCT has positive effect on toughness of AISI M2 steel, minor in terms of impact toughness and resistance to crack initiation, but significant in terms of fracture toughness and resistance to crack propagation.

In the case of steel B (AISI M3:2; Fig. 5) there is an increase in impact toughness of about 22% obtained by DCT when steel is quenched from high austenitizing temperature and tempered at lower temperature. (from 37.5 kJ m ^{2} for B1-CHT to 45.83 ± 2.89 kJ m ^{2} for B2-DCT). However, for lower austenitizing temperature and lower hardness ranges, although in general giving higher toughness values, no difference could be observed between CHT and DCT treated samples (B3-CHT/B4-DCT = 50/50 kJ m ^{2}). On the other hand, DCT has negative effect on fracture toughness of steel B. It decreases fracture toughness for both groups, insignificantly for high austenitizing/low tempering group by ~1% (B1-CHT = 9.63 ± 1.35 MPa$\sqrt{m}$ and B2-DCT = 9.52 ± 0.92 MPa$\sqrt{m}$), but significantly by about 21% for low austenitizing/high tempering temperature subgroups (B3-CHT = 15.42 ± 0.89 MPa$\sqrt{m}$ and

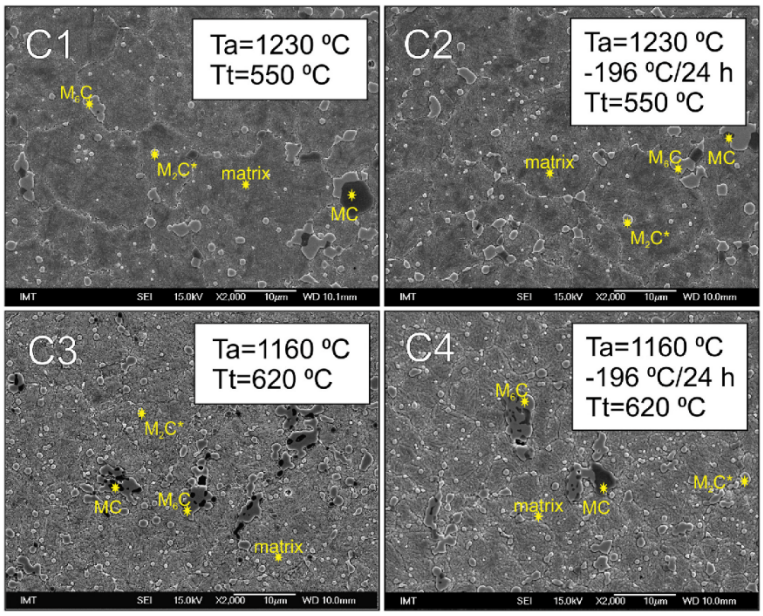

Fig. 3. Microstructure obtained by scanning electron microscope for all four groups of steel C (AISI M35). Groups C1/C3 are conventional heat-treated and C2/C4 are deep cryogenic treated.

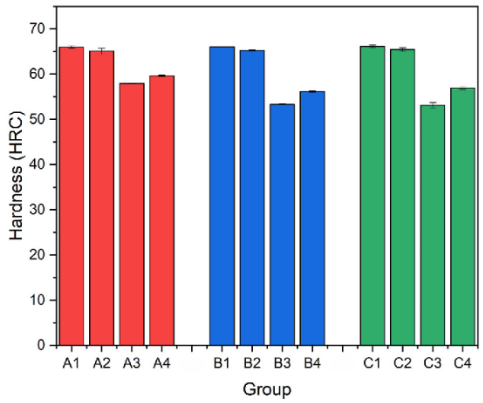

Fig. 4. Hardness for all 3 high-speed steel grades, for all four treatments, where A1-A3, B1–B3, C1–C3 are conventional heat-treated and A2-A4, B2–B4, C2–C4 are deep cryogenic treated. a) Results for (AISI M2) steel A, b) results for (AISI M3:2) steel B, c) results for (AISI M35) steel C.

B4-DCT = 12.13 ± 1.07 MPa$\sqrt{m}$).

The results of impact toughness for steel C group (AISI M35) are given in Fig. 5 a. In both cases, high or low austenitizing temperature DCT negatively influences on the impact toughness. The values of DCT subgroups are up to 5% lower than for CHT samples (C1-CHT/C2-DCT = 34.38 ± 3.12/33.33 ± 3.61 kJ m ^{2} and C3-CHT/C4-DCT = 41.66 ± 2.94/39.58 ± 2.94 kJ m ^{2}). On the other hand, fracture toughness of steel C is more or less unaffected by the heat treatment, as shown in Fig. 5 b. For all four groups, implementing DCT or not, fracture toughness of steel C (AISI M35) is in the range of 13 MPa$\sqrt{m}$. (C1-CHT 15.43 ± 2.25 MPa$\sqrt{m}$, C2-DCT 14.57 ± 1.64 MPa$\sqrt{m}$, C3-CHT 13.97 ± 0.7 MPa$\sqrt{m}$ and C4-DCT 13.83 ± 1.22 MPa$\sqrt{m}$) It is suggested, that DCT has no or very limited effect on the fracture and impact toughness of steel C, where the effect is being rather negative. The results indicate that the most significantly positive effect of DCT on toughness is obtained for steel A, for steel C is insignificant, while in steel B positive as well as negative effect can be observed, depending preferentially on the heat treatment conditions and fracture mode.

3.2.3. *Compressive strength and strain-hardening exponent*

In Fig. 9, the compressive strength results (black columns) and values of strain-hardening exponent (red squares) are provided for all three steels (A-C).

In Fig. 6 a, results for steel A (AISI M2) are given. In the case of first subgroup (A1-CHT/A2-DCT), DCT has negative effect on the compressive strength (A1-CHT/A2-DCT = 11.38 ± 1.59/9.38 ± 0.84 GPa) and reduces strain-hardening exponent (A1/A2 = 0.47 ± 0.08/0.39 ± 0.03), decreasing it by 18% and 17%, respectively. In the second case (lower austenitizing temperature), DCT has positive effect on the compressive strength, increasing it by 7% (A3-CHT/A4-DCT = 6.67 ± 0.12/7.16 ± 0.42 GPa). On the other hand, strain-hardening exponent remains practically unaffected (2% increase) (n ≈ 0.32) (A3-CHT/A4-DCT 0.32 ± 0/0.33 ± 0.02), especially when taking scattering into account. Similar trends as found for steel A can be observed also for steel B (AISI M3:2), as shown in Fig. 6 b. In B1-CHT/B2-DCT group the values for compressive strength (B1-CHT/B2-DCT = 12.47 ± 0.29/11.58 ± 0.35

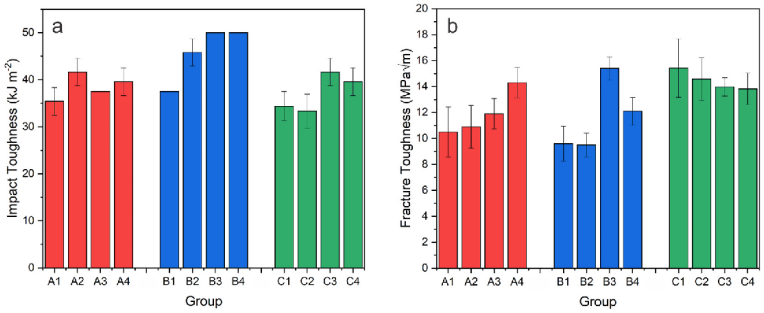

Fig. 5. a) Impact toughness for all 3 steel grades and b) fracture toughness, for all four treatments, where A1-A3, B1–B3, C1–C3 are conventional heat-treated and A2-A4, B2–B4, C2–C4 are deep cryogenic treated.

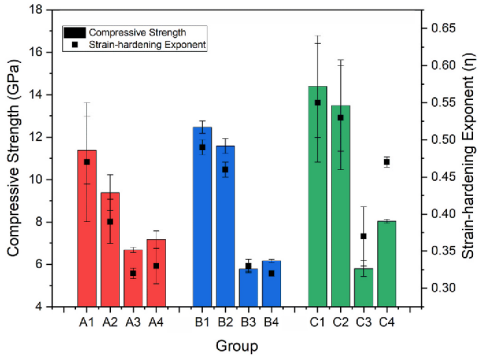

Fig. 6. Compressive strength and strain-hardening exponent for all 3 steel grades (AISI M2, AISI M3.2 and AISI M35), for all four treatments, where A1-A3, B1–B3, C1–C3 are conventional heat-treated and A2-A4, B2–B4, C2–C4 are deep cryogenic treated.

GPa) and strain-hardening exponent (B1-CHT/B2-DCT = 0.49 ± 0.01/0.46 ± 0.01) are decreased by 7% and 6%, respectively. For lower austenitizing temperature and lower hardness group (B3-CHT/B4-DCT), the DCT samples again show approx. 7% higher values of compressive strength (B3-CHT/B4-DCT = 5.78 ± 0.11/6.16 ± 0.08 GPa), while strain-hardening exponent remains at about 0.33 (B3-CHT/B4-DCT = 0.33 ± 0/0.32 ± 0) (↓ 3%). Among the three investigated HSS, C steel (AISI M35) shows the most positive influence of DCT on material strength. In the case of high austenitizing temperature and high hardness (C1-CHT/C2-DCT) both, compressive strength (C1-CHT/C2-DCT = 14.38 ± 2.41/13.49 ± 2.15 GPa) and strain-hardening exponent (C1-CHT/C2-DCT = 0.55 ± 0.08/0.53 ± 0.07) are still decreased (7% and 4%, accordingly) with DCT. However, due to the high SD, the negative influence of DCT can be regarded as insignificant. In the second case, with quenching performed from lower austenitizing temperature (C3-CHT/C4-DCT), the effect of DCT is largely positive. By the implementation of DCT compressive strength (C3-CHT/C4-DCT = 5.81 ± 0.37/8.04 ± 0.09 GPa) is increased by 39% and strain-hardening exponent by 30% (C3-CHT/C4-DCT = 0.37 ± 0.04/0.48 ± 0), greatly improving ductility of the material.

3.2.4. Fatigue resistance

The *k* (fatigue linear slope coefficient) values of steel AISI M2 (A) (Fig. 7 a) for the first subgroups (preferred hardness; A1-CHT/A2-DCT) are 6.36/6.48, respectively. It can be seen, that a 2% increase in the k is obtained after DCT, which suggests that DCT treated AISI M2 steel hardened from the high austenitizing temperature (A2-DCT) has a slightly lower possibility for faster crack propagation and failure, and thus better fatigue life. In this case DCT also improved fatigue limit by 2%, with the fatigue limits for A1-CHT/A2-DCT case being 245/250 MPa, respectively. In the second case of lower austenitizing and higher tempering temperature (promoting toughness; A3-CHT/A4-DCT) the DCT degrades fatigue properties of the AISI M2 steel, thus having negative effect. Fatigue life remains similar (A3-CHT = 7.25/A4-DCT = 7.01) and fatigue limit reduced by 6% (A3-CHT = 265 MPa/A4-DCT = 250 MPa). The number of cycles at high stress level of 350 MPa was for A1-CHT at 7000 cycles, for A2-DCT 8100 cycles, A3-CHT 19400 cycles and for A4-DCT 20000 cycles, respectively. This indicates that the effect of DCT on fatigue response of AISI M2 steel depends also on heat treatment conditions, i.e. austenitizing and tempering temperature. AISI M2 steel hardened from high austenitizing temperature and tempered at lower temperatures has a positive fatigue response, when treated additionally with DCT, whereas the other combination of heat treatment parameters yields a negative influence of DCT.

The fractographic analysis of steel A (Fig. 7 b-e and SM2) indicates that DCT generally promotes a flatter cleavage surface (compare Fig. 7 b with Fig. 7 c and Fig. 7 d with Fig. 7 e), which correlates to the refined martensite structure after DCT. As a result, the crack expansion is also different, at which the cracking is more direct for the CHT samples, whereas for DCT sample the cracks exhibit higher degree of branching. Furthermore, the larger M_6C carbides display cracking, which is more frequently observed for DCT sample. This indicates that the matrix and carbides exhibit higher degree of cohesion after DCT, which allows higher resistance to stress cracking of the matrix through dislocation pinning on carbides. Both facts indicate that the DCT steel A is more resistant to crack propagation, which correlates well with the increased fatigue strength for both sample groups of steel A. For the subgroups A1/A2 the fatigue limit increase is associated with the higher fraction of spherical $M_{23}C_6$ carbides, which relates to the increase to resistance of crack initiation through dislocation agglomeration by stress distribution among a plane of carbides, effectively reducing the local stress concentrations. However, the increased carbide density for A4-DCT for is detrimental to the fatigue limit that results from the different morphology of precipitated $M_{23}C_6$ carbides. As can be seen from the insert of Fig. 7 e, the carbides are more sharp-formed leading to higher local stress concentrations. As a result, the carbides act as nano notches, which allows formation of nanocracks on their orifices that can

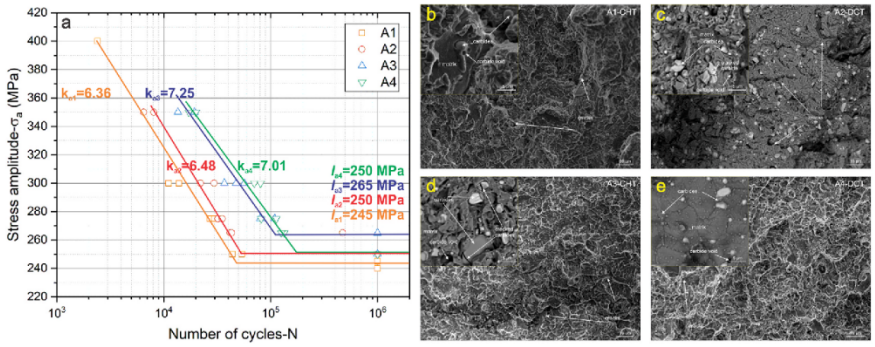

Fig. 7. Fractography of A1-A4 (a–d) and fatigue values of A group of steel AISI M2, where A1/A3 are conventionally heat-treated and A2/A4 are deep cryogenic treated.

interconnect easily due to the high carbide density and growth of cracks over the critical length required for crack propagation through the matrix.

The values of the slope of the linear regression *k* for AISI M3:2 steel (B) (Fig. 8 a) substantially increases for subgroups B1/B2 (by 50%), when combining heat treatment with DCT; B1-CHT/B2-DCT (7.76/11.67), whereas for B3-CHT/B4-DCT (8.21/7.68) it decreases for roughly 7%. Number of cycles at the stress level of 350 MPa decreased from 7500 to 6900 cycles when combining DCT and high austenitizing/low tempering temperature (B1-CHT - > B2-DCT), while it dropped from 40000 to 36000 for the second case (B3-CHT - > B4-DCT). The fatigue limits for the first condition (high austenitizing - low tempering temperature; B1-CHT/B2-DCT) are 295 MPa and 310 MPa, respectively, representing an improvement of about 5%. However, in the second case (low austenitizing – high tempering temperature; B3-CHT/B4-DCT) fatigue limit for AISI M3:2 steel is deteriorated by DCT, dropping from 325 MPa to 310 MPa. To summarize, in the case of AISI M3:2 steel DCT considerably improves fatigue properties of the AISI M3:2 steel, but only when combined with high austenitizing and low tempering temperatures (B2-DCT), i.e. when promoting hardness over toughness.

The fractograms of steel B indicate that steel B displays a finer texture of the cracking surface, which is a result of the generally finer microstructure compared to steel B and C. For subgroups B1/B2, the fractography results indicate similar effects of DCT on cracking as observed for steel A. The DCT sample B2-DCT exhibits more flatter material cleavages, but with higher branching degree, compared to the CHT sample B1-CHT. The higher magnification images (see inserts of Fig. 8 b-c) indicate that the cracking of the matrix-CHT dominates the crack propagation process, at which the ridges around carbides display more plastic-like deformation of the matrix. This indicates a more ductile nature of the matrix, which is associated with higher resistance to cracking initiation and with it improved fatigue limit. In contrast, the subgroups B3/B4 display opposite trend, with the DCT sample B4-DCT (Fig. 8 e) displaying lower ductility of the matrix, which is indicated by the lack of ductile ridges that were found for CHT sample B3-CHT (Fig. 8 d). Additionally, as seen for sample A4-DCT, sample B4-DCT shows also more cuboidal-shaped carbides, which further enhances the crack initiation within the sample. As a result, of all these features, both the resistance against crack initiation as well as propagation is reduced, which is complementary to the fatigue measurements.

For steel C (AISI M35) (Fig. 9 a) DCT has negligible effect on fatigue life (k in the range of 6–7), especially when taking scattering and SD into account. Nevertheless, DCT has a strong positive effect on the fatigue limit and with it on the prolonged life of steel AISI M35. The fatigue limits for the first case (high austenitizing – low tempering temperature; C1-CHT/C2-DCT) are 225/240 MPa, respectively (increased by 6%) and for the second case (low austenitizing – high tempering temperature) 250/280 MPa (12% prolonged fatigue life). Number of cycles at high

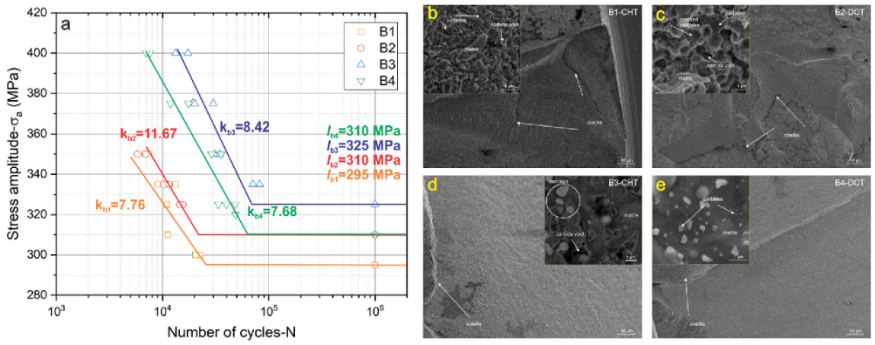

Fig. 8. Fractography of B1–B4 (a–d) and fatigue values of B group of steel AISI M3:2, where B1/B3 are conventional heat-treated and B2/B4 are deep cryogenic treated.

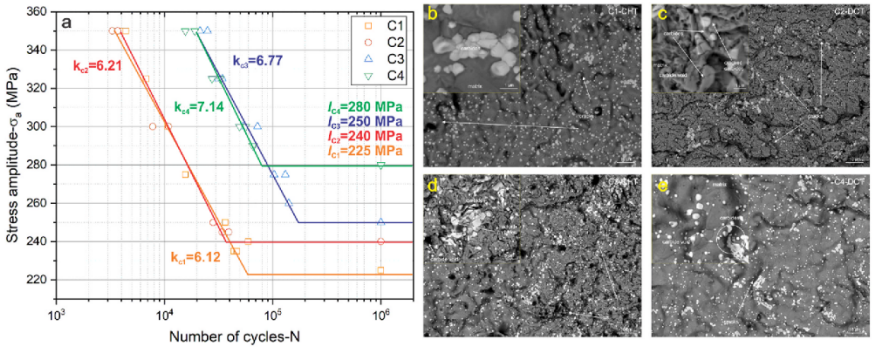

Fig. 9. Fractography of C1–C4 (a–d) and fatigue values of C group of steel AISI M35, where C1/C3 are conventional heat-treated and C2/C4 are deep cryogenic treated.

stress level (350 MPa) for the high harness case (C1/C2) is in the range of 4000 cycles and for the high toughness case (C3/C4) of 20000 cycles. To sum up, DCT has a general positive effect on the fatigue properties of AISI M35 steel and it is the only steel where regardless of the heat treatment parameters DCT gives high fatigue life and improved fatigue limit.

For steel C, the fractographic analysis (Fig. 9 b-e) indicates that the cracking of the material is noticeably similar between CHT and DCT samples for both heat treatment groups. The cracking topography, crack branching and occurrence of cracked carbides is similar for all four samples, indicating that the ductility of the matrix as well as the cohesion of the matrix with carbides did not change with DCT. This also goes well together with the similar fatigue strength behavior of DCT samples compared to their CHT counterparts observed from the fatigue measurements (Fig. 9 e). The significant difference between CHT and DCT samples is the increased density of spherical $M_{23}C_6$ carbides. Similarly, as postulated for steel A4-DCT, the increased number of the small carbides results in a redistribution of the stress concentrations that lead to improved resistance to crack initiation. Since for steel C the denser carbides are spherically shaped for both heat treatment groups, the fatigue limit improves regardless of the selection of heat treatment parameters.

4. Discussion

4.1. Hardness

In selected steels, two different phenomena are observed in relationship to hardness. For the lower austenitization and higher tempering temperature, the preferred state is the increase of hardness by application of DCT. The reason for increase in hardness is related to more effective the change of retained austenite into martensite, as shown in our previous investigations [25,26]. The direct transformation into martensite by crossing the martensite finish temperature with DCT alters the carbide precipitation as the austenite decomposition does not occur with tempering in contrast to CHT samples [31]. As a result, the increased number and density of homogeneously distributed carbides (determined from microstructural analysis by SEM/TEM) that result from the austenite conversion and additional carbide nucleation are additional reasons for the increase of the overall hardness of the material. The decrease of hardness is observed with the heat treatment from the higher austenitizing and lower tempering temperature. The most possible explanation of this phenomenon in observed steels is in the decreased carbon content in the martensitic matrix after DCT leading to reduced solid solution strengthening. The reduced carbon content in the matrix after DCT was proven by microstructure evolution analysis with energy-dispersive X-ray spectroscopy EDS (see SM 1) and XPS. Interesting correlation can be extracted with Co content in HSS. Despite the known fact, that Co can cause decrease in hardness, when present in certain steels, in selected HSS, the Co seems to be advantageous. In Co-containing steels (steel M3:2 (B) and steel M35 (C)) the hardness increased, whereas the steel without Co (steel AISI M2 (A) displayed a proportionally lower hardness increase after DCT in the case of lower austenitization and higher tempering temperature.

4.2. Impact and fracture toughness

Based on the microstructural observations of our previous studies [25,26], the carbide clusters potentially explain the fracture toughness improvement of steel A after DCT regardless of the heat treatment parameters. The clusters or agglomerates are in both cases reduced and are considerably less often found in the DCT samples. The large clusters, resulting from the varying decomposition of M_2C carbides, act as localized weak points that provide the means for sudden local material failure and crack propagation. Similar holds for steel C, however, the clusters are still highly present after DCT, although less in number compared to CHT samples. As a result, the fracture toughness is similar for all samples, but due to the general statistical probability of the clusters being less often present in the crack propagation path, the mean values are in general higher for the DCT samples compared to their CHT counterparts. For PM steel B (AISI M3:2) the clusters are not present and instead the density of carbides and the size of prior austenite grains (PAG) can play an important role, as reported in study by Zheng et al., 2018 [32]. In the case of higher austenitization and lower tempering temperature the number of carbides is lower and the PAG are larger compared to the other heat treatment regime, which results in the lower fracture toughness as the PAG boundaries act as weak points and give way to the crack propagation. For this reason, the fracture toughness is similar for both CHT and DCT samples. In the case of lower austenitization and higher tempering temperature the carbide density is significantly higher and the average PAG size is much smaller, which then increases the fracture toughness. For the case of the DCT treated material, the smaller $M_{23}C_6$ carbides form in significantly larger quantity, which reduces the mean carbide distance significantly. Such a microstructure allows fast bridging and crack propagation through the carbides, resulting in the reduced fracture toughness compared to the CHT variant that correlate to the hardness increase after DCT. The impact toughness is more related to the cohesion and the composition of the

matrix. For all steels, the martensitic laths are smaller for the heat treatment with lower austenitizing temperature and higher tempering temperature compared to the other heat treatment, as clearly shown by our previous investigations [25,26]. For both treatments and all steels, the martensitic laths are generally smaller when the steels are DCT. The refinement of martensitic laths correlates well with the increase of the impact toughness. In the case of steel C (AISI M35), the refinement of laths after DCT is considerably lower compared to steels A (AISI M2) and B (AISI M3:2). This explains the insignificant change in impact toughness after DCT for both heat treatments. The increase of impact toughness is also related to the decreased carbon content (decrease of in average 7–36% regarding to each group) in the martensitic solid solution during deep cryogenic treatment, provided in SM 2. This increases the toughness of the steel matrix and the energy absorption of the matrix. Similar behavior was observed in high-vanadium alloy steel in the study conducted by Li et al., 2016 [33].

4.3. Compressive strength and strain-hardening exponent

The general trend of the compressive strength correlates well with the hardness trend of the steels based on the selected heat treatment and presence of DCT. However, the explanation of compressive strength relation to the DCT effect is considerably more complicated, as this property is influenced by all the microstructural characteristics. For the case of higher austenitization and lower tempering temperature, for steel A (AISI M2) the decrease of the compressive strength is considered to be a result of the decomposition of the M_2C carbides and the increased precipitation of smaller $M_{23}C_6$ carbides. The carbides act as indenting hard particulates that cause local rupture of the material due to their incoherent boundaries and lead to reduced compressive strength. This is further enhanced by the formation of carbides at the PAG boundaries that cause intergranular fracturing and faster material failure. Similarly, the effect is also present for steels B (AISI M3:2) and C (AISI M35) and can be explained in a similar fashion. The difference between the steels is in the presence of carbide clusters, as discussed in previous section. As a result, the SD of the compressive strength is higher for steels A (AISI M2) and C (AISI M35), due to the statistical probability of the inclusion of carbide clusters in the fracturing process. Since, the amount of carbide clusters is lower for both steels after DCT; the SD is narrower for the DCT samples compared to their CHT counterparts. For PM steel B (AISI M3:2), no clusters are present, which results in a significantly narrower SD compared to the other two steels and the SD is similar for DCT and CHT variants. The strain-hardening exponent in this case follows the trend of the compressive strength changes, as the fracturing around the carbides limits the strain-hardening effect of the matrix, despite the matrix being more depleted of alloying elements and in general showing increased toughness. For the heat treatment with lower austenitization temperature and higher tempering temperature, the trend is inverse for all steels that results in an increase of the compressive strength after DCT. The reason for such behavior lies in the much finer microstructure (PAG size, martensite grain size and average carbide size) obtained after the heat treatment that already decreases significantly the compressive strength (due to the increased fraction of interface areas and grain boundaries). However, after DCT the increased precipitation of fine $M_{23}C_6$ carbides takes place. The nucleation and growth of the fine carbides results in the overall increase in the compressive strength of the material, as due to the fine microstructure, the increase in carbide volume increases the overall direct strength of the material and does not significantly increase the critical cracking distance between carbides. An additional contribution to the improvement of compressive strength can be also related to the reduced residual stresses of the steels that has been confirmed in our previous research by Jovičević-Klug et al., 2021 [34]. As a result of the increased fine carbide precipitation, the matrix is depleted of alloying elements and results in the increase of the ductility of the material (see SM 1). However, on the contrary, the increase of carbides still increases the overall stiffness of the material, leading to reduced strain-hardening. These contradicting effects balance out and result in the insignificant change of the strain-hardening exponent for steels A (AISI M2) and B (AISI M3:2). For steel C (AISI M35), the strain-hardening exponent increases after carbide precipitation induced by DCT, since the steel incorporates larger quantities of Co that induces higher ductility of the matrix after depletion with other alloying elements, which was also observed by Gogte et al., 2012 [35].

4.4. Fatigue properties

Overall DCT has positive effect on the fatigue properties (fatigue life and fatigue limit) of HSS if combined with high austenitization temperatures and seeking high hardness levels. Otherwise, DCT shows negative effect, especially in terms of fatigue limit. Exception is high Co-containing steel C (AISI M35), with DCT improving its fatigue limit regardless of the heat treatment parameters. Based on the acquired results, the effect of DCT on the fatigue behavior of HSS is strongly influenced by the steel type and chemical composition, in this specific case Co-content, as well as selected heat treatment parameters: austenitizing and tempering temperature. The change of the heat treatment parameters (Ta, DCT and Tt) influence on the change in the microstructure (carbides size, distribution and number, precipitation of finer $M_{23}C_6$ carbides), which affect the fatigue behavior in HSS. The origin of the incremental changes of the fatigue life for steels A and C originates additionally to the $M_{23}C_6$ carbides also from the presence of M_2C carbides that influence the crack propagation and are detrimental to the fatigue life. Similar conclusion about the influence of carbide clusters and smaller carbides on fatigue properties of HSS has been also observed by Sohar et al., 2009 [36]. For steel C the M_2C carbide clusters are similarly present for CHT and DCT samples (just slightly lower), the k value and fatigue life are practically unaltered by DCT. On the other hand, for steel A, a stronger reduction in the number of clusters is present after DCT, which together with changes in the matrix ductility behavior transcends towards improved fatigue properties. However, due to the increased density of $M_{23}C_6$ carbides by DCT the fatigue life may even get reduced (higher change for group A3-A4 than for A1-A2). As a result of such a counteractive action, the fatigue life increase for group A1-A2 is more pronounced than for group A3-A4. For steel B, representing PM steel type, the M_2C clusters are significantly smaller and present in smaller amount, which reduce their effect on the fatigue life. As a result, the fatigue life of steel B is directly related to the stiffness change (work-hardening discussed in previous section), which has a negative consequence on the fatigue properties, as the cracking is shifted towards more brittle character. The change is thus a result of carbide precipitation, which can be described through hardness and fracture toughness alteration. Increased hardness combined with lower toughness result in deteriorated fatigue life of steel B. The fatigue limit accordingly deteriorates or improves for both steel A and B, depending on the heat treatment parameters selection and morphology of DCT induced precipitated carbides. The trend based on different heat treatment parameters, albeit being similar to the fatigue life, originates from the modification of the martensitic laths through tempering that reduces their stiffness and strength for the case of higher tempering temperature. As a result, the additionally precipitated carbides during DCT act as stress concertation points due to their sharper forms and result in local cracking initialization of the softer yet weaker matrix and lower fatigue limit. In contrast, for lower tempering temperature, the martensitic matrix is sufficiently strong to translate the high stresses and the precipitated carbides have a rounder form resulting in the cracking to originate from the direct flexibility of the system, which is increased with the depletion of the matrix of alloying elements through DCT-induced carbide precipitation. For these steels, the improved fatigue behavior can be also attributed to the increase of MC (VC) particle size after DCT (proved by our previous studies [25,26]), which additionally can cause the decrease of flexural stresses with increased VC carbide size, suggested already by Nakajima et al., 2007 [37]. In

addition to carbide size and increased carbide precipitation after DCT, also the chemical composition of the HSS plays important role in improved fatigue behavior. As it can be observed for steel C (AISI M35), with the highest concentration of Co, the fatigue limit behavior is improved significantly as compared to the other two HSS, with similar observation being made by Warren 2012 [38]. It is postulated that the high Co content allows the formation of the $M_{23}C_6$ carbides in a more limited manner, which in response induces larger carbides with lower density after DCT as compared to steels A and B. The carbides are also more spherical, which reduces the crack initialization possibility near the carbide-matrix interface. As a result, the direct increase of carbides number for steel C increases the ductility of the matrix material and hardens the material without causing a negative impact on the crack initiation probability, which leads to an increase in fatigue life of steel C with DCT for both heat treatment variations.

4.5. Influence of heat treatment parameters on effectiveness of deep cryogenic treatment

Different trends observed in relation to the heat treatment parameters (austenitization and tempering temperatures) indicate that DCT influence on HSS properties is related to the selected processing temperatures.

The dependency of the DCT effectiveness is graphically presented in Fig. 10, indicating the percentile change of individual steel properties after DCT, with the CHT state set as a reference value. The results clearly indicate that DCT provides a general positive effect on HSS properties in the case of lower austenitization temperature and higher tempering temperature (except for fatigue behavior for A and B steel, which have no or very low content of Co). The positive effect of DCT for this heat treatment mainly originates from the increased carbide precipitation and the refinement of the martensitic lath structure and depletion of martensitic matrix of alloying elements, described in detail in our previous study [25]. On the contrary, DCT has a negative effect on the hardness, compressive strength and strain-hardening exponent, when the higher austenitization temperature and lower tempering temperature is selected. The main reason for such a change lies in the carbon and alloying elements depletion of the matrix that is a consequence of the increased carbide precipitation [25]. However, as a result of the same

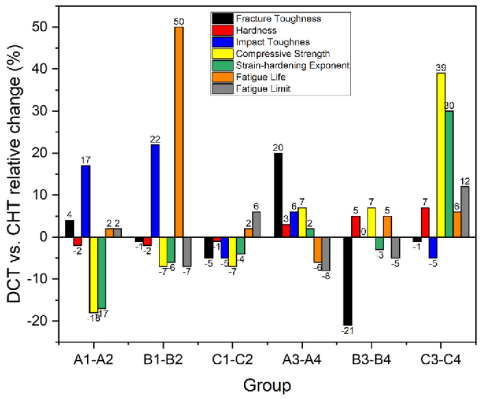

Fig. 10. Change in mechanical properties (y-axis) of HSS groups (x-axis) with the inclusion of DCT as compared to the conventional heat treatment (CHT), left side groups with high austenitization/low tempering temperature (CHT-A1, B1, C1; DCT-A2, B2, C2). Right side groups with low austenitization/high tempering temperature (CHT-A3, B3, C3; DCT-A4, B4, C4).

change of microstructural features, the fracture and impact toughness of selected steels is generally increased, which is also heavily related to the decomposition of M_2C carbides and reduction of carbide clusters, being related to properties of wrought steels A and C. This is also the reason for lower amount of M_2C carbides and other carbide dynamic being observed in steel B. Obtained results clearly indicate that DCT has higher impact on wrought steels than on PM steels (steel B), as has also been observed in other studies [20].

5. Conclusions

In high-speed steels AISI M2, AISI M3:2 and AISI M35, DCT promotes more homogeneous microstructure with more intense precipitation of carbides (up to 40%). As shown previously, it also induces formation of finer martensitic laths and carbides. The modification of the microstructure can be directly related to the modified properties of HSS steels under different heat treatment conditions. For the selected HSS, DCT in general has a positive effect on the selected steel properties (toughness, hardness, fatigue resistance, compressive strength and strain hardening exponent), when combined with heat treatment from low austenitizing and high tempering temperatures. However, compressive strength, hardness and strain-hardening exponent are deteriorated when combined with high austenitizing and low tempering temperatures, whereas the impact toughness and fatigue resistance generally improve with DCT. The main reason for increased hardness and strength in the heat treatment with higher austenitization and lower tempering temperature in DCT subgroups, is in the increased number of precipitated carbides, while increase in toughness and fatigue resistance can be correlated to the depleted carbon content and higher plasticity of the finer martensitic matrix. The strain-hardening exponent is modified by DCT in a limited manner, as the increased carbide precipitation and the depletion of the matrix of alloying elements create a counteracting effect, resulting in minimal changes of strain-hardening exponent. However, in the case of AISI M35 steel, the high Co content promotes the carbide precipitation, resulting in improved strain-hardening exponent. For the second heat treatment subgroups with lower austenitization and higher tempering temperature and with application of DCT, the reduction of hardness, fatigue resistance and strength are related to the depletion of carbon and other alloying elements content in the matrix that results in the reduced solid-solution strengthening of the matrix. In response the fracture toughness increases, whereas the impact toughness generally improves due to the refined martensite lath structure. To conclude, DCT can be a useful tool for the improvement of mechanical properties of high-speed steels. However, the effect and level of improvement obtained by DCT greatly depends on the composition and type of steel as well as heat treatment parameters, i.e. austenitizing and tempering temperature, with lower austenitizing and higher tempering temperatures in general resulting in improved properties.

Funding

This work was supports by Slovenian Research Agency (ARRS) [J2-9211 and P2-0050].

Data availability

The raw/processed data required to reproduce these findings cannot be shared at this time as the data also forms part of an ongoing study.

CRediT authorship contribution statement

Patricia Jovičević-Klug: Investigation, Visualization, Conceptualization, Writing – original draft, Writing – review & editing. **Gašper Puš:** Visualization, Writing – original draft. **Matic Jovičević-Klug:** Investigation, Visualization, Writing – review & editing. **Borut Žužek:** Visualization, Writing – review & editing. **Bojan Podgornik:**

Conceptualization, Supervision, Writing – review & editing.

Declaration of competing interest

The authors declare that they have no known competing financial interests or personal relationships that could have appeared to influence the work reported in this paper.

Acknowledgements

Authors would like to thank IMT colleagues Branko Zvonar for the help with heat treatments and Nataša Lipovšek for metallographic preparation of samples.

Appendix A. Supplementary data

Supplementary data to this article can be found online at https://doi.org/10.1016/j.msea.2021.142157.

References

[1] P. Jovičević-Klug, B. Podgornik, Review on the effect of deep cryogenic treatment of metallic materials in automotive applications, Metals 10 (2020) 434, https://doi.org/10.3390/met10040434.
[2] D. Senthilkumar, Cryogenic treatment:shallow and deep, in: G.E. Totten, R. Colas (Eds.), Encyclopedia of Iron, Steel, and Their Alloys, Taylor and Francis, NY, USA, New York, NY, 2016, pp. 995–1007, https://doi.org/10.1081/E-EISA-120052805.
[3] P. Baldissera, C. Delprete, Deep cryogenic treatment: a bibliographic review, Open Mech. Eng. J. 2 (2008) 1–11, https://doi.org/10.2174/1874155X00802010001.
[4] S. Paul, A.B. Chattopadhyay, Environmentally conscious machining and grinding with cryogenic cooling, Mach. Sci. Technol. 10 (2007) 87–131.
[5] J.N. Jones, C.B. Rogers, The acoustic effect of cryogenically treating, J. Acoust. Soc. Am. 114 (2013) 2349.
[6] N. Govindaraju, A.L. Shakeel, M. Pradeep Kumar, Experimental investigations on cryogenic cooling in the drilling of AISI 1045 steel, Mater. Manuf. Process. 29 (2014) 1417–1421.
[7] D. Senthilkumar, I. Rajendran, Optimization of Deep Cryogenic Treatment to Reduce Wear Loss of 4140 Steel, Materials and Manufacturing Processes, 2012, https://doi.org/10.1080/10426914.2011.593237.
[8] M. Pellizzari, A. Molinari, L. Girardini, L. Maldarelli, Deep cryogenic treatment of AISI M2 high-speed steel, Int. J. Microstruct. Mater. Prop. 3 (2008) 383–390, https://doi.org/10.1504/IJMMP.2008.018742.
[9] S.Q. Zheng, X. Bai, S.H. Li, J.X. Liang, K.Y. Zhao, Influence of cryogenic treatment on the microstructure and reversed austenite in super martensitic stainless steel, J. Iron Steel Res. 27 (2015) 63–67, https://doi.org/10.13228/j.boyuan.issn1001-0963.20150171.
[10] S. Zhirafar, A. Rezaeian, M. Pugh, Effect of cryogenic treatment on the mechanical properties of 4340 steel, J. Mater. Process. Technol. (2007), https://doi.org/10.1016/j.jmatprotec.2006.12.046.
[11] P. Jovičević-Klug, B. Podgornik, Comparative study of conventional and deep cryogenic treatment of AISI M3:2 (EN 1.3395) high-speed steel, J. Mater. Res. Technol. 9 (2020) 13118–13127, https://doi.org/10.1016/j.jmrt.2020.09.071.
[12] A. Ciski, T. Babul, M. Duchek, Sub-zero treatments of case-carburized 18CrNiMo7-6 steel, in: 9th Youth Symposium on Experimental Solid Mechanics, 2010, pp. 108–111.
[13] G. Hoyle, High Speed Steels, Butterworths, University of Michigan, 1988. https://books.google.si/books/about/High_Speed_Steels.html?id=qOJTAAAAMAAJ&redir_esc=y. (Accessed 15 March 2021).
[14] B. Podgornik, I. Paulin, B. Zajec, S. Jacobson, V. Leskovšek, Deep cryogenic treatment of tool steels, J. Mater. Process. Technol. 229 (2016) 398–406, https://doi.org/10.1016/j.jmatprotec.2015.09.045.
[15] F.J. da Silva, S.D. Franco, Á.R. Machado, E.O. Ezugwu, A.M. Souza, Performance of cryogenically treated HSS tools, Wear 261 (2006) 674–685, https://doi.org/10.1016/j.wear.2006.01.017.
[16] M. Pellizzari, D. Caliskanoglu, A. Fernández, J.I. Barbero, B. Pena, T. Uemit, R. Pizarro Sanz, R. Elvira Eguizabal, L.A. Alava, Influence of different deep cryogenic treatment routes on the properties of high speed steel, HTM J. Heat Treat. Mater. 67 (2012) 111–117.
[17] C. Gogte, D. Peshwe, A. Likhite, S. Lomte, On the mechanism of the effect of the cryogenic treatment on high speed steels, Adv. Mater. Res. (2011). https://doi.org/10.4028/www.scientific.net/AMR.383-390.7138.
[18] V. Leskovšek, M. Kalin, J. Vižintin, Influence of deep-cryogenic treatment on wear resistance of vacuum heat-treated HSS, Vacuum 80 (2006) 507–518, https://doi.org/10.1016/j.vacuum.2005.08.023.
[19] S.S. Gill, J. Singh, R. Singh, H. Singh, Effect of cryogenic treatment on AISI M2 high speed steel: metallurgical and mechanical characterization, J. Mater. Eng. Perform. 21 (2012) 1320–1326, https://doi.org/10.1007/s11665-011-0032-z.
[20] M. Pellizzari, Influence of deep cryogenic treatment on the properties of conventional and PM high speed steels, Metallurgia Italiana 100 (2008) 17–22.
[21] R. Sola, R. Giovanardi, G. Parigi, P. Veronesi, A novel methods for fracture toughness evaluation of tool steels with post-tempering cryogenic treatment, Metals 7 (2017) 75, https://doi.org/10.3390/met7030075.
[22] D.G. Fantineli, C.T. Parcianello, T.S. Rosendo, A. Reguly, M.D. Tier, Effect of heat and cryogenic treatment on wear and toughness of HSS AISI M2, J. Mater. Res. Technol. 9 (2020) 12354–12363, https://doi.org/10.1016/j.jmrt.2020.08.090.
[23] D. Candane, Effect of cryogenic treatment on microstructure and wear characteristics of AISI M35 HSS, Int. J. Mater. Sci. Appl. 2 (2013) 60, https://doi.org/10.11648/j.ijmsa.20130202.14.
[24] J. Jeleńkowski, A. Ciski, T. Babul, Effect of deep cryogenic treatment on substructure of HS6-5-2 high speed steel, J. Achiev. Mater. Manuf. Eng. 43 (2010) 80–87.
[25] P. Jovičević-Klug, M. Jovičević-Klug, B. Podgornik, Effectiveness of deep cryogenic treatment on carbide precipitation, J. Mater. Res. Technol. 9 (2020) 13014–13026, https://doi.org/10.1016/j.jmrt.2020.09.063.
[26] P. Jovićević-Klug, M. Jenko, M. Jovićević-Klug, B. Šetina Batič, J. Kovač, B. Podgornik, Effect of deep cryogenic treatment on surface chemistry and microstructure of selected high-speed steels, Appl. Surf. Sci. 548 (2021) 1–11.
[27] B. Podgornik, G. Puš, B. Žužek, V. Leskovšek, M. Godec, Heat treatment optimization and properties correlation for H11-type hot-work tool steel, Metall. Mater. Trans. 49 (2018) 455–462, https://doi.org/10.1007/s11661-017-4430-1.
[28] H.M. Rietveld, A profile refinement method for nuclear and magnetic structures, J. Appl. Crystallogr. 2 (1969) 65–71, https://doi.org/10.1107/s0021889869006558.
[29] H. Toraya, A new method for quantitative phase analysis using X-ray powder diffraction: direct derivation of weight fractions from observed integrated intensities and chemical compositions of individual phases, J. Appl. Crystallogr. 49 (2016) 1508–1516, https://doi.org/10.1107/S1600576716010451.
[30] B. Podgornik, B. Žužek, V. Leskovšek, Experimental evaluation of tool steel fracture toughness using circumferentially notched and precracked tension bar specimen, Mater. Perform. Char. 3 (2014) 87–103.
[31] P. Jovićević-Klug, M. Jovićević-Klug, T. Sever, D. Feizpour, B. Podgornik, Impact of steel type, composition and heat treatment parameters on effectiveness of deep cryogenic treatment, J. Mater. Res. Technol. (2021) 1–23, in progres.
[32] Y. Zheng, F. Wang, C. Li, Y. Li, J. Cheng, R. Cao, Effect of microstructure and precipitates on mechanical properties of Cr–Mo–V alloy steel with different austenitizing temperatures, ISIJ Int. 58 (2018) 1126–1135, https://doi.org/10.2355/isijinternational.ISIJINT-2017-531.
[33] H. Li, W. Tong, J. Cui, H. Zhang, L. Chen, L. Zuo, The influence of deep cryogenic treatment on the properties of high-vanadium alloy steel, Mater. Sci. Eng. 662 (2016) 356–362, https://doi.org/10.1016/j.msea.2016.03.039.
[34] M. Jovičević-Klug, P. Jovičević-Klug, J. McCord, B. Podgornik, Investigation of microstructural attributes of steel surfaces through magneto-optical Kerr effect, J. Mater. Res. Technol. 11 (2021) 1245–1259.
[35] C.L. Gogte, D.R. Peshwe, R.K. Paretkar, Influence of cobalt on the cryogenically treated W-Mo-V high speed steel, in: Advances in Cryogenic Engineering, Spokane, WA, USA, 2012, pp. 1175–1182, https://doi.org/10.1063/1.4707039.
[36] C.R. Sohar, A. Betzwar-Kotas, C. Gierl, B. Weiss, H. Danninger, Fatigue behaviour of M2 and M42 high speed steel up to the gigacycle regime, Kovove Mater. 47 (2009) 147–158.
[37] T. Nakajima, H. Hosokawa, K. Shimojima, Influence of cobalt content on the fatigue strength of WC-Co hardmetals, Mater. Sci. Forum 534–536 (2007) 1201–1204. https://doi.org/10.4028/www.scientific.net/msf.534-536.1201.
[38] W.M. Garrison, Cobalt and the toughness of steel, in: Materials Science Forum, Trans Tech Publications Ltd, 2012, pp. 3–10. https://doi.org/10.4028/www.scientific.net/MSF.710.3.

3.2 Friction, Wear Resistance and Galling

The purpose of this subchapter is to provide and test DCT as a new affordable and noncomplex approach to improve friction properties, sliding and impact wear resistance and galling resistance of HSS. This study is also continuing research of the DCT investigation, where different properties are tested in order to provide systematic research of DCT. Testing of steels was performed under dry sliding conditions in order to focus solely on the change of materials properties and induced mechanisms of DCT. The tribology testing involved different contact type, prevailing wear mechanisms (abrasion, adhesion and mix of both of them) and loading conditions (low to high stress conditions). The results also confirm observations from previous studies that DCT does not only affect the microstructure, mechanical properties and fatigue, but also the friction, wear resistance and galling properties. The DCT effect on friction, wear resistance and galling depends on the HSS type (wrought/PM) and chemical composition, final microstructure and heat treatment parameters, as well as contact conditions and wear mode. Generally, DCT improves the dynamic impact wear and galling resistance. This again suggests that DCT is a complex mechanism, which can have, with the same heat treatment parameters and same testing conditions, a different effect. This also indicates that more research is needed for understanding the DCT mechanism for proposed application in various industries.

Brief discussion: The testing of friction, wear resistance (sliding wear resistance and dynamic impact wear) and galling in correlation to DCT showed complex dependencies on both material as well as testing conditions. The improvement of sliding wear resistance is contributed to the increased precipitation of finer carbides $M_{23}C_6$ and with this also the overall hardening of the material, resulting in increased hardness and toughness. However, in terms of abrasive wear resistance, DCT improves it up to 75 % for lower hardness and higher toughness state of the material under high sliding conditions. Whereas for low-speed conditions, the effect is opposite by increasing the wear rate up to 10 %. The improvement is associated with the softer matrix and higher precipitation of carbides. With high sliding speeds, the increased toughness promotes localized deformation of the softened matrix material (high contact temperatures), which in return causes the displacement of the carbides on the contact surface. This forms a densely populated carbide layer deeper within the matrix, which protects the matrix from further nominal friction forces and wear. This effect strongly depends on the size and shape of carbides. For friction results, DCT has no significant effect under abrasive conditions. Under conditions favoring adhesion, DCT has an evidently positive effect, resulting from the more homogenous microstructure, precipitation of finer carbides and solid solution hardened with Co. These modifications allow the reduced adhesion on a macro scale, which is indicated by the 25 % decrease of the friction coefficient. In the case of a mixture of abrasive and adhesive wear, DCT generally improves the combined abrasive/adhesive wear resistance of HSS, when the high hardness case is investigated (up to 90 % improvement). The overall negative effect under lower hardness conditions is attributed to the tougher matrix, which may lead to the sticking and tearing of the matrix and with it microcracking of the HSS. This exposes the carbides, which can act as abrasive third-body particles on the material itself, as well as causes further microploughing and microcracking. The improvement of impact wear is strongly correlated to the increased volumetric amount and more homogeneous distribution of $M_{23}C_6$ carbides induced by DCT. Additionally, DCT also generally improves the galling resistance, leading to an improvement of up to 50 %. The positive influence is a result of the more refined microstructure and higher amount of carbides compared to CHT counterparts, which creates a more durable and homogeneous surface that strongly resists the adhesion and agglomeration of the counter body material.

The ***author's contribution***, as the first author, to the **paper *Effect of Deep Cryogenic Treatment on Wear and Galling Properties of High-Speed Steels*** published in Materials was: conceptualization, investigation, planning of experiments, visualization, evaluation and writing (original draft and editing).

This subchapter addresses thesis ***Hypotheses 1, 2 and partly 3***.

materials

MDPI

Article

Effect of Deep Cryogenic Treatment on Wear and Galling Properties of High-Speed Steels

Patricia Jovičević-Klug [1,2,*], Marko Sedlaček [2], Matic Jovičević-Klug [3] and Bojan Podgornik [1,2]

[1] Institute of Metals and Technology, Lepi pot 11, 1000 Ljubljana, Slovenia; bojan.podgornik@imt.si
[2] Jožef Stefan International Postgraduate School, Jamova cesta 39, 1000 Ljubljana, Slovenia; marko.sedlacek@imt.si
[3] Max-Planck-Institute für Eisenforschung, Max-Planck-Straße 1, 40237 Düsseldorf, Germany; m.jovicevic-klug@mpie.de
* Correspondence: patricia.jovicevicklug@imt.si; Tel.: +386-1-4701-990

Abstract: New approaches to improving wear resistance with an affordable and noncomplex technology, such as deep cryogenic treatment, (DCT0), are receiving attention. The aim of this study is to investigate the effect of DCT on the friction and wear performance of high-speed steels. AISI M2, AISI M3:2 and AISI M35 were heat-treated under different conditions, and then investigated under dry sliding conditions. Tribological testing involved different contact conditions, prevailing wear mechanisms and loading conditions. The DCT effect on sliding wear resistance depends on HSS steel grade, as well as contact conditions and wear mode, whereas it improves the dynamic impact of the wear and galling resistance.

Keywords: deep cryogenic treatment; high speed steel; wear; galling; impact loading

Citation: Jovičević-Klug, P.; Sedlaček, M.; Jovičević-Klug, M.; Podgornik, B. Effect of Deep Cryogenic Treatment on Wear and Galling Properties of High-Speed Steels. *Materials* **2021**, *14*, 7561. https://doi.org/10.3390/ma14247561

Academic Editor: Andrzej Dzierwa

Received: 17 November 2021
Accepted: 8 December 2021
Published: 9 December 2021

1. Introduction

In tool industry high-speed steels (HSS), such as AISI M2; AISI M4 and AISI M42, are most commonly used for cutting tools (saw blades, knives, drill bits, etc.). HSS are preferred materials for cutting tools, as they have a high hardness (above 60 HRC), high wear resistance and high thermal resistance [1]. The tool's performance is determined not only by the material's intrinsic properties, but also by the surface properties, including friction, abrasive and adhesive wear resistance, galling resistance and resistance to mechanical and thermal cracking, i.e., fatigue. In addition, tools can be exposed to very demanding and complex loading conditions (chemical, mechanical, thermal, tribological, etc.). As a consequence, different approaches to improving tool properties and increasing tool performance for a prolonged lifecycle are applied, such as heat treatment, thermo-chemical treatments, surface texturing and coatings [1].

The easiest way to manipulate steel properties and performance is to change the heat treatment parameters (austenitizing and tempering temperature, quenching speed, etc.) to induce microstructural changes and, in turn, the mechanical, tribological and corrosion properties of the processed steel [2]. Another method for modifying the microstructure is the introduction of additional processing of the material, such as deep cryogenic treatment (DCT). DCT is used as a supplementary processing method and was proven to be effective in prolonging tool life by changing the material's mechanical properties (hardness, fracture toughness, compressive and tensile strength, impact toughness, etc.) [3]. During DCT, the material is exposed for certain time to temperatures below −160 °C, which influences the microstructure development. In steels, it induces more homogenous carbides distribution, a higher precipitation of carbides and matrix change (increased amount of martensite and reduction in retained austenite) [4]. However, DCT performance is dependent on the selected soaking temperature, soaking time, cooling and heating rate and placement of DCT within the heat treatment process (before or after tempering) [5].

The literature review on DCT-treated HSS in relation to tribological properties, including wear resistance, showed that the majority of studies concentrated on AISI M2, as the most commonly used HSS. Leskovšek et al., 2006 [6], Pellizzari et al., 2008 and 2012 [7–9], Fantineli et al., 2020 [10] and Zhou et al., 2020 [11] clearly stated that DCT has a positive effect on the abrasive wear resistance of AISI M2 steel, whereas studies on other HSS are rather limited and show contradictory results in terms of wear resistance change after DCT. This is proposed to be a consequence of different microstructural changes (carbide precipitation, carbide distribution and characteristics of the matrix), which then influences the material's mechanical and tribological properties [6–9]. Nevertheless, most cases indicate DCT to have a positive effect [4,12,13]; some negative effects on wear resistance were also reported [8]. Most of the research is focused on abrasive wear resistance, while resistance to adhesive wear, galling and dynamic impact wear has rarely been investigated, not only in connection to DCT, but also more generally in connection to selected HSS. Furthermore, it is known that steel type, composition and heat treatment conditions all determine the impact and effectiveness of DCT on changes in microstructure, which consequently influences the changes in the materials' properties [7,14–16]. To overcome the contradictory results and to acquire a clear understanding of DCT impact on HSS wear and tribological properties, testing results must be correlated to microstructural changes induced by DCT.

For the above reasons, the aim of this study is (1) to explore the effect of deep cryogenic treatment (DCT) on the wear and galling resistance of three different high-speed steels of the same type (Mo-type), but with a different ratio of alloying elements (C, V, Co) that are manufactured by different manufacturing technologies (wrought/powder-metallurgy (P/M)). The next aim is (2) to test the influence of the chemical composition of HSS in relation to different heat treatments (higher/lower austenitization temperature and lower/higher tempering temperature) and how this reflects on the tribological properties. (3) In order to provide deeper understanding of the DCT mechanism on wear and galling resistance, testing under different contact and loading conditions to provoke different wear mechanisms was performed and evaluated.

2. Materials and Methods

2.1. Materials and Heat Treatment

All three high-speed steels, AISI M2 (M.N. 1.3343, EN HS6-5-2, wrought steel), AISI M3:2 (M.N. 1.3395, EN HS6-5-3, P/M steel) and AISI M35 (M.N. 1.3243, EN HS6-5-2-5, wrought steel), were obtained in the form of rolled, peeled and soft annealed rods, from the following producers: Sij Ravne, Ravne, Slovenia (AISI M2 and AISI M35) and HSM, Georgensgmuend, Germany (AISI M3:2). Samples for specific testing were then machined from these rods: abrasive/adhesive wear and dynamic impact wear test discs (Ø 20.0 × 8.0 mm), and test cylinders for galling tests (Ø 10.5 × 100.0 mm). After heat treatment all samples were also surface polished down to Ra = 0.05 µm (the surface roughness was the same for both heat treatments regimes and for all three steel grades), and then subjected to heat treatment. The measured chemical composition and selected mechanical properties of each steel grade is provided in Table 1.

Table 1. Measured chemical composition of AISI M2, AISI M3:2 and AISI M35 steel (wt. %). Analyzed values measured with ICP-OES Agilent 720.

Steel (AISI)	C	Mn	S	Cr	Mo	W	V	Co	Fe
M2	0.90	0.28	0.002	4.00	4.70	6.00	1.70	-	base
M3:2	1.29	0.31	0.006	3.90	4.80	6.75	3.00	0.69	base
M35	0.90	0.34	0.004	4.10	5.20	6.20	2.01	4.50	base

For all three steel grades, two sets of heat treatment parameters were used to evaluate the effect of selected austenitizing/tempering temperatures. First set of specimens (A1–A2, B1–B2, C1–C2) was hardened at upper austenitizing temperature, as recommended by the steel producer, and then tempered at lower temperature in order to promote higher

hardness over toughness. The second set (A3–A4, B3–B4, C3–C4) was hardened at lower austenitizing temperature and tempered at higher tempering temperature, therefore promoting a higher toughness over hardness. Each set from the individual steel group was austenitized and quenched in a single step in a horizontal vacuum furnace Ipsen VTTC324-R. Quenching was performed with N_2 gas at a pressure of 5 bars with an average quenching rate of 7–8 °C/s. After hardening, one group of specimens from each steel and heat treatment set was conventionally heat-treated (CHT) (A1, A3, B1, B3, C1, C3) (control group), comprising of triple tempering according to a steel producer recommendation. The second group was subjected to DCT, which was performed immediately after quenching by gradual immersion (approximate cooling rate of 10 °C/s) of the samples (A2, A4, B2, B4, C2, C4) in liquid nitrogen for 24 h, followed by a single tempering cycle. Heat treatment parameters of each set are given in Table 2.

Table 2. Heat treatment of AISI M2, AISI M3:2 and AISI M35 steel samples, where samples 1 and 3, marked as CHT samples, were conventionally heat-treated, and samples 2 and 4, marked as DCT samples, were deep cryogenic heat-treated. In addition to heat treatment parameters, hardness (HRC), fracture toughness (KIc; MPa$\sqrt{m}$) and impact toughness (KV; J) are provided for each sample subgroup [17].

Steel (AISI)	Subgroup	Austenitizing (°C/min)	DCT (°C/h)	Tempering (°C/h)	HRC	K_{Ic} * (MPa$\sqrt{m}$)	KV ** (J)
M2 (A)	A1-CHT (A1)	1230/2	-	3x 550/1	66	10	3
	A2-DCT (A2)	1230/2	−196/24	1x 550/1	65	11	3
	A3-CHT (A3)	1180/2	-	3x 620/1	58	12	3
	A4-DCT (A4)	1180/2	−196/24	1x 620/1	60	14	3
M3:2 (B)	B1-CHT (B1)	1180/2	-	3x 540/2	66	10	3
	B2-DCT (B2)	1180/2	−196/24	1x 540/2	65	10	4
	B3-CHT (B3)	1050/2	-	3x 600/2	53	15	4
	B4-DCT (B4)	1050/2	−196/24	1x 600/2	56	12	4
M35 (C)	C1-CHT (C1)	1230/2	-	3x 550/2	66	13	3
	C2-DCT (C2)	1230/2	−196/24	1x 550/2	65	13	4
	C3-CHT (C3)	1160/2	-	3x 620/2	53	13	3
	C4-DCT (C4)	1160/2	−196/24	1x 620/2	57	13	3

* measured by circumferentially notched and fatigue pre-cracked tensile bar specimen [18], ** measured by Charpy V-notch impact test.

2.2. *Testing Methods*

2.2.1. Reciprocating Sliding Tests

Abrasive/adhesive wear resistance and coefficient of friction were determined under reciprocating dry sliding conditions using ball-on-flat contact configuration (Figure 1a) with a stroke length of 4 mm. The testing was performed with 3 different wear mechanism conditions typically found in cutting by utilizing different counter bodies (all of the same size; Ø 20 mm): Al_2O_3 (~1750 HV), favoring abrasive wear; AISI 52100 (100Cr6; ~700 HV) favoring a combination of abrasive/adhesive wear; and AISI 304L (~300 HV), favoring pure adhesive wear. Four different loading conditions were applied, using two loads and two sliding speeds (high sliding speed/high load, low sliding speed/high load, high sliding speed/low load and low sliding speed/low load). High-load conditions corresponded to contact pressure of 1.5 GPa (Al_2O_3 ball) and 1.0 GPa (AISI 52100 and 304L ball), obtained by applying load of 102 N and 40 N, respectively. Whereas for low load conditions, contact pressures of 1.0 GPa (Al_2O_3) and 0.8 GPa (AISI 52100 and 304L) were achieved with the application of a load of 40 N and 20 N, respectively. The high sliding speed of 0.12 m/s was achieved at a frequency of 15 Hz and the low sliding speed of 0.01 m/s at frequency of 1 Hz. The summary of all conditions is presented in Table 3. Dry sliding wear and friction tests were performed at room conditions, with a total sliding time and distance of 7500 s/60 m (low sliding speed) and 1667 s/200 m (high sliding speed). The measurements were performed at least 3 times for each condition and sample group.

Table 3. Sliding conditions.

Sliding Condition	Speed (m/s)	Contact Pressure (GPa)
Condition 1 (Al_2O_3/AISI 52100/AISI 304L)	0.12	102/40/40
Condition 2 (Al_2O_3/AISI 52100/AISI 304L)	0.01	102/40/40
Condition 3 (Al_2O_3/AISI 52100/AISI 304L)	0.12	30/20/20
Condition 4 (Al_2O_3/AISI 52100/AISI 304L)	0.01	30/20/20

The wear volume of the HSS disc samples was measured using 3D confocal focus variation microscope (Alicona InfiniteFocus, Raaba/Graz, Austria) and the specific wear rate [19] was calculated afterwards based on Equation (1), where W is wear volume in mm^3, F_N is normal load in N, and S is sliding distance in m:

$$k = \frac{W}{F_N \times S} \left[\frac{mm^3}{Nm}\right] \quad (1)$$

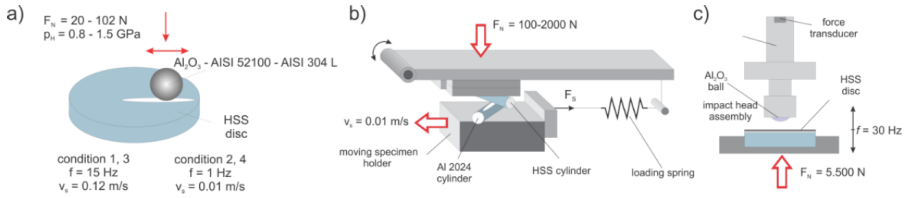

Figure 1. Schematic representation of different testing methods. (**a**) Reciprocating sliding: ball-on-flat contact configuration. (**b**) Cross-cylinder galling test. (**c**) Dynamic impact wear testing.

The wear scars were also investigated with scanning electron microscope (SEM; JSM-6500F, Jeol, Tokyo, Japan), to identify/confirm prevailing wear mechanisms and wear related failures and defects. Coefficient of friction (COF) was recorded continuously during sliding, and then the average value for the steady–state conditions (800–1666 s for sliding speed of 0.12 m/s and 500–7500 s for sliding speed of 0.01 m/s) was determined for all three counter-body conditions.

2.2.2. Galling

The effect of material resistance against galling, defined as an accumulation of work material on the tool surface and commonly observed in forming operations such as deep drawing and extrusion, was evaluated under progressively increasing loading conditions by a cross-cylinder load-scanning test rig (Figure 1b) [17], thus simulating metal forming. Al2024 cylinders in a T6 condition (Ø10 mm × 100 mm; 155 HB) were used as a moving counter-body, representing one of many very difficult materials in cold form. All Al specimens were polished and cleaned with ethanol to achieve clean and equal surface condition (Ra = 0.1 µm) for all tests. Galling tests, repeated three times for each tool steel specimens group, were performed dry, using sliding speed of 0.01 m/s and normal load from 100 N to 2000 N, resulting in severe plastic deformation of the Al cylinder during testing. For determining the critical loads for galling initiation and gross galling (transfer layer) formation, the wear tracks after sliding were analyzed using 3D confocal focus variation microscope (Alicona InfiniteFocus, Raaba/Graz, Austria) at specific loading regions, which were selected based on the coefficient of friction evolution during sliding [20]. All friction data were processed with the LOESS (locally weighted smoothing) method with a 0.06-point span.

2.2.3. Dynamic Impact Wear

In order to investigate the dynamic impact wear properties, servo-hydraulic dynamic testing machine Instron 8802, Norwood, MA-USA was used. Tests were performed in such a way that the HSS disc samples were constantly impacted against a static alumina ball (Al_2O_3) at an impact frequency of 30 Hz (Figure 1c). Test was regulated through the monitoring of the impact force, which varied in a sinusoidal form with a compressive force peak of 5.5 kN, and corresponded to a contact pressure of 3.5 GPa. At maximum displacement amplitude, the ball and the test sample were completely separated with a 0.5 mm gap. Tests were limited to 300,000 cycles and performed at normal room conditions ($T = 23 \pm 3$ °C; $RH = 50 \pm 10\%$). In order to prevent adhesion of wear debris to the ball, the steel disc contact surface was lubricated with lithium grease before the experiment. For each specimen, the test was repeated at least three times and for each test a fresh Ø 32 mm Al_2O_3 ball was used. After testing, the wear volume of the steel sample was measured using 3D confocal focus variation microscope (Alicona InfiniteFocus, Raaba/Graz, Austria).

2.2.4. Microstructure of Selected High-Speed Steels

Microstructure analysis and explanation of the possible mechanism related to microstructure of all three HSS (AISI M2, AISI M3:2 and AISI M35) is based on our previous studies by Jovičević-Klug et al., 2020 [16] and Jovičević-Klug et al., 2021 [21]. The main finding of microstructure analysis of all three HSS showed that the matrix is lath martensite, whereas retained austenite (RA) was found in all three cases < 1 vol. %. The carbides present in all three steels, independent of the heat treatment regimens, are MC (M = V), M_6C (Mo, W, Fe), M_2C (Mo, V, W) and $M_{23}C_6$ (Cr, Fe). DCT increases the precipitation of carbides, induces the size reduction in carbides, and reduces amount of RA; martensitic laths are smaller and have preferable orientated along [101] and [001] directions, and oxidation state of DCT samples is changed.

3. Results

3.1. Sliding Wear Resistance

3.1.1. Conditions Favoring Abrasive Wear (Al_2O_3 Counter-Body)

COF and wear rate (k) results for conventionally and deep cryogenic heat-treated HSS (AISI M2, AISI M3:2 and AISI M35) tested under reciprocating dry sliding conditions against Al_2O_3 ball, which favors abrasive wear, are shown in Figure 2. Under the abrasive wear conditions used in this investigation, the steady-state COF is generally independent of the heat treatment process (CHT or DCT) and HSS grade. However, it changes depending on the sliding condition (load and sliding speed), as shown in Figure 2a–c. Under high-load/high sliding speed, COF is in the range of 0.5–0.55, except for steel C that is hardened from the lower austenitizing temperature (C3, C4), where it increases to 0.6. By switching to high load/low sliding speed conditions, COF increases to ~0.6 and, for low load/high sliding speed, increases to ~0.7. For low load/low sliding speed, COF decreases slightly to ~0.65, while for steel C, hardened from the lower austenitizing temperature (C3, C4), it again shows slightly higher values of 0.7. In terms of abrasive wear resistance (Figure 2d–f), the first observation is that for all three HSS wear scars of DCT samples (Figure 2d) are narrower compared to CHT samples (Figure 2d) by roughly 25%. For steel A, wear rates are in the range of 2.0×10^{-6}–18.0×10^{-6} mm^3/Nm. If hardened from high austenitization temperature and followed by a low tempering temperature (promoted hardness; A1, A2), DCT does not show any noticeable effect, except at low load/low sliding speed conditions, under which approximately a 10% increase in wear rates can be observed (Figure 2d). On the other hand, when hardened from a low austenitization temperature (promoting toughness; A3, A4), DCT greatly improves the abrasive wear resistance of steel A under high sliding speed conditions (~75%) but deteriorates it with low sliding speeds (2–3 times). In the case of steel B ($k = 0.1 \times 10^{-6}$–5.0×10^{-6} mm^3/Nm), DCT improves its abrasive wear resistance under high sliding speed conditions regardless of the austenitization/tempering temperatures, with the improvement being in the range of 30–60%. However, under low

sliding speed conditions in combination with a high austenitization temperature and low tempering temperature, DCT results in a reduced abrasive wear resistance (up to 4 times), while with low austenitization temperature and high tempering temperature followed by DCT causes an improvement of up to 40%, especially for low loading conditions (Figure 2e). Finally, for steel C (k = 1.0×10^{-6}–35.0×10^{-6} mm^3/Nm) there is a general trend of negligible to only minor negative effectd on abrasive wear resistance, when applying DCT treatment (Figure 2f).

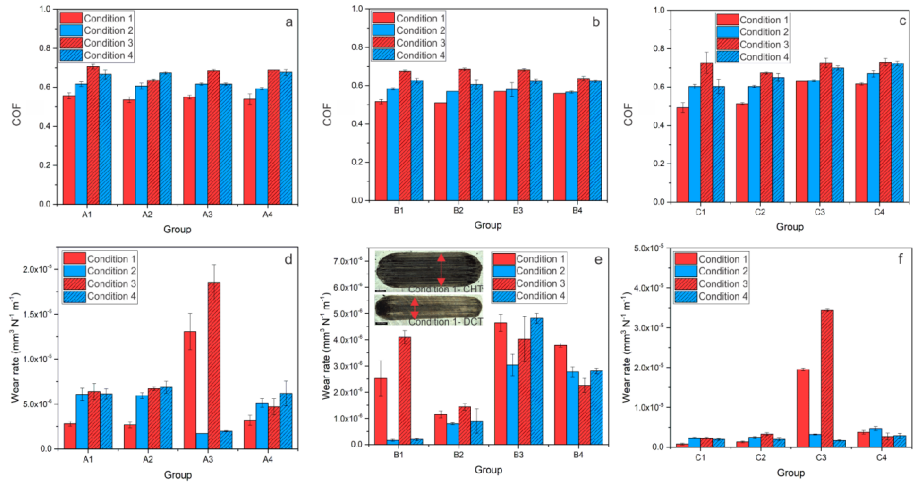

Figure 2. Results of abrasive wear conditions (Al_2O_3 counter-body) for all three steels; A (AISI M2), B (AISI M3:2) and C (AISI M35), where (**a**–**c**) is steady-state coefficient of friction for each condition and (**d**–**f**) is wear rate for each steel at certain condition. (**e**) the insert shows the average representation of wear scar for all three steels of conventionally (CHT) and deep cryogenically heat-treated samples; the black scale represents 500 µm.

3.1.2. Conditions Favoring Combination of Abrasive and Adhesive Wear (AISI 52100 Counter-Body)

Analysis of the wear scars under the combination of abrasive/adhesive wear (AISI 52100 counter-body) showed a similar trend, as observed for pure abrasive wear conditions, with wear scars of DCT samples being narrower compared to CHT samples by about 15%. COF and wear rate results for CHT- and DCT-treated HSS tested under the mixed condition of abrasive and adhesive wear are shown in Figure 3. In general, for steel A, COF decreased from 0.5–0.6 (CHT sample) to 0.3–0.4 after DCT, which is a reduction of 20–25% (Figure 3a). Steel B shows no significant changes in COF. However, for high austenitizing temperature groups (B1-B2), CHT group (B1) has a decreasing and the DCT group has an increasing COF trend as the contact conditions intensify, as shown in Figure 3b. The origin of such behavior could be in different prevailing wear mechanisms for DCT and CHT samples. Steel C (Figure 3c) also shows different trends depending on the heat treatment. There is no significant difference in COF between the CHT and DCT group for a higher austenitizing and lower tempering temperature (C1-C2). However, for the second heat treatment regime of a lower austenitizing and higher tempering temperature, the DCT samples have about 20–25% lower COF (0.5–0.6) as compared to CHT samples (0.6–0.7), similar to that observed for steel A. With regard to wear resistance (Figure 3d–f), involving a combination of abrasive and adhesive wear, steel A wear rates are in the range of 0.5–5.0 $\times 10^{-7}$ mm^3/Nm (Figure 3d). In this case, (steel A) DCT has a positive effect on wear resistance for high sliding speed conditions (contact conditions 1 and 3),

but detrimental under low-speed conditions (contact conditions 2 and 4), regardless of the austentizing and tempering temperature. Steel B wear rate results are in range of 0.5–7.0 $\times$ 10^{-7} mm^3/Nm, with DCT generally resulting in a negative trend. The only exceptions are high load and low sliding speed conditions (Figure 3e). Finally, for steel C, wear rates are in the range of 0.1–85 $\times$ 10^{-7} mm^3/Nm, for which a generally positive trend of improved wear resistance is observed for DCT samples, especially when combined with lower austenitizing and higher tempering temperature (Figure 3f), similar to the conditions favoring abrasive wear (Figure 2f).

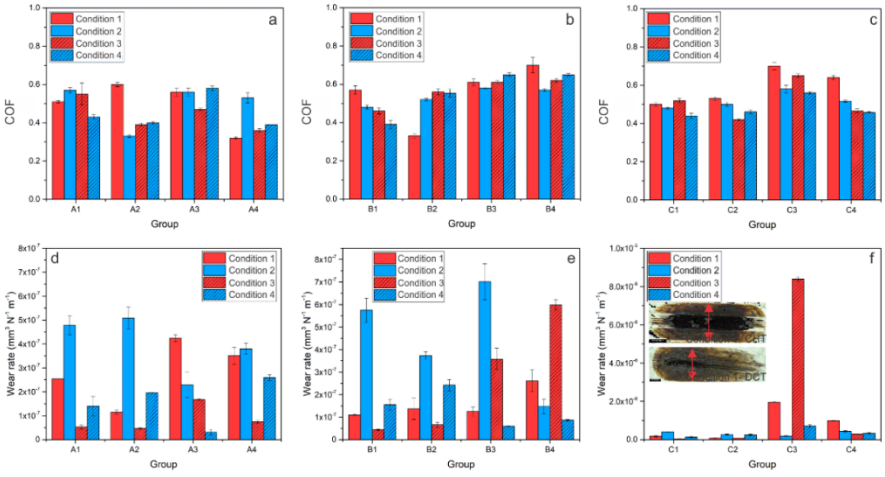

Figure 3. COF and wear rate results for contact conditions favoring a combination of abrasive and adhesive wear for all three steels, A (AISI M2), B (AISI M3:2) and C (AISI M35), where (**a**–**c**) is steady-state coefficient of friction for each condition and (**d**–**f**) is the wear rate for each steel at certain condition. (**f**) the insert presents the average representation of wear scar for all three steels of conventionally (CHT) and deep cryogenically heat-treated specimens; the black scale represents 500 µm.

3.1.3. Conditions Favoring Combination of Abrasive and Adhesive Wear (AISI 304L Counter-Body)

Additionally, in the case of a softer counter-body (AISI 304L) favoring adhesive wear, wear scars for DCT samples are generally narrower when compared to their CHT counterparts, although not by more than 10%. The COF results of steel A show no significant difference between DCT and CHT treatments (COF is between 0.4–0.6). The only noticeable exception is at the low sliding speed conditions and low austenitizing temperature, with the DCT samples displaying a 20–25% lower steady-state friction (Figure 4a). Steel B and C (Figure 4b,c) show a general trend of COF improvement with DCT when adhesive wear prevails. Adhesive wear resistance for steel A (k = 0.1–2.25 $\times$ 10^{-5} mm^3/Nm) improves with DCT (up to 35%) for high sliding speed conditions (condition 1 and 3), while it deteriorates under slow sliding speed conditions (conditions 2 and 4; Figure 4d). In the case of steel B, DCT generally has a positive trend, improving adhesive wear resistance by 10–65% (k = 0.1–1.6 $\times$ 10^{-5} mm^3/Nm). The only exception is a low austenitizing temperature and low load/low sliding speed condition (condition 4) (Figure 4e). For steel C, the adhesive wear rate is in the range of 0.1–5.5 $\times$ 10^{-5} mm^3/Nm. While, for high austenitizing and low tempering temperatures, DCT has no evident effect, it significantly improves adhesive wear resistance (by up to 90%) when combined with low austenitizing and high tempering temperatures (Figure 4f).

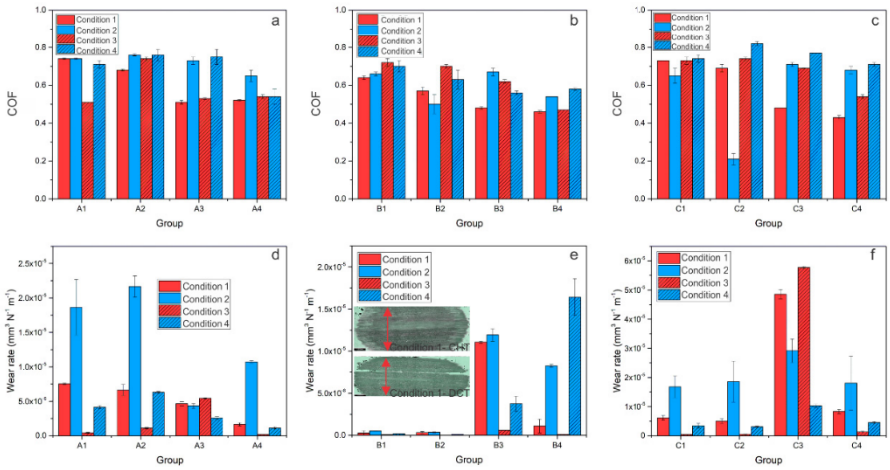

Figure 4. COF and wear rate results for contact conditions favoring adhesive wear for all three steels A (AISI M2), B (AISI M3:2) and C (AISI M35), where (**a**–**c**) is a steady-state coefficient of friction for each condition and (**d**–**f**) is wear rate for each steel at a certain condition. (**e**) The insert shows the average representation of the wear scars for all three steels of conventionally (CHT) and deep cryogenically heat-treated samples, the black scale represents 500 µm.

3.2. Galling

The galling test results (Figure 5a–f) generally show a positive trend of DCT on galling initiation and Al transfer layer formation on HSS. The results were evaluated by monitoring the coefficient of friction (COF) as a function of the load and identifying abrupt changes in friction, indicating galling initiation and transfer layer formation [17]. (Figure 5a–c). Furthermore, the amount of transferred and adhered Al material to the HSS contact surface at four different loads (300 N, 500N, 1000 N and 1500 N; Figure 5d–f) is determined to evaluate the galling processes. The results of steel A (AISI M2) (Figure 5a) show an abrupt increase in COF already, at low loads of about 400 N and 500 N, when conventionally heat treated from higher (A1) and lower (A3) austenitization temperatures, respectively, followed by a high and unstable COF due to stochastic deposition and the removal of Al material. The application of DCT results in postponed friction increase to higher load values of 700 N (A2) and 1000 N (A4). However, when analyzing the adhered amount of Al material to the steel A cylinder, DCT does not show any improvement if combined with a high austenitizing temperature and low tempering temperature, at least not before the extensive plastic deformation of Al counter cylinders takes place (1500 N). However, for a low austenitization temperature and high tempering temperature (A3–A4) the amount of adhered Al material was reduced by 30% with DCT, which is observed across a broad load range (300–1500 N). For steel B (AISI M3:2) (Figure 5e), the increase in friction takes place between 600 N and 800 N when conventionally heat treated (B1, B3), at which a low austenitization temperature and high tempering temperature (B3) results in a 15–40% smaller amount of transferred Al material. Similar to steel A, the inclusion of DCT provides an improved galling resistance, but only when combined with lower austenitization and higher tempering temperature (B4). In this case, an abrupt increase in friction, indicating gross galling, is postponed to 1200 N and the amount of adhered material in the low-to-mid load range (300–1000 N) is reduced by ~20% as compared to CHT counterpart (B3), as shown in Figure 5b,e.

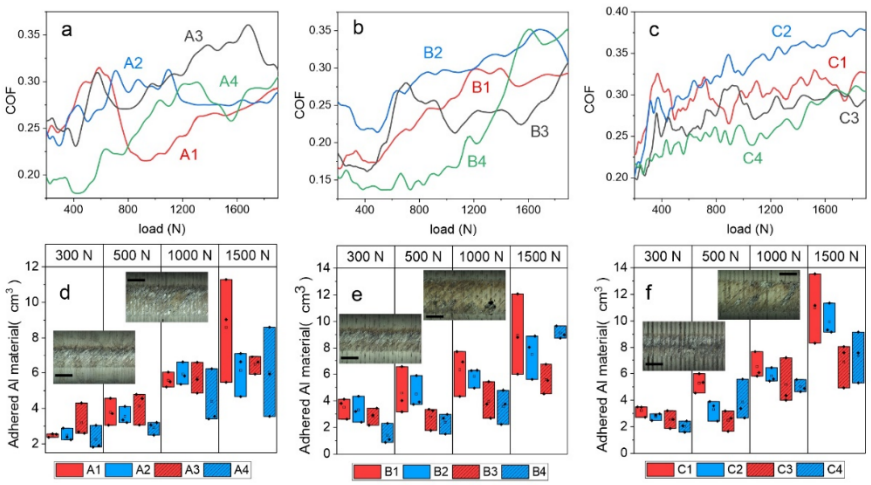

Figure 5. Resulting deposited volume of aluminum material from the counter body at specific normal loads for all heat-treated states of steels (**a**) A, (**b**) B and (**c**) C. Within the diagrams, exemplar images of areas at different loads displaying complete adhesion of counter body material, and a region indicating delamination of adhered material, are provided. In (**d**–**f**), the representative friction coefficient (COF) profiles versus applied load of each heat-treated state of steels, A, B and C, are presented, respectively. (**d**–**f**) The inserts show the average representation of galling for all three steels of conventionally (CHT) and deep cryogenically heat-treated samples; the black scale represents 500 μm.

In the case of steel C, the coefficient of friction shows a similar trend for all four heat treatment regimes (Figure 5f). In all cases, COF steadily increases with load, with galling initiation already indicated at a high value of approximately 300 N. With a low austenitizing temperature and high tempering temperature (C1-C2), the friction values are lower compared to the other heat treatment procedure (C3-C4), whether combined with DCT or not. In terms of adhered Al material, DCT provides up to a 50% improvement in galling resistance when combined with a high austenitizing/low tempering temperature (C2), while its beneficial effects are more or less lost for the other case (low austenitizing/high tempering temperature; C4).

3.3. Dynamic Impact Wear

In Figure 6, the dynamic impact wear (DIW) properties of the investigated steels, A (AISI M2), B (AISI M3:2) and C (AISI M35), are presented in the form of disc wear volume as a function of heat treatment. In the case of steel A, the dynamic impact wear volume is between 0.6×10^4 mm^3 and 1.8×10^4 mm^3, and is lowered by using a lower austenitization temperature (A3) and/or DCT (A2, A4) by 30–40%, as shown in Figure 6a. Dynamic impact wear results for material B are presented in Figure 6b. It can be seen that for steel B, DCT has a positive effect on DIW resistance, especially when DCT is combined with a low austenitization temperature and high tempering temperature (B3, B4). In this case, the dynamic impact wear volume of steel B is reduced from 8.0×10^4 mm^3 to 1.0×10^4 mm^3, which is lower than for both CHT and DCT samples heat treated from a high austenitization and low tempering temperature, as shown in Figure 6b. In the case of steel C, DCT has only a minor improvement effect (~10%) on steel DIW resistance when high austenitization and low tempering temperatures are applied, as shown in Figure 6c. By using low austenitization and high tempering temperatures, the DIW properties of steel C are more strongly improved with DCT, reducing the wear volume from $\sim 3 \times 10^4$ mm^3 to $\sim 1.75 \times 10^4$ mm^3.

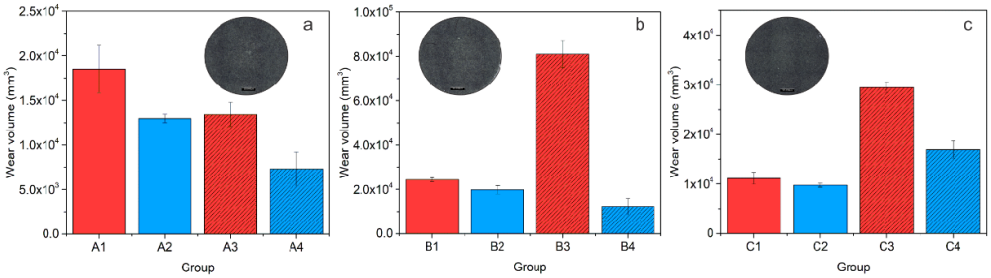

Figure 6. Dynamic impact wear (DIW) as a function of heat treatment for all three steels, where A stands for AISI M2 (**a**), B for AISI M3:2 (**b**) and C for AISI M35 (**c**). (**a**–**c**) Insert photos show the average representation of wear scar for each steel grade for conventionally (CHT) and deep cryogenically heat-treated samples; the black scale represents 500 µm.

4. Discussion

4.1. Sliding Wear Resistance (Abrasive and Adhesive Wear)

Detailed microstructure analysis of the investigated HSS after CHT and DCT is presented in Jovičević-Klug et al., 2020 [16] and Jovičević-Klug et al., 2021 [21]. As described, for all three HSS steels, the matrix is composed of lath martensite (hardness of 53–63 HRC), with the retained austenite (RA) being under 1 vol. %. In addition, carbides in the form of MC (enriched with V; hardness of 2500–3000 HV [22]), M_6C (enriched with W, Mo and Fe; hardness of 1100–1700 HV [23]) and $M_{23}C_6$ (enriched with Fe and C; hardness of 1000–1450 HV [24]) are observed (Supplementary Material Table S1). However, the number of carbides is higher in DCT samples compared to CHT samples, which mostly originates from the increased number of precipitated $M_{23}C_6$ carbides (30% higher volume fraction and up to 140% increased number). Additionally, after DCT, the microstructure is more homogenous and the average size of carbides is up to 20% smaller compared to CHT counterparts [16]. Aside from DCT, the heat treatment regime (austenitizing and tempering temperature) also defines the number of precipitated carbides, with a lower austenitizing and higher tempering temperature resulting in up to a 40% higher number of precipitated carbides. The increased number of MC carbides is observed for steel B (AISI M3:2) and M_6C for steels A (AISI M2) and C (AISI M35). In this case, the application of DCT increases the volumetric fraction of carbides (mostly $M_{23}C_6$ carbides) for steels A and B, whereas, for steel C, the volumetric fraction of carbides remains similar, although is finer after DCT. The increased precipitation of finer carbides, such as $M_{23}C_6$, can improve wear resistance by the overall hardening of the material. Aside from this, DCT-induced microstructural changes also resulted in changes in mechanical properties (proven in the study by Jovičević-Klug et al., 2021 [17]), including increased hardness and toughness.

In terms of the abrasive wear resistance (Figure 7a,b), DCT generally has no dominant effect on heat treatment conditions that favor high hardness (high austenitizing/low tempering temperature), with the matrix hardness being the dominant factor. One exception is PM steel B, which has a higher volume fraction and more uniform carbides. However, under conditions favoring a higher toughness (low austenitizing/high tempering temperature) DCT improves the abrasive wear resistance of HSS steels for high sliding speed conditions, while it decreases it under low-speed conditions. The general tendency of a more pronounced effect of DCT on abrasive wear resistance at lower austenitizing and higher tempering conditions is associated with the softer matrix, higher precipitation of carbides and a higher toughness, also typical for PM steels. In this case, DCT promotes the increased precipitation of finer carbides and their more homogeneous distribution, facilitating improvement in toughness as well as hardness (Table 2). It is proposed that, at high sliding speeds, the increased toughness allows for the localized deformation of the softened matrix material due to high contact temperatures, which, in turn, allow the

displacement of the carbides on the contact surface and deeper into the matrix (indicated by vertical red arrows in Figure 7b), protecting the matrix from nominal friction forces and wear. In turn, the initial removal of material mostly results from the accommodation of this effect, which is then considerably reduced with the intensified agglomeration of carbides over time. However, at low sliding speeds, the absence of the matrix softening promotes carbides pull-out (mostly MC carbides, as also observed by Pellizzari et al., 2012 [9]) and microcracking ($M_{23}C_6$ and M_6C), which may act as third-body particles and cause microploughing, thus resulting in an increased wear rate at an increased level of carbides precipitation via DCT. This effect strongly depends on the size and shape of carbides. These carbides are smaller and more uniform, with a smaller size having a negative effect, thus switching favor toward DCT, as observed for PM steel B.

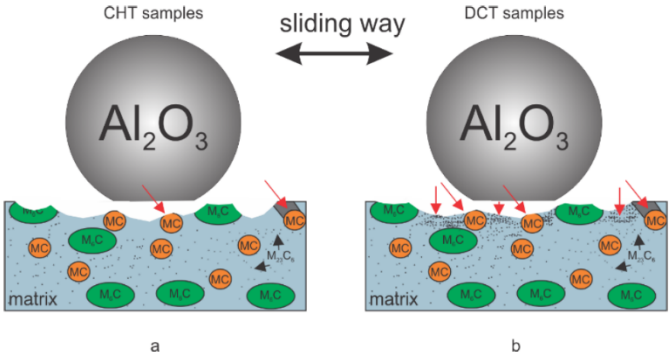

Figure 7. Schematic representation of sliding dynamics during sliding ball-on-flat contact testing for (**a**) conventional heat-treated samples and (**b**) deep cryogenic heat-treated samples. The red arrows indicate the movement of carbides and the agglomeration of them on the wear surface during the sliding test.

In wear testing, which favors abrasive wear (Al_2O_3 counter-ball), abrasive wear is combined with surface oxidation and oxidative wear (dark grey areas in Figure 8, Supplementary Material Figure S1), mainly observed in the carbide–matrix boundary during high sliding speed conditions. Regarding this aspect, an additional improvement is expected from DCT since the oxide development by the high flash temperatures is reduced, due to a higher amount of carbides and a refined lath structure of the matrix that decreases the amount of absorbed oxygen and build-up of the oxide layer [21]. An important factor also has the mean carbide size as suggested by Vardavoulias 1994 [25]. The carbides, whose mean size is less than or equal to the oxide layer thickness ($M_{23}C_6$), are incorporated into the densified and hardened surface zone. Overtime, the hardened zone leads to reduced wear of the matrix, being more pronounced for DCT treatment and intensifying the precipitation of very fine $M_{23}C_6$ carbides.

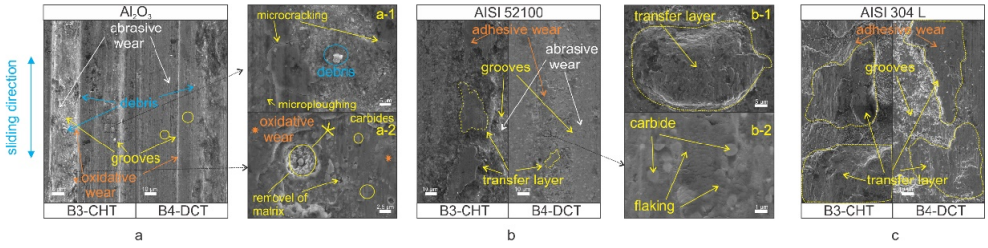

Figure 8. Examples of wear scars for the same wear condition 1 (102 N/15 Hz/0.12 m/s) for (**a**) conventionally heat-treated sample and (**b**) deep cryogenic heat-treated sample. (**a**,**a-1**,**a-2**) SEM micrographs of B3-CHT (**left**) and B4-DCT (**right**) of sample under mentioned conditions with counter-body Al_2O_3. (**b**,**b-1**,**b-2**) SEM micrographs of B3-CHT (**left**) and B4-DCT (**right**) of sample under mentioned conditions with counter-body AISI 52100. (**c**) SEM micrographs of B3-CHT (**left**) and B4-DCT (**right**) of sample under mentioned conditions with counter-body AISI 304L.

The testing against an AISI 304L counter ball promoted adhesive wear combined with oxidative wear (Figure 8(b-1,c)). For all steels, heat treatment and contact conditions applied a high degree of AISI 304L counter ball wear, and transfer layers formation took place. Again, for a high hardness case (high austenitizing/low tempering conditions) and matrix properties defining adhesive wear resistance, DCT shows no distinctive effect. However, for a higher toughness case (low austenitizing/high tempering temperature) and the promotion of carbides precipitation with a lower adhesion tendency, DCT has an evidently positive effect, being the most evident for steel C (AISI M35), followed by steel B (AISI M3:2) and A (AISI M2). In the case of steel C, DCT most evidently facilitates the precipitation of finer and more homogeneously distributed carbides, with the matrix material being more segmented by the homogeneously distributed carbides and solid solution hardened with Co, thus reducing adhesion on a macro scale, as also indicated by a decrease in friction. Steel A shows lower volume fraction of carbides while PM steel B already has a very homogeneous carbides distribution, reducing the positive effect of DCT.

In the case of a mixture of abrasive and adhesive wear (AISI 52100 counter-ball), wear grooves are combined with the formation of transfer layers and flaking (Figure 8(b-2)), which additionally intensify the wear of the material. Compared to pure abrasive wear (Al_2O_3 counter-ball) DCT generally improves the combined abrasive/adhesive wear resistance of HSS for a high hardness case (high austenitizing/low tempering temperatures). Increased precipitation and the more homogeneous distribution of carbides reduces the adhesive component with a harder matrix being less prone to sticking and tearing. However, the promoted toughness depends on the steel grade, having a similar effect on pure abrasive wear for steel A, a predominantly negative effect for steel B and a predominantly positive effect for steel C. In the case of steel A, displaying the highest hardness and the lowest fraction of carbides, abrasive wear predominates, thus showing the same effect of DCT as for pure abrasive wear conditions. In the case of steel C with the finest carbides and Co, the strengthened matrix-adhesive wear dominates, which is greatly reduced by DCT, while for steel B, a high-volume fraction of carbides and increased toughness increase the likelihood of the material sticking and cold welding to the counter ball, which is then followed by the localized tearing of the surface and intensified wear.

4.2. Galling Resistance

In the case of the galling tests, a generally positive effect of DCT is observed (Supplementary Material Figure S2). The improvement of galling resistance with DCT, similar for adhesive wear resistance, is considered to be a consequence of microstructure and hardness changes. The DCT leads to an increase in $M_{23}C_6$ carbides precipitation, which allows for the development of a hardened surface that resists localized branching and tearing that would normally result in higher galling. Furthermore, the more even

distribution of carbides leads to a more homogeneous and even surface and reduces local surface roughness (confirmed by a previous study [21]). Regarding this aspect, the residual stresses of the surface can be a potentially defining parameter, since the material can produce a higher cracking of the surface with normal loads, when internal tensile stresses are present. Based on previous studies [8,26], it is confirmed that DCT generally reduces the tensile stresses or even changes them into a compressive character. The galling tests shown in relation to the heat treatment also have a generally higher impact on DCT in the case of lower austenitizing and higher tempering temperatures, which also yield a considerably lower friction coefficient and lower adhered volume for all HSS with DCT. This is believed to occur from the much more refined microstructure, due to the smaller prior austenite grains, smaller martensitic lath structure and larger carbide amount compared to the opposite heat treatment [17], which creates a more durable and homogeneous surface that more strongly resists the adhesion and agglomeration of the counter body material (Figure 9a,b). For the treatment with a higher austenitizing and lower tempering temperature, the friction coefficient is generally higher for DCT than for the CHT samples, which are considered to be related to the general higher toughness of the matrix material after DCT. However, as the galling test is in a single stroke configuration and the aluminum material is much softer, this does not directly affect galling intensity. Both DCT and CHT samples from this heat treatment group (groups 1–2) display similar deposited volumes at various, selected, normal load values (Figure 5a–c). Only steel C, with a considerable amount of Co shows a tendency towards a lower volume deposition with DCT. Steel C also sees a more linear increase in COF than steels A and B. This is considered to be related to the solid solution hardening of the matrix with Co that is not depleted from the matrix by carbide precipitation. As a result, such a matrix state, in combination with the increased toughness and higher number of carbides (volumetrically similar), leads to a linear change of COF with an applied load, as well as a linear displacement in friction properties with the application of DCT.

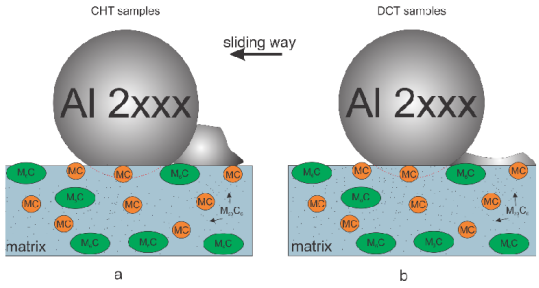

Figure 9. Schematic representation of galling testing of steels corresponding to (**a**) conventional samples and (**b**) deep cryogenic heat-treated samples.

4.3. Dynamic Impact Wear

For the impact wear tests, abrasive wear combined with oxidative wear, microcracking and microploughing were dominant for all steels investigated when treated with either CHT or DCT. In all cases, the softer martensitic matrix is worn faster than surrounding carbides, which can be pulled out or microcracked, thus intensifying impact wear. However, a clear correlation with the carbide precipitation can be determined. For all steel grades, a general tendency has a reduced impact wear with the increased volumetric amount and more homogeneous distribution of $M_{23}C_6$ carbides obtained by DCT. This is concordant with the theory of carbide agglomeration and the subsequent hardening of the matrix of the contact surface, which prevents further wear propagation over time. From this perspective, the increase in impact wear resistance with DCT is also influenced by the

increased toughness of the material, since it does not only allow for a deeper movement of carbides into the matrix, but also reduces the probability of the cracking of the matrix with external loading. It should be noted that the increased amount of $M_{23}C_6$ carbides does not directly relate to an increase in hardness, which results in an inconsistent relationship between hardness and impact wear resistance. However, for steel C, this relation still holds; for this steel the volumetric change in $M_{23}C_6$ carbides is negligible, which results in a stronger correlation with the hardness/toughness change in the material with different heat treatment procedures that impact wear properties.

5. Conclusions

The effect of deep cryogenic treatment (DCT) on sliding wear, impact wear and galling behavior of selected high-speed steels (HSS) (AISI M2, AISI M3:2 and AISI M35) was investigated in correlation with selected austenitization and tempering temperatures and different wear conditions and modes. The DCT effect on sliding wear resistance depended on the HSS steel grade, as well as the contact conditions and wear mode, whereas on dynamic impact wear and galling resistance, DCT had a generally positive effect:

1. The positive effect of DCT on the tribological properties of HSS is attributed to a more homogenous microstructure, an increase in precipitation of finer carbides, the modification of different carbide types, and the generally reduced mean carbide diameter that, consequently, led to better mechanical properties.
2. The eventual negative effect of DCT is related to the combined effect of increased volume fraction of carbides and a tougher matrix, which, under certain contact conditions (combined abrasive/adhesive wear), may lead to the sticking and tearing of the matrix material, and the microcracking and pull-outs of carbides. This exposes carbide–matrix boundaries, which act as the starting locations for oxidative wear, while loose carbides may act as abrasive third-body particles.
3. Through the homogeneous distribution of fine carbides over the contact surface, DCT greatly reduces the adhesion and galling of counter-material, while a tougher matrix and increased volume fraction of carbides provides an improved impact wear resistance of HSS. Under sliding, DCT generally reduces abrasive wear. However, the presence of an adhesive component and carbides pull-out may shift the trend in the opposite direction, especially when combined with milder contact conditions.
4. The selection of the heat treatment regime influences the performance of DCT and, consequently, the changes in the microstructure, mechanical properties and tribological properties of HSS. The most optimal heat treatment regime promoting wear resistance improvement by DCT is hardening from lower austenitizing temperature and high temperature tempering, which promotes carbides precipitation and high toughness over hardness.
5. Alloying elements and steel type influence the type, shape and precipitation of carbides, and thus affect the wear and galling properties. The most positive effect of DCT on wear resistance is obtained for high-alloyed Co-containing steel C (AISI M35), with DCT mainly resulting in the refinement of carbides. At lower alloying element contents (steel A; AISI M2), the effect of DCT diminishes, while, for PM steels with very uniform carbides, the positive effect of DCT becomes a negative effect when abrasive wear is accompanied with adhesion.

Supplementary Materials: The following are available online at https://www.mdpi.com/article/10.3390/ma14247561/s1, Supplementary Material Table S1, The phase results for all three high-speed steels; Supplementary Material Figure S1, Oxidation; Supplementary Material Figure S2, Galling testing.

Author Contributions: Conceptualization P.J.-K.; Methodology P.J.-K., M.S. and M.J.-K.; Investigation P.J.-K., M.S. and M.J.-K.; Resources P.J.-K. and B.P.; Writing—original draft preparation P.J.-K., M.S. and M.J.-K.; Writing—review and editing P.J.-K., M.S., M.J.-K. and B.P.; Visualization P.J.-K.; Supervision B.P. All authors have read and agreed to the published version of the manuscript.

Funding: This research was funded by Slovenian Research Agency (ARRS), Ljubljana, Slovenia, grant numbers P2-0050 and J2-9211.

Institutional Review Board Statement: Not applicable.

Informed Consent Statement: Not applicable.

Data Availability Statement: The raw/processed data required to reproduce these findings cannot be shared at this time as the data also forms part of an ongoing study.

Acknowledgments: Acknowledgements go to our IMT colleagues: B. Zvonar, for the help with heat treatments; N. Lipovšek and T. Kranjec, for the help in the metallographic lab; and G. Puš, for the help in mechanical lab.

Conflicts of Interest: The authors declare no conflict of interest.

References

1. Podgornik, B.; Majdic, F.; Leskovsek, V.; Vizintin, J. Improving tribological properties of tool steels through combination of deep-cryogenic treatment and plasma nitriding. *Wear* **2012**, *288*, 88–93. [CrossRef]
2. Porter, D.A.; Easterling, K.E.; Sherif, M.Y.A. *Phase Transformations in Metals and Alloys*, 3rd ed.; CRC Press, Taylor & Francis Group: Boca Raton, FL, USA, 2009; ISBN 978-1-4398-8357-0.
3. Senthilkumar, D. Cryogenic Treatment: Shallow and Deep. In *Encyclopedia of Iron, Steel, and Their Alloys*; Totten, G.E., Colas, R., Eds.; Taylor and Francis: New York, NY, USA, 2016; pp. 995–1007, ISBN 9781351254496.
4. Jovičević-Klug, P.; Podgornik, B. Comparative study of conventional and deep cryogenic treatment of AISI M3:2 (EN 1.3395) high-speed steel. *J. Mater. Res. Technol.* **2020**, *9*, 13118–13127. [CrossRef]
5. Oppenkowski, A.; Weber, S.; Theisen, W. Evaluation of factors influencing deep cryogenic treatment that affect the properties of tool steels. *J. Mater. Process. Technol.* **2010**, *210*, 1949–1955. [CrossRef]
6. Leskovšek, V.; Kalin, M.; Vižintin, J. Influence of deep-cryogenic treatment on wear resistance of vacuum heat-treated HSS. *Vacuum* **2006**, *80*, 507–518. [CrossRef]
7. Pellizzari, M.; Molinari, A.; Girardini, L.; Maldarelli, L. Deep cryogenic treatment of AISI M2 high-speed steel. *Int. J. Microstruct. Mater. Prop.* **2008**, *3*, 383–390. [CrossRef]
8. Pellizzari, M. Influence of deep cryogenic treatment on the properties of conventional and PM high speed steels. *Metall. Ital.* **2008**, *100*, 17–22.
9. Pellizzari, M.; Caliskanoglu, D.; Fernández, A.; Barbero, J.I.; Pena, B.; Uemit, T.; Pizarro Sanz, R.; Elvira Eguizabal, R.; Alava, L.A. Influence of different deep cryogenic treatment routes on the properties of high speed steel. *HTM J. Heat Treat. Mater.* **2012**, *67*, 111–117. [CrossRef]
10. Fantineli, D.G.; Parcianello, C.T.; Rosendo, T.S.; Reguly, A.; Tier, M.D. Effect of heat and cryogenic treatment on wear and toughness of HSS AISI M2. *J. Mater. Res. Technol.* **2020**, *9*, 12354–12363. [CrossRef]
11. Zhou, L.; Min, N.; Li, H.; Wu, X. Nanoscratch and internal friction investigations of deep cryogenic treated M2 high-speed steel. *Heat Treat. Surf. Eng.* **2020**, *1*, 109–114. [CrossRef]
12. Candane, D. Effect of Cryogenic Treatment on Microstructure and Wear Characteristics of AISI M35 HSS. *Int. J. Mater. Sci. Appl.* **2013**, *2*, 60. [CrossRef]
13. Cicek, A.; KIvak, T.; Uygur, I.; Ekici, E.; Turgut, Y. Performance of cryogenically treated M35 HSS drills in drilling of austenitic stainless steels. *Int. J. Adv. Manuf. Technol.* **2012**, *60*, 65–73. [CrossRef]
14. Jovičević-Klug, P.; Jovičević-Klug, M.; Sever, T.; Feizpour, D.; Podgornik, B. Impact of Steel Type, Composition and Heat Treatment Parameters on Effectiveness of Deep Cryogenic Treatment. *J. Mater. Res. Technol.* **2021**, *14*, 1007–1020. [CrossRef]
15. Jeleńkowski, J.; Ciski, A.; Babul, T. Effect of deep cryogenic treatment on substructure of HS6-5-2 high speed steel. *J. Achiev. Mater. Manuf. Eng.* **2010**, *43*, 80–87.
16. Jovičević-Klug, P.; Jovičević-Klug, M.; Podgornik, B. Effectiveness of deep cryogenic treatment on carbide precipitation. *J. Mater. Res. Technol.* **2020**, *9*, 13014–13026. [CrossRef]
17. Jovičević-Klug, P.; Puš, G.; Jovičević-Klug, M.; Žužek, B.; Podgornik, B. Influence of heat treatment parameters on effectiveness of deep cryogenic treatment on properties of high-speed steels. *Mater. Sci. Eng. A* **2022**, *829*, 142157. [CrossRef]
18. Podgornik, B.; Žužek, B.; Leskovšek, V. Experimental Evaluation of Tool Steel Fracture Toughness Using Circumferentially Notched and Precracked Tension Bar Specimen. *Mater. Perform. Charact.* **2014**, *3*, 87–103. [CrossRef]
19. Williams, J. *Engineering Tribology*; Cambridge University Press: New York, NY, USA, 2005; ISBN 978-0-521-60988-3.
20. Podgornik, B.; Hogmark, S.; Pezdirnik, J. Comparison between different test methods for evaluation of galling properties of surface engineered tool surfaces. *Wear* **2004**, *257*, 843–851. [CrossRef]
21. Jovičević-Klug, P.; Jenko, M.; Jovičević-Klug, M.; Šetina Batič, B.; Kovač, J.; Podgornik, B. Effect of Deep Cryogenic Treatment on Surface Chemistry and Microstructure of Selected High-Speed Steels. *Appl. Surf. Sci.* **2021**, *548*, 149257. [CrossRef]
22. Roberts, G.A.; George, A.; Cary, R.A. *Tool Steels*; American Society for Metals: San Marcos, CA, USA, 1980; ISBN 0871700964.

23. Wilmes, S.; Zwick, G. Effect of Niobium and Vanadium As an Alloying Element in Tool Steels With High Chromium Content. In Proceedings of the 6th International Tooling Conference: The Use of Tool Steels: Experience and Research, Karlstad, Sweden, 10–13 September 2002; pp. 269–287.
24. Inoue, A.; Arakawa, S.; Masumoto, T. Effect of Alloying Elements on Defect Structure and Hardness of M23C6 Type Carbides. *Trans. Jpn. Inst. Met.* **1979**, *20*, 585–592. [CrossRef]
25. Vardavoulias, M. The role of hard second phases in the mild oxidational wear mechanism of high-speed steel-based materials. *Wear* **1994**, *173*, 105–114. [CrossRef]
26. Jovicevic-Klug, M.; Jovicevic-Klug, P.; McCord, J.; Podgornik, B. Investigation of microstructural attributes of steel surfaces through magneto-optical Kerr effect. *J. Mater. Res. Technol.* **2021**, *11*, 1245–1259. [CrossRef]

Chapter 4

Effect of Deep Cryogenic Treatment on Surface Properties

The purpose of this chapter is to provide insight of how DCT influences not only the whole bulk of the material, but also the surface of the material. Dedicated research of the DCT influence on the material's surface and properties has until now not been researched due to the general understanding that DCT influences the material equally throughout the entire volume and surface. However, with this study, the first proof is provided that surface properties are tailored differently than the bulk of the investigated material, which is determined with a combination of different techniques (SEM, EDS, EBSD, and X-ray photoelectron spectroscopy (XPS)). The DCT effect is analyzed through the modification of the microstructure, chemical composition, phase change and binding state of the alloying elements. The selected materials were three groups of HSS, namely AISI M2, AISI M3:2 and AISI M35. This chapter delivers also a first-time evaluation of oxidation states and oxygen absorbance of the surface in HSS, also in relation to applied DCT. The study indicates that martensitic laths after the application of DCT are smaller, sharper and generally more oriented along specific crystal directions of prior austenite grains.

Brief discussion: Results show that the size modification of martensitic laths via DCT is influenced through selected tempering temperature, which defines the carbon segregation and recrystallization. In addition, DCT samples display a more rounded form of the ends of the martensitic laths, which is also attributed to the different microstructural evolution with DCT compared to CHT. DCT also influences the martensitic laths orientation, resulting from the different way of retained austenite transformation through direct diffusionless process (for DCT) or through diffusional decomposition during tempering (for CHT). For this reason, the general orientation of the prior austenite grains is preserved through martensitic subdivision of austenite grains with DCT, leading to congregated directional growth of martensite along the <1 0 1> and <0 0 1> directions. XPS results indicate the tendency of a lower amount of oxide presence for DCT samples, which is related to the larger amount of carbides that display overall a larger surface to volume ratio, thus hindering oxide formation. Additionally, this is also associated with the higher absorption of oxygen on the DCT samples' surfaces, as there is less hindrance of absorption by the larger patches of carbides and flatter surface (formed due to the smaller martensitic laths). The distinct vanadium metallic peak, which is higher for DCT, indicates the increased number of vanadium precipitated carbides in DCT material compared to the CHT counterpart. Additionally, the oxide peaks of tungsten are lower in intensity for DCT samples, which supports the reduced oxide presence. Furthermore, these results provide further understanding of DCT and overall microstructure and surface behavior, which could be used in the explanation of improved oxidation and corrosion resistance after DCT application. Finally, the results of this study prove that the DCT influence is not only bounded to the bulk of the material and bulk properties, but it also strongly influences the surface and its properties in a completely separate fashion.

The ***author's contribution,*** as the first author, to the paper ***Effect of deep cryogenic treatment on surface chemistry and microstructure of selected high-speed steels***, published in Applied

Surface Science, was: conceptualization, investigation, planning of experiments, visualization, evaluation and writing (original draft and editing).

This chapter addresses thesis ***Hypotheses 2 and 3***.

Applied Surface Science 548 (2021) 149257

Contents lists available at ScienceDirect

Applied Surface Science

journal homepage: www.elsevier.com/locate/apsusc

Full Length Article

Effect of deep cryogenic treatment on surface chemistry and microstructure of selected high-speed steels

Patricia Jovičević-Klug [a,b,*], Monika Jenko [a,b], Matic Jovičević-Klug [a], Barbara Šetina Batič [a], Janez Kovač [b,c], Bojan Podgornik [a,b]

[a] Institute of Metals and Technology, Lepi pot 11, 1000 Ljubljana, Slovenia[1]
[b] Jožef Stefan International Postgraduate School, Jamova cesta 39, 1000 Ljubljana, Slovenia[2]
[c] Department of Surface Technology and Optoelectronics – F4, Institute Jožef Stefan, Jamova cesta 39, 1000 Ljubljana, Slovenia[3]

ARTICLE INFO

Keywords:
High-speed steel
Deep cryogenic treatment (DCT)
Scanning electron microscope (SEM)
Energy-dispersive X-ray spectroscopy (EDS)
Electron backscatter diffraction (EBSD)
X ray photoelectron spectroscopy (XPS)

ABSTRACT

The purpose of this study is to provide a systematic, complementary research of deep cryogenically treated (DCT) steels AISI M2, M3:2 and M35 including scanning electron microscopy (SEM), energy dispersive X-ray spectroscopy (EDS), electron backscatter diffraction (EBSD) and X-ray photoelectron spectroscopy (XPS). The DCT effect on selected steels was analyzed through modification of microstructure, chemical composition, phase change and chemical state of the present elements, when comparing conventional heat-treated (CHT) and DCT samples. The XPS results provide input into the understanding of oxidation dynamics of DCT samples and DCT influence on the microstructure using EBSD, as the major interpretation tool. It is confirmed, that martensitic laths are sharper, smaller and generally more oriented along specific crystal directions of prior austenite grains within DCT samples compared to CHT counterparts. A first-time evaluation of oxidation states and oxygen absorbance of the surface of selected high-speed steels is conducted with XPS, which is correlated with the microstructural changes induced by DCT. Depth profile XPS analysis of CHT and DCT samples was also conducted that shows the oxidation layer thickness and elemental gradients. These results provide further understanding of DCT dynamic on the overall microstructure and the corresponding surface behavior of the selected steels.

1. Introduction

Steels are an important group of materials that are required for various applications in everyday life. The subgroups such as stainless steels, high-speed steels (HSS), constructional steels, hot work and cold work tool steels etc. are constantly used for forming cutting tools, construction of living habitat, medicine, music, tools and electronics and many other applications. For these reasons, constant improvement of techniques concerning heat treatment of steels are being debated and researched. One of these upcoming solutions for improvement of steel properties whilst simultaneously cutting production costs is deep cryogenic treatment (DCT). The primary focus of DCT was a complete transformation and elimination of retained austenite, not normally provided with conventional heat treatment. Consequently, DCT utilized as an additional step within the process of conventional heat treatment, improves certain properties of steels such as fracture and impact toughness, hardness, fatigue, wear and corrosion resistance [1–5]. DCT may also cut costs, as it reduces the required amount of tempering cycles, for instance instead of three cycles only one cycle of tempering is needed, when DCT is applied on tools [6]. In recent studies, different mechanisms are being proposed to explain the effect and consequence of DCT on steel properties. The two most commonly noted mechanisms are transformation of retained austenite into martensite [7–9] and precipitation of finer carbides and its redistribution [10–12]. However, in certain cases such well understood mechanisms cannot explain the change of properties that transpire for certain steels when exposed to DCT. Furthermore, specific less often used mechanisms provide only sensible correlation for specific grade of steel and does not apply to other

* Corresponding author at: Institute of Metals and Technology, Lepi pot 11, 1000 Ljubljana, Slovenia.
E mail address: patricia.jovicevicklug@imt.si (P. Jovičević-Klug).
[1] info@imt.si.
[2] info@mps.si.
[3] info@ijs.si.

https://doi.org/10.1016/j.apsusc.2021.149257
Received 2 October 2020; Received in revised form 2 February 2021; Accepted 4 February 2021
Available online 8 February 2021

grades, even if they are from the same steel group or category [5].

The underlying processes that occur during DCT have been extensively researched using microstructural characterization methods such as light and electron microscopy on a variety of different steel grades and types [13–16]. Recent scientific contributions disclose the improvement of some mechanical properties occurring for DCT HSS to be related to refinement of secondary carbides [17–20] and precipitation of specific additional carbides of complex origin [21,22]. Also other high-resolution exotic methods [23,24] have given the opportunity to provide additional insight and information about such phenomena.

However, there is still a lack of in-depth understanding of the microstructural changes induced by DCT at different levels and how these correlate with the surface properties. Specifically, the state of the surface in terms of its oxidation dynamics and roughness related to the exposure of HSS to DCT has not been evaluated and correlated with microstructural (carbide) changes induced by DCT.

For the above reasons, this study aims at providing a complementary systematic approach to DCT effect, where microstructural, chemical and phase properties were taken into account for various steels from the HSS group. Chemical composition was analyzed in detail to obtain any indication of a significant change during DCT on the steel, such as different chemical composition of matrix/carbides and phase change during DCT. Using X-ray photoelectron spectroscopy (XPS), the change of chemical state of the elements present within the surface of the samples was investigated. Furthermore through XPS analysis, the oxidation state of the surface and the chemical binding of individual elements are probed and correlated with the microstructural changes induced by DCT. Therefore, the XPS results provide a link between oxide formation and oxygen absorbance to the surface construct that forms as a result of the underlying microstructure of the material.

All these results potentially indicate possible mechanism(s) in selected HSS that occur during DCT application. Furthermore, the results give indications to the cause of the change of the surface and bulk properties and the applicability of certain mechanism for the interpretation of these changes. HSS AISI M2, M3:2 and M35 were chosen as they are extensively researched tool steels and have versatile applicability (cutting tools etc.). The three different HSS were also chosen to determine, if the type and amount of various alloying elements (example Co) play a significant role on the phase transformation and other dynamics during DCT.

2. Materials and methods

2.1. Materials

HSS AISI M2 (designated as steel A, SIJ group), M3:2 (designated as steel B, ERAsteel) and M35 (designated as steel C, Dörrenberg, Edelstahl GmbH) were selected for this study. All three steels were supplied in the form of soft annealed, peeled and rolled bars. The actual chemical composition for all three HSS in mass fraction is provided in Table 1. The samples for scanning electron microscope, electron backscatter diffraction and X-ray photoelectron spectroscopy were obtained from the same heat treated master sample and then prepared for various analysis techniques (cut, ground, polished and in case of SEM and EBSD etched). Master samples from each group of HSS were first austenitized and quenched followed by particular heat treatment protocol for each group.

Table 1
The chemical composition of selected high-speed steels in wt.%.

M2 (A)	C	Mn	S	Cr	Mo	V	W	Co
	0.90	0.28	0.002	4.00	4.70	1.70	6.00	–
M3:2 (B)	**C**	**Mn**	**S**	**Cr**	**Mo**	**V**	**W**	**Co**
	1.29	0.31	0.006	3.90	4.80	3.00	5.90	0.69
M35 (C)	**C**	**Mn**	**S**	**C**	**Mo**	**V**	**W**	**Co**
	0.90	0.34	0.004	4.11	5.20	2.01	6.22	4.52

All samples were treated in a horizontal vacuum furnace, IPSEN VTTC324-R. Quenching was done by nitrogen gas at 5 bars. After quenching, samples were divided into two groups, first group was conventionally heat treated (CHT) (A1, B1, C1) and second group(s) was treated by deep cryogenic treatment (DCT) followed by one cycle of tempering (A2, B2, C2). The CHT was performed in accordance with the recommended protocol for HSS involving triple tempering. Deep cryogenic treatment was performed immediately after quenching with a gradual immersion of selected samples (A2, B2, C2) in liquid nitrogen. The protocol and parameters for all 6 heat treatments are provided in Table 2, with the austenitizing and tempering parameters selected based on the available tempering diagrams and the particular steel producer recommendations.

2.2. Methods

2.2.1. Chemical analysis

Chemical analysis was conducted on all three steels to confirm the chemical composition of each steel grade. Chemical analysis was measured by X-ray fluorescence (XRF), Thermo Scientific Niton XL3t GOLDD+, and Inductively Coupled Plasma Optical Emission Spectrometry, ICP-OES Agilent 720. Analysis of the chemical composition of the M2, M3:2 and M35 shows that the actual compositions are more or less within the standard range (Table 1). The variations are expected to have a negligible effect on the final properties of selected steel grades after heat treatment. Nevertheless, the presence of Co, Cu, Mn and S poses a possible difference in the behavior of the steel during heat treatment. However, no negative effects of Mn, Cu, S and Co on the microstructure were observed.

2.2.2. Microscopy

Samples were firstly investigated by light microscope ZEISS Axio Imager, Carl Zeiss, Oberkochen, Germany, at Institute of Metals and Technology (IMT) to obtain an overall picture of the microstructure, such as grains size, grain boundaries and phases present in the samples.

The used scanning electron microscope (SEM) was JSM-6500F, Jeol, Tokyo, Japan at IMT. For the energy-dispersive X-ray spectroscopy (EDS) program INCA, Oxford Instruments Analytical, UK was used. The electron backscatter diffraction (EBSD) was conducted using ZEISS Crossbeam 550 FIB-SEM Gemini II, Germany at IMT. SEM-EBSD mapping was performed under vacuum conditions below 10^{-6} mbar, acceleration voltage of 15 kV and current of approximately 5 nA. The size of the scanned area was $22 \times 17\ \mu m^2$ and step size 0.4 μm. EBSD was used for the interpretation of phase differences between DCT and CHT samples. The interpretation of the results was performed with Oin Software, AMETEK, Mahwah, NJ, USA.

2.2.3. XPS analysis

In addition to the microscopic investigations, X-ray photoelectron spectroscopy (XPS) was performed at Jožef Stefan Institute, with the electron spectrometer PHI-TFA XPS, Physical Electronics, Chanhassen, MN, USA. Al K-alpha was used as X-ray monochromatic source with the emission energy of 1486 eV. The sampled area was 0.4 mm in diameter and analysis depth was around 3–5 nm. A hemispheric analyzer detector of electron energy with 16 channels was used. All samples were surveyed with XPS across a wide energy range (0–1200 eV). These spectra were measured with the energy resolution of about 1.2 eV in order to identify and quantify the presence of different elements in the spectrum (samples). Multiple XPS spectra with high-energy resolution (0.65 eV) were then recorded on two different surface locations of the samples in order to identify the chemical state of the elements present in the samples. This way the peaks of C (1s), Co (2p), Fe (2p), Mo (3d), O (1s), W (4f) and W (4d) were recorded. Additionally, XPS depth profiles of chemical composition were recorded on the samples C1 and C2 down to the depth of about 10 nm. The samples were bombarded with Ar ions with energy of 3 keV over range of 3×3 mm. The velocity of ion etching

Table 2
Heat treatment parameters for M2, M3:2 and M35 steel.

Group	Subgroup	Austenitizing		DCT		Tempering (°C/h)
		Temperature (°C)	Time (min)	Temperature (°C)	Immersion time (h)	
A	A1	1230	2	–	–	3x550/1
	A2	1230	2	−196	24	550/1
B	B1	1180	2	–	–	3x540/2
	B2	1180	2	−196	24	540/2
C	C1	1230	2	–	–	3x550/2
	C2	1230	2	−196	24	550/2

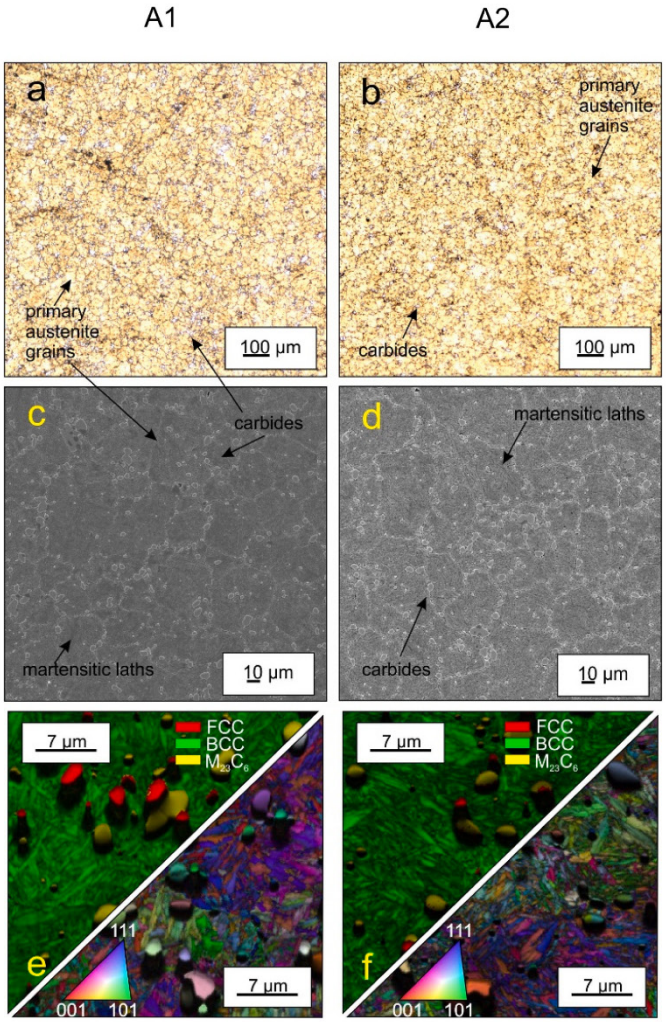

Fig. 1. Images obtained by light microscope (a and b), scanning electron microscope by secondary electrons imaging (SEM-SEI) (c and d) and by electron back-scattered diffraction (EBSD) and orientation (inverse pole figures) (e and f) for A1 (conventional heat treatment) and A2 (deep cryogenic treatment) of AISI M2.

rate was about 1 nm/min.

3. Results and discussion

3.1. SEM-EDS results

Light microscope images (Fig. 1a–b, Fig. 2a–b, Fig. 3a–b) were mainly obtained to get an overall picture of the microstructure of each subgroup of all three steel types. The evaluation of type, size, number and distribution of different phases was provided as an orientation for further analysis with SEM and XPS.

Secondary electron imaging (SEI) images (Fig. 1c–d) of steel A (AISI M2) show precipitation of fine carbides within a lath-type martensite matrix. These micrographs reveal spherical carbide precipitation of MC (M = V) (bright), M_6C (M = Fe, Mo, W) (dark), M_2C (M = Fe, Mo, W) (bright) and $M_{23}C_6$ (M = Fe, Cr) (dark). With additional measurements (including also transmission electron microscope - TEM), it was proven that MC, M_6C and M_2C are primary carbides and $M_{23}C_6$ are secondary

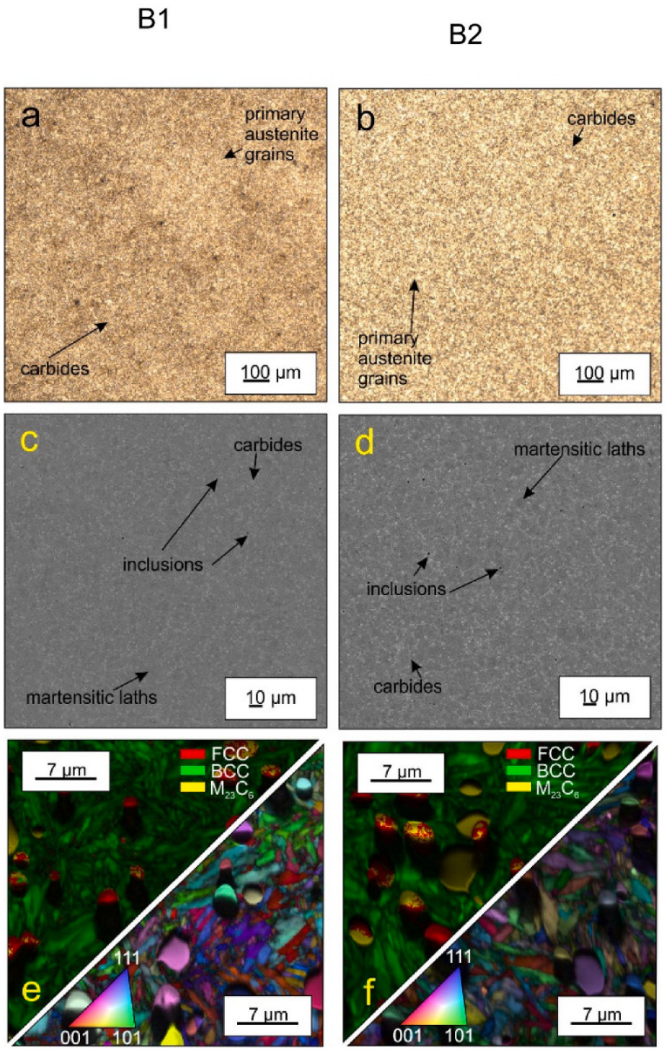

Fig. 2. Images obtained by light microscope (a and b), scanning electron microscope by secondary electrons (SEM-SEI) (c and d) and by electron backscattered diffraction (EBSD) and orientation (inverse pole figures) (e and f) for B1 (conventional heat treatment) and B2 (deep cryogenic treatment) of AISI M3:2.

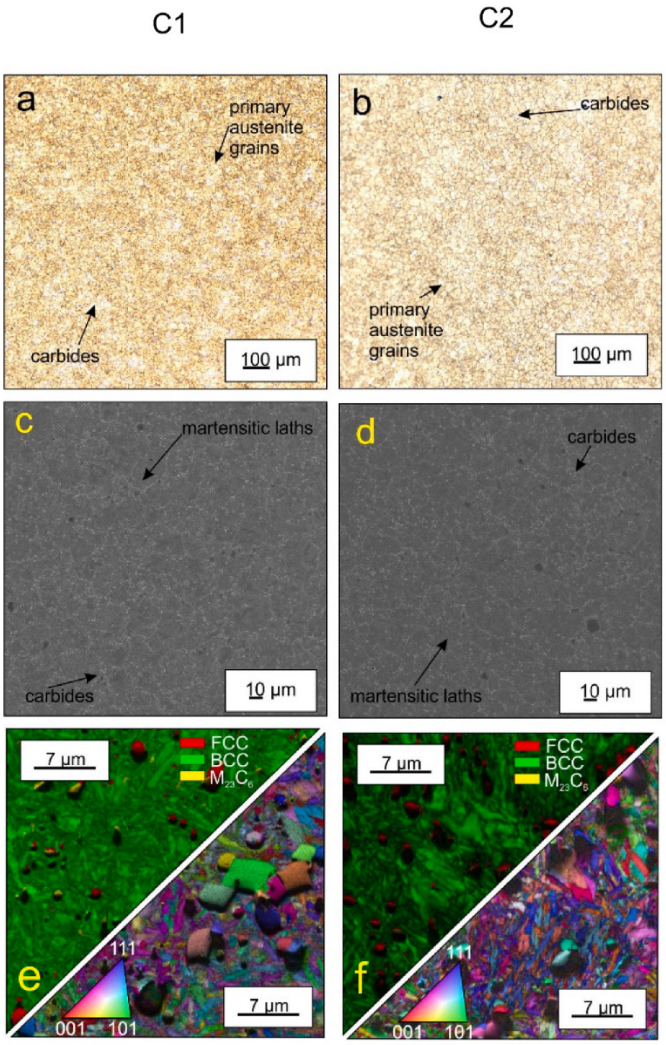

Fig. 3. Images obtained by light microscope (a and b), scanning electron microscope by secondary electrons (SEM-SEI) (c and d) and by electron backscattered diffraction (EBSD) and orientation (inverse pole figures) (e and f) for C1 (conventional heat treatment) and C2 (deep cryogenic treatment) of AISI M35.

carbides [21]. For this research the identification of the generation of carbides in all three steels was done with regards to the original state of microstructure of steel before heat-treatment. As compared to conventional heat treatment, DCT samples (A2) have less agglomerated carbides. They are also more homogenously distributed and larger in number. The average number of carbides in CHT (A1) samples is 25% lower as compared to the samples treated with DCT (A2).

SEI images of steel B (M3:2) (Fig. 2c–d) and steel C (M35) (Fig. 3c–d) show similar relation as in steel A, where fine carbide precipitation occurs within the lath martensite matrix. The carbides are the same types as found for steel A, where MC, M_6C and M_2C are primary carbides and $M_{23}C_6$ are secondary carbides. On average, for steel B DCT increased volume fraction of carbides by about 4% and for steel C by about 17%, where also less agglomerated and more homogenously distributed carbides can be observed.

The number of precipitated carbides have increased significantly after DCT, with the strongest DCT influence being found for M2 HSS (A). A possible explanation of the carbide phenomena (refinement of carbides and higher number) in DCT samples is the shrinkage pressure, which is induced by large temperature change when the sample is placed

from room temperature to deep cryogenic temperature. Under the shrinkage pressure, the crystal defect-vacancies, which are formed by the deformation, are reduced. The dislocations merge to form longer dislocations and with it future sub-boundaries. At the same time, twins and slip lines occur in the matrix, which additionally promote the formation of new sub-boundaries in the matrix (retained austenite/martensite [25]. Furthermore, the lattice distortion of the matrix (usually martensite) leads to segregation of alloying elements and carbon to nearby defects, where these locations act as potential centers for forming clusters and later development into carbide nuclei. The location and size of defects influences the potential carbide size and shape [26]. Thermodynamic modeling of the effect of cryogenic temperatures on the carbide evolution of selected steels indicate existence of preexisting M_7C_3 carbides that presumably form due to the aforementioned phenomenon [21]. The M_7C_3 carbides act as nucleation sites and intermediate stage for the formation of secondary carbides observed in the final structures of selected HSS. The additional contribution to the increased number of carbides is also the transformation of retained austenite into martensite during DCT [5], which is also induced by the shrinkage pressure.

3.2. SEM-EBSD results

To define phases in CHT and DCT samples and the differences between the two heat treatments (CHT and DCT), SEM-EBSD analysis was conducted (Fig. 1e–f, Fig. 2e–f, Fig. 3e–f). The selected EBSD colors are set as green, red and yellow, at which the green color stands for BCC lattice, red for FCC lattice and yellow represents $M_{23}C_6$ carbides. Due to the similar characteristic Kikuchi patterns (the position of the lattice points), the red color also marks different types of the carbides, such as MC, M_2C. Consequently, a detailed and precise analysis was carried out to distinguish between retained austenite and carbides. The inverse pole figures were used to show orientation of certain phases in the microstructure. The orientation directions are presented from red color for [0 0 1] to blue color for the [1 1 1] and green color for the [1 0 1], all the intermediate color shades correspond to the directions between these orientations. Shadowing on EBSD and IPF-Z maps is a result of the protruding carbides, which are less polished due to their higher hardness compared to the martensite matrix. The results of EBSD and IPF-Z maps are post-processed by filter application, image inversion and interpretation and correction of the data.

The SEM-EBSD results of the AISI M2 steel (A) (Fig. 1e–f) indicate and confirm that the matrix consists of lath martensite, where the laths are on average smaller in DCT sample (A2). The EBSD maps show the low defect content level of the martensite and carbides. The martensite orientation of CHT laths is in all lattice directions (A1), whereas in DCT sample (A2), the laths are oriented mostly along the [1 0 1] and [0 0 1] directions. EBSD also indicates that no retained austenite could be detected in both CHT (A1) and DCT (A2) samples. The reasons for no detection of RA in both samples could be in the location of measurements and very small patches (islands) of RA at the primary austenitic grain boundaries. Secondly, next to RA, carbide growth and cluster formation (nucleus) can occur and therefore obscure the RA position due to shading. The third option is the successful selection of CHT heat treatment procedure with triple tempering, explicitly aimed at obtaining minimum quantities of RA. The EBSD confirms that the carbides within all three steels are MC, M_2C, M_6C and $M_{23}C_6$.

The EBSD results of the AISI M3:2 steel (B) (Fig. 2e–f)) show similar phase identification, where the matrix is also lath martensite, but with a significantly higher number of carbides compared to steel A. Martensitic laths in CHT sample are on average 10% larger than those found in DCT sample. The growth of martensitic laths in steel B samples (B1) is observed to be similar as in steel A, with the laths in DCT samples (B2) being mostly oriented along the [1 0 1] and [0 0 1] directions. Similarly, as for steel A, no RA was observed in both samples B1 and B2.

The results of EBSD for the M35 steel (C) (Fig. 3e–f); indicate similar presence of phases as for the other two investigated HSS. The majority of laths in CHT sample (C1) grow in the [1 1 1] to [0 0 1] direction, with some exceptions growing along the [1 0 1]. In the DCT sample (C2) the similar change in growth, as with the other two HSS can be observed along the direction of [1 0 1]. Laths are on average 15% smaller in the DCT sample (C2) as compared to CHT counterpart (C1). Comparable to the other two steels, no RA was observed in CHT and DCT treated samples.

The possible explanation of the different lath size between CHT and DCT samples could be in tempering duration and/or temperature history (DCT). During tempering (in CHT triple tempering and in DCT only single tempering) of the HSS, the segregation of carbon and recrystallization (lath coarsening) of the martensitic structure occurs [27,28]. Due to the two additional cycles of tempering, it is proposed that the coarsening of the martensite occurs in CHT samples, while elimination of two tempering cycles and use of subzero temperature (−196 °C) the laths are finer. As a result, DCT has an additional positive effect on the steel properties [5,6]. Additionally, the smaller martensitic laths in DCT treated samples (A2, B2 & C2) also show, more rounded tips, which can be explained by different microstructural evolution compared to CHT samples (A1, B1 & C1); as described in Chapter 3.1.

The possible explanation for the change in the orientation of martensitic laths with DCT, proven by Hase et al. (2006) [29], is that the new orientation in DCT is a consequence of the subdivision of austenite by newly generated orientations of phases formed with austenite transformation during DCT. This was proven for bainite phase and it is suggested that the mechanism occurs also for the martensite phase, which correlates well with the results within this research. This mechanism also explains the congregated directional growth of martensite laths that are aligned based on the orientation of preexisting austenite grains.

3.3. XPS results

The main purpose of XPS was to see, if DCT (exposure of the steel to extreme cooling) influences the chemical state and chemical processes of the present elements in each steel. For steel C, depth profile analysis was also performed. It is important to point out, that XPS method is limited to the focusing of the X-ray beam and the results are obtained from an area with diameter of 0.4 mm. As a result, the chemical composition of many carbides, which have smaller size (range of 100 nm), cannot be determined for which other techniques were utilized for this purpose [21].

XPS spectrums for A1 (CHT) and A2 (DCT) are presented in Fig. 4, for B1 (CHT) and B2 (DCT) in Fig. 6 and for C1 (CHT) and C2 (DCT) in Fig. 7. Traces of Ca and Si are detected on the surface of all three steel samples, which are considered as contaminants. Due to the similarity of the chemical composition of the HSS steel samples, similar spectrums were obtained for all three steels regardless of the heat treatment strategy (CHT or DCT).

Within the spectrums, C1s peaks are identifiable (Fig. 4a, Fig. 6a, Fig. 7a), out of which the first smaller peak (289 eV) indicates carbonate and the stronger one at 284.5 eV indicates the C-C and C-H bonds. For O1s spectrum (Fig. 4b, Fig. 6b, Fig. 7b), the first stronger peak at 532 eV indicates absorbed oxygen and the smaller peak at 530 eV corresponds to the oxide state. Fe peaks occurred around 711 eV (greater peak) and 707 eV (smaller peak). The first Fe peak represents oxide (Fe(3+) oxidation state) and the second peak corresponds to elementary (metallic) Fe, which is interpreted as the matrix peak of selected steels. The peaks of Cr, W and Mo are also present in all three steels, for both heat treatments. Cr peaks occur in the range of 547.5 eV (Cr metal), as the most representative peak for presence of Cr carbides in the matrix, second one at around 576 eV (Cr (+3) oxide) and third at around 580 eV (Cr (+4) oxide). Mo spectrums are presented in Fig. 4c, Fig. 6c, Fig. 7c, from which the main peak can be seen at 233 eV, which indicates Mo (+6) oxidation state. The peak of Mo metal occurs at around 228 eV. In

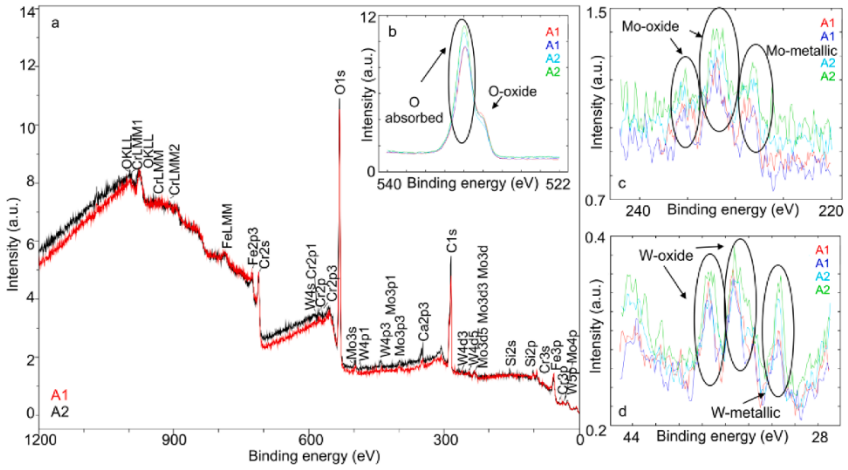

Fig. 4. a) X-ray photoelectron spectroscopy (XPS) surface spectrum from A1 (conventional heat treatment) (red color) and A2 (deep cryogenic treatment) (black color) AISI M2 samples. b) XPS spectrum of O1s on the surface of samples. c) XPS spectrum of Mo3d on the surface of samples. d) XPS spectrum of W4f on the surface of samples. For b and c, red and dark blue lines represent A1 spectrums and light blue and light green lines A2 spectrums. (For interpretation of the references to color in this figure legend, the reader is referred to the web version of this article.)

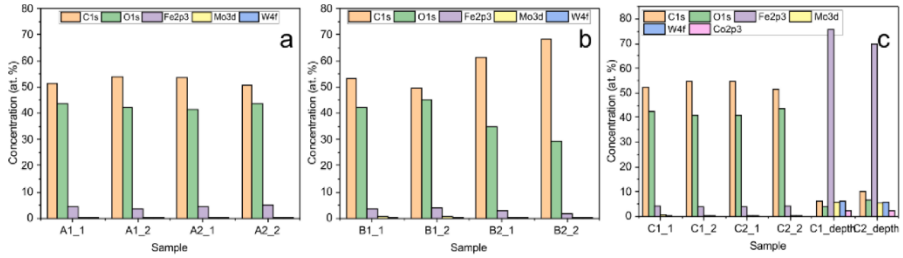

Fig. 5. Concentrations of selected peaks in (a) AISI M2 steel, (b) AISI M3:2 and (c) AISI M35 steel. For AISI M35 steel the concentrations for CHT and DCT samples after ion etching (depth of about 10 nm) are also provided.

the samples, Mo is mainly present in the carbides together with Fe and C. Fig. 4d, Fig. 6d, Fig. 7d show the spectra of W for CHT and DCT samples. The main two peaks (33 eV and 37 eV) are again dedicated to the oxides W(+6), whereas the W metal peak is also present at 31.5 eV. Similarly as Mo, W is also mainly bonded in carbides. V peaks are present in B and C steels, due to the higher amount of V present in these two steels. The interpretation of V peaks is not included, due to the low amplitude of characteristic XPS peaks. In the case of AISI M35 steel (C), Co peaks at 780 eV and 795 eV are also present in the spectrum, corresponding to metallic Co and Co(+2) respectively. The oxide peak is considerably broad, which corresponds to overlapping of the characteristic peaks of Co_3O_4 state.

From the results of AISI M2 steel (A), it can be concluded that there is an insignificant difference between CHT (A1) and DCT (A2) samples in terms of the overall chemical composition. Furthermore, the XPS spectrum confirms the presence of carbide forming elements in both samples. The intensities in A1 and A2 of C1s, O1s, Fe2p3, Mo3d and W4f (Fig. 5) are similar. The small difference in intensity of individual elements between samples can be explained by the varying presence of the oxides, carbonates, contaminants and adventitious carbon. The locally higher values of peak intensities can be also dedicated to the local change of the charging of the surface, change in sample surface condition and localized change in the number of chemical bonds. Nevertheless, for Mo3d and W4f peaks, an increase of the metallic specific peak is visible for A2 compared to A1 at 228.5 eV and 31.5 eV respectively (see Fig. 4c–d). These two specific peaks correspond to the state of the elements in carbide form [30,31]. This data support the SEM results from Section 3.2 that show an increase in the precipitation of carbides. Additionally, the sample comparison shows also a tendency of a smaller amount of oxides present for the DCT sample (A2). This could be related to the fact that a larger amount of carbides is present (see Section 3.2) with overall larger surface to volume ratio, that hinder oxide formation. Additionally, the number of carbide agglomerates is lower in DCT sample and could be a reason for the higher absorption of oxygen on the samples surface after DCT as there is less hindrance of absorption by the larger patches of carbides.

Spectrums for AISI M3:2 (B1-CHT and B2-DCT) are shown in Fig. 6. B1 and B2 have almost similar characteristic peaks. However, B1 has for specific elements a stronger peak intensity. Concerning the overall chemical composition, it is suggested, that similarly as for M2 steel no

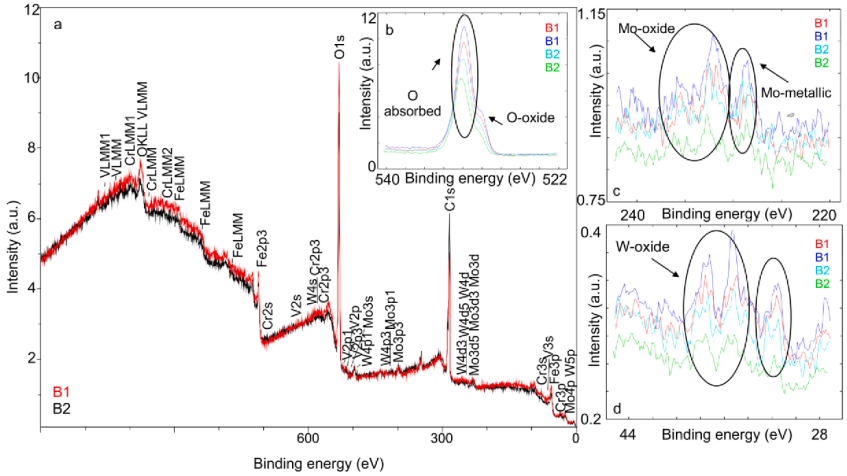

Fig. 6. a) X-ray photoelectron spectroscopy (XPS) surface spectrum from B1 (conventional heat treatment) (red color) and B2 (deep cryogenic treatment) (black color) AISI M3:2 samples. b) XPS spectrum of O1s on the surface of samples. c) XPS spectrum of Mo3d on the surface of samples. d) XPS spectrum of W4f on the surface of samples. For b and c, red and dark blue lines represent B1 spectrums and light blue and light green lines B2 spectrums. (For interpretation of the references to color in this figure legend, the reader is referred to the web version of this article.)

significant difference is visible between CHT (B1) and DCT (B2) samples. The XPS spectrums confirm the presence of carbide forming elements in both samples. The intensities of O1s, Fe2p3, are higher in the CHT sample (B1) as in DCT sample (B2), by roughly 26% (see Fig. 5). The reason for such a difference is a result of the higher carbon signal, which most probably is a result of a thicker layer of adventitious carbon. The proportionally lower oxide signal peak of the oxygen characteristic peak and other metal characteristic peaks supports this claim. Nevertheless, even with normalizing the peak intensities with the change in carbon signal, a lower absorption of oxygen is determined for DCT sample compared to its CHT counterpart. This is presumed to be a result of steel B not forming carbide agglomerates, because of which the surface to volume ratio of the small carbides is similar for both CHT and DCT samples. As a result, the higher amount of carbides in DCT sample does not allow high absorption of oxygen as the area of exposed iron matrix is lower. The metallic peak of carbide-forming Mo and W show no significant difference between CHT and DCT samples (see Fig. 6c–d), which goes well in hand with the indifference of oxygen oxide peak for the two samples. An additional contributing factor for the lower absorption of oxygen in DCT samples could also be the flatter surface (less exposed area) that forms due to the smaller martensitic laths. This has been measured additionally using surface confocal microscopic analysis (Keyence VHX 7000, Itasca, IL, USA) that proved that DCT sample has a much smoother surface than its CHT counterpart (see Supplementary Material 1).

Vanadium peaks also occur at 512.5 eV (V as metal), 513.5 eV for V (+2) and 516.5 eV for V(+4), the peaks are present in B and C steel in both CHT and DCT samples. V metal states, indicating presence of V in the precipitated carbides, show increased values in DCT sample and support the claim of higher carbide amount in the DCT sample (data not shown).

For AISI M35 steel (C), additional Co is detected for both samples (C1 and C2), which is present in the matrix or in carbides. In sample C1 the spectrum has slightly higher intensities in the higher binding energy range as sample C2 (Fig. 7e). This could be related to the higher inelastic scattering caused by a rougher surface in sample C1 compared to C2. The second reason also coincides with the surface measurements of steel B (see Supplementary Material 1). The oxide state of oxygen, similarly as for steel A, points to the lower oxide formation for DCT sample that result from the higher carbide number with larger surface to volume ratio. However, the absorption of oxygen seems to show no trend with relation to the treatment of steel C and varies based on position on the sample. This can be correlated with the large agglomerates present in steel C, which are considerably larger compared to those found in steel A. As a result, their seldom occurrence and large size can be the reason for such varying oxygen absorption peak. Similarly as in steel A, the W and Mo peaks indicate a difference between CHT and DCT sample in both metallic and oxide characteristic peaks (see Fig. 7c–d). The metallic Mo peak is proportionally higher in intensity for DCT sample compared to CHT sample. This coincides well with the increased precipitation of carbides, which was observed for DCT steel C (C2, Fig. 3d). Additionally, the oxide peaks of W are considerably lower in intensity for DCT sample compared to its CHT counterpart, which supports the claim of reduced oxide presence derived from the lower intensity of the oxygen oxide peak. Based on XPS results of steel C shows the largest impact of DCT on the carbide formation among the HSS investigated.

To determine the influence of the oxidation layer on the XPS spectrum, both C1 and C2 samples were etched with Ar ions down to the depth of 10 nm. Intermediate chemical measurements were made and chemical data of the state before and after etching was compared (Fig. 8a). From the spectrums of C1 depth profile and C2 depth profile, a significant change in the intensity of the signal for the binding energy from 1200 eV to 700 eV (2–3× increase of the signal) can be observed. The reason for the increase of the XPS signal is in the purer material, with no oxidation layer. The depth profile measurements show a carbon drop to low levels after about 1 min of etching, which corresponds well with the preexisting layer (about 1 nm) of adventitious carbon. The oxide layer is considerably thicker extending up to 4 nm (4 min of etching time to reach low levels of oxygen) for both DCT and CHT samples. The depth profile measurements show no significant difference between the two differently heat-treated samples of steel C (Fig. 8b–c). The XPS measurements of samples C1 and C2 after etching present no

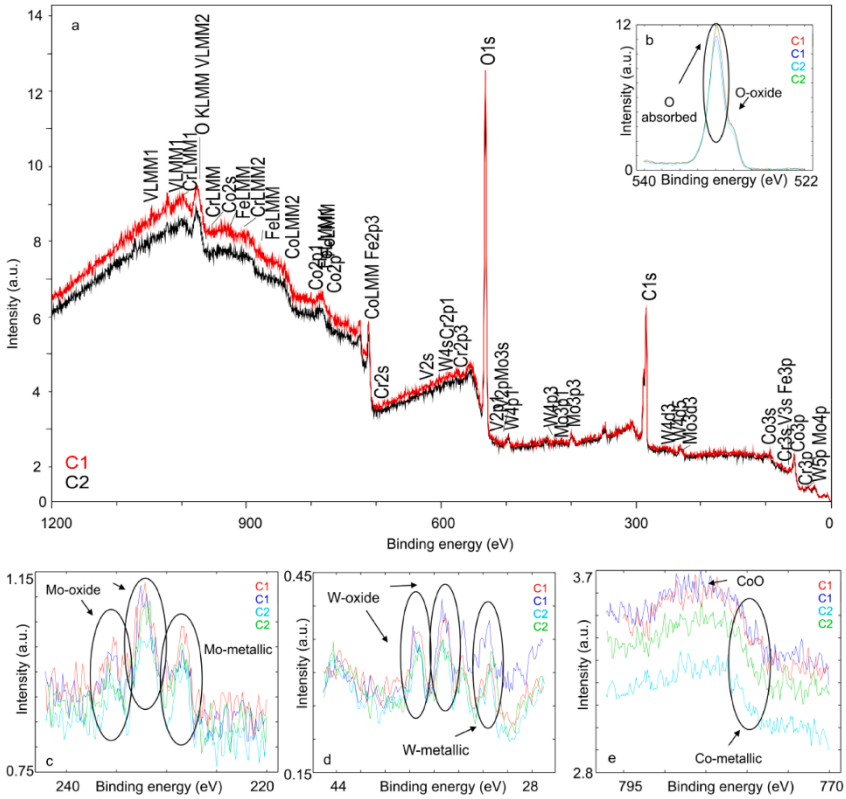

Fig. 7. a) X-ray photoelectron spectroscopy (XPS) surface spectrum from C1 (conventional heat treatment) (red color) and C2 (deep cryogenic treatment) (black color) AISI M35 samples. b) XPS spectrum of O1s on the surface of samples. c) XPS spectrum of Mo3d on the surface of samples. d) XPS spectrum of W4f on the surface of samples. For b and c, red and dark blue lines represent C1 spectrums and light blue and light green lines the C2 spectrums. D) XPS spectrum of Co2p. (For interpretation of the references to color in this figure legend, the reader is referred to the web version of this article.)

significant difference between the two samples. The individual characteristic peaks of Fe, W and Mo are very similar in intensity between CHT and DCT samples. However, the typical carbide related carbon peak, revealed by etching, is slightly higher in intensity for DCT sample compared to CHT counterpart, which matches the findings of larger number of carbides in DCT sample. The indifference of the metal peaks from both samples is considered to originate from the overlapping of the carbide and pure metal characteristic peaks and the significantly lower intensity of carbide characteristic peaks (intensity scales with area fraction of carbides, which is about 10%).

From XPS spectrums, it can be concluded, that DCT has generally an influence on the formation of carbides for the selected HSS. AISI M2 (A) A and M35 (C) steels show notable changes, which correlate well with the microstructural observations, conducted with SEM and support the claim of larger number of carbides (overall larger surface to volume presence in the material). For AISI M3:2 steel (B) the XPS results show no significant trend in terms of DCT influence on the carbide formation, which also goes in hand with the considerably smaller change in number of carbides and the general absence of carbide clusters.

4. Conclusions

The effectiveness of DCT was investigated by the combination of light microscopy, SEM; SEM-EDS; SEM-EBSD and XPS.

Light microscope images provided information about the grains and grain boundaries, precipitates and phases of each subgroup of all three steel types. The obtained results from the light microscope confirmed high amount of carbides present for all three samples and similar distribution of phases.

SEM imaging provided the overall images of the CHT and DCT samples, from which an increased number of precipitated carbides was observed for DCT samples by 17%, 4% and 25% for steels M2, M3:2 and M35 respectively. The phenomenon can be explained by the shrinkage pressure and transformation of the retained austenite into martensite as well as by the formation of additional nuclei and intermediate carbide formations induced by exposure of selected steels to cryogenic temperatures.

SEM-EBSD technique provided the information of DCT influence on the texture, phases and morphology of the microstructure. The data indicates, that the martensitic laths in DCT samples are smaller and less

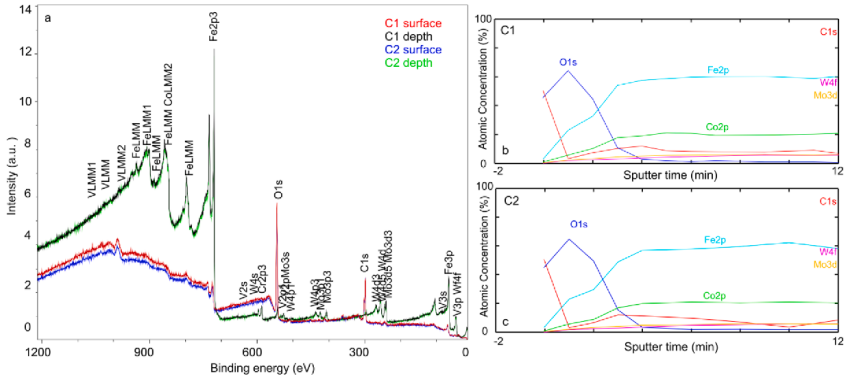

Fig. 8. a) Spectrum comparison of the surface (C1-red, C2-blue) and depth (C1-black, C2-green) X-ray photoelectron spectroscopy (XPS) of the C1 (conventional heat treatment) and C2 (deep cryogenic treatment) samples. b) C1 atomic concentration depth profile of elected oxidation states. c) C2 atomic concentration depth profile of elected oxidation states. (For interpretation of the references to color in this figure legend, the reader is referred to the web version of this article.)

sharpened compared to CHT and the laths are more orientated towards the orientation of preexisting austenite grains, mainly along the [1 0 1] and [0 0 1] direction. The less stochastically aligned laths are considered to form due to the subdivision of primary austenite grains that occurs with exposure to cryogenic temperatures.

From XPS spectrums it was observed, that DCT has an insignificant impact on the chemical structure of the sample. However, the oxide formation and metallic state peaks of W and Mo support the observations of higher number of precipitates and larger surface to volume ratio of carbides in the selected steels (clearly observed for steels M2 and M35 due to their larger increase of carbide numbers with DCT). Additionally, the reduced amount of carbide clusters after DCT could be correlated to the oxygen absorption and oxide state of oxygen of individual steel samples. Furthermore, oxygen absorption analysis and XPS background analysis, also indicate the effect of DCT on the refinement of martensitic laths in the matrix, resulting in a smoother surface. Overall, the XPS results confirm the pre-dominant influence of DCT on the microstructure (grains, phases etc.), which then leads to the change of the steel's properties (hardness, fracture toughness, tribological properties etc.).

Finally, the presented results provide useful input into the DCT dynamic of the selected high-speed steels and provide a way of interpreting XPS data in terms of the DCT effect on carbide refinement and precipitation. Overall, DCT influences both carbide precipitation and the matrix by introducing a finer microstructure and smoother surface formation.

Funding

This work was supported by Slovenian Research Agency -ARRS [J2-9211 and P2-0050].

CRediT authorship contribution statement

Patricia Jovičević-Klug: Conceptualization, Investigation, Visualization, Writing - original draft. **Monika Jenko:** Supervision, Writing - review & editing. **Matic Jovičević-Klug:** Visualization, Writing-review & editing. **Barbara Šetina Batič:** Investigation, Visualization. **Janez Kovač:** Resources, Investigation. **Bojan Podgornik:** Supervision, Writing - review & editing.

Declaration of Competing Interest

The authors declare that they have no known competing financial interests or personal relationships that could have appeared to influence the work reported in this paper.

Acknowledgments

Acknowledgement goes to IMT chemical and metallographic labs and microscope operators.

Appendix A. Supplementary material

Supplementary data to this article can be found online at https://doi.org/10.1016/j.apsusc.2021.149257.

References

[1] D. Senthilkumar, Effect of deep cryogenic treatment on residual stress and mechanical behaviour of induction hardened En 8 steel, Adv. Mater. Process. Technol. 2 (2016) 427–436, https://doi.org/10.1080/2374068X.2016.1244326.

[2] P. Baldissera, C. Delprete, Deep cryogenic treatment: a bibliographic review, Open Mech. Eng. J. 2 (2008) 1–11, https://doi.org/10.2174/1874155X00802010001.

[3] H.B. Patil, P.B. Chavan, S.H. Kazi, Effects of cryogenic on tool steels-a review, Int. J. Mech. Prod. Eng. 1 (2013) 31–36.

[4] C.A. Dumasia, V.A. Kulkarni, K. Sonar, A review on the effect of cryogenic treatment on metals, Int. Res. J. Eng. Technol. 4 (2017) 2402–2406. https://irjet.net/archives/V4/i7/IRJET-V4I7490.pdf.

[5] P. Jovičević-Klug, B. Podgornik, Review on the effect of deep cryogenic treatment of metallic materials in automotive applications, Metals. 10 (2020) 434, https://doi.org/10.3390/met10040434.

[6] A. Molinari, M. Pellizzari, S. Gialanella, G. Straffelini, K.H. Stiasny, Effect of deep cryogenic treatment on the mechanical properties of tool steels, J. Mater. Process. Technol. 118 (2001) 350–355, https://doi.org/10.1016/S0924-0136(01)00973-6.

[7] S. Li, M. Xiao, G. Ye, K. Zhao, M. Yang, Effects of deep cryogenic treatment on microstructural evolution and alloy phases precipitation of a new low carbon martensitic stainless bearing steel during aging, Mater. Sci. Eng., A (2018), https://doi.org/10.1016/j.msea.2018.07.012.

[8] P. Jurči, M. Dománková, J. Ptačinová, M. Pašák, M. Kusý, P. Priknerová, Investigation of the microstructural changes and hardness variations of sub-zero treated Cr-V ledeburitic tool steel due to the tempering treatment, J. Mater. Eng. Perform. 27 (2018) 1514–1529, https://doi.org/10.1007/s11665-018-3261-6.

[9] M. Pellizzari, Influence of Deep Cryogenic Treatment on the heat treatment of steel and selected non ferrous alloys. (Cu-Be alloys), Int. Heat Treat. Surf. Eng. 4 (2010) 105–109.

[10] M. Pérez, C. Rodríguez, F.J. Belzunce, The use of cryogenic thermal treatments to increase the fracture toughness of a hot work tool steel used to make forging dies, Procedia Mater. Sci. 3 (2014) 604–609, https://doi.org/10.1016/j.mspro.2014.06.100.

[11] D. Hradil, M. Duchek, T. Hrbáčková, A. Ciski, Gas nitriding with deep cryogenic treatment of high-speed steel, Acta Metallurgica Slovaca. 24 (2018) 187–193, https://doi.org/10.12776/ams.v24i2.1058.

[12] Y. Yao, Y. Zhou, Effects of deep cryogenic treatment on wear resistance and structure of GB 35CrMoV steel, Metals. 8 (2018) 502, https://doi.org/10.3390/met8070502.

[13] A. Idayan, A. Gnanavelbabu, K. Rajkumar, Influence of deep cryogenic treatment on the mechanical properties of AISI 440C bearing steel, in: Procedia Engineering, Elsevier Ltd, 2014, pp. 1683–1691. doi: 10.1016/j.proeng.2014.12.319.

[14] K. Amini, M. Negahbani, H. Ghayour, The effect of deep cryogenic treatment on hardness and wear behavior of the H13 tool steel, Metallurgia Italiana. 107 (2015) 53–58.

[15] D. Senthilkumar, Cryogenic treatment: shallow and deep, in: G.E. Totten, R. Colas (Eds.), Encyclopedia of Iron, Steel, and Their Alloys, Taylor and Francis, NY, USA, New York, NY, 2016, pp. 995–1007, https://doi.org/10.1081/E-EISA-120052805.

[16] M. Pellizzari, A. Molinari, Deep cryogenic treatment of cold work tool steel, in: 6th International Tooling Conference, Stockholm, Sweden, n.d., pp. 657–669.

[17] P. Jovičević-Klug, B. Podgornik, Comparative study of conventional and deep cryogenic treatment of AISI M3:2 (EN 1.3395) high-speed steel, J. Mater. Res. Technol. 9 (2020) 13118–13127, https://doi.org/10.1016/j.jmrt.2020.09.071.

[18] S.S. Gill, J. Singh, R. Singh, H. Singh, Effect of cryogenic treatment on AISI M2 high speed steel: metallurgical and mechanical characterization, J. Mater. Eng. Perform. 21 (2012) 1320–1326, https://doi.org/10.1007/s11665-011-0032-z.

[19] J. Li, X. Yan, X. Liang, H. Guo, D.Y. Li, Influence of different cryogenic treatments on high-temperature wear behavior of M2 steel, Wear 376–377 (2017) 1112–1121, https://doi.org/10.1016/j.wear.2016.11.041.

[20] M. Pellizzari, A. Molinari, L. Girardini, L. Maldarelli, Deep cryogenic treatment of AISI M2 high-speed steel, Int. J. Microstruct. Mater. Prop. 3 (2008) 383–390, https://doi.org/10.1504/IJMMP.2008.018742.

[21] P. Jovičević-Klug, M. Jovičević-Klug, B. Podgornik, Effectiveness of deep cryogenic treatment on carbide precipitation, J. Mater. Res. Technol. 9 (2020) 13014–13026, https://doi.org/10.1016/j.jmrt.2020.09.063.

[22] C.L. Gogte, D.R. Peshwe, R.K. Paretkar, Influence of cobalt on the cryogenically treated W-Mo-V high speed steel, in: Advances in Cryogenic Engineering, Spokane, WA, USA, 2012, pp. 1175–1182. Doi: 10.1063/1.4707039.

[23] M. Villa, M. Somers, Cryogenic treatment of an AISI D2 steel: the role of isothermal martensite formation and "martensite conditioning", Cryogenics 110 (2020), 103131 https://doi.org/10.1016/j.cryogenics.2020.103131.

[24] Y. Meng, M. Villa, K.V. Dahl, T.L. Christiansen, M.A.J. Somers, Synchrotron X-ray diffraction investigation of the effect of cryogenic treatment on the microstructure of Ti-6Al-4V, Appl. Surf. Sci. 502 (2020), https://doi.org/10.1016/j.apsusc.2019.144087.

[25] Z. Shengquan, W. Bing, W. Shizhuo, Z. Changzhong, W. Xijing, Z. Zhongke, Effect of cryogenic treatment on extruded copper structures, in: IOP Conference Series: Materials Science and Engineering, 20–22 September, 2019, Jiaozuo, Henana, China, 2019, pp. 1–10. doi: 10.1088/1757-899X/688/3/033087.

[26] Y.Y. Su, L.H. Chiu, F.S. Chen, S.C. Lin, Y.T. Pan, Residual stresses and dimensional changes related to the lattice parameter changes of heat- treated JIS SKD 11 tool steels, Mater. Trans. 55 (2014) 831–837.

[27] G.R. Speich, W.C. Leslie, Tempering of steel, Metall Trans. 3 (1972) 1043–1054, https://doi.org/10.1007/BF02642436.

[28] S. Li, M. Xiao, G. Ye, K. Zhao, M. Yang, Effects of deep cryogenic treatment on microstructural evolution and alloy phases precipitation of a new low carbon martensitic stainless bearing steel during aging, Mater. Sci. Eng., A 732 (2018) 167–177, https://doi.org/10.1016/j.msea.2018.07.012.

[29] K. Hase, C. García-Mateo, H.K.D.H. Bhadeshia, Bimodal size-distribution of bainite plates, Mater. Sci. Eng., A 438–440 (2006) 145–148.

[30] C.B. Rodella, D.H. Barrett, S.F. Moya, S.J.A. Figueroa, M.T.B. Pimenta, A.A. S. Curvelo, V. Teixeira Da Silva, Physical and chemical studies of tungsten carbide catalysts: effects of Ni promotion and sulphonated carbon, RSC Adv. 5 (2015) 23874–23885, https://doi.org/10.1039/c5ra03252k.

[31] L. Jin, A. Chen, Y. Wang, P. Wang, Effect of cryogenic treatment on microstructure and properties of copper alloy, Jinshu Rechuli/Heat Treatment of Metals. 43 (2018) 199–202, https://doi.org/10.13251/j.issn.0254-6051.2018.09.041.

Chapter 5

Impact of Steel Type, Composition and Heat Treatment Parameters

The main aim of this chapter is to challenge some theories how chemical composition of ferrous alloy, type and selected heat treatment parameters, such as austenitizing and tempering temperature, influence the DCT performance. Additionally, to the final state of the microstructure, the evolution of microstructure through different stages of heat treatment as well as initial matrix state (ferritic, martensitic, bainitic etc.) before the heat treatment also define the effectiveness of DCT. The results indicate that the DCT effect on the final microstructure of steels is strongly related to the chemical composition of individual steel and the predefined matrix microstructure (as delivered stage). This also relates to the steel type (tool steel, bearing steel or stainless steel). This study also showed that generally DCT increases precipitation of carbides and induces their more homogenous distribution, regardless of the type of matrix (bainite/martensite/pearlite). The study also shows that not only martensitic laths, but also bainitic laths display preferable crystallographic orientation, which indicates the complex nature of DCT in different steels and that one mechanism cannot be applied for all ferrous alloys. Thus, more research and analyses are needed to understand the underlying mechanism(s) and their impact on the investigated materials. The study also indicates that the increased carbide precipitation after DCT is correlated with the higher carbon content, whereas the content of other alloying elements does not proportionally upscale the precipitation behavior.

Brief discussion: The obtained results provide a guide towards the optimal heat treatment regime for selected steel type (tool steel, bearing steel and stainless steel) for the most positive and influential effect of incorporated DCT, which was determined to be higher austenitizing and lower tempering temperature. With these parameters, the steels' properties are considered to improve with DCT due to the stronger carbide precipitation (stainless steel up to 94 %, hot work tool steel up to 50 %, bearing steel up to 15 % and cold work tool steel up to 10 %). Furthermore, DCT positively modifies the matrix through size and morphological refinement, increased homogeneity and more even redistribution of alloying elements. The decrease of retained austenite can be observed after the application of DCT even up to 93 % and the preferential orientation of bainitic/martensitic matrix domains along the <1 0 1> and <0 0 1> direction is documented. Furthermore, the interesting observation of M_7C_3 carbide precipitation was observed in DCT chromium-bearing steel, which is also correlated to the increased precipitation of $M_{23}C_6$ carbides. This dynamic is considered to be related to the redistribution of the alloying elements, namely carbon and chromium, and consequential homogenization of the matrix after DCT. Moreover, the microstructure evolution is related to the steel type, chemical composition as well as the prior microstructure set through the austenitization and quenching, which in some cases modified the DCT effect to be higher with lower austenitizing and higher tempering temperature. The research delivers proof to the complex nature and interdependency of the DCT effect. As such, it provides reasonable explanation for the dichotomy of the DCT effect in previous studies due to the lack of insight and consideration on the complex relations and interdependency with all considered parameters that the DCT effectiveness depends on.

The ***author's contribution*** to the paper ***Impact of steel type, composition and heat treatment parameters on effectiveness of deep cryogenic treatment***, published in Journal of Materials Research and Technology, was: conceptualization, validation, investigation, planning of experiments, visualization, evaluation and writing (original draft and editing).

This article addresses thesis ***Hypotheses 1, 2 and 3***.

JOURNAL OF MATERIALS RESEARCH AND TECHNOLOGY 2021;14:1007–1020

Available online at www.sciencedirect.com

jmr&t Journal of Materials Research and Technology

journal homepage: www.elsevier.com/locate/jmrt

Original Article

Impact of steel type, composition and heat treatment parameters on effectiveness of deep cryogenic treatment

Patricia Jovičević-Klug [a,b,*], *Matic Jovičević-Klug* [a], *Tina Sever* [a], *Darja Feizpour* [a], *Bojan Podgornik* [a,b]

[a] *Institute of Metals and Technology, Lepi pot 11, 1000, Ljubljana, Slovenia*
[b] *Jožef Stefan International Postgraduate School, Jamova cesta 39, 1000, Ljubljana, Slovenia*

ARTICLE INFO

Article history:
Received 29 April 2021
Accepted 6 July 2021
Available online 10 July 2021

Keywords:
Steel
Deep cryogenic treatment
Microstructure
Precipitation
Carbide evolution
Heat treatment

ABSTRACT

In recent years, promising technique of deep cryogenic treatment (DCT) is taking a new step in improving properties of various materials, especially steels. This study is focusing on influence of selected heat treatment process involving deep cryogenic treatment on the microstructure and microstructural evolution of four different steel grades (bearing steel 100Cr6, cold work tool steel X210Cr12, hot work tool steel X38CrMoV5-3 and stainless steel X17CrNi16-2). The study was performed for different heat treatment conditions, focused on effectiveness of DCT when using different austenitizing and tempering temperatures. The evolution of the microstructure was investigated in a sequential manner with various analytical techniques. The study indicates that the microstructure and microstructural evolution and changes are strongly related to the chemical composition of steel and the predefined matrix microstructure. DCT increases precipitation of carbides and induce their more homogenous distribution. The magnitude of increased carbide precipitation after DCT is correlated with the higher carbon content, whereas the content of other alloying elements does not scale with the precipitation behavior. The obtained results indicate that incorporation of DCT with heat treatment with higher austenitizing and lower tempering temperature is the most suitable for improving steels' properties with DCT, due to the stronger impact of DCT on the carbide precipitation and matrix modification.

1. Introduction

In recent years, deep cryogenic treatment (DCT) is rising as an important tool (part of heat treatment) for improving properties of ferrous and non-ferrous alloys such as: wear [1] and corrosion resistance [2], hardness [3] and fracture toughness, without additional application of coatings, surface engineering or any other surface finishing. Literature reviews on DCT show that tool steels and high-speed steels [4–7] are

* Corresponding author.
E-mail address: patricia.jovicevicklug@imt.si (P. Jovičević-Klug).
https://doi.org/10.1016/j.jmrt.2021.07.022

most commonly associated with DCT testing and improvement of properties. Whereas stainless and bearing steel grades are not usually selected for testing and modification with DCT [6]. This occurs, as on the one hand, the applicability and critical properties are different for stainless and bearing steels compared to tool steels, and on the other hand DCT is still a technique in development for the application on various steels, such as stainless and bearing steels. Tool steels (cold and hot work tool steels) and stainless steels are commonly used in industry for rolls, press tools, punches, bushes, fasteners, bolts, pump and propeller shafts [8,9]; whereas bearing steel is used for bearings in rotating machinery [10]. For the application of DCT, the main purpose of the process is to reduce retained austenite (RA) and consequently convert it into daughter phase martensite [6]. This causes the increase in hardness and reduces residual stresses (improvement of wear resistance) [11], which is favorable in tool industry for prolonged material/tool lifecycles. However, such general modification is considered not useful for some stainless and bearing steels, since the presence of austenite in the microstructure is associated with increased corrosion resistance [12], better toughness, increased ductility and elongation [13,14]. However, for martensitic stainless steels and bearing steels used for high friction applications the main concern are hardness, surface quality and fatigue resistance, which can be effectively modified with DCT.

These improvements of mechanical and tribological properties result from microstructural changes after DCT such as: carbon redistribution and site reduction, more homogeneous and increased precipitation of fine submicroscopic carbides (secondary and tertiary) and refinement of martensitic laths [4]. The common accepted theories of DCT influence on the increased carbide precipitation state that: (1) the carbide formation is a consequence of phase change from retained austenite into martensite [15,16]; (2) local plastic deformation during heat treatment causes segregation of carbon atoms through dislocation to local deformed areas during tempering, which acts as nuclei for future carbides [17]; (3) carbide precipitation is a product of contraction and expansion of the martensitic lattice [18] and finally (4) the increase in precipitated carbides is a function of the carbides and their placement in the matrix [19]. The factors influencing the DCT effectiveness are DCT soaking temperature, DCT soaking time, warming/cooling rate of DCT and placement of DCT in the heat treatment scheme [17]. Furthermore, the effectiveness of DCT on steels is also influenced by the austenitization and tempering temperatures [17,20–22]. This effectiveness is related to the chemical composition of each steel that influences the microstructure and mechanisms during heat treatment (conventional heat treatment (CHT) or DCT). Alloying elements such as Cr, Mo, V and Mn, at which the latter is a weak carbide former, induce additional carbide precipitation in steels [23]. As a result, these elements are considered as the major influencing factors for determining the DCT effectiveness on steels from a chemical standpoint. Cr is one of the leading alloying elements that is used in various steel grades and types that leads to the reduction of Ac1, as well as modifies the solubility energy of other alloying elements [24]. Consequently, Cr induces finer carbide precipitation and alteration of the microstructural changes with the application of different heat treatments [25]. This is also directly connected with the DCT influence on the C redistribution, homogenization and increased C clustering with localized depletion of the matrix that effectively change the macroscopic properties of the material/tool [26]. All these interdependencies lead to a complex interrelated system, requiring careful understanding and an in-depth progressive research of the dependencies contributing to the effect of DCT for different steels.

For this reason, this research intends to resolve the connection of DCT effect with relation to chemical composition (low/high carbon and low/high chromium content) and steel type (tool steel, stainless steel, bearing steel), as well as heat treatment conditions (austenitizing and tempering temperature) that lead to changes in the microstructural dynamics and thermodynamic processes. The study focuses on the microstructural changes concerning carbide precipitation, carbide type and distribution, matrix type and possible mechanisms of carbide formation, with the conventional heat treatment taken as a reference. The aim is thus to explain possible phenomena behind DCT in different steel types at different heat treatment temperatures and to provide theoretical background in the development of carbides under DCT, based on the predefined steel matrix structure.

2. Experimental

2.1. *Material and heat treatment*

In this work, four different steel grades (tool steels X38CrMoV5-3 (D) and X210Cr12 (Y), martensitic stainless steel X17CrNi16-2 (E) and bearing steel 100Cr6(X)) were used. The selected steels are chosen due to different chemical composition, ranging from low carbon/high chromium (X17CrNi16-2), low to medium carbon/chromium (X38CrMoV5-3 and 100Cr6) to high carbon/high chromium steel (X210Cr12). Steels were also chosen based on their different matrix microstructure, commonly obtained after heat treatment. The steels X210Cr12 and X17CrNi16-2 have preferentially a martensitic matrix; X38CrMoV5-3 has a bainitic/martensitic matrix and 100Cr6 a ferritic/pearlitic matrix. Steels were delivered in the form of rolled, peeled and soft annealed bars with Ø20 mm. The chemical composition of all four steel grades is shown in Table 1.

The heat treatment procedure of each steel is schematically presented in Fig. 1 and their individual parameters in Table 2, at which two combinations of austenitizing and tempering temperature are selected for each steel grade. For the first treatment, high austenitizing temperature and low tempering temperature is used, aimed at high primary carbides dissolution rate. For the second treatment, low austenitizing and high tempering temperature is used. For each treatment a control group with CHT (D1, D3, E1, E3, X1, X3, Y1, Y3) and tested group with DCT (D2, D4, E2, E4, X2, X4, Y2, Y4) are devised. All samples were heat treated in a horizontal vacuum furnace Ipsen VTTC324-R. The quenching was performed in N_2 gas at pressure of 1.05 bar (EN X38CrMoV5-3) or

Table 1 – Chemical composition of selected steels in mass contents (wt. %). Analyzed values measured with ICP-OES Agilent 720.

Steel grade (EN)	C	Mn	S	Cr	Si	Ni	V	Mo	Fe
X17CrNi16-2	0.17	0.83	0.017	15.22	0.29	1.50	–	0.11	Base
X38CrMoV5-3	0.38	0.43	0.001	4.91	0.30	0.14	0.57	2.92	Base
100Cr6	0.93	0.41	0.004	1.41	0.30	–	–	–	base
X210Cr12	2.07	0.35	0.002	12.40	0.23	0.11	0.16	0.13	base

5 bars (EN X210Cr12, EN X17CrNi16-2 and 100Cr6). The parameters of the conventional heat treatment (control group) (CHT) were chosen according to the suppliers' recommendations for the heat treatment of each steel grade aimed at obtaining high hardness (first treatment D1-D2, E1-E2, X1-X2, Y1-Y2) or high toughness (D3-D4, E3-E4, X3-X4, Y3-Y4). The tested DCT group of samples was exposed to DCT performed after quenching in a controlled environment with gradual immersion in liquid nitrogen for 24 h (cooling and warming rate of about 10 °C min^{-1}). After reaching room temperature DCT treated samples were finalized by single-step tempering.

Samples for microstructural analysis were cut from bigger cylindrical samples (Ø 10 × 100 mm), taken after designated heat treatments (Table 2) as well as at the intermediate states of the individual heat treatment (see scheme in Fig. 1). X-ray diffraction (XRD) and scanning electron microscopy (SEM) samples were prepared in size of 10 mm diameter and 5 mm thickness. The XRD and SEM samples were embedded in resin and ground with 320, 500, 800, and 1200 grit SiC paper. Their surface was polished with 3 μm and 1 μm diamond suspension as per standard metallographic procedure. For transmission electron microscopy (TEM) and scanning TEM (STEM), samples were prepared from 3 mm wide, around 1 mm high and 1 mm thick lamellas, which were thinned by grinding and polishing using SiC papers to around 100–150 μm thickness and additionally ion-milled using JEOL EM-09100IS Ion Slicer (JEOL, Tokyo, Japan) to electron transparency.

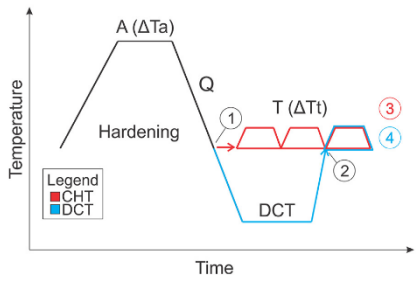

Fig. 1 – Scheme of heat treatment with selected heat treatment temperature (ΔTa and ΔTt). The position within the heating procedure of individual steel states analyzed for each heat treatment is indicated in the scheme with numbers (1- quenched before DCT (QBDCT), 2-quenched after DCT (ADCT), 3-final microstructure after conventional heat treatment (CHT) procedure, 4-final microstructure after deep cryogenic heat treatment (DCT) procedure).

2.2. *Microstructural and phases analysis*

To provide a systematic investigation of the possible underlying mechanism/s of DCT in different steels, microstructural changes were studied with SEM, energy-dispersive X-ray spectroscopy (EDS), electron backscatter diffraction (EBSD), XRD, TEM, STEM. Metallographically prepared samples were first inspected with light microscopy (Zeiss Axio Imager.Z2m with Zen software, Carl Zeiss AG, Germany) and scanning electron microscopy (Jeol JSM-6500F, Jeol Ltd., Japan). The samples were afterwards also inspected after being etched for 5 s with 5% Nital (D, X group) or 10% ferric chloride (E, Y group). Chemical composition of individual microstructural features was also analyzed by energy-dispersive X-ray spectroscopy (EDS) with 15 keV electron beam (Oxford EDS INCA Energy 450, detector type INCA X-SIGHT LN2, Oxford Instruments, UK). The size and distribution analysis of carbides was conducted with program INCA (so-called featuring) and by post processing of multiple SEM images through gray level and common contrast feature analysis using Fiji [27]. The analysis for each steel grade and heat treatment was conducted on the most representative sample area of 400 × 400 μm^2. Carbide distribution is presented with relative frequency (the number of carbides per area) and area fraction (percentage of steel area occupied by carbides) in correlation with the carbide size threshold for selected steels. The carbide size is expressed as carbide equivalent diameter (ECD) [28]. Samples were also later prepared for electron backscatter diffraction (EBSD) analysis, by polishing with 3 μm and 1 μm diamond suspension and finished with colloidal silica. EBSD was performed on Zeiss CrossBeam 550 (Carl Zeiss AG, Germany) with Edax EBSD system (Hikari Super plus camera with Apex and OIM Analysis software, EDAX, Ametek Inc., US). The measured crystallographic orientations are denoted by red color for [0 0 1], blue color for [1 1 1] and green color for [1 0 1], with their corresponding vector summations represented by intermediate color shades (inverse pole figures). Large phases (down to 1 μm) were determined with EDS stoichiometry analysis and Kikuchi pattern analysis. Their presence and distribution were also confirmed with EBSD. The EBSD mappings were performed locally at 2500x magnification to observe the shape of the matrix features and individual carbides. Area of 43.3 × 33.7 μm^2 was inspected with 100 nm step size for each sample. The volumetric fraction of phases was also determined with XRD. The XRD analysis was carried out on PANalytical 3040/60, Almelo, Netherlands. The XRD data was measured from 15° to 90° of 2θ angle. The phase identification

Table 2 – Heat treatment of selected steel samples, where CHT samples were conventionally heat-treated and DCT were deep cryogenic heat treated.

Steel (EN)	Subgroup	Austenitizing (°C/min)	DCT (°C/h)	Tempering (°C/h)
X38CrMoV5-3 (D)	1-CHT (D1)	1080/20	–	3 × 525/2
	2-DCT (D2)	1080/20	−196/24	1 × 525/2
	3-CHT (D3)	1030/20	–	3 × 600/2
	4-DCT (D4)	1030/20	−196/24	1 × 600/2
X17CrNi16-2 (E)	1-CHT (E1)	1050/30	–	1 × 480/2
	2-DCT (E2)	1050/30	−196/24	1 × 480/2
	3-CHT (E3)	980/30	–	1 × 600/2
	4-DCT (E4)	980/30	−196/24	1 × 600/2
100Cr6 (X)	1-CHT (X1)	870/30	–	1 × 150/1
	2-DCT (X2)	870/30	−196/24	1 × 150/1
	3-CHT (X3)	830/30	–	1 × 350/1
	4-DCT (X4)	830/30	−196/24	1 × 350/1
X210Cr12 (Y)	1-CHT (Y1)	980/20	–	1 × 350/2
	2-DCT (Y2)	980/20	−196/24	1 × 350/2
	3-CHT (Y3)	950/20	–	1 × 300/2
	4-DCT (Y4)	950/20	−196/24	1 × 300/2

was performed using COD database references and their fractions were evaluated using a combination of Rietveld refinement [29] and Toraya method [30]. For the TEM microstructural characterization (bright- and dark-field imaging, elemental EDS analyses, selected area diffraction,) and STEM (imaging, elemental EDS analyses, line and profile analyses, and elemental mapping) microstructural characterization, JEOL JEM-2100 HR TEM microscope operating at 200 kV accelerating voltage was employed. SingleCrystal software was utilized for the characterization of the electron diffraction patterns. The TEM/STEM analyses and characterization of different phases for each steel grade and heat treatment was conducted on the most representative sample areas. For concise description of the microstructural characteristics and changes only selected results are presented. Nevertheless, the data that is not shown is still considered and used for elucidation of results and phenomena.

3. Results

3.1. *Microstructure analysis*

Light microscopy (LM) images (Fig. 2 a–d, Fig. 4 a–d, Fig. 5 a–d, Fig. 7 a–d,) were used in order to obtain an overview picture of the microstructure and general microstructural evolution of different steel grades depending on the heat treatment strategy applied. The evaluation of size, type, number, volume fraction and distribution of different phases was conducted with SEM (Fig. 2 e-l, Fig. 4 e-l, Fig. 5 e-l, Fig. 7 e-l), XRD and TEM. Results are presented in regards to the steel carbon content (from low to high carbon content).

3.1.1. *Stainless steel (X17CrNi16-2) and hot work tool steel (X38CrMoV5-3) with low carbon content (C 0.17 and 0.38 wt. %, respectively)*

For stainless steel X17CrNi16-2 (low C 0.17, and high Cr 15.22 and Ni 1.50 wt. %), a lath-type martensite matrix with RA (Fig. 3 a-2) is observed for all four heat treatment groups (E1–E4; Fig. 2). However, martensitic laths are on average 50% coarser after first heat treatment process with high austenitizing and low tempering temperature (↑ΔTa and ↓ΔTt) as compared to the second one (↓ΔTa and ↑ΔTt). Furthermore, for DCT samples after both heat treatments, the martensitic laths are smaller as compared to their CHT counterparts, in general preferably orientated along [101] and [001] (Fig. 2 i-l), whereas CHT counterpart do not show any preferable orientation. Additional difference is observed in the vol. % of RA in the matrix. RA fraction determined by XRD was found larger for CHT samples (RA_{E1} = 15 vol. %, RA_{E3} = 2 vol. %) as compared to the DCT samples (RA_{E2} = 1 vol. %, RA_{E4} = <1 vol. %), especially for high austenitizing/low tempering treatment conditions (15-fold), as shown in Table 3. Results were confirmed also by EBSD (Fig. 2 i-l). The majority of carbides in the investigated stainless steel are of two major types, M_3C_2 (enriched with Cr and Fe) and $M_{23}C_6$ (enriched with Cr and Fe), proven by XRD, SEM-EBSD and TEM (Fig. 2, Fig. 3 a-1, a-3, Table 3). Both types are present mostly in spherical form with the M_3C_2 carbides occasionally displaying faceted form, which are more apparent for the samples with lower austenitization temperature (E3 and E4). Carbides are present in clusters and chains throughout the samples on the location of previous austenitic grain boundaries (PAGB). The TEM results disclose that additionally to the confirmed carbide groups (M_3C_2 (Pnma) and $M_{23}C_6$ ($Fm\bar{3}m$)) also M_2C (Pnnm), and M_7C_3 (Pnma) can be found, all enriched with Cr and Fe. The matrix is confirmed to be martensite (I4/mmm) and some RA ($Fm\bar{3}m$). The carbides nucleate preferentially on the martensitic lath boundaries and demonstrate nanocluster growth in carbon enriched areas for all samples (CHT and DCT). Exemplar TEM image and SAED of interlath $M_{23}C_6$ is presented in Fig. 3 a-3.

In both cases of DCT groups (E2, E4) an increased carbide precipitation in-between martensitic laths is observed. For the first heat treatment process (↑ΔTa and ↓ΔTt) increased precipitation of $M_{23}C_6$ carbides (E1 → E2; ~15%). Whereas for the second heat treatment process (↓ΔTa and ↑ΔTt) decreased precipitation of $M_{23}C_6$ and increased precipitation of M_3C_2 carbides occurs (Table 3). Furthermore, analysis of the total number of carbides revealed that DCT promotes carbides precipitation, especially for lower austenitizing temperatures,

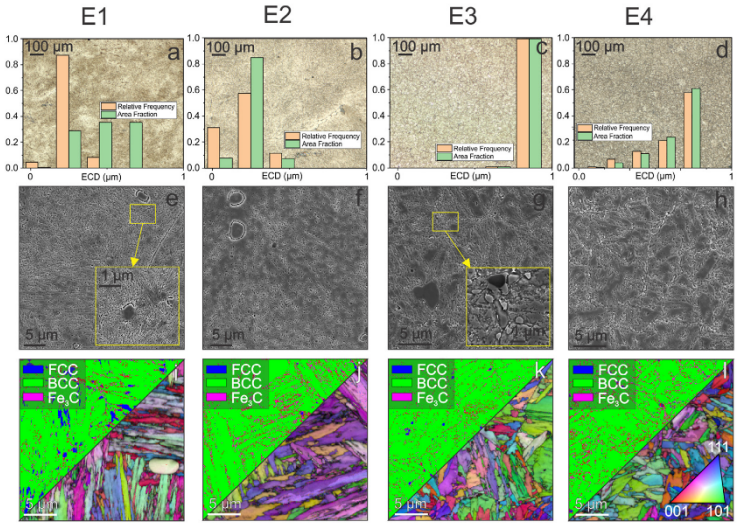

Fig. 2 – Microstructure analysis of X17CrNi16-2 stainless steel (E) with light microscope (LM) (a–d), scanning electron microscope (SEM) (e–h), electron backscattered diffraction (EBSD) and orientation (inverse pole figures) (i–l).

thus enhancing precipitation rate for this case. Number of carbides increased from 30,600 mm^{-2} (E1) to 41,500 mm^{-2} (E2) and from 17,100 mm^{-2} (E3) to 33,100 mm^{-2} (E4), corresponding to increased precipitation of 35% and 94%, respectively. Carbides distribution and size analysis, confirmed by SEM-EBSD and TEM observation, also reveals that DCT promotes precipitation of finer carbides (≤0.5 μm) with increased relative frequency for first heat treatment group (↑ΔTa and ↓ΔTt) (Fig. 2 a-d). Similarly, for the second heat treatment case (↓ΔTa and ↑ΔTt) the average carbides size decreased from 0.90 μm (E3) to 0.75 μm (E4), as shown in Fig. 2 a-d.

For hot work tool steel X38CrMoV5-3 (low C 0.38 and moderate Cr 4.91 wt. %) a matrix composed of lower bainite, RA (~2%) and lath-type martensite is observed for the first two groups (D1–D2), while only martensite and individual patches of RA (~1%) are found for the second group (D3–D4).

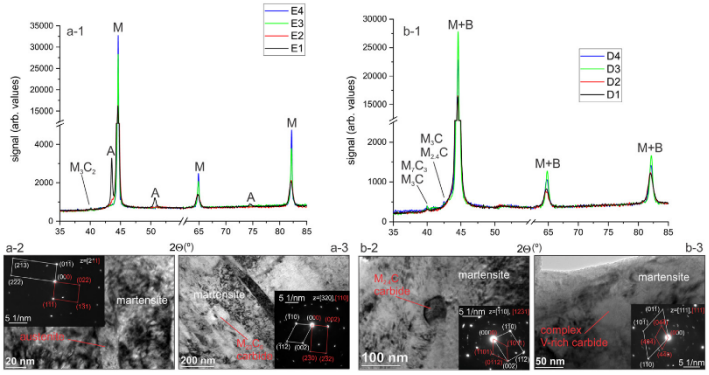

Fig. 3 – Images (a-1 and b-1) represent X-ray diffraction (XRD) spectres for stainless steel X17CrNi16-2 (a-1) and hot work tool steel X38CrMoV5-3 (b-1), where M stands for martensite, B bainite, A austenite, M_XC_Y for specific type of carbides. Under XRD spectres, TEM images of individual features of the microstructure with their corresponding selective area electron diffraction (SAED) are presented for stainless steel X17CrNi16-2 (a-2, a-3) and hot work tool steel X38CrMoV5-3 (b-2, b-3).

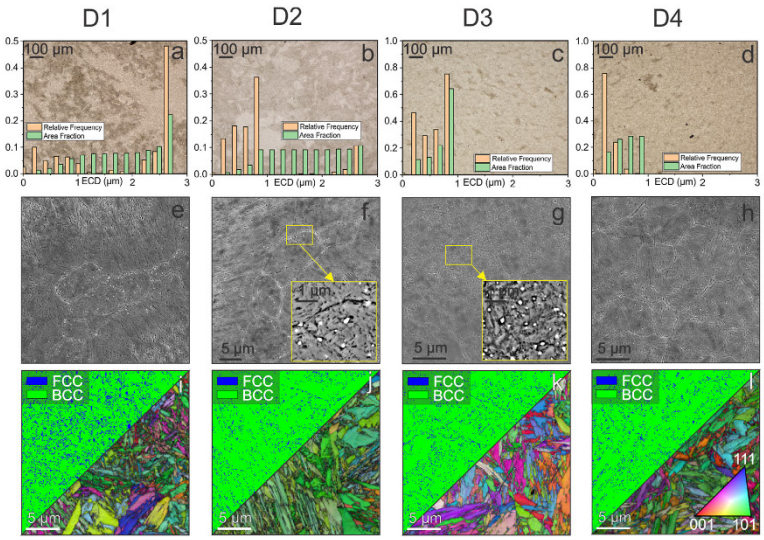

Fig. 4 – Microstructure analysis of X38CrMoV5-3 hot work tool steel (D) with light microscope (LM) (a–d), scanning electron microscope (SEM) (e–h), electron backscattered diffraction (EBSD) and orientation (inverse pole figures) (i–l).

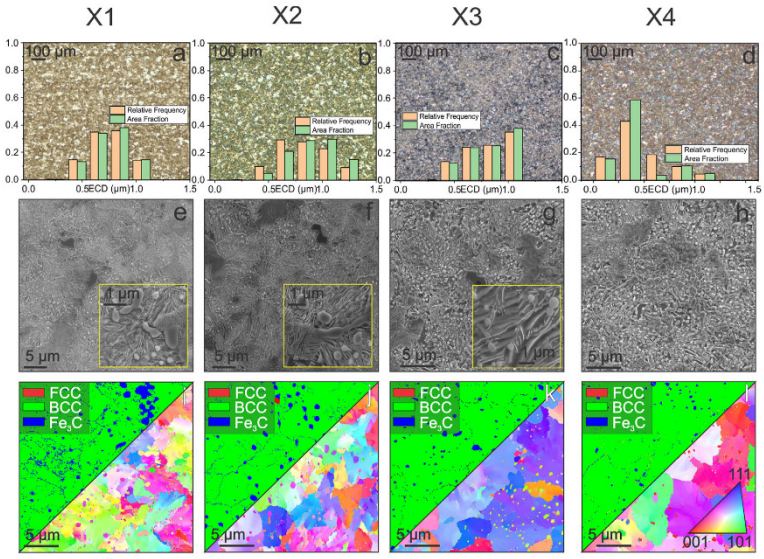

Fig. 5 – Microstructure analysis of 100Cr6 bearing steel (X) with light microscope (LM) (a–d), scanning electron microscope (SEM) (e–h), electron backscattered diffraction (EBSD) and orientation (inverse pole figures) (i–l).

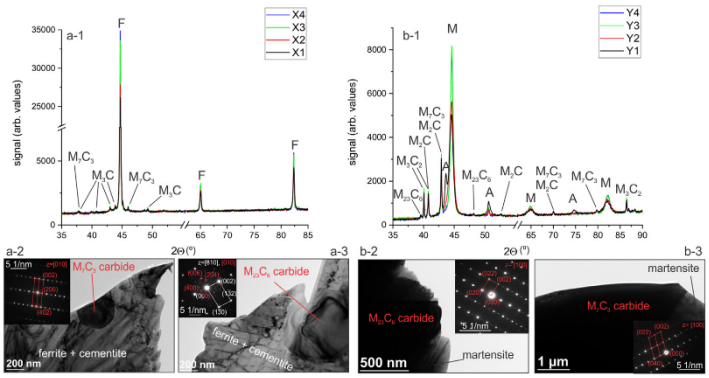

Fig. 6 – Images (a-1 and b-1) represent X-ray diffraction (XRD) spectres for bearing steel 100Cr6 (a-1) and cold work tool steel X210Cr12 (b-1), where M stands for martensite, F ferrite (pearlite), A austenite, M_XC_Y for specific type of carbides. Under XRD spectres, TEM images of individual features of the microstructure with their corresponding selective area electron diffraction (SAED) are presented for bearing steel 100Cr6 (a-2, a-3) and cold work tool steel X210Cr12 (b-2, b-3).

Martensitic/bainitic laths are on average larger for the second heat treatment process (↓ΔTa and ↑ΔTt), by roughly 40–50% (Table 4). However, for both groups, DCT samples show finer and more oval shaped martensitic laths as compared to their CHT counterparts (Fig. 4 i-l). Furthermore, although no difference in RA could be detected between DCT and CHT samples, DCT for first heat treatment group results in reduced amount of bainite (B_{D1} = 33 vol. %; B_{D2} = 26 vol. %) and higher amount of martensite (M_{D1} – 35 vol. %, M_{D2} – 40 vol. %). In contrast, no notable difference could be detected in subgroups D3–D4. SEM-EBSD, XRD and TEM (Fig. 3 b-1, b-2, b-3) confirmed two types of carbides, Fe_3C (large portion originates as cementite from bainite) and $(Cr, Fe)_7C_3$. The latter are spherical shaped carbides, which are present in the steel more or less in dispersed groups at the locations of PAGB (Fig. 3, Fig. 4). As mentioned, for the second heat treatment group

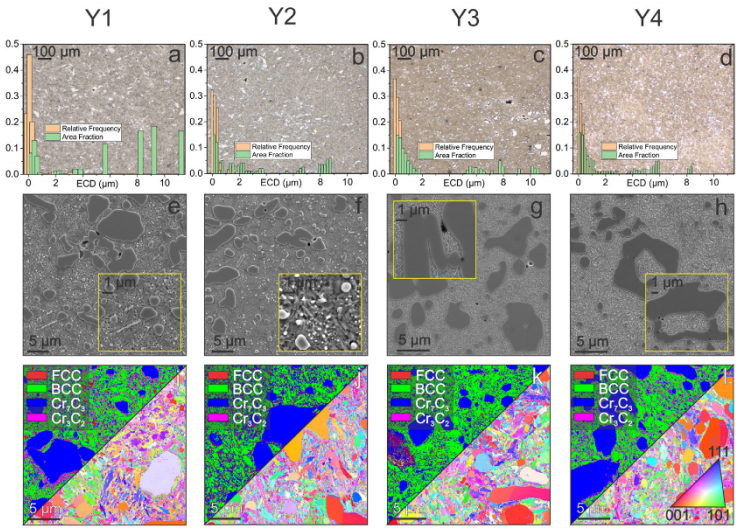

Fig. 7 – Microstructure analysis of X210Cr12 cold work tool steel (Y) with light microscope (LM) (a–d), scanning electron microscope (SEM) (e–h), electron backscattered diffraction (EBSD) and orientation (inverse pole figures) (i–l).

Table 3 – X17CrNi16-2 stainless steel vol. % of phases for each group (E1-E4) and also for microstructural evolution during DCT heat treatment (E2 QBDCT: sample after quenching and before exposure to DCT, E2 ADCT: sample after quenching and DCT and before tempering).

X17CrNi16-2	E1	E2	E3	E4	E2 QBDCT	E2 ADCT
Matrix (vol. %):						
Martensite	62	74	81	80	94.5	97
RA	15	1	2	<1	3.5	1
Carbides (vol. %):						
$(Cr, Fe)_3C_2$	3	3	4.5	6.5	2	1.5
$(Cr, Fe)_{23}C_6$	20	22	12.5	13	<1	<1

(subgroups D3–D4) the matrix does not hold any bainite. Therefore, minute amount of Fe_3C carbides is present and increased amount of Fe_7C_3 carbides is observed (Table 4).

The TEM results additionally identified the presence of $Fe_{2.4}C$ (Im-3m) carbides (Fig. 3 b-2) and complex form of carbide embryos in the form of $Fe_{125}C_7$ (Fm-3m) enriched with V in all four groups (Fig. 3 b-3). Observation of the carbides showed that they preferentially nucleate on the martensitic/bainitic lath boundaries or within the martensitic laths (Fig. 3 b-2, b-3).

The distribution and size analysis has also identified the trend of higher number of carbides in D steel after DCT as compared to CHT, which is true for both heat treatment groups. For first group (↑ΔTa and ↓ΔTt), the number of carbides increased from 11,600 mm^{-2} (D1) to 13,400 mm^{-2} (D2) and for the second group (↓ΔTa and ↑ΔTt) from 7300 mm^{-2} (D3) to 8000 mm^{-2} (D4), corresponding to an increase of 16% and 9%, respectively. In D1 (Fig. 4 a, e) two distinct peaks of relative frequency can be observed, one below 0.25 μm and another at about 2.75 μm. The first indicates the Fe_3C carbides and the second Fe_7C_3. Whereas, in D2 (Fig. 4 b, f) sample the majority of carbides are below 1 μm, with lower ECD. In the second heat treatment process (D3–D4) all carbides are smaller than 1 μm (Fig. 4 c-d, g-h), with the highest relative frequency for D3 at around 0.85 μm and for D4 at around 0.25 μm. The SEM-EBSD analysis of X38CrMoV5-3 steel confirmed the matrix composition and low RA content, where for both DCT samples (D2 and D4) a preferable orientation of martensitic laths along [101] and [001] is observed, whereas CHT samples do not indicate preferable orientation. Although XRD analysis showed no difference in RA between DCT and CHT samples, EBSD still indicates lower amount of RA after DCT as compared to the CHT counterparts.

3.1.2. Bearing steel (100Cr6) with medium carbon content (C 0.93 wt. %)

The matrix of bearing steel (high C 2.07, high Cr 12. wt. %) is similar for all four sample groups (X1-X4). In the matrix, ferrite and pearlite dominate, with a small fraction of martensite (1–2 vol. %) and RA (<1 vol. %) (Table 5, Fig. 6 a-1). Additionally, the pearlite structure shows ferritic leaves (troostite), which indicates the presence of upper bainite before tempering. In the first heat treatment process (↑ΔTa and ↓ΔTt) the pearlite structures are 50–60% smaller than in the second process (↓ΔTa and ↑ΔTt). However, the comparison of CHT vs. DCT samples did not indicate any additional shrinkage of matrix, as observed in other three steels. Carbides are homogenously distributed through the matrix of all four sample groups (X1-X4). Carbides, being in greater amount as for other three steel grades, due to different matrix, are mainly of M_7C_3 type (enriched with Cr and Fe) and M_3C type (enriched with Fe) (Fig. 5, Fig. 6 a-1, a-2, Table 5). Both carbide types are of spherical shape, whereas pure Fe_3C is also in lamellar form as cementite (Fig. 6 a-2, a-3). TEM discloses that additional carbides $Fe_{2.4}C$, $Fe_{23}C_6$ (Fig. 6 a-3) and M_5C_2 (enriched with Cr and Fe) are present. These smaller carbides nucleate mainly within the troostite matrix, with the M_5C_2 being more frequent in DCT samples. As shown in Table 5, also increased precipitation of M_7C_3 carbides can be observed after DCT treatments (X1 → X2 for 10% and X3 → X4 for 34%), which is related to the increased formation of M_5C_2 carbides after DCT.

In both heat treatments the total number of carbides increases with DCT, by 15% for first heat treatment (X1 = 86,600 mm^{-2} > X2 = 99,900 mm^{-2}) and by merely 3% for second heat treatment group (X3 = 89,200 mm^{-2} > X4 = 91,600 mm^{-2}). For group X1 (Fig. 5 a) carbides are mainly in 0.65–0.85 μm range, which remains more or less the same for X2 (0.65–1.05 μm; Fig. 5 b). However, in the second heat treatment (↓ΔTa and ↑ΔTt; X3-X4), DCT samples have a predominant trend of precipitation of much smaller carbides (ECD_{X3} = 1.05 μm → ECD_{X4} = 0.40 μm), as shown in Fig. 5 c-d.

Table 4 – X38CrMoV5-3 hot work tool steel XRD vol. % of phases for each group (D1–D4) and also for microstructural evolution during DCT heat treatment (D2 QBDCT: sample after quenching and before exposure to DCT, D2 ADCT: sample after quenching and exposure to DCT and before tempering).

X38CrMoV5-3	D1	D2	D3	D4	D2 QBDCT	D2 ADCT
Matrix (vol. %):						
Martensite	35	40	87.5	87.5	46	48
Bainite (Ferrite)	33	26	–	–	23	22
RA	2	2	1	1	6.5	3.5
Carbides (Vo. %):						
$(Cr, Fe)_7C_3$	5	7	7.5	7.5	1.5	3.5
Fe_3C (incl. cementite)	25	25	4	4	23	23

Table 5 – 100Cr6 bearing steel vol. % of phases for each group (X1-X4) and also for microstructural evolution during DCT heat treatment (X2 QBDCT: sample after quenching and before exposure to DCT, X2 ADCT: sample after quenching and exposure to DCT and before tempering).

100Cr6	X1	X2	X3	X4	X2 QBDCT	X2 ADCT
Matrix (vol. %):						
Martensite	2	2	1	1	2	2
Ferrite	51	46.5	48.5	47.5	58.5	58
RA	<1	<1	<1	<1	<1	<1
Carbides (vol. %):						
$(Cr, Fe)_7C_3$	8.5	9.5	11.5	17.5	4	4.5
Fe_3C (incl. cementite)	38	41.5	38.5	33.5	35	35

The SEM-EBSD results confirm the multiphase matrix of 100Cr6 steel. For all samples a preferable orientation of matrix is visible, however, no specific trends in relation to the heat treatment state and presence of DCT is visible (Fig. 5 i-l).

3.1.3. *Cold work tool steel (X210Cr12) with high carbon content (C 2.07 wt. %)*

For cold work tool steel X210Cr12 (high C 2.07 wt. %, high Cr 12.40 wt. %) a predominant lath-type martensite matrix is observed for all four heat treatment groups (Y1-Y4). However, for Y1 also large amount (15 vol. %) of retained austenite (RA) is found, whereas for other subgroups the RA presence is minute (1–2 vol. %). Martensitic laths are finer for the first heat treatment group (↑ΔTa and ↓ΔTt), being 30–40% finer as compared to the second heat treatment. Application of DCT treatment further refines martensitic laths by 30–40%, as well as reduces fraction of RA. In Y1 from 15 vol. % to 2 vol. % (Y2) and in Y3 from 2 vol. % to below 1 vol. % (Y4), as shown in Table 6. Carbides present in the samples are of three types: M_3C_2, $M_{23}C_6$ and M_7C_3, all enriched with Cr and Fe (Fig. 6 b-1, Fig. 7, Table 6). The $M_{23}C_6$ (Fig. 6 b-2) and M_7C_3 (Fig. 6 b-3) types are spherically shaped, whereas the M_3C_2 are considerably larger and more block-like.

The analysis of distribution and size of carbides has identified the trend of increased number of carbides after DCT (Y1 → Y2 by about 10% and Y3 → Y4 by 5%). For Y1 three distinct peaks of relative frequency can be observed, each peak corresponding to each detected carbide group (Fig. 7 a, Table 6). The one below 1 μm corresponds to $M_{23}C_6$, whereas the 2–3 μm and above 6 μm correspond to M_3C_2 and M_7C_3, respectively. However, area fraction indicates a stronger contribution from the larger carbides, despite the greater number of smaller ones. After DCT (Y2, Fig. 7 b) the majority of carbides is smaller than 1 μm. In the second heat treatment (Y3–Y4), CHT and DCT subgroups show similar values, with predominantly fine carbides and mean ECD below 1 μm (Fig. 7 c-d). The results also confirm the higher phase fraction of both M_3C_2 and $M_{23}C_6$ carbides (by 15% and 43%, respectively) in Y2 subgroup (DCT) as compared to Y1 (CHT), whereas for second heat treatment process only the vol. % of $M_{23}C_6$ carbide phase has increased by DCT (by 40%), but at the cost of reduced quantity of M_7C_3 carbides (by 26%).

Table 6 – X210Cr12 cold work tool steel vol. % of phases for each group (Y1–Y4) and also for microstructural evolution during DCT heat treatment (Y2 QBDCT: sample after quenching and before exposure to DCT, Y2 ADCT: sample after quenching and exposure to DCT and before tempering).

X210Cr12	Y1	Y2	Y3	Y4	Y2 QBDCT	Y2 ADCT
Matrix (vol. %):						
Martensite	**48**	**57**	**56.5**	**57**	**51.5**	**60.5**
RA	**15**	**2**	**1.5**	**<1**	**11**	**2**
Carbides (vol. %):						
$(Cr, Fe)_7C_3$	20	19.5	17	12.5	20	20.5
$(Cr, Fe)_3C_2$	10	11.5	10	9	12	11.5
$(Cr, Fe)_{23}C_6$	7	10	15	21	5.5	5.5

3.2. *Microstructure evolution during deep cryogenic treatment*

To resolve the effect of DCT on microstructural changes and possible effect on properties, the microstructure evolution was monitored from start to finish of the heat-treatment process. Based on microstructural results of the differently heat-treated sample groups and the effect of DCT on microstructure, only the groups with higher austenitizing and lower tempering temperature (D1–D2, E1–E2, X1–X2, Y1–Y2) were selected for the evolution path analysis, since they generally exhibited stronger DCT influence on the microstructure.

3.2.1. *Stainless steel (X17CrNi16-2)*

As shown in Table 3 stainless steel X17CrNi16-2 directly after quenching from 1050 °C (E2 QBDCT; Fig. 8 a) contains 94.5 vol. % martensite, 3.5 vol. % RA and about 3 vol. % carbides. After DCT (E2 ADCT; Fig. 8 a) the amount of RA is reduced to 1 vol. % and martensite fraction increased to 97 vol. %, whereas the amount of carbide phase remains the same. However, when comparing samples after tempering (E1 and E2), for the sample that undergone DCT (E2) the amount of RA remained unchanged (approx. 1 vol. %), with the amount of martensite shifted to 74 vol. % as compared to 62 vol. % in E1 and carbides precipitation increased to 25 vol. % as compared to 23 vol. % in E1. The XRD results (Fig. 8 a) confirm the increased content of austenite after tempering in E1 sample, indicating that the 15% of austenite originates from the austenite reversion transformation (ART) of martensite and stabilization of martensite by DCT. The martensitic matrix is determined to be morphologically similar before and after DCT and no special groupings of smaller martensite laths were found to develop after DCT. This suggests that additional nanoscopic precipitation needs to occur during DCT in order to obstruct the ART effect. This furthermore indicates that DCT influences the development of martensitic laths (refinement and relaxation) during tempering.

3.2.2. *Hot work tool steel (X38CrMoV5-3)*

After quenching from the upper austenitizing temperature (1080 °C) microstructure of hot work tool steel X38CrMoV5-3 (D2 QBDCT; Table 4) is composed of 46 vol. % martensite, 23 vol. % bainite, 6.5 vol. % RA and ~1.5 vol. % carbides (M_7C_3). After DCT treatment (D2 ADCT), the martensite phase content increased to 48 vol. %, while RA phase was cut in half (by 46%), down to 3.5 vol. %. Furthermore, although after tempering the amount of RA was decreased down to 2 vol. % for CHT (triple tempering; D1) and DCT treatment (single tempering; D2), DCT hinders decomposition of martensite by 15–20% (Fig. 8 b), as well as promotes carbides precipitation by ~40%. For this steel, also no significant difference is visible for the morphology of martensite matrix after DCT, which suggests the influence of DCT on the development of martensitic laths during tempering.

3.2.3. *Bearing steel (100Cr6)*

For bearing steel 100Cr6 no change in RA and martensite content could be observed between different heat treatment phases, as shown in Table 5 and Fig. 8 c. There is only

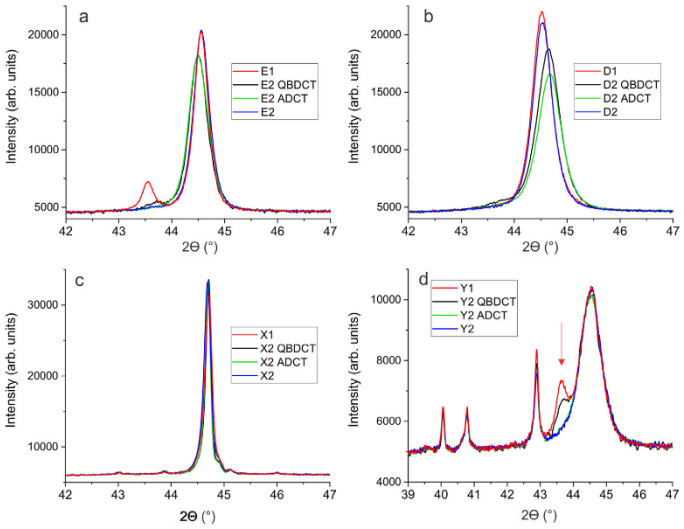

Fig. 8 – X-ray diffraction (XRD) of E1, D1, X1, Y1 (red line), E2, D2; X2, Y2 (blue line), E2-D2-X2-Y2 QBDCT (black line) and E2-D2-X2-Y2 ADCT (green line). With red arrow on d figure is marked peak for austenite.

minimum deviation in phase composition between quenched (X2 QBDCT), and quenched and DCT treated sample (X2 ADCT). However, after final tempering incorporation of DCT resulted in promoted ferrite/perlite phase transformation. By application of DCT (X2) the amount of ferrite decreased during tempering from 58 vol. % to 46.5 vol. %, as compared to CHT (X1), with the decrease to just 51 vol. %. On the other hand, DCT increases carbide phase content, already after quenching (from 39 vol. % in X2 QBDCT to 39.5 vol. % in X2 ADCT), but mainly after tempering (from 46.5 vol. % in X1 to 51 vol. % in X2). The results indicate that the effect of DCT for bearing steel is more related to the carbides precipitation and depletion of the matrix of alloying elements. This suggests that similar as for steel E (stainless steel), nanoscopic precipitation must to occur after DCT application.

3.2.4. *Cold work tool steel (X210Cr12)*

In the case of cold work tool steel X210Cr12 the microstructure after quenching (Y2 QBDCT) is composed of 51.5 vol. % martensite, 11 vol. % RA and 37.5 vol. % carbides (Table 6, Fig. 8 d). After exposure to DCT (Y2 ADCT), the martensite phase content increased by 17% (to 60.5 vol. %) and RA phase decreased by 82% (down to just 2 vol. %), while carbides content remained more or less unchanged (at 37.5 vol. %). When combined with tempering (Y2) the amount of martensite and RA stayed more or less the same (57 vol. % and 2 vol. %), whereas the amount of $M_{23}C_6$ carbides almost doubled. On the other hand, conventionally treated sample (Y1) shows less stable microstructure after quenching, with the fraction of RA being increased during tempering (from 11 vol. % to 15 vol. %), caused by austenite reversion due to ART and less pronounced $M_{23}C_6$ carbides precipitation (Table 6). For this steel, the DCT effect is most noticeable from all steel grades in relation to the matrix modification. The microstructural evolution clearly shows that the matrix displays more homogeneous structure, which is visible by the stronger localized etching of the matrix after quenching (Fig. 9 a) and after CHT (Fig. 9 c) than after quenching and DCT (Fig. 9 b) and heat treatment with DCT (Fig. 9 d). This indicates that DCT directly influences the distribution of alloying elements and the homogeneity of the microstructure, which then directly influences the carbide precipitation.

4. Discussion

4.1. *Microstructural changes of matrix during deep cryogenic treatment*

Microstructure, microstructural changes and DCT effect in all four steels were strongly linked with the type and chemical composition of the steel. The DCT samples of stainless steel X17CrNi16-2 and cold work tool steel X210Cr12 before (ADCT) and after tempering show reduced amount of RA compared to CHT samples, which confirms theory that DCT reduces the amount of RA and converts it into martensite [6]. Interesting observation was also made in hot work tool steel X38CrMoV5-3, where despite the fact that the bainite (ferrite) was the main matrix phase, the presence of RA directly after DCT (sample D-ADCT) was reduced and matrix phase was increased. Whereas for bearing steel 100Cr6 no change of the matrix was observed. This clearly shows that DCT has predominantly stronger

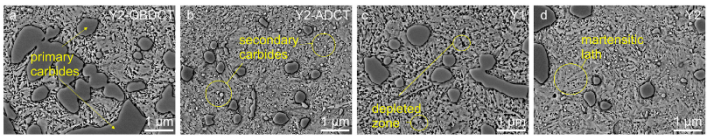

Fig. 9 – a) sample before exposure to deep cryogenic treatment (DCT), b) sample after DCT, c) sample without DCT (control group-CHT) and d) sample at the end of heat treatment with included DCT. Each image has a marked feature present in all samples.

effect on bainitic/martensitic steels, as compared to ferritic/pearlitic steels.

Not only that DCT has a positive influence on the matrix composition of preferable phases, but also the martensitic/bainitic laths and structures were found to be generally more refined, rounded and preferably oriented along [101] and [001], as also reported by Jovičević-Klug et al., 2021 [31] for high-speed steels. The preferable orientation of laths after DCT can have a considerable influence on steel properties, as indicated by work of Burik and Pešek 2015 [32] and Jakob et al., 2019 [33], and proven by Jovičević-Klug et al., 2021 [21,31]. In addition, the study has also proven that already after DCT exposure (in liquid nitrogen at −196 °C for 24 h), without any additional tempering, the drastic reduction of RA takes place.

4.2. *Carbide precipitation induced by deep cryogenic treatment*

Carbide precipitation, distribution and size have been shown to be influenced by DCT in all four selected steels. After application of DCT, increased precipitation of carbides occurred compared to their CHT counterparts. In DCT samples, carbides are also more homogenously distributed, smaller and more spherically shaped. The possible explanation for increased carbide precipitation in DCT samples results from the low temperature of DCT and consequential volumetric contraction of phases, which causes movement of carbon atoms into the nearby dislocations (microvoids). These microvoids later act as nucleus for carbides during change of temperature [15,16] or tempering process [19]. Furthermore, directly after DCT (samples ADCT) increased fraction of secondary M_7C_3 carbides was observed. Increased precipitation of M_7C_3 carbides is present, not only in high-Cr content steel (X210Cr12), but also in medium- (X38CrMoV5-3) and low-Cr steels (100Cr6), which indicates that for formation of such carbide, high content of Cr is not necessary. This additionally supports the theory about volumetric contractions of phases. Another observed phenomena is the increased number of $M_{23}C_6$ carbides for X210Cr12 and X17CrNi16-2 steels, which can be directly linked to the induced precipitation of M_7C_3 carbides [4]. DCT also induced precipitation of smaller carbides in the matrix, as proven by particles distribution (ECD), SEM and TEM analysis. The formation of these carbides is considered to be related to the redistribution of the alloying elements, such as C and Cr, and consequential homogenization of the matrix after DCT, which was most clearly visible for steel X210Cr12. Furthermore, DCT was found to have an effect on carbides precipitation even in steels with non-martensitic matrix composition such as bainite/pearlite, thus indicating versatile application of DCT.

4.3. *Effect of carbon and chromium content on effectiveness of deep cryogenic treatment*

Correlation of C and Cr content on the DCT effectiveness was studied through the selected four steel grades, ranging from low to high C and Cr grade steels. C plays an important role in carbides formation. During DCT carbon atoms are moved to dislocations, produced by high degree of RA and martensite contractions and local plastic deformation, which then results in increased carbides precipitation [17]. As a result, with the higher C content in steel, the higher carbide precipitation and effect of DCT can be expected. Results for high carbon content steels (100Cr6 – 0.93 wt. % and X210Cr12–2.07 wt. %) confirm this theory, both in general showing more intense carbides precipitation after DCT as compared to the other two steels with lower C content. Correspondingly, the highest carbides precipitation rate and improvement by DCT was determined for cold work tool steel X210Cr12 with the highest C content. Furthermore, in all investigated steels depleted C matrix was confirmed by EDS measurements (not shown), being correlated to the higher carbide precipitation.

High presence of Cr in steel should induce Cr–Fe rich carbides formation during DCT [34]. Indeed, in both steels with high Cr content, X210Cr12 and X17CrNi16-2, the precipitation of same carbide types enriched with Cr and Fe was observed (M_3C_2 and $M_{23}C_6$). However, despite containing almost 5% of Cr the precipitated amount (relative frequency) of carbides was the lowest for X38CrMoV5-3 tool steel. The mechanism of promoted $M_{23}C_6$ carbides precipitation can be observed in both high-Cr steels, where C and Cr content in matrix is reduced by precipitation of these carbides, leading to destabilization of RA and subsequent increase of martensite phase, as also proven by Liu et al., 2007 [34]. The slight decrease of eutectic M_7C_3 carbides in X20Cr12 steel directly after DCT (Y ADCT), followed by more than 40% increase in favorite $M_{23}C_6$ formation after tempering (Y2 vs. Y1) additionally confirms the DCT dynamics related to C and Cr content and their more homogeneous distribution in the matrix.

4.4. *Temperature effect on deep cryogenic treatment performance*

Selected temperatures of austenitizing and tempering have an effect on the microstructure and microstructural evolution as well as on the DCT performance [22]. The noticeable

difference between high austenitizing/low tempering (samples 1 and 2) and low austenitizing/high tempering (samples 3 and 4) groups are coarser matrix features in the second case. This trend is mainly related to higher tempering temperature, which increases the average size of martensite laths. However, for stainless steel X17CrNi16-2 the opposite trend was observed, related to the chemical composition of low C and presence of Ni, causing increased size of martensitic laths and packed orientation in [111] direction [35]. Regardless of this, for both heat treatment groups incorporating DCT, refined martensitic laths are found, potentially leading to improved mechanical properties through the Hall–Petch relation [36]. The similar observation of decreased martensitic laths was also observed by Yan et al., 2020 [37]. Several authors [38,39] have suggested that in addition to the chemical composition also the local stress formed by newly formed neighbor laths and their plastic relaxation during RA to martensite transformation can cause size change of martensitic laths. This explanation can be directly linked to DCT and martensite laths refinement, as the RA transformation occurs in all martensitic steels. However, this phenomenon is not activated during immersion in liquid nitrogen, but requires higher temperatures (tempering) for the effect of DCT on martensite lath refinement to occur. In terms of effectiveness of DCT on carbides precipitation, the effect of the heat treatment conditions is not so straightforward. As shown by the results of this investigation, the precipitation also depends on the steel type and composition. For high-C and high-Cr steel (Y-X20Cr12) with very high fraction of carbides in general no particular effect of austenitizing/tempering temperature on the intensity of DCT effect could be observed. However, for lower austenitizing temperature more intense decrease in larger M_7C_3 and M_3C_2 carbide types was detected. Switching to low-Cr steel (X-100Cr6), DCT effect on intensified M_7C_3 carbides precipitation and carbides size reduction becomes more pronounced for the lower austenitizing temperature case (X3 → X4). However, at reduced C content (D-X38CrMoV5-3 and E-X17CrNi16-2) increased precipitation of finer carbides with DCT is more emphasized when using high austenitizing/low tempering temperatures.

5. Conclusions

The study investigated four different steel grades; stainless steel (X17CrNi16-2), bearing steel (100Cr6), cold work tool steel (X38CrMoV5-3) and hot work tool steel (X210Cr12), for the effect and effectiveness of DCT on their microstructure and its evolution. The following conclusions have been established:

1. Microstructure and microstructural changes in all four steels are strongly linked with the chemical composition and prior matrix composition of each individual steel.
2. The transformation of retained austenite into other steel phases is more pronounced after higher austenitization and lower tempering temperature. The effectiveness of DCT on the matrix changes is mainly related to the homogenization of the matrix and redistribution of alloying elements. The increased refinement of the matrix substructures with DCT occurs only after thermal activation with tempering.
3. Generally, the application of DCT increased precipitation of carbides after tempering. Carbides are also more homogenously distributed, smaller and more spherically shaped. However, DCT has higher effect on C enriched steels in correlation with carbides precipitation and distribution. Cr enriched steels had higher precipitation of carbides. However, the relation with regards to the magnitude of increased precipitation does not correlate with the Cr fraction in the steels.
4. For DCT samples, bainitic/martensitic laths are finer with more oval-shaped ends and display a preferable crystallographic orientation along [101] and [001] direction.
5. The DCT process induces the preferential formation of secondary transiting carbides M_7C_3 and $M_{2.4}C$, which directly induce the increased formation of $M_{23}C_6$ and M_7C_3 carbides. The dissolution of primary carbides is slightly increased after DCT, which is related to the increased nucleation of secondary carbides and redistribution of alloying elements in the matrix.
6. In general the preferable heat treatment conditions for the possible improvement of steels' properties through microstructure refinement and more intense carbides precipitation by application of DCT are higher austenitizing and lower tempering temperatures. However, this is also steel type related, with better DCT effectiveness switching toward lower austenitizing/higher tempering temperatures for high-C steels.

Author contributions

P.J.-K.: Conceptualization, Visualization, Validation, Methodology, Investigation, Writing-Original Draft, Resources, Writing-Review & Editing.

M.J.-K.: Methodology, Investigation, Visualization, Writing-Original Draft, Writing-Review & Editing.

T.S.: Methodology, Writing-Review & Editing.

D.F.: Methodology, Writing-Review & Editing.

B.P.: Conceptualization, Supervision, Validation, Resources, Writing-Review & Editing.

All authors have read and agreed to the published version of the manuscript.

Funding

This work was supported by Slovenian Research Agency (ARRS), Ljubljana, Slovenia [No. P2-0050 & No. J2-9211].

Declaration of Competing Interest

The authors declare that they have no known competing financial interests or personal relationships that could have appeared to influence the work reported in this paper.

Acknowledgement

Acknowledgement goes to colleagues Branko Zvonar (IMT) for the help with heat treatment of samples, Nataša Lipovšek (IMT) for the help in the metallographic lab and Miro Pečar (IMT) for the preparation of TEM lamellae.

REFERENCES

[1] Šolić S, Godec M, Schauperl Z, Donik Č. Improvement in abrasion wear resistance and microstructural changes with deep cryogenic treatment of austempered ductile cast iron (ADI). Metall Mater Trans A: Phy Metall Mater Sci 2016;47:5058–70. https://doi.org/10.1007/s11661-016-3659-4.

[2] Bhale P, Shastri H, Mondal AK, Masanta M, Kumar S. Effect of deep cryogenic treatment on microstructure and properties of AE42 Mg alloy. J Mater Eng Perform 2016;25:3590–8. https://doi.org/10.1007/s11665-016-2238-6.

[3] Amini K, Negahbani M, Ghayour H. The effect of deep cryogenic treatment on hardness and wear behavior of the H13 tool steel. Metall Ital 2015;107:53–8.

[4] Jovičević-Klug P, Jovičević-Klug M, Podgornik B. Effectiveness of deep cryogenic treatment on carbide precipitation. J Mater Res Technol 2020;9:13014–26. https://doi.org/10.1016/j.jmrt.2020.09.063.

[5] Akincioğlu S, Gökkaya H, Uygur İ. A review of cryogenic treatment on cutting tools. Int J Adv Manuf Technol 2015;78:1609–27. https://doi.org/10.1007/s00170-014-6755-x.

[6] Baldissera P, Delprete C. Deep cryogenic treatment: a bibliographic review. Open Mech Eng J 2008;2:1–11. https://doi.org/10.2174/1874155X00802010001.

[7] Kalsi NS, Sehgal R, Sharma VS. Cryogenic treatment of tool materials: a review. Mater Manuf Process 2010;25:1077–100. https://doi.org/10.1080/10426911003720862.

[8] Rajasekhar A. Heat-Treatment-Methods-Applied-To-AISI-431-Martensitic-Stainless-Steels.doc. Int J Sci Eng Res 2015;6.

[9] Aouici H, Bouchelaghem H, Yallese MA, Elbah M, Fnides B. Machinability investigation in hard turning of AISI D3 cold work steel with ceramic tool using response surface methodology. Int J Adv Manuf Technol 2014;73:1775–88. https://doi.org/10.1007/s00170-014-5950-0.

[10] Romanowicz PJ, Szybiński B. Fatigue life assessment of rolling bearings made from AISI 52100 bearing steel. Materials 2019;12. https://doi.org/10.3390/ma12030371.

[11] Jovičević-Klug P, Podgornik B. Comparative study of conventional and deep cryogenic treatment of AISI M3:2 (EN 1.3395) high-speed steel. J Mater Res Technol 2020;9:13118–27. https://doi.org/10.1016/j.jmrt.2020.09.071.

[12] Mudali UK, Pujar MG. Pitting corrosion of austenitic stainless steels and their weldments. Corrosion of austenitic stainless steels. Elsevier; 2002. p. 74–105. https://doi.org/10.1533/9780857094018.106.

[13] Nakagawa H, Miyazaki T. Effect of retained austenite on the microstructure and mechanical properties of martensitic precipitation hardening stainless steel. J Mater Sci 1999;34:3901–8. https://doi.org/10.1023/A:1004626907367.

[14] Akhavan Tabatabae B, Ashrafizadeh F, Hassanli AM. Influence of retained austenite on the mechanical properties of. ISIJ Int 2011;51:471–5.

[15] Akhbarizadeh A, Shafyei A, Golozar MA. Effects of cryogenic treatment on wear behavior of D6 tool steel. Mater Des 2009;30:3259–64. https://doi.org/10.1016/j.matdes.2008.11.016.

[16] Amini K, Nategh S, Shafyei A. Influence of different cryotreatments on tribological behavior of 80CrMo12 5 cold work tool steel. Mater Des 2010. https://doi.org/10.1016/j.matdes.2010.05.028.

[17] Oppenkowski A, Weber S, Theisen W. Evaluation of factors influencing deep cryogenic treatment that affect the properties of tool steels. J Mater Process Technol 2010;210:1949–55. https://doi.org/10.1016/j.jmatprotec.2010.07.007.

[18] Meng F, Tagashira K, Azuma R, Sohma H. Role of eta-carbide precipitations in the wear resistance improvements of Fe-12Cr-Mo-V-1.4C tool steel by cryogenic treatment. ISIJ Int 1994;34:205–10. https://doi.org/10.2355/isijinternational.34.205.

[19] Collins DN, Dormer J. Deep cryogenic treatment of a D2 cold-work tool steel. Heat Treat Met 1997;3:71–4.

[20] Preciado M, Bravo PM, Alegre JM. Effect of low temperature tempering prior cryogenic treatment on carburized steels. J Mater Process Technol 2006;176:41–4. https://doi.org/10.1016/j.jmatprotec.2006.01.011.

[21] Jovičević-Klug P, Puš G, Žužek B, Podgornik B. Effect of deep cryogenic treatment on mechanical properties of steels EN HS6-5-2, HS6-5-3, HS6-5-2-5, X38CrMoV5-3 and X17CrNi16-2. Mater Sci Eng: A 2021 [in prog].

[22] Villa M, Somers MAJ. On the role of isothermal martensite formation during cryogenic treatment of steels. HTM 2019;75:263–86. https://doi.org/10.3139/105.110420.

[23] Totten GEPD, editor. Steel heat treatment. Metallurgy and Technologies. 1 2007. p. 1558. https://doi.org/10.1201/NOF0849384523.ch6.

[24] Ali M, Nyo T, Kaijalainen A, Hannula J, Porter D, Kömi J. Influence of chromium content on the microstructure and mechanical properties of thermomechanically hot-rolled low-carbon bainitic steels containing niobium. Appl Sci 2020;10:344. https://doi.org/10.3390/app10010344.

[25] Beswick JM. The effect of chromium in high carbon bearing steels. Metall Trans A 1987;18:1897–906. https://doi.org/10.1007/bf02647019.

[26] Li H, Tong W, Cui J, Zhang H, Chen L, Zuo L. The influence of deep cryogenic treatment on the properties of high-vanadium alloy steel. Mater Sci Eng 2016;662:356–62. https://doi.org/10.1016/j.msea.2016.03.039.

[27] Schindelin J, Arganda-Carreras I, Frise E, Kaynig V, Longair M, Pietzsch T, et al. Fiji: an open-source platform for biological-image analysis. Nat Methods 2012;9:676–82. https://doi.org/10.1038/nmeth.2019.

[28] Kostoj V, Mithieux JD, Fröhlich T. Influence of chromium carbide size on the austenitization kinetics of a martensitic stainless steel measured by dilatometry. Solid State Phenom 2011;172–174:426–31.

[29] Rietveld HM. A profile refinement method for nuclear and magnetic structures. J Appl Crystallogr 1969;2:65–71. https://doi.org/10.1107/s0021889869006558.

[30] Toraya H. A new method for quantitative phase analysis using X-ray powder diffraction: direct derivation of weight fractions from observed integrated intensities and chemical compositions of individual phases. J Appl Crystallogr 2016;49:1508–16. https://doi.org/10.1107/S1600576716010451.

[31] Jovičević-Klug P, Jenko M, Jovičević-Klug M, Šetina Batič B, Kovač J, Podgornik B. Effect of deep cryogenic treatment on surface chemistry and microstructure of selected high-speed steels. Appl Surf Sci 2021;548:1–11.

[32] Burik P, Pešek L. Effect of crystallographic orientation on mechanical properties of steel sheets by depth sensing indentation. Metal 2015:1–5.

[33] Jakob S, Leitner A, Lorich A, Eidenberger-Schober M, Knabl W, Pippan R, et al. Influence of crystal orientation and Berkovich tip rotation on the mechanical characterization of grain boundaries in molybdenum.

Mater Des 2019;182:107998. https://doi.org/10.1016/j.matdes.2019.107998.

[34] Liu H huai, Wang J, Shen B luo, shan Yang H, Gao S ji, Huang S jiu. Effects of deep cryogenic treatment on property of 3Cr13Mo1V1.5 high chromium cast iron. Mater Des 2007;28:1059–64. https://doi.org/10.1016/j.matdes.2005.09.007.

[35] Sun C, Fu P, Liu H, Liu H, Du N, Gao Y. The effect of lath martensite microstructures on the strength of medium-carbon low-alloy steel. Crystals 2020;10. https://doi.org/10.3390/cryst10030232.

[36] Zhang C, Wang Q, Ren J, Li R, Wang M, Zhang F, et al. Effect of microstructure on the strength of 25CrMo48V martensitic steel tempered at different temperature and time. Mater Des 2012;36:220–6. https://doi.org/10.1016/j.matdes.2011.11.026.

[37] Yan Z, Liu K, Eckert J. Effect of tempering and deep cryogenic treatment on microstructure and mechanical properties of Cr–Mo–V–Ni steel. Mater Sci Eng 2020;787:139520. https://doi.org/10.1016/j.msea.2020.139520.

[38] Shtremel MA, Andreev YG, Kozlov DA. Structure and strength of lath martensite. Met Sci Heat Treat 1999;41:140–5.

[39] Morito S, Tanaka H, Konishi R, Furuhara T, Maki T. The morphology and crystallography of lath martensite in Fe-C alloys. Acta Mater 2003;51:1789–99. https://doi.org/10.1016/S1359-6454(02)00577-3.

Chapter 6

Conclusions and Future Outlook

6.1 Conclusions

This thesis provides a detailed overview of the effect of deep cryogenic treatment (DCT) on selected ferrous alloys, as a potential technology for enhancing various of ferrous alloys. Additionally, the thesis also challenges the current theories on DCT and its implications on microstructure evolution of metallic materials and their properties. Several important findings related to the microstructure changes during DCT and factors that influence DCT performance are proposed as well as their consequential influence on the final properties of treated ferrous alloys (steels).

From this thesis, the following major conclusions can be drawn:

I. DCT performance on investigated steels is strongly influenced by steel type, chemical composition and heat treatment parameters. The ratio of alloying elements influences the microstructure and precipitation of the carbides and depletion of the matrix. Whereas the steel type with its prior matrix composition influences the later effects of DCT.

II. DCT increases the density of precipitation of carbide in matrix (even up to 140 %, depending on the carbide type). Generally, the carbides are smaller and more spherically shaped with DCT. The average size of carbides is also on average smaller with DCT and more homogeneously distributed. The change in the density of the carbides does not necessarily change their volumetric ratio in the material. For some steels, the volume ratio of specific carbides, such as $M_{23}C_6$, is increased with DCT, reaching thermodynamically calculated theoretical values that are conventionally achievable with extended tempering times, far longer than those used in practice. However, for other steels, the carbide fraction remains similar as that of conventionally heat-treated (CHT) counterparts. This is associated with the influence of alloying elements on the carbide precipitation and thus the effect of DCT on it.

III. The increased precipitation of carbides is strongly correlated with precipitation and evolution of smaller cuboidal carbides, which is proposed to evolve from M_7C_3 and $M_{2.4}C$ carbides, for which initial nucleation and alloying condition evolves during deep cryogenic temperatures.

IV. Observations showed that DCT has a higher effect on carbon-enriched steels in correlation with carbides precipitation and distribution. Whereas for chromium-enriched steels, DCT only increases the precipitation of carbides.

V. The transformation of retained austenite after the application of DCT is more pronounced after higher austenitization and lower tempering temperature (up to 90 %). Generally, the amount of retained austenite (including also reverted austenite) is reduced to 1 vol. % with DCT. DCT also has an effect on the matrix, which is mainly

related to the homogenization of the matrix, redistribution of alloying elements and refinement, which occurs after tempering. Another observation is that DCT makes bainitic/martensitic laths finer with more oval-shaped ends, which display a preferable crystallographic orientation along <101> and <001> direction, which is associated with the orientation of preexisting austenite grains.

VI. Surface analysis showed that the reduced amount of carbide clusters after DCT could be correlated to the oxygen absorption and oxide state. Additionally, oxygen absorption analysis also indicated the effect of DCT on the refinement of martensitic laths in the matrix, resulting in a smoother surface.

VII. The modification of the microstructure can be directly related to the modified mechanical properties, fatigue and wear resistance of steels under different heat treatment conditions (austenitizing and tempering temperature). Compressive strength, hardness and strain-hardening exponent are deteriorated when combined with high austenitizing and low tempering temperatures, whereas the impact toughness and fatigue resistance generally improve with DCT.

VIII. The main reason for increased hardness and compressive strength with DCT is in the increased number of precipitated carbides, while the increase in toughness and fatigue resistance can be correlated to the depleted carbon content and higher plasticity of the finer martensitic matrix. DCT has a limited effect on the strain-hardening exponent.

IX. In specific cases, where carbide changes are relatively small, the reduction of hardness, fatigue resistance and strength are related to the depletion of carbon and other alloying elements' content in the matrix which results in the reduced solid-solution strengthening of the matrix.

X. The effect of deep cryogenic treatment on wear resistance was tested with sliding wear, impact wear and galling behavior. DCT effect on sliding wear is strongly correlated to chemical composition and type of steel, contact conditions as well as wear mode. On the other hand, DCT has a predominant positive effect on dynamic impact wear and galling resistance.

XI. The positive effect of DCT on tribological properties is attributed to a more homogenous microstructure, increased precipitation of finer carbides, modification of different carbide types and the generally reduced mean carbide diameter.

XII. For the negative effect of DCT on tribological properties, the combined effect of increased volume fraction of carbides and a tougher matrix is considered, which could lead to the sticking and tearing of the matrix material, and with it microcracking and pull-outs of carbides.

XIII. In general, the preferable heat treatment conditions for the possible improvement of mechanical, fatigue and tribological properties through microstructure refinement and more intense carbides precipitation by application of DCT are higher austenitizing and lower tempering temperatures for stainless steel, cold and hot work tool steels and bearing steel. However, this is strongly dependent on steel type (chemical composition and type), with better DCT effectiveness switching toward lower austenitizing/higher tempering temperatures for high carbon steels and HSS.

6.2 Tested Hypotheses

The conclusion about the proposed thesis hypotheses is presented for each hypothesis separately.

I. **Hypothesis 1:** *In addition to the parameters of the deep cryogenic treatment process, the efficiency of deep cryogenic treatment and thus the final properties of the material are also influenced by the parameters of the basic heat treatment of steel (higher/lower austenitizing and tempering temperature).*

Hypothesis 1 was fully confirmed, as it was proven that the selected austenitizing and tempering temperature have a strong effect on DCT dynamics, with preferable heat treatment route with lower austenitizing and higher tempering temperature for improved final properties for high-speed steels.

II. **Hypothesis 2:** *The effect of deep cryogenic treatment is not the same for all types of steels, but depends on the type and chemical composition of steel or main alloying elements, where deep cryogenic treatment affects the mechanical and anti-wear properties, corrosion resistance and fatigue resistance.*

Hypothesis 2 was also fully confirmed, as the results show that the steel chemical composition and steel type (wrought/PM) have a strong effect on the DCT performance during heat treatment. However, more detailed research and advanced testing methods with in-situ option should be used in order to unravel the importance of each alloying element during DCT.

III. **Hypothesis 3:** *Deep cryogenic treatment causes microstructural changes at the macro, micro and nano-level and affects the dynamics of precipitation and growth of phases. At the same time, deep cryogenic treatment enables the achievement of a fine-grained microstructure with a homogeneous distribution of finer carbides with an increased degree of nucleation or precipitation and a reduced tendency for clustering. Furthermore, in the metal matrix, deep cryogenic treatment leads to the elimination of retained austenite and the formation of very fine lattice martensite by non-diffuse martensitic transformation before and during deep cryogenic treatment.*

For the last, third hypothesis, the microstructure changes induced by DCT were successfully proven with consistent observation of the microstructure evolution during heat treatment (as delivered state, after quenching, after DCT and after tempering-final state) and with analysis of the final microstructure state.

6.3 Future Outlook

The results in this thesis have proven that DCT is a very good opportunity to achieve significant technical development in materials science in order to be at the same time a green and effective technology, with the influence on bulk and surface of the material in a positive manner.

For future research of the DCT phenomenon, it is suggested to extend research of the mechanism by incorporating additional advance in-situ techniques in order to observe specific details with both high temporal and high spatial resolution. With such measurements, the consequential influence on the change of properties (chemical, tribological, fatigue, mechanical, corrosion, electromagnetic etc.) of different steel grades within the same steel group can be analyzed and tailored to obtain strongest positive yield of DCT on materials properties.

The present thesis provides an important piece of the puzzle about the understanding of DCT and systematic testing of different ferrous alloys with DCT. The research also acts as a good fundamental basis for continued research and development of DCT for present and future applications in various industries with the strongest contribution to the usage of DCT for tailoring ferrous alloys.

References

[1] C. A. Dumasia, V. A. Kulkarni, and K. Sonar, “A Review on the Effect of Cryogenic Treatment on Metals,” *International Research Journal of Engineering and Technology*, vol. 4, no. 7, pp. 2402–2406, 2017.

[2] B. Podgornik, I. Paulin, B. Zajec, S. Jacobson, and V. Leskovšek, “Deep cryogenic treatment of tool steels,” *Journal of Materials Processing Technology*, vol. 229, pp. 398–406, 2016, doi: 10.1016/j.jmatprotec.2015.09.045.

[3] C. L. Gogte, A. Likhite, D. Peshwe, A. Bhokarikar, and R. Shetty, “Effect of cryogenic processing on surface roughness of age hardenable AA6061 alloy,” *Materials and Manufacturing Processes*, vol. 29, no. 6, pp. 710–714, 2014, doi: 10.1080/10426914.2014.901526.

[4] J. Indumathi, J. Bijwe, A. K. Ghosh, M. Fahim, and N. Krishnaraj, “Wear of cryo-treated engineering polymers and composites,” *Wear*, vol. 225–229, no. 1, pp. 343–353, 1999, doi: 10.1016/S0043-1648(99)00063-0.

[5] A. Bensely, A. Prabhakaran, D. Mohan Lal, and G. Nagarajan, “Enhancing the wear resistance of case carburized steel (En 353) by cryogenic treatment,” *Cryogenics (Guildf)*, vol. 45, no. 12, pp. 747–754, 2006, doi: 10.1016/j.cryogenics.2005.10.004.

[6] W. Reitz and J. Pendray, “Cryoprocessing of materials: A review of current status,” *Materials and Manufacturing Processes*, vol. 16, no. 6, pp. 829–840, 2001, doi: 10.1081/AMP-100108702.

[7] S. S. Gill, H. Singh, R. Singh, and J. Singh, “Cryoprocessing of cutting tool materials - A review,” *International Journal of Advanced Manufacturing Technology*, vol. 48, no. 1–4, pp. 175–192, 2010, doi: 10.1007/s00170-009-2263-9.

[8] P. Jovičević-Klug and B. Podgornik, “Review on the Effect of Deep Cryogenic Treatment of Metallic Materials in Automotive Applications,” *Metals (Basel)*, vol. 10, no. 4, pp. 434, 2020, doi: 10.3390/met10040434.

[9] R. F. Barron *et al.*, “Cryogenic engineering conference/international cryogenic materials conference. Boston, MA, USA,” *Cryogenics (Guildf)*, vol. 26, no. 1, pp. 49–51, 1986, doi: 10.1016/0011-2275(86)90198-0.

[10] P. Baldissera and C. Delprete, “Deep Cryogenic Treatment: A Bibliographic Review,” *The Open Mechanical Engineering Journal*, vol. 2, no. 1, pp. 1–11, 2008, doi: 10.2174/1874155X00802010001.

[11] W. Foerg, “History of cryogenics: The epoch of the pioneers from the beginning to the year 1911,” *International Journal of Refrigeration*, vol. 25, no. 3, pp. 283–292, 2002, doi: 10.1016/S0140-7007(01)00020-2.

[12] R. G. Scurlock, “A matter of degrees: A brief history of cryogenics,” *Cryogenics (Guildf)*, vol. 30, no. 6, pp. 483–500, 1990, doi: 10.1016/0011-2275(90)90048-H.

[13] R. N. Richardson, “The cooling potential of cryogens, Part I: The early development of refrigeration and cryogenic cooling technology,” *Ecolibrium*, vol. 2, pp. 10–14, 2003.

[14] K. D. Timmerhaus and T. M. Flynn, “Properties of Cryogenic Fluids,” in *Cryogenic Process Engineering*, 1989, pp. 13–38. doi: 10.1007/978-1-4684-8756-5_2.

[15] K. D. Timmerhaus and T. M. Flynn, “Cryogenic Process Engineering,” in *Cryogenic Engineering*, 2007, pp. 3–27. doi: http://dx.doi.org/10.1016/B0-12-227410-5/00156-3.

[16] S. Kalia, “Cryogenic processing: A study of materials at low temperatures,” *Journal of Low Temperature Physics*, vol. 158, no. 5–6, pp. 934–945, 2010, doi: 10.1007/s10909-009-0058-x.

[17] K. Prudhvi and V. V. Lakshmi, “Cryogenic Tool Treatment,” *Imperial Journal of Interdisciplinary Research*, vol. 2, no. 9, pp. 1204–1211, 2016.

[18] D. Senthilkumar, “Thermophysical behavior of cryogenically treated silicon carbide for nanofluids,” *Materials and Manufacturing Processes*, vol. 29, no. 7, pp. 819–825, 2014, doi: 10.1080/10426914.2014.892976.

[19] J. N. Jones and C. B. Rogers, “The Acoustic Effect of Cryogenically Treating,” *Journal of the Acoustical Society of America*, vol. 114, no. 4, pp. 2349–2349, 2013.

[20] K. S. Raj, J. J. Monica, K. Nirmalkumar, and M. N. A. G. Taj, “Cryogenic Treatment,” *International Journal of Engineering Science Invention Research and Development*, vol. 1, pp. 325–332, 2015.

[21] J. Singh, A. Kumar, and J. Singh, “Effect of cryogenic treatment on metals and alloys,” *International Journal of Advanced Research*, vol. 5, no. 3, pp. 1035–1045, 2017.

[22] P. Stratton, “Cold Treatment on Case-Hardened Steel,” *Heat Treating Progress*, vol. 3–4, no. 4, pp. 45–48, 2008, doi: 10.3139/105.110134.

[23] T. P. Sweeney, “Deep cryogenics: the great cold debate,” *Heat Treating*, vol. 18, no. 2, pp. 28–33, 1986.

[24] P. Jurči, J. Ptačinová, M. Sahul, M. Dománková, and I. Dlouhy, “Metallurgical principles of microstructure formation in sub-zero treated cold-work tool steels – a review,” *Matériaux and Techniques*, vol. 106, no. 1, pp. 104–113, 2018, doi: 10.1051/mattech/2018022.

[25] D. Das, A. K. Dutta, and K. K. Ray, “Influence of varied cryotreatment on the wear behavior of AISI D2 steel,” *Wear*, vol. 266, no. 1–2, pp. 297–309, 2009, doi: 10.1016/j.wear.2008.07.001.

[26] D. Das, A. K. Dutta, and K. K. Ray, “Sub-zero treatments of AISI D2 steel: Part I. Microstructure and hardness,” *Materials Science and Engineering: A*, vol. 527, no. 9, pp. 2182–2193, 2010, doi: 10.1016/j.msea.2009.10.070.

[27] D. Das, A. K. Dutta, and K. K. Ray, “Sub-zero treatments of AISI D2 steel: Part II. Wear behavior,” *Materials Science and Engineering: A*, vol. 527, no. 9, pp. 2194–2206, 2010, doi: 10.1016/j.msea.2009.10.071.

[28] D. N. Collins, “Deep cryogenic treatment of tool steels: A review,” *Heat Treatment of Metals*, vol. 23, no. 2, pp. 40–42, 2010, doi: 10.1080/10426911003720862.

[29] D. Senthilkumar, “Cryogenic Treatment: Shallow and Deep,” in *Encyclopedia of Iron, Steel, and Their Alloys*, no. 1, G. E. Totten and R. Colas, Eds. New York, NY: Taylor and Francis: NY, USA, 2016, pp. 995–1007.

[30] S. J. Gobbi, V. J. Gobbi, and G. Reinke, “Ultra Low Temperature Process Effects on Micro-Scale Abrasion of Tool Steel AISI D2,” *Materials Science and Technology*, vol. 35, no. 11, pp. 1355-1364, 2018, doi: 10.1080/02670836.2019.1624018.

[31] B. Podgornik, D. Uršič, and I. Paulin, “Effectiveness of deep cryogenic treatment in improving mechanical and wear properties of cold work tool steels,” *International Journal of Microstructure and Materials Properties*, vol. 12, no. 3–4, pp. 216, 2017, doi: 10.1504/IJMMP.2017.091098.

[32] P. Jovičević-Klug, M. Jovičević-Klug, T. Sever, D. Feizpour, and B. Podgornik, “Impact of Steel Type, Composition and Heat Treatment Parameters on Effectiveness of Deep Cryogenic Treatment,” *Journal of Materials Research and Technology*, vol. 14, no. 9-10, pp. 1–23, 2021, doi: 10.1016/j.jmrt.2021.07.022.

[33] P. Jovičević-Klug, M. Jovičević-Klug, and B. Podgornik, “Effectiveness of deep cryogenic treatment on carbide precipitation,” *Journal of Materials Research and Technology*, vol. 9, no. 6, pp. 13014–13026, 2020, doi: 10.1016/j.jmrt.2020.09.063.

[34] P. Jovičević-Klug and B. Podgornik, “Comparative study of conventional and deep cryogenic treatment of AISI M3:2 (EN 1.3395) high-speed steel,” *Journal of Materials Research and Technology*, vol. 9, no. 6, pp. 13118–13127, 2020, doi: 10.1016/j.jmrt.2020.09.071.

[35] V. Leskovšek and B. Podgornik, “Vacuum heat treatment, deep cryogenic treatment and simultaneous pulse plasma nitriding and tempering of P/M S390MC steel,” *Materials Science and Engineering A*, vol. 531, pp. 119–129, 2012, doi: 10.1016/j.msea.2011.10.044.

[36] H. huai Liu, J. Wang, B. luo Shen, H. shan Yang, S. ji Gao, and S. jiu Huang, “Effects of deep cryogenic treatment on property of 3Cr13Mo1V1.5 high chromium cast iron,” *Materials and Design*, vol. 28, no. 3, pp. 1059–1064, 2007, doi: 10.1016/j.matdes.2005.09.007.

[37] F. Diekman, “Cold and Cryogenic Treatment of Steel,” in *Steel Heat Treating Fundamentals and Processes-ASM Handbook*, J. Dossett and G. E. Totten, Eds. Cleveland, OH, USA: ASM International, 2013, pp. 382–386.

[38] J. Gayda and L. J. Ebert, “The effect of cryogenic cooling on the tensile properties of metal-matrix composites,” *Metallurgical Transactions A*, vol. 10, no. 3, pp. 349–353, 1979, doi: 10.1007/BF02658344.

[39] D. Senthilkumar, “Effect of deep cryogenic treatment on residual stress and mechanical behaviour of induction hardened En 8 steel,” *Advances in Materials and Processing Technologies*, vol. 2, no. 4, pp. 427–436, 2016, doi: 10.1080/2374068X.2016.1244326.

[40] D. Senthilkumar, I. Rajendran, M. Pellizzari, and J. Siiriainen, “Influence of shallow and deep cryogenic treatment on the residual state of stress of 4140 steel,” *Journal of Materials Processing Technology*, vol. 211, no. 3, pp. 396–401, 2011, doi: 10.1016/j.jmatprotec.2010.10.018.

[41] M. Jovicevic-Klug, P. Jovicevic-Klug, J. McCord, and B. Podgornik, “Investigation of microstructural attributes of steel surfaces through magneto-optical Kerr effect,” *Journal of Materials Research and Technology*, vol. 11, no. 3-4, pp. 1245–1259, 2021, doi: 10.1016/J.JMRT.2021.01.106.

[42] A. Levy and J. M. Papazian, “Finite Element Analysis of Whisker-Reinforced SiC/Al Composites Subjected to Cryogenic Temperature Thermal Cycling,” *Journal of Engineering and Technology*, vol. 115, no. 1, pp. 129–133, 1993.

[43] P. Jovičević-Klug, M. Jovičević-Klug, and B. Podgornik, “Unravelling the Role of Nitrogen in Surface Chemistry and Oxidation Evolution of Deep Cryogenic Treated High-Alloyed Ferrous Alloy,” *Coatings*, vol. 12, no. 2, p. 213, 2022, doi: 10.3390/coatings12020213.

[44] A. Y. L. Yong, K. H. W. Seah, and M. Rahman, “Performance of cryogenically treated tungsten carbide tools in milling operations,” *International Journal of Advanced Manufacturing Technology*, vol. 32, no. 7–8, pp. 638–643, 2007, doi: 10.1007/s00170-005-0379-0.

[45] L. He and Z. Q. Shi, “Effect of deposition temperature on electric conduction and microstructure of Au films,” *Solid-State Electronics*, vol. 39, no. 12, pp. 1811–1815, 1996, doi: 10.1016/S0038-1101(96)00089-5.

[46] Z. Q. Shi, R. L. Wallace, and W. A. Anderson, “High Barrier Height Schottky Diodes on n-{InP} by Low Temperature Deposition,” *Applied Physics Letters*, vol. 59, pp. 446–448, 1991, doi: 10.1109/ICIPRM.1991.147433.

[47] S. Paul and A. B. Chattopadhyay, “Effects of cryogenic cooling by liquid nitrogen jet on forces, temperature and surface residual stresses in grinding steels,” *Cryogenics (Guildf)*, vol. 35, no. 8, pp. 515–523, 1995, doi: 10.1016/0011-2275(95)98219-Q.

[48] N. K. Singh, A. Nayak, and V. Singh, “Effect of cryogenics on treated steel,” *in the proceedings of National Conference on Refrigeration and Air Conditioning,* Indian Institute of Technology Guwahati: Bhopal, India, 2014.

[49] K. Bán, A. Lovas, L. Novák, and K. Csach, “The influence of low temperature treatments on the H solubility and the Curie temperature of Fe-B based glasses,” *Czechoslovak Journal of Physics*, vol. 54, no. 4, pp. 12–15, 2004, doi: 10.1007/s10582-004-0048-9.

[50] P. Jurči, M. Dománková, J. Ptačinová, M. Pašák, M. Kusý, and P. Priknerová, “Investigation of the Microstructural Changes and Hardness Variations of Sub-Zero Treated Cr-V Ledeburitic Tool Steel Due to the Tempering Treatment,” *Journal of Materials Engineering and Performance*, vol. 27, no. 4, pp. 1514–1529, 2018, doi: 10.1007/s11665-018-3261-6.

[51] M. el Mehtedi, P. Ricci, L. Drudi, S. el Mohtadi, M. Cabibbo, and S. Spigarelli, “Analysis of the effect of Deep Cryogenic Treatment on the hardness and microstructure of X30 CrMoN 15 1 steel,” *Materials and Design*, vol. 33, no. 1, pp. 136–144, 2012, doi: 10.1016/j.matdes.2011.07.030.

[52] P. Jovičević-Klug, G. Puš, M. Jovičević-Klug, B. Žužek, and B. Podgornik, “Influence of heat treatment parameters on effectiveness of deep cryogenic treatment on properties of high-speed steels,” *Materials Science and Engineering: A*, vol. 829, pp. 142157, 2022, doi: 10.1016/j.msea.2021.142157.

[53] G. Prieto, W. R. Tuckart, and J. E. P. Ipiña, “Influence of a cryogenic treatment on the fracture toughness of an AISI 420 martensitic stainless steel,” *Materiali in Tehnologije*, vol. 51, no. 4, pp. 591–596, 2017, doi: 10.17222/mit.2016.126.

[54] F. Cajner, V. Leskovsek, D. Landek, and H. Cajner, “Effect of deep-cryogenic treatment on high speed steel properties,” *Materials and Manufacturing Processes*, vol. 24, no. 7-8, pp. 743-746, 2009, doi: 10.1080/10426910902809743.

[55] P. H. S. Cardoso, C. L. Israel, M. B. da Silva, G. A. Klein, and L. Soccol, “Effects of deep cryogenic treatment on microstructure, impact toughness and wear resistance of an AISI D6 tool steel,” *Wear*, vol. 456–457, no. 9, pp. 203382, 2020, doi: 10.1016/j.wear.2020.203382.

[56] Z. Weng, K. Gu, K. Wang, X. Liu, and J. Wang, “The reinforcement role of deep cryogenic treatment on the strength and toughness of alloy structural steel,” *Materials Science and Engineering: A*, vol. 772, no. 9-10, pp. 138698, 2020, doi: 10.1016/j.msea.2019.138698.

[57] H. Li, W. Tong, J. Cui, H. Zhang, L. Chen, and L. Zuo, “The influence of deep cryogenic treatment on the properties of high-vanadium alloy steel,” *Materials Science and Engineering: A*, vol. 662, no. 3-4, pp. 356–362, 2016, doi: 10.1016/J.MSEA.2016.03.039.

[58] M. Villa, K. Pantleon, and M. A. J. Somers, “Evolution of compressive strains in retained austenite during sub-zero Celsius martensite formation and tempering,” *Acta Materialia*, vol. 65, pp. 383–392, 2014, doi: 10.1016/j.actamat.2013.11.007.

[59] P. Jovičević-Klug, M. Sedlaček, M. Jovičević-Klug, and B. Podgornik, “Effect of deep cryogenic treatment on corrosion properties of various high-speed steels,” *Materials*, vol. 14, no. 1, pp. 1–16, 2021, doi: 10.3390/met11010014.

[60] R. N. Wurzbach and W. DeFelice, “Improving component wear performance through cryogenic treatment,” *Lubrication Excellence*, vol. 1, pp. 1-7, 2004.

[61] B. Podgornik and V. Leskovšek, “Wear mechanisms and surface engineering of forming tools,” *Materiali in Tehnologije*, vol. 49, no. 3, pp. 313–324, 2015, doi: 10.17222/mit.2015.005.

[62] D. Das, A. K. Dutta, and K. K. Ray, “Correlation of microstructure with wear behaviour of deep cryogenically treated AISI D2 steel,” *Wear*, vol. 267, no. 9–10, pp. 1371–1380, 2009.

[63] J. Li, X. Yan, X. Liang, H. Guo, and D. Y. Li, “Influence of different cryogenic treatments on high-temperature wear behavior of M2 steel,” *Wear*, vol. 376–377, no, 3-4, pp. 1112–1121, 2017, doi: 10.1016/j.wear.2016.11.041.

[64] D. Korade, K. V. Ramana, and K. Jagtap, “Wear and Fatigue Behaviour of Deep Cryogenically Treated H21 Tool Steel,” *Transactions of the Indian Institute of Metals*, vol. 73, no. 4, pp. 843–851, 2020, doi: 10.1007/s12666-019-01834-6.

[65] A. Akhbarizadeh, A. Shafyei, and M. A. Golozar, “Effects of cryogenic treatment on wear behavior of D6 tool steel,” *Materials and Design*, vol. 30, no. 8, pp. 3259–3264, 2009, doi: 10.1016/j.matdes.2008.11.016.

[66] B. Podgornik, F. Majdic, V. Leskovsek, and J. Vizintin, “Improving tribological properties of tool steels through combination of deep-cryogenic treatment and plasma nitriding,” *Wear*, vol. 288, no. 5, pp. 88–93, 2012, doi: 10.1016/j.wear.2011.04.001.

[67] J. Voglar, Ž. Novak, P. Jovičević-Klug, B. Podgornik, and T. Kosec, “Effect of Deep Cryogenic Treatment on Corrosion Properties of Various High-Speed Steels,” *Metals (Basel)*, vol. 11, no. 1, p. 14, 2020, doi: 10.3390/met11010014.

[68] A. Jaswin and M. L. Dhasan, “Effect of Cryogenic Treatment on Corrosion Resistance and Thermal Expansion of Valve Steels,” *International Journal of Engineering Technology, Management and Applied Sciences*, vol. 3, no. 3, pp. 2349–4476, 2015.

[69] S. Ramesh, B. Bhuvaneswari, G. S. Palani, D. M. Lal, and N. R. Iyer, “Effects on corrosion resistance of rebar subjected to deep cryogenic treatment,” *Journal of Mechanical Science and Technology*, vol. 31, no. 1, pp. 123–132, 2017, doi: 10.1007/s12206-016-1211-5.

[70] P. Jovičević-Klug, T. Kranjec, M. Jovičević-Klug, T. Kosec, and B. Podgornik, “Influence of the Deep Cryogenic Treatment on AISI 52100 and AISI D3 Steel’s Corrosion Resistance,” *Materials 2021, Vol. 14, Page 6357*, vol. 14, no. 21, pp. 6357, 2021, doi: 10.3390/ma14216357.

[71] M. Jovičević-Klug, P. Jovičević-Klug, T. Kranjec, and B. Podgornik, “Cross-effect of Surface Finishing and Deep Cryogenic Treatment on Corrosion Resistance of AISI M35 steel,” *Journal of Materials Research and Technology*, vol. 14, no. 9–10, pp. 2365–2381, 2021, doi: doi.org/10.1016/j.jmrt.2021.07.134.

[72] X. Gong, Z. Wu, and F. Zhao, “Effect of Deep Cryogenic Treatment on the Microstructure and the Corrosion Resistance of AZ61 Magnesium Alloy Welded Joint,” *Metals (Basel)*, vol. 7, no. 5, pp. 179, 2017, doi: 10.3390/met7050179.

[73] P. Jovičević-Klug, M. Jenko, M. Jovičević-Klug, B. Šetina Batič, J. Kovač, and B. Podgornik, “Effect of Deep Cryogenic Treatment on Surface Chemistry and Microstructure of Selected High-Speed Steels,” *Applied Surface Science*, vol. 548, no. 5, pp. 1–11, 2021, doi: 10.1016/j.apsusc.2021.149257.

[74] P. Baldissera and C. Delprete, “Cryogenic treatment and fatigue resistance”*,* in *Cryogenics: Theory, Processes and Applications,* London, UK, Nova Science*,* 2011.

[75] A. Bensely *et al.*, “Fatigue behaviour and fracture mechanism of cryogenically treated En 353 steel,” *Materials and Design*, vol. 30, no. 8, pp. 2955–2962, 2009, doi: 10.1016/j.matdes.2009.01.003.

[76] J. Singh, S. L. Mannan, T. Jayakumar, and D. R. G. Achar, “Fatigue life extension of notches in AISI 304L weldments using deep cryogenic treatment,” *Engineering Failure Analysis*, vol. 12, no. 2, pp. 263–271, 2005, doi: 10.1016/j.engfailanal.2004.03.008.

[77] P. Baldissera and C. Delprete, “Deep cryogenic treatment of AISI 302 stainless steel: Part II - Fatigue and corrosion,” *Materials and Design*, vol. 31, no. 10, pp. 4731–4737, 2010, doi: 10.1016/j.matdes.2010.05.015.

[78] L. A. Alava, G. Artola, I. Guinea, and M. Muro, “On the Influence of Cryogenic Steps on Heat Treatment Processes,” *Materials Performance and Characterization*, vol. 6, no. 5, pp. 837–849, 2017, doi: 10.1520/MPC20170017.

[79] J. M. Crissman, J. A. Sauer, and A. E. Woodward, “Dynamic mechanical behavior of some high polymers at temperatures from 6°K.: Polyethylene, nylon 66, polypropylene, poly(vinyl chloride), poly-(d,l-propylene oxide), polybutene-1, poly(4-methyl-pentene-1),

poly(methyl methacrylate), poly(ethyl methacrylat," *Journal of Polymer Science Part A: General Papers*, vol. 2, no. 12, pp. 5075–5091, 1964, doi: 10.1002/pol.1964.100021205.

[80] C. D. Armeniades and E. Baer, "Structural origin of the cryogenic relaxations in poly(ethylene terephthalate)," *Journal of Polymer Science Part A-2: Polymer Physics*, vol. 9, no. 8, pp. 1345–1369, 1971, doi: 10.1002/pol.1971.160090801 .

[81] V. Frosini and A. E. Woodward, "Effects of orientation on dynamic shear behavior of some amorphous polymers from 4.2° to 300°K," *Journal of Polymer Science Part A-2: Polymer Physics*, vol. 7, no. 3, pp. 525–536, 1969, doi: 10.1002/pol.1969.160070307.

[82] J. D. Darwin, D. Mohan Lal, and G. Nagarajan, "Optimization of cryogenic treatment to maximize the wear resistance of 18% Cr martensitic stainless steel by Taguchi method," *Journal of Materials Processing Technology*, vol. 195, no. 1–3, pp. 241–247, 2008, doi: 10.1016/j.jmatprotec.2007.05.005.

[83] T. Sonar, S. Lomte, and C. Gogte, "Cryogenic Treatment of Metal – A Review," in *Materials Today: Proceedings*, 2018, vol. 5, pp. 25219–25228. doi: 10.1016/j.matpr.2018.10.324.

[84] M. Pellizzari, A. Molinari, L. Girardini, and L. Maldarelli, "Deep cryogenic treatment of AISI M2 high-speed steel," *International Journal of Microstructure and Materials Properties*, vol. 3, no. 2–3, pp. 383–390, 2008, doi: 10.1504/IJMMP.2008.018742.

[85] M. Vengatesh, R. Srivignesh, T. Pradeep, and N. R. Karthik, "Review on Cryogenic Trearment of Steels," *International Research Journal of Engineering and Technology*, vol. 3, no. 10, pp. 417–422, 2016.

[86] G. Zhou, S. Deng, W. Wei, and Q. Liu, "Effect of multiple deep cryo-treating and tempering on microstructure and property evolution of high carbon bearing steel," *Materials Research Express*, vol. 7, no. 6, pp. 066529, 2020, doi: 10.1088/2053-1591/AB9C63.

[87] L. A. Alava, "Multistage cryogenic treatment of materials", *in the proceedings 5th International Conference Recent Trends in Structural Materials*, Research Institute COMTES: Bilbao, Spain, 2014.

[88] A. Ciski, P. Nawrocki, T. Babul, and D. Hradil, "Multistage cryogenic treatment of X153CrMoV12 cold work steel," in *5th International Conference Recent Trends in Structural Materials*, vol. 461, pp. 0120121–0120126. doi: 10.1088/1757-899X/461/1/012012.

[89] P. Jimbert, M. Iturrondobeitia, J. Ibarretxe, and R. Fernandez-Martinez, "Influence of Cryogenic Treatment on Wear Resistance and Microstructure of AISI A8 Tool Steel," *Metals*, vol. 8, no. 12, pp. 1038, 2018, doi: 10.3390/met8121038.

[90] X. G. Yan and D. Y. Li, "Effects of the sub-zero treatment condition on microstructure, mechanical behavior and wear resistance of W9Mo3Cr4V high speed steel," *Wear*, vol. 302, no. 1–2, pp. 854–862, 2013, doi: 10.1016/j.wear.2012.12.037.

[91] M. Pellizzari, "Influence of deep cryogenic treatment on the properties of conventional and PM high speed steels," *Metallurgia Italiana*, vol. 100, no. 8, pp. 17–22, 2008.

[92] M. Pellizzari *et al.*, "Influence of different deep cryogenic treatment routes on the properties of high speed steel," *HTM Journal of Heat Treatment and Materials*, vol. 67, no. 2, pp. 111–117, 2012, doi: 10.3139/105.110141.

[93] P. Jovičević Klug, M. Jovičević Klug, and B. Podgornik, "Deep cryogenic treatment of AlSI 431 and AlSI 52100 steels," in the proceedings of *CEC-ICMC 2021*, Centennial Conferences: virtual, 2021.

[94] Y. Su, N. He, L. Li, and W. Zhao, "Effects of cryogenic nitrogen gas jet on machinability of Ti-alloy in high speed milling," *China Mechanical Engineering*, vol. 17, no. 11, pp. 1183–1187, 2006.

[95] R. F. Barron, "Cryogenic treatment of metals to improve wear resistance," *Cryogenics (Guildf)*, vol. 22, no. 8, pp. 409–413, 1982, doi: 10.1016/0011-2275(82)90085-6.

[96] A. R. Jha, *Cryogenic Technology and Applications*. Cerritos, CA, USA: Elsevier Publishing, 2006.

[97] M. Roberts, “Safe Use of Cryogenic Materials,” *UK Research and Innovation*, no. 1.5, pp. 1–28, 2018.

[98] A. Damir, A. Sadek, and H. Attia, “Characterization of Machinability and Environmental Impact of Cryogenic Turning of Ti-6Al-4V,” *Procedia CIRP*, vol. 69, pp. 893–898, 2018, doi: 10.1016/J.PROCIR.2017.11.070.

[99] K. Gu, B. Zhao, Z. Weng, K. Wang, H. Cai, and J. Wang, “Microstructure evolution in metastable β titanium alloy subjected to deep cryogenic treatment,” *Materials Science and Engineering A*, vol. 723, pp. 157–164, 2018, doi: 10.1016/j.msea.2018.03.003.

[100] J. W. Kim, J. A. Griggs, J. D. Regan, R. A. Ellis, and Z. Cai, “Effect of cryogenic treatment on nickel-titanium endodontic instruments,” *International Endodontic Journal*, vol. 38, no. 6, pp. 364–371, 2005, doi: 10.1111/j.1365-2591.2005.00945.

[101] H. F. Rush, “Cryogenic Material Selection, Availability, and Cost Considerations”, *NASA*, pp. 0-5, 1983.

[102] T. Malone, P. Torres, P. Chen, T. Malone, P. Torres, and R. Bond, “Effects of Cryogenic Treatment on the Residual Stress,” *NASA*, pp. 0–4, 2001.

[103] P. Chen, T. Malone, P. Torres, and R. Bond, “Effects of Cryogenic Treatment on the Residual Stress,” *NASA*, pp. 0–4, 2001.

[104] L. T. Popoola, A. S. Grema, G. K. Latinwo, B. Gutti, and A. S. Balogun, “Corrosion problems during oil and gas production and its mitigation,” *International Journal of Industrial Chemistry*, vol. 4, no. 1, pp. 1–15, 2013, doi: 10.1186/2228-5547-4-35/figures/20.

[105] D.-H. Park, S.-W. Choi, J.-H. Kim and J.-M. Lee, “Cryogenic mechanical behavior of 5000- and 6000-series aluminum alloys: Issues on application to offshore plants,” *Cryogenics (Guildf)*, vol. 146, no. 1, pp. 44–58, 2004, doi: 10.1016/j.cryogenics.2015.02.001.

[106] P. Jovičević-Klug, T. Kranjec, M. Jovičević-Klug, and B. Podgornik, “Modification of Steel Corrosion Resistance in Seawater with Deep Cryogenic Treatment,” *in the proceedings of the 60th Conference of Metallurgists, COM 2021,* The Canadian Institute of Mining, Metallurgy and Petroleum: virtual, 2021.

[107] P. Jovičević-Klug *et al.*, “Assessment of deep cryogenic heat-treatment impact on the microstructure and surface chemistry of austenitic stainless steel,” *Surfaces and interfaces*, vol. accepted, 2022.

[108] C. J. Ming, “Cryogenic Treatment of Music Wire,” in master thesis, Singapore, Singapore: National University of Singapore 2004.

[109] E. Bartolomé, B. Bozzo, P. Sevilla, O. Martínez-Pasarell, T. Puig, and X. Granados, “ABS 3D printed solutions for cryogenic applications,” *Cryogenics (Guildf)*, vol. 82, pp. 30–37, 2017, doi: 10.1016/j.cryogenics.2017.01.005.

[110] L. Tegg, I. McCarroll, T. Sato, M. Griffith, and julie Cairney, “Nanoporous metal tips as frameworks for analysing frozen liquids with atom probe tomography,” *Microscopy and Microanalysis*, vol. 27, pp. 1512–1513, 2021, doi: 10.1017/S1431927621005572.

[111] J. Sun, A. Su, T. Wang, W. Chen, and W. Guo, “Effect of laser shock processing with post-machining and deep cryogenic treatment on fatigue life of GH4169 super alloy,” *International Journal of Fatigue*, vol. 119, no. 2, pp. 261–267, 2019, doi: 10.1016/j.ijfatigue.2018.10.012.

[112] D. Mohan Lal, S. Renganarayanan, and A. Kalanidhi, “Cryogenic treatment to augment wear resistance of tool and die steels,” *Cryogenics (Guildf)*, vol. 41, no. 3, pp. 149–155, 2001, doi: 10.1016/S0011-2275(01)00065-0.

[113] N. B. Dhokey, A. R. Hake, V. T. Thavale, R. Gite, and R. Batheja, “Microstructure and Mechanical Properties of Cryotreated SAE8620 and D3 Steels,” *Current Advances in Materials Sciences Research (CAMSR) Microstructure*, vol. 1, no. 1, pp. 23–27, 2014.

[114] I. Uygur, H. Gerengi, Y. Arslan, and M. Kurtay, “The Effects of Cryogenic Treatment on the Corrosion of AISI D3 Steel,” *Materials Research*, vol. 18, no. 3, pp. 569–574, 2015, doi: 10.1590/1516-1439.349914.

[115] N. W. Khun, E. Liu, A. W. Y. Tan, D. Senthilkumar, B. Albert, and D. Mohan Lal, "Effects of deep cryogenic treatment on mechanical and tribological properties of AISI D3 tool steel," *Friction*, vol. 3, no. 3, pp. 234–242, 2015, doi: 10.1007/s40544-015-0089-z.

[116] H. Singh and R. Khanna, "Parametric Optimization of Cryogenic-Treated D-3 for Cutting Rate in Wire Electrical Discharge Machining," *Journal of Engineering and Technology*, vol. 1, no. 2, pp. 59–64, 2011, doi: 10.4103/0976-8580.86633.

[117] M. Pellizzari and A. Molinari, "Deep cryogenic treatment of cold work tool steel," *in the proceedings of 6th International Tooling Conference 2002,* Karlstad University: Karlstad, Sweden, 2002

[118] J. Li, X. Cai, Y. Wang, and X. Wu, "Multiscale Analysis of the Microstructure and Stress Evolution in Cold Work Die Steel during Deep Cryogenic Treatment," *Materials*, vol. 11, no. 11, pp. 2122–2133, 2018, doi: 10.3390/ma11112122.

[119] V. G. Gavriljuk *et al.*, "Low-temperature martensitic transformation in tool steels in relation to their deep cryogenic treatment," *Acta Materialia*, vol. 61, no. 5, pp. 1705–1715, 2013, doi: 10.1016/j.actamat.2012.11.045.

[120] K. Amini, A. Akhbarizadeh, and S. Javadpour, "Effect of deep cryogenic treatment on the formation of nano-sized carbides and the wear behavior of D2 tool steel," *International Journal of Minerals, Metallurgy and Materials*, vol. 19, no. 9, pp. 795–799, 2012, doi: 10.1007/s12613-012-0630-2.

[121] S. E. Vahdat, S. Nategh, and S. Mirdamadi, "Effect of microstructure parameters on tensile toughness of tool steel after deep cryogenic treatment," *International Journal of Precision Engineering and Manufacturing*, vol. 15, no. 3, pp. 497–502, 2014, doi: 10.1007/s12541-014-0363-4.

[122] S. E. Vahdat and K. S. Niaki, "XRD, STEM, and Tensile Properties of AISI S1 Tool Steel after Deep Cryogenic Treatment," *Advanced Materials Research*, vol. 1088, pp. 195–199, 2015, doi: 10.4028/www.scientific.net/AMR.1088.195.

[123] L. Tóth, "Examination of the properties and structure of tool steel en. 1.2379 due to different heat treatments," *European Journal of Materials Science and Engineering,* vol. 3, no. 3, pp. 1–7, 2017.

[124] B. Podgornik, U. Borovšak, F. Megušar, and K. Košir, "Performance of low-friction coatings in helium environments," *Surface and Coatings Technology*, vol. 206, no. 22, pp. 4651–4658, 2012, doi: 10.1016/j.surfcoat.2012.05.040.

[125] N. Dhokey and K. Bawane, "Cryogenic treatment*", in the proceedings of the 7th International Conference on Fracture Fatigue and Wear*, Ghent University: Ghent, Belgium, 2018.

[126] K. Sanjeev, S. Rakesh, and S. Vishal, "Study of the Effect of Deep Cryogenic Treatment on the Mechanical Properties of Hot Die Steel AISI-H13," *Journal on Material Science*, vol. 4, no. 2, pp. 9–18, 2016, doi: 10.26634/jms.4.2.8125.

[127] A. Molinari, M. Pellizzari, S. Gialanella, G. Straffelini, and K. H. Stiasny, "Effect of deep cryogenic treatment on the mechanical properties of tool steels," *Journal of Materials Processing Technology*, vol. 118, no. 1–3, pp. 350–355, 2001, doi: 10.1016/S0924-0136(01)00973-6.

[128] M. Pérez, C. Rodríguez, and F. J. Belzunce, "The Use of Cryogenic Thermal Treatments to Increase the Fracture Toughness of a Hot Work Tool Steel Used to Make Forging Dies," *Procedia Materials Science*, vol. 3, pp. 604–609, 2014, doi: 10.1016/j.mspro.2014.06.100.

[129] V. Bhawar, S. Khot, P. Kattire, M. Mehta, and R. Singh, "Influence of Deep Cryogenic Treatment (DCT) on Thermo Mechanical Performance of AISI H13 Tool Steel," *Journal of Materials Science and Chemical Engineering*, vol. 5, no. 1, pp. 91–101, 2017, doi: 10.4236/msce.2017.51013.

[130] D. Korade, K. V. Ramana, and K. Jagtap, “Influence of Cryogenic Treatment on the Tribological Behaviour of AISI H21 Tool Steel,” *Material Research*, vol. 22, no. 1, pp. 1–12, 2019, doi: 10.1590/1980-5373-MR-2017-0745.

[131] C. A. Dumasia and V. A. Kulkarni, “Effect of cryogenic treatment on EN8 steel used for press tool,” *Global Journal of Engieering Science and Research Management*, vol. 4, no. 8, pp. 39–54, 2017, doi: 10.5281/zenodo.841202.

[132] P. V. G. Krishna, K. Kishore, T. Srihari, and S. Venkataiah, “Performance Evaluation of Cryogenic Treated HSS Drill,” *Global Journal of Researches in Engineering Mechanical & Mechanics*, vol. 13, no. 7, pp. 23–28, 2013, doi: 10.12966/abc.02.07.2015.

[133] T. V. S. Reddy, T. Somakumar, M. V. Reddy, R. Venkatram, and A. Setnhilkumar, “Turning studies of deep cryogenic treated P-40 tungsten carbide cutting tool inserts- Technical communication,” *Machining Science and Technology*, vol. 13, no. 2, pp. 269–281, 2009, doi: 10.1080/10910340902979754.

[134] D. Senthilkumar, “Influence of deep cryogenic treatment on hardness and toughness of En31 steel,” *Advances in Materials and Processing Technologies*, vol. 5, no. 1, pp. 114–122, 2019, doi: 10.1080/2374068X.2018.1530426.

[135] A. J. Vimal, A. Bensely, D. M. Lal, and K. Srinivasan, “Deep cryogenic treatment improves wear resistance of en 31 steel,” *Materials and Manufacturing Processes*, vol. 23, no. 4, pp. 369–376, 2008, doi: 10.1080/10426910801938098.

[136] C. H. Surberg, P. Stratton, and E. Lingenhöle, “The influence of cold treatment on case-hardened steel,” *Heat Treating Progress*, vol. 8, no. 2, pp. 45–48, 2008, doi: 10.1016/S1006-7191(08)60012-5.

[137] A. Bensely, D. Senthilkumar, D. Mohan Lal, G. Nagarajan, and A. Rajadurai, “Effect of cryogenic treatment on tensile behavior of case carburized steel-815M17,” *Materials Characterization*, vol. 58, no. 5, pp. 485–491, 2007, doi: 10.1016/j.matchar.2006.06.019.

[138] A. Ciski, T. Babul, and M. Duchek, “Sub-zero treatments of case-carburized 18CrNiMo7-6 steel,” in *9th Youth Symposium on Experimental Solid Mechanics*, 2010, pp. 108–111.

[139] D. Senthilkumar and I. Rajendran, “Influence of Shallow and Deep Cryogenic Treatment on Tribological Behavior of En 19 Steel,” *Journal of Iron and Steel Research International*, vol. 18, no. 9, pp. 53–59, 2011, doi: 10.1016/S1006-706X(12)60034-X.

[140] D. Senthilkumar and I. Rajendran, “Optimization of deep cryogenic treatment to reduce wear loss of 4140 steel,” *Materials and Manufacturing Processes*, vol. 27, no. 5, pp. 567-572, 2012, doi: 10.1080/10426914.2011.593237.

[141] D. Senthilkumar, J. Bracke, and N. Slootsman, “Corrosion and elastic behaviour of cryogenically treated en 19 steel,” *Corrosion Management*, vol. 117, pp. 16–21, 2014.

[142] A. V. Pradeep, S. V. Satya Prasad, L. V. Suryam, Y. Kesava Rao, and D. Kesava, “Effect of Cryogenic Treatment on Tool Life of HSS Tool (S400) and Surface Finish of the Material in Turning of SS304,” *IOP Conference Series: Materials Science and Engineering*, vol. 149, no. 1, pp. 1–11, 2016, doi: 10.1088/1757-899X/149/1/012010.

[143] N. B. Dhokey and A. R. Hake, “Instability in wear mechanism and its relevance to microstructural features in cryotreated T42,” *Tribology - Materials, Surfaces & Interfaces*, vol. 7, no. 4, pp. 193–200, 2013, doi: 10.1179/1751584X13Y.0000000047.

[144] N. B. Dhokey, A. Hake, S. Kadu, I. Bhoskar, and G. K. Dey, “Influence of cryoprocessing on mechanism of carbide development in cobalt-bearing high-speed steel (M35),” *Metallurgical and Materials Transactions A: Physical Metallurgy and Materials Science*, vol. 45, no. 3, pp. 1508–1516, 2014, doi: 10.1007/s11661-013-2067-2.

[145] N. B. Dhokey, J. V. Dandawate, R. Rawat, N. B. Dhokey, J. V. Dandawate, and R. Rawat, “Effect of Cryosoaking Time on Transition in Wear Mechanism of M2 Tool Steel,” *ISRN Tribology*, vol. 2013, pp. 1–6, 2013, doi: 10.5402/2013/408016.

[146] K. Shanmugam and S. D. Pathak, “Study on the effect of cryogenic treatment of T1, T4 and M42 high-speed steels,” *Indian Journal of Science and Technology*, vol. 9, no. 41, pp. 7–10, 2016, doi: 10.17485/ijst/2016/v9i41/101977.

[147] F. J. da Silva, S. D. Franco, Á. R. Machado, E. O. Ezugwu, and A. M. Souza, “Performance of cryogenically treated HSS tools,” *Wear*, vol. 261, no. 5–6, pp. 674–685, 2006, doi: 10.1016/j.wear.2006.01.017.

[148] H. Li, W. Tong, J. Cui, H. Zhang, L. Chen, and L. Zuo, “The influence of deep cryogenic treatment on the properties of high-vanadium alloy steel,” *Materials Science and Engineering A*, vol. 662, pp. 356–362, 2016, doi: 10.1016/j.msea.2016.03.039.

[149] D. Hradil, M. Duchek, T. Hrbáčková, and A. Ciski, “Gas Nitriding With Deep Cryogenic Treatment of High-Speed Steel,” *Acta Metallurgica Slovaca*, vol. 24, no. 2, pp. 187–193, 2018, doi: 10.12776/ams.v24i2.1058.

[150] J. Y. Huang, Y. T. Zhu, X. Z. Liao, I. J. Beyerlein, M. A. Bourke, and T. E. Mitchell, “Microstructure of cryogenic treated M2 tool steel,” *Materials Science and Engineering A*, vol. 339, no. 1–2, pp. 241–244, 2003, doi: 10.1016/S0921-5093(02)00165-X.

[151] M. A. J. Somers and T. L. Christiansen, “Low temperature gaseous surface hardening of stainless steel,” *Thermochemical Surface Engineering of Steels*, vol. 171, no. 11, pp. 52–23, 2015, doi: 10.1533/9780857096524.4.557.

[152] M. A. J. Somers and T. L. Christiansen, “Gaseous processes for low temperature surface hardening of stainless steel,” in *Thermochemical Surface Engineering of Steels: Improving Materials Performance*, 2015, vol. 1, no. 1, pp. 581–614. doi: 10.1533/9780857096524.4.581.

[153] A. Idayan, A. Gnanavelbabu, and K. Rajkumar, “Influence of Deep Cryogenic Treatment on the Mechanical Properties of AISI 440C Bearing Steel,” *Procedia Engineering*, vol. 97, pp. 1683–1691, 2014, doi: 10.1016/j.proeng.2014.12.319.

[154] P. Baldissera and C. Delprete, “Deep cryogenic treatment of AISI 302 stainless steel: Part II - Fatigue and corrosion,” *Materials and Design*, vol. 31, no. 10, pp. 4731–4737, 2010, doi: 10.1016/j.matdes.2010.05.015.

[155] P. Baldissera and C. Delprete, “Deep Cryogenic Treatment: Effects on Mechanical Properties of AISI 302 Stainless Steel and 18NiCrMo5 Carburized Steel,” *Key Engineering Materials*, vol. 417–418, pp. 793–796, 2009, doi: 10.4028/www.scientific.net/KEM.417-418.793.

[156] D. S. Nadig, M. R. Bhat, V. K. Pavan, and C. Mahishi, “Effects of Cryogenic Treatment on the Strength Properties of Heat Resistant Stainless Steel (07X16H6),” *IOP Conference Series: Materials Science and Engineering*, vol. 229, no. 1, pp. 1–6, 2017, doi: 10.1088/1757-899X/229/1/012014.

[157] M. Villa, M. F. Hansen, and M. A. J. Somers, “Martensite formation in Fe-C alloys at cryogenic temperatures,” *Scripta Materialia*, vol. 141, pp. 129–132, 2017, doi: 10.1016/j.scriptamat.2017.08.005.

[158] M. A. Jaswin and D. M. Lal, “Impact Behavior of Cryogenically Treated En 52 and 21-4N Valve Steels,” *International Journal of Mechanical, Industrial Science and Engineering*, vol. 8, no. 1, pp. 159–164, 2014, doi: 10.5281/zenodo.1090751.

[159] A. R. Suresh and I. Rajendran, “Investigations on Deep Cryogenically Treated Low Alloy Steel Impregnated with WS2,” *Materials Today: Proceedings*, vol. 5, no. 2, pp. 6736–6745, 2018, doi: 10.1016/j.matpr.2017.11.332.

[160] L. B. Ramos, L. Simoni, R. G. Mielczarski, M. R. O. Vega, R. M. Schroeder, and C. de F. Malfatti, “Tribocorrosion and Electrochemical Behavior of DIN 1.4110 Martensitic Stainless Steels After Cryogenic Heat Treatment,” *Materials Research*, vol. 20, no. 2, pp. 460–468, 2017, doi: 10.1590/1980-5373-mr-2016-0341.

[161] P. Baldissera and C. Delprete, “Effects of deep cryogenic treatment on static mechanical properties of 18NiCrMo5 carburized steel,” *Materials and Design*, vol. 30, no. 5, pp. 1435–1440, 2009, doi: 10.1016/j.matdes.2008.08.015.

[162] A. Fedorikova, “Effect of plastic deformation on mechanical properties of austenitic stainless steel under cryogenic condition,” in *Metallurgy Junior*, 2018, pp. 39–42.

[163] S. Li, M. Xiao, G. Ye, K. Zhao, and M. Yang, “Effects of deep cryogenic treatment on microstructural evolution and alloy phases precipitation of a new low carbon martensitic stainless bearing steel during aging,” *Materials Science and Engineering A*, vol. 732, pp. 167–177, 2018, doi: 10.1016/j.msea.2018.07.012.

[164] M. Villa, K. Pantleon, and M. A. J. Somers, “Enhanced carbide precipitation during tempering of sub-zero Celsius treated AISI 52100 bearing steel,” *in the proceedings Heat Treat & Surface Engineering Conference & Expo*, Heat Treating Society: Chennai, India, 2013

[165] M. Preciado and M. Pellizzari, “Influence of deep cryogenic treatment on the thermal decomposition of Fe-C martensite,” *Journal of Materials Science*, vol. 49, no. 23, pp. 8183–8191, 2014, doi: 10.1007/s10853-014-8527-2.

[166] R. Sri Siva, D. Mohan Lal, P. Kesavan Nair, and M. Arockia Jaswin, “Influence of cryogenic treatment on the wear characteristics of 100Cr6 bearing steel,” *International Journal of Minerals, Metallurgy and Materials*, vol. 21, no. 1, pp. 46–51, 2014, doi: 10.1007/s12613-014-0863-3.

[167] A. Bensely, D. Senthilkumar, S. Harish, D. Mohan Lal, A. Nagarajan, and P. Paulin, “Cryogenic treatment of gear steel,” *GearSolutions*, no. 10, pp. 36–51, 2011.

[168] M. Pellizzari, “Influence of Deep Cryogenic Treatment on the heat treatment of steel and selected non ferrous alloys. (Cu-Be alloys),” *International Heat Treatment and Surface Engineering*, vol. 4, no. 3, pp. 105–109, 2010, doi: 10.1179/174951410X12712449937243.

[169] F. Hu, K. Wu, P. D. Hodgson, and A. A. Shirzadi, “Refinement of Retained Austenite in Super-bainitic Steel by a Deep Cryogenic Treatment,” *ISIJ International*, vol. 54, no. 1, pp. 222–226, 2014, doi: 10.2355/isijinternational.54.222.

[170] F. H. Çakir and O. N. Çelik, “The effects of cryogenic treatment on the toughness and tribological behaviors of eutectoid steel,” *Journal of Mechanical Science and Technology*, vol. 31, no. 7, pp. 3233–3239, 2017, doi: 10.1007/s12206-017-0613-3.

[171] N. Min, H. M. Li, C. Xie, and X. C. Wu, “Experimental investigation of segregation of carbon atoms due to sub-zero cryogenic treatment in cold work tool steel by mechanical spectroscopy and atom probe tomography,” *Archives of Metallurgy and Materials*, vol. 60, no. 2, pp. 1110–1113, 2015, doi: 10.1515/amm-2015-0268.

[172] M. Preciado, P. M. Bravo, and J. M. Alegre, “Effect of low temperature tempering prior cryogenic treatment on carburized steels,” *Journal of Materials Processing Technology*, vol. 176, no. 1–3, pp. 41–44, 2006, doi: 10.1016/j.jmatprotec.2006.01.011.

[173] L. A. Alava, “Austenite stability of austempered ductile iron (ADI) in sub-zero conditions,” *in the proceedings of 71st World Foundry Congress 2014*, World Foundry Organization: Bilbao, Spain, 2014.

[174] R. Thornton, T. Slatter, A. H. Jones, and R. Lewis, “The effects of cryogenic processing on the wear resistance of grey cast iron brake discs,” *Wear*, vol. 271, no. 9–10, pp. 2386–2395, 2011, doi: 10.1016/j.wear.2010.12.014.

[175] C. H. Surberg, P. Stratton, and K. Lingenhöle, “Effect of deep cold treatment on two case hardening steels,” *Acta Metallurgica Sinica (English Letters)*, vol. 21, no. 1, pp. 1–7, 2008, doi: 10.1016/S1006-7191(08)60012-5.

[176] Y. Gao, B. H. Luo, Z. H. Bai, B. Zhu, and S. Ouyang, “Effects of deep cryogenic treatment on the microstructure and properties of WC-Fe-Ni cemented carbides,” *International*

Journal of Refractory Metals and Hard Materials, vol. 58, pp. 42–50, 2016, doi: 10.1016/j.ijrmhm.2016.03.010.

[177] B. Podgornik, V. Leskovšek, and B. Arh, "The effect of heat treatment on the mechanical, tribological and load-carrying properties of PACVD-coated tool steel," *Surface and Coatings Technology*, vol. 232, pp. 528–534, 2013, doi: 10.1016/j.surfcoat.2013.06.019.

[178] B. Podgornik, V. Leskovšek, and J. Vižintin, "Influence of Deep-Cryogenic Treatment on Tribological Properties of P/M High-Speed Steel," *Materials and Manufacturing Processes*, vol. 24, no. 7–8, pp. 734–738, 2009.

[179] D. H. Park, S. W. Choi, J. H. Kim, and J. M. Lee, "Cryogenic mechanical behavior of 5000- and 6000-series aluminum alloys: Issues on application to offshore plants," *Cryogenics (Guildf)*, vol. 68, pp. 44–58, 2015, doi: 10.1016/j.cryogenics.2015.02.001.

[180] A. L. Woodcraft, "Predicting the thermal conductivity of aluminium alloys in the cryogenic to room temperature range," *Cryogenics (Guildf)*, vol. 45, no. 6, pp. 421–431, 2005, doi: 10.1016/j.cryogenics.2005.02.003.

[181] K. M. Asl, A. Tari, and F. Khomamizadeh, "Effect of deep cryogenic treatment on microstructure, creep and wear behaviors of AZ91 magnesium alloy," *Materials Science and Engineering A*, vol. 523, no. 1–2, pp. 27–31, 2009, doi: 10.1016/j.msea.2009.06.003.

[182] K. X. Gu, J. J. Wang, Z. Yuan, H. Zhang, Z. Q. Li and B. Zhao., "The Effect of Cryogenic Treatment on the Microstructure and Properties of Ti-6Al-4V Titanium Alloy," *Materials Science Forum*, vol. 747–748, pp. 899–903, 2013, doi: 10.4028/www.scientific.net/MSF.747-748.899.

[183] A. Ciski, "Deep cryogenic treatment of high speed steel," *in the proceedings of COMAT, Recent trends in structural materials*, COMAT: Pilsen, Czech Republic, 2012.

[184] D. N. Korade, K. V. Ramana, K. R. Jagtap, and N. B. Dhokey, "Effect of Deep Cryogenic Treatment on Tribological Behaviour of D2 Tool Steel - An Experimental Investigation," *Materials Today: Proceedings*, vol. 4, no. 8, pp. 7665–7673, 2017, doi: 10.1016/j.matpr.2017.07.100.

[185] Z. Hu, H. Zheng, G. Liu, and H. Wu, "Effects of Cryogenic Treatment after Annealing of Ti-6Al-4V Alloy Sheet on Its Formability at Room Temperature," *Metals (Basel)*, vol. 8, no. 295, pp. 1–16, 2018, doi: 10.3390/met8050295.

[186] G. Hemath Kumar, H. Mohit, and R. Purohit, "Effect of Deep Cryogenic Treatment on Composite Material for Automotive Ac System," *Materials Today: Proceedings*, vol. 4, no. 2, pp. 3501–3505, 2017, doi: 10.1016/j.matpr.2017.02.240.

[187] X. Wang, Y. Lv, S. Lv, H. Liu, and H. Ni, "Effect of cryogenic treatment on microstructure and properties of acrylonitrile–butadiene–styrene," *Emerging Materials Research*, vol. 6, no. 1, pp. 35–39, 2017, doi: 10.1680/jemmr.16.00066.

[188] P. Jimbert, M. Iturrondobeitia, J. Ibarretxe, and R. Fernandez-Martinez, "Influence of Cryogenic Treatment on Wear Resistance and Microstructure of AISI A8 Tool Steel," *Metals (Basel)*, vol. 8, no. 12, pp. 1038–1049, 2018, doi: 10.3390/met8121038.

[189] V. F. Steier, E. S. Ashiuchi, L. Reißig, and J. A. Araújo, "Effect of a Deep Cryogenic Treatment on Wear and Microstructure of a 6101 Aluminum Alloy," *Advances in Materials Science and Engineering*, vol. 2016, no. 1582490, pp. 1–12, 2016, doi: 10.1155/2016/1582490.

[190] M. Levine and C. White, "Material damping experiments at cryogenic temperatures," *Optical Materials and Structures Technologies*, vol. 5179, pp. 165–176, 2003, doi:10.1117/12.506838.

[191] R. F. Barron and R. H. Thompson, "Effect of Cryogenic Treatment of Corrosion Resistance," *in the proceedings of International Cryogenics Materials Conference*, Cryogenics Society: Boston, MA, USA, 1991

[192] F. Iacopi, J. H. Choi, K. Terashima, P. M. Rice, and G. Dubois, “Cryogenic plasmas for controlled processing of nanoporous materials,” *Physical Chemistry Chemical Physics*, vol. 13, no. 9, pp. 3634–3637, 2011, doi: 10.1039/c0cp02660c.

[193] D. J. Kamody, “Cryogenics process update,” *Advance Materials and Processes*, vol. 155, no. 6, pp. 67–59, 1999.

[194] R. Cryderman, D. Rickert, K. Puzak, J. Speer, D. Matlock, and M. Burnett, “Effects of Chemical Composition, Heat Treatment, and Microstructure in Splittable Forged Steel Connecting Rods,” *SAE International Journal of Materials and Manufacturing*, vol. 8, no. 3, pp. 765–773, 2015, doi: 10.4271/2015-01-0522.

[195] S. Zhirafar, A. Rezaeian, and M. Pugh, “Effect of cryogenic treatment on the mechanical properties of 4340 steel,” *Journal of Materials Processing Technology*, vol. 186, no. 1–3, pp. 298–303, 2007, doi: 10.1016/j.jmatprotec.2006.12.046.

[196] F. Niessen, M. Villa, and M. A. J. Somers, “Martensite Formation from Reverted Austenite at Sub-zero Celsius Temperature,” *Metallurgical and Materials Transactions A*, vol. 49, no. 11, pp. 5241–5245, 2018, doi: 10.1007/s11661-018-4887-6.

[197] B. K. Anil Kumar, M. G. Ananthaprasad, and K. Gopalakrishna, “Action of Cryogenic chill on Mechanical properties of Nickel alloy Metal Matrix Composites,” in *IOP Conference Series: Materials Science and Engineering*, 2016, vol. 149, no. 1, pp. 1–11. doi: 10.1088/1757-899X/149/1/012116.

[198] W. S. Lee and C. R. Lin, “Deformation behavior and microstructural evolution of 7075-T6 aluminum alloy at cryogenic temperatures,” *Cryogenics (Guildf)*, vol. 79, pp. 26–34, 2016, doi: 10.1016/j.cryogenics.2016.07.007.

[199] K. E. Moore and N. N. Collins, “Cryogenic Treatment of Three Heat Treated Tool Steels,” *Key Engineering Materials*, vol. 86–87, pp. 47–54, 1993, doi: 10.5860/CHOICE.33-5121.

[200] A. Oppenkowski, S. Weber, and W. Theisen, “Evaluation of factors influencing deep cryogenic treatment that affect the properties of tool steels,” *Journal of Materials Processing Technology*, vol. 210, no. 14, pp. 1949–1955, 2010, doi: 10.1016/j.jmatprotec.2010.07.007.

[201] L. Tóth, “The properties and structure of tool steel en. 1.2379 due to different heat treatments,” *European Journal of Materials Science and Engineering*, vol. 2, no. 3, p.p.1-10, 2018.

[202] M. Kus, P. Jurci, and J. Durica, “Microstructure and Hardness of Cold Work Vanadis 6 Steel after Subzero Treatment at − 140 °C ,” *Advances in Materials Science and Engineering*, vol. 2018, pp. 1–7, 2018, doi: 10.1155/2018/6537509.

[203] J. Li, X. Cai, Y. Wang, and X. Wu, “Multiscale Analysis of the Microstructure and Stress Evolution in Cold Work Die Steel during Deep Cryogenic Treatment,” *Materials*, vol. 11, no. 11, pp. 2122–2133, 2018, doi: 10.3390/ma11112122.

[204] G. Sayegh, “High energy density beams (electron beam and laser beam) for heat treatment of metals,” *in the proceedings of 3rd International Congress on: Heat Treatment of Materials,* Heat Treatment Society: Shanghai, China, 1983.-

[205] K. Gu, H. Zhang, B. Zhao, J. Wang, Y. Zhou, and Z. Li, “Effect of cryogenic treatment and aging treatment on the tensile properties and microstructure of Ti-6Al-4V alloy,” *Materials Science and Engineering A*, vol. 584, pp. 170–176, 2013, doi: 10.1016/j.msea.2013.07.021.

[206] S. Paul and A. B. Chattopadhyay, “Environmentally conscious machining and grinding with cryogenic cooling,” *Machining Science and Technology*, vol. 10, no. 1, pp. 87–131, 2007, doi: 10.1080/10910340500534316.

[207] P. F. Stratton, “Optimising nano-carbide precipitation in tool steels,” *Materials Science and Engineering A*, vol. 449–451, pp. 809–812, 2007, doi: 10.1016/j.msea.2006.01.162.

[208] V. Leskovšek and B. Podgornik, “Simultaneous ion nitriding and tempering after deep cryogenic treatment of PM S390MC HSS,” *International Heat Treatment and Surface Engineering*, vol. 7, no. 3, pp. 115–119, 2013, doi: 10.1179/1749514813Z.00000000066.

[209] Y. T. Lin, M. C. Wang, Y. Zhang, Y. Z. He, and D. P. Wang, “Investigation of microstructure evolution after post-weld heat treatment and cryogenic fracture toughness of the weld metal of AA2219 VPTIG joints,” *Materials and Design*, vol. 113, pp. 54–59, 2017, doi: 10.1016/j.matdes.2016.10.010.

[210] A. Cicek, T. KIvak, I. Uygur, E. Ekici, and Y. Turgut, “Performance of cryogenically treated M35 HSS drills in drilling of austenitic stainless steels,” *International Journal of Advanced Manufacturing Technology*, vol. 60, no. 1–4, pp. 65–73, 2012, doi: 10.1007/s00170-011-3616-8.

[211] B. Podgornik, V. Leskovšek, M. Godec, and B. Senčič, “Microstructure refinement and its effect on properties of spring steel,” *Materials Science and Engineering A*, vol. 599, pp. 81–86, 2014, doi: 10.1016/j.msea.2014.01.054.

[212] J. A. Mathews, “Austenite and Austenitic Steels,” *AIME*, vol. 71, pp. 568–596, 1925.

[213] I. A. Revis, A. M. Levinson, V. S. Naletov, and S. A. Popov, “Use of cryogenic treatment to restore worn plug gages,” *Chemical and Petroleum Engineering*, vol. 10, no. 5, p. 474, 1974.

[214] M. Koneshlou, K. Meshinchi Asl, and F. Khomamizadeh, “Effect of cryogenic treatment on microstructure, mechanical and wear behaviors of AISI H13 hot work tool steel,” *Cryogenics (Guildf)*, vol. 51, no. 1, pp. 55–61, 2011, doi: 10.1016/j.cryogenics.2010.11.001.

[215] D. J. Kamody, “Process for the Cryogenic Treatment of Metal Containing Materials, US Patent 5, 259, 200,” 1993.

[216] H. Berns, N. Krasokha, and M. Seifert, “Nitrogen and Ausforming to Improve Stainless Martensitic Steels,” *Steel Research InInternational*, vol. 85, no. 7, pp. 1200–1208, 2014, doi: 10.1002/srin.201300299.

[217] K. Amini, A. Akhbarizadeh, and S. Javadpour, “Investigating the effect of holding duration on the microstructure of 1.2080 tool steel during the deep cryogenic heat treatment,” *Vacuum*, vol. 86, no. 10, pp. 1534–1540, 2012, doi: 10.1016/j.vacuum.2012.02.013.

[218] V. Leskovšek and B. Ule, “Influence of deep cryogenic treatment on vacuum heat-treated high-speed steel,” *International Heat Treatment and Surface Engineering*, vol. 29, no. 3, pp. 72–76, 2002, doi: 10.1179/174951508X446385.

[219] F. Meng, K. Tagashira, and H. Sohma, “Wear resistance and microstructure of cryogenic treated Fe-1.4Cr-1C bearing steel,” *Scripta Metallurgica et Materialia*, vol. 31, no. 7, pp. 865–868, 1994, doi: 10.1016/0956-716X(94)90493-6.

[220] E. Demir and I. Toktas, “Effects of cryogenic treatment on residual stresses of AISI D2 tool steel,” *Kovove Materialy*, vol. 56, no. 3, pp. 153–161, 2018, doi: 10.4149/km20183153.

[221] M. Koneshlou, A. K. Meshinchi, and F. Khomamizadeh, “Effect of cryogenic tratment on microstucture, mechanical and wear behaviors of AISI H13 hot work tool steel,” *Cryogenics (Guildf)*, vol. 51, no. 1, pp. 55–61, 2011, doi: 10.1016/j.cryogenics.2010.11.001.

[222] M. Villa and M. A. J. Somers, “Cryogenic treatment of an AISI D2 steel: The role of isothermal martensite formation and ‘martensite conditioning,’” *Cryogenics (Guildf)*, vol. 110, no. 12, pp. 103131, 2020, doi: 10.1016/j.cryogenics.2020.103131.

[223] V. A. Landa, “The secondary martensitic transformation resulting from tempering tool steels,” *Metal Science and Heat Treatment*, vol. 5, no. 3, pp. 125–129, 1963, doi: 10.1007/BF00655394.

Bibliography

Publications Related to the Thesis

Journal Articles

P. Jovičević-Klug, N. Lipovšek, M. Jovičević-Klug, M. Mrak, J. Ekar, B. Ambrožič, G. Dražić, J. Kovač, and B. Podgornik, "Assessment of deep cryogenic heat-treatment impact on the microstructure and surface chemistry of austenitic stainless steel," *Surfaces and Interfaces*, *accepted,* 2022.

P. Jovičević-Klug, A. S. Guštin, M. Jovičević-Klug, B. Šetina Batič, A. Lebar, and B. Podgornik, "Coupled Role of Alloying and Manufacturing on Deep Cryogenic Treatment Performance on High-alloyed Ferrous Alloys," *Journal of Materials Research and Technology*, vol. 18, no. 5-6, pp. 3184-3197, 2022, doi: 10.1016/j.jmrt.2022.04.025.

M. Jovičević-Klug, T. Verbovšek, P. Jovičević-Klug, B. Šetina Batič, B. Ambrožič, G. Dražić. and B. Podgornik, "Revealing the Pb Whisker Growth Mechanism from Al-Alloy Surface and Morphological Dependency on Material Stress and Growth Environment," *Materials*, vol. 15, no. 7, p. 2574, 2022, doi: 10.3390/ma15072574.

P. Jovičević-Klug, M. Jovičević-Klug, and B. Podgornik, "Unravelling the Role of Nitrogen in Surface Chemistry and Oxidation Evolution of Deep Cryogenic Treated High-Alloyed Ferrous Alloy," *Coatings*, vol. 12, no. 2, p. 213, 2022, doi: 10.3390/coatings12020213.

M. Jovičević-Klug, R. Rezar, P. Jovičević-Klug, and B. Podgornik, "Influence of deep cryogenic treatment on natural and artificial aging of Al-Mg-Si alloy EN AW 6026," *Journal of Alloys and Compounds*, vol. 899, p. 163323, 2022, doi: 10.1016/j.jallcom.2021.163323.

P. Jovičević-Klug, G. Puš, M. Jovičević-Klug, B. Žužek, and B. Podgornik, "Influence of heat treatment parameters on effectiveness of deep cryogenic treatment on properties of high-speed steels," *Materials Science and Engineering A*, vol. 829, p. 142157, 2022, doi: 10.1016/j.msea.2021.142157.

P. Jovičević-Klug, M. Jenko, M. Jovičević-Klug, B. Šetina Batič, J. Kovač, and B. Podgornik, "Effect of Deep Cryogenic Treatment on Surface Chemistry and Microstructure of Selected High-Speed Steels," *Applied Surface Science*, vol. 548, no. 15, pp. 1–11, 2021, doi: 10.1016/j.apsusc.2021.149257.

M. Jovičević-Klug, P. Jovičević-Klug, J. McCord, and B. Podgornik, "Investigation of Microstructural Attributes of Steel Surfaces through Magneto-optical Kerr Effect," *Journal of Materials Research and Technology,* vol. 11, no. 3-4, pp. 1245–1259, 2021, doi: 10.1016/j.jmrt.2021.01.106.

P. Jovičević-Klug, M. Jovičević-Klug, T. Sever, D. Feizpour, and B. Podgornik, "Impact of Steel Type, Composition and Heat Treatment Parameters on Effectiveness of Deep Cryogenic Treatment," *Journal of Materials Research and Technology*, vol.14, no. 9-10, pp. 1007-1020, 2021, doi: 10.1016/j.jmrt.2021.07.022.

M. Jovičević-Klug, P. Jovičević-Klug, T. Kranjec, and B. Podgornik, "Cross-effect of Surface Finishing and Deep Cryogenic Treatment on Corrosion Resistance of AISI M35 steel," *Journal of Materials Research and Technology*, vol. 14, no. 9–10, pp. 2365–2381, 2021, doi: 10.1016/j.jmrt.2021.07.134.

P. Jovičević-Klug, N. Lipovšek, M. Jovičević-Klug, and B. Podgornik, "Optimized preparation of deep cryogenic treated steel and Al-alloy samples for optimal microstructure imaging results," *Materials Today Communications*, vol. 27, no. 6, pp. 102211, 2021, doi: doi.org/10.1016/j.mtcomm.2021.102211.

P. Jovičević-Klug, T. Kranjec, M. Jovičević-Klug, T. Kosec, and B. Podgornik, "Influence of the Deep Cryogenic Treatment on AISI 52100 and AISI D3 Steel's Corrosion Resistance," *Materials*, vol. 14, no. 21, pp- 6357, 2021, doi: 10.3390/ma14216357.

P. Jovičević-Klug, M. Sedlaček, M. Jovičević-Klug, and B. Podgornik, "Effect of deep cryogenic treatment on corrosion properties of various high-speed steels," *Materials*, vol. 14, no. 1, pp. 1–16, 2021, doi: 10.3390/ma14247561.

J. Voglar, Ž. Novak, P. Jovičević-Klug, B. Podgornik, and T. Kosec, "Effect of Deep Cryogenic Treatment on Corrosion Properties of Various High-Speed Steels," *Metals*, vol. 11, no. 1, p. 14, 2020, doi: 10.3390/met11010014.

M. Jovičević-Klug, P. Jovičević-Klug, T. Sever, D. Feizpour, and B. Podgornik, "Extraordinary nanocrystalline Pb whisker growth from Bi-Mg-Pb pools in aluminum alloy 6026 moderated through oriented attachment," *Nanomaterials*, vol. 11, no. 7, pp. 1842, 2021, doi: 10.3390/nano11071842.

P. Jovičević-Klug, M. Jovičević-Klug, and B. Podgornik, "Effectiveness of deep cryogenic treatment on carbide precipitation," *Journal of Materials Research and Technology*, vol. 9, no. 6, pp. 13014–13026, 2020, doi: 10.1016/j.jmrt.2020.09.063.

P. Jovičević-Klug and B. Podgornik, "Comparative study of conventional and deep cryogenic treatment of AISI M3:2 (EN 1.3395) high-speed steel," *Journal of Materials Research and Technology*, vol. 9, no. 6, pp. 13118–13127, 2020, doi: 10.1016/j.jmrt.2020.09.071 .

P. Jovičević-Klug and B. Podgornik, "Review on the Effect of Deep Cryogenic Treatment of Metallic Materials in Automotive Applications," *Metals*, vol. 10, no. 4, p. 434, 2020, doi: 10.3390/met10040434.

Conference Proceedings (Abstracts)

B. Podgornik, P. Jovičević Klug, J. Ekar and J. Kovač, "Impact of deep cryogenic treatment on nitridability and properties of nitrided hot work tool steel*," in the proceedings of the 27th International Federation for Heat Treatment and European Conference on Heat Treatment*, International Federation for Heat Treatment and Surface Engineering: Salzburg, Austria, 2022.

P. Jovičević Klug and B. Podgornik, "Deep Cryogenic Treatment of AISI H11, AISI H13 and AISI H21 Hot Work Tool Steels,*" in the proceedings of the 27th International Federation for Heat Treatment and European Conference on Heat Treatment*, International Federation for Heat Treatment and Surface Engineering: Salzburg, Austria, 2022.

T. Sever, M. Jovičević Klug, P. Jovičevič Klug, D. Feizpour and B. Podgornik. "Extraordinary Nanocrystalline Pb Whisker Growth from Bi-Mg-Pb Pools in Aluminum Alloy 6026," *in the proceedings of the 4th Slovenian Microscopy Symposium,* Slovene Society for Microscopy: Ankaran, Slovenia, 2022.

B. Podgornik, P. Jovičević Klug, and M. Jovičević Klug, "Altering tribological properties of tools steel through deep cryogenic treatment utilization," *in the proceedings of the 12th Tooling Conference & Exhibition – Tooling*, Austrian Society for Metallurgy and Materials: Orebro, Sweden, 2022.

P. Jovičević-Klug, T. Kranjec, M. Jovičević-Klug, and B. Podgornik, "Modification of Steel Corrosion Resistance in Seawater with Deep Cryogenic Treatment," *in the proceedings of the 60th Conference of Metallurgists, COM 2021,* The Canadian Institute of Mining, Metallurgy and Petroleum, virtual conference, Canada, 2021.

P. Jovičevič Klug, M. Jovičević Klug, and B. Podgornik, "Potential in Deep Cryogenic Treatment of Non-ferrous Alloys," *in the proceedings of the European Cryogenics Days 2021*, Cryogenics Society of Europe: virtual conference, the Netherlands, 2021.

M. Jovičević Klug, P. Jovičević Klug, and B. Podgornik, "Utilization of Magneto-optical Kerr Effect Microscopy for Microstructural Characterization of Steels," *in the proceedings of the TMS 2021 Virtual : 150th annual meeting & exhibition,* the American Institute of Mining, Metallurgical, and Petroleum Engineers: Orlando, FL, USA, 2021.

P. Jovičević Klug, M. Jovičevič Klug, and B. Podgornik, "*Applicability of Deep Cryogenic Treatment in Emerging Industries,*" *in the proceedings of the TMS 2021 Virtual : 150th annual meeting & exhibition*; the American Institute of Mining, Metallurgical, and Petroleum Engineers: Orlando, FL, USA, 2021.

P. Jovičević Klug, M. Jovičević Klug, and B. Podgornik, " Deep cryogenic treatment of AlSI 431 and AlSI 52100 steels," *in the proceedings of the 23rd Cryogenic Engineering Conference*

and International Cryogenic Materials Conference, Cryogenic Society of Europe: Cern, Switzerland, 2021.

M. Jovičević Klug, P. Jovičević Klug, and B. Podgornik, "Deep cryogenic treatment as the next processing step in the steel industry," *in the proceedings of the 60th annual conference of metallurgists,* the metallurgy and materials society of the Canadian intitute of mining, metallurgy and petrolum: Westmount, Canada, 2021.

P. Jovičević Klug, T. Kranjec, M. Jovičević Klug, and B. Podgornik, "Modification of steel corrosion resistance in seawater with deep cryogenic treatment," *in the proceedings of the 60th annual conference of metallurgists,* the metallurgy and materials society of the Canadian intitute of mining, metallurgy and petrolum: Westmount, Canada, 2021.

P. Jovičević Klug, M. Jovičević Klug, and B. Podgornik, "Deep cryogenic treatment of AlSi 431 and AlSi 52100 steels," *in the proceedings of the Cryogenic Engineering Conference and International Cryogenic Materials Conference*, Centennial Conferences: Cern, Switzerland, 2021.

M. Jovičević Klug, P. Jovičević Klug, and B. Podgornik, "Extraordinary Pb whisker growth from Bi-Mg-Pb pools in aluminum alloy 6026," *in the poceedings of the 32nd Canadian Materials Science Conference,* University of Toronto*:* Toronto, Canada, 2021.

P. Jovičević Klug, M. Jovičević Klug, and B. Podgornik, "Novel method for surface chemistry dynamics analysis of HSS steel induced by deep cryogenic treatment,*in the poceedings of the 32nd Canadian Materials Science Conference,* University of Toronto*:* Toronto, Canada, 2021.

M. Jovičević Klug, P. Jovičević Klug, L. Thormählen, J. McCord, and B. Podgornik, "Microstructural and residual stress evaluation of bulk martensitic steels with micrometer-sized grains through magneto-optical Kerr effect," *in the proceedings of the INTERMAG 2021*, IEEE Magnetics Societ: Lyon, France, 2021.

P. Jovičević Klug and B. Podgornik, "Importance of deep cryogenic treatment in present, emerging and future industries," *in the proceedings of the 13th Jožef Stefan International Postgraduate School Students' Conference and 15th Young Researchers' Day of Chemistry, Material Science, Biochemistry and Environment,* Jožef Stefan International Postgraduate School: Ljubljana, Slovenia, 2021.

P. Jovičević Klug, M. Jovičević Klug, L. Thormählen, J. McCord, and B. Podgornik, "Analysis of microstructural attributes of bulk martensitic steel surfaces with micrometersized grains through magneto-optical Kerr effect," *in the proceedings of the Joint European Magnetic Symposia 2020*, the European Magnetism Association: Porto, Portugal, 2020.

P. Jovičević Klug and B. Podgornik, "Systematic Development of Deep Cryogenic Treatment of Steels as the Next Processing Step in Emerging Industries," *in the proceedings of the International Materials Applications and Technologies*, ASM Heat Treating Society: Cleveland, OH, USA, 2020.

P. Jovičević Klug and B. Podgornik, "Deep cryogenic treatment as the next processing step in steel industry," *in the proceedings of the 12th Jožef Stefan International Postgraduate School Students' Conference and 14th Young Researchers' Day of Chemistry, Material Science, Biochemistry and Environment,* Jožef Stefan International Postgraduate School: Ljubljana, Slovenia, 2020.

P. Jovičević Klug and B. Podgornik, "Systematic Development of Deep Cryogenic Treatment of Steels as the Next Processing Step in Emerging Industries," *in the proceedings of the International Materials Applications and Technologies 2020:* ASM Heat Treatment Society: Cleveland, Ohio, USA, 2020.

P. Jovičević Klug and B. Podgornik, "Deep cryogenic treatment of metallic materials in automotive applications : a review," *in the proceedings of the European Conference on Heat Treatment: Heat treatment and surface engineering for automotive: proceedings*, Associazione Italiana di Metallurgia: Bardolino, Italy, 2019.

P. Jovičević Klug and B. Podgornik, "Deep cryogenic treatment of metallic materials," *in the proceedings of the 11th Jožef Stefan International Postgraduate School Students' Conference and 13th Young Researchers' Day of Chemistry, Material Science, Biochemistry and Environment,* Jožef Stefan International Postgraduate School; Planica, Slovenia, 2019.

P. Jovičević Klug and B. Podgornik, "Deep cryogenic treatment of high speed steels," *in the proceedings of the 26th IFHTSE congress 2019: dedicated to the 180th anniversary of Dmitry*

Chernov, International Federation for Heat Treatment and Surface Engineering: Moscow, Russia, 2019.
P. Jovičević Klug and B. Podgornik, "Deep cryogenic treatment of high speed steels M2, M3:2 and M35," *in the proceedings of the 27th International Conference on Materials and Technology*; Institute of Metals and Technology: Portorož, Slovenia, 2019.
P. Jovičević Klug and B. Podgornik, "Deep cryogenic treatment of high speed steels," *in the proceedings of the 27th International Conference on Materials and Technology*; Institute of Metals and Technology: Portorož, Slovenia, 2019.

Book Chapter

P. Jovičević-Klug and B. Podgornik, "Deep Cryogenic Treatment of Metallic Materials," Encyclopedia MDPI AG, pp. 1–11, 2020.

Other Publications

P. Jovičević Klug, "Deep cryogenic treatment of metallic materials : overview of DCT influence on different steel grades," self-published, Ljubljana, Slovenia, 2021.
P. Jovičević Klug, "Deep Cryogenic Treatment of High-speed (M2, M3:2 and M35), Hot Work Tool (1.2367) and Stainless Steels (AISI 431) : I. phase," self-published, Ljubljana, Slovenia, 2020.
P. Jovičević Klug, "Deep cryogenic treatment of metallic materials," self-published, Ljubljana, Slovenia, 2019.

Editor/Guest Editor

P. Jovičević Klug, M. Jovičević-Klug and L. Toth., Coatings MDPI: Special Issue: Mechanical, Corrosive and Tribological Degradation of Metal Coatings and Modified Metallic Surfaces, 2021-2022.
P. Jovičević-Klug et al., 13th Jožef Stefan International Postgraduate School Students' Conference and 15th Young Researchers' Day, Ljubljana, Slovenia, 2021.
P. Jovičević-Klug et al., 12th Jožef Stefan International Postgraduate School Students' Conference and 14th Young Researchers' Day, Ljubljana, Slovenia, 2020.
P. Jovičević-Klug et al., 11th Jožef Stefan International Postgraduate School Students' Conference and 13th Young Researchers' Day, Planica, Slovenia, 2019.

Biography

Patricia Jovičević Klug (née Jovičević, and also known as Jovičević-Klug) studied Geology at the Faculty of Natural Sciences and Engineering, University of Ljubljana, concluding her bachelor studies in 2013 with the thesis entitled “Heavy Metal Content in some Children’s Sandpits in Ljubljana and Surroundings”, under the supervision of Prof. Nina Zupančič, Faculty of Natural Sciences and Engineering, University of Ljubljana. She continued her studies at the University of Kiel, Faculty of Mathematics and Natural Sciences, where she finished two international master degrees. The first master degree was done in the field of Marine Geosciences with the thesis entitled “Factors Controlling Radiogenic Neodymium Isotope Composition of Seawater and Sediments in the Mozambique Channel”, under the supervision of Prof. Martin Frank, Helmholtz Centre for Ocean Research Kiel (GEOMAR) and Dr. Ed Hathorne, Helmholtz Centre for Ocean Research Kiel (GEOMAR). The second master degree was done in the field of Sustainability, Society and Environment with the thesis entitled “Greenhouse Gases CH_4, CO_2, N_2O and its Emissions to the Atmosphere from Soil in Controlled Environment with Emphasis on N_2O”, under the supervision of Prof. Karl Mühling, Institute of Plant Nutrition and Soil Science Kiel and Dr. Britta Pitann, Institute of Plant Nutrition and Soil Science Kiel.

She received the Zois Scholarship from 2006 to 2013.

From 2018 to 2022, she has been employed as a young researcher at the Institute of Metals and Technology. In 2018, she enrolled in the doctoral studies of Nanosciences and Nanotechnologies at the Jožef Stefan International Postgraduate School. Her main research work within her doctoral studies and her dissertation revolved around the field of cryogenics, more specifically deep cryogenic treatment of ferrous and non-ferrous alloys.